

Dissertation zur Erlangung des Doktorgrades
der Fakultät für Chemie und Pharmazie
der Ludwig-Maximilians-Universität München

Functional Characterization of the *Saccharomyces cerevisiae*
Chromatin Remodeler INO80

Vanessa Laura Erna Niebauer

aus

Fensterbach, Deutschland

2020

Erklärung

Diese Dissertation wurde im Sinne von §7 der Promotionsordnung vom 28. November 2011 von Herrn Prof. Dr. Karl-Peter Hopfner betreut.

Eidesstattliche Versicherung

Diese Dissertation wurde eigenständig und ohne unerlaubte Hilfe erarbeitet.

München, den 18.06.2020

Vanessa Laura Erna Niebauer

Dissertation eingereicht am:	18.06.2020
1. Gutachter:	Herr Prof. Dr. Karl-Peter Hopfner
2. Gutachter:	Herr PD Dr. Philipp Korber
Mündliche Prüfung am:	29.07.2020

This thesis has been prepared from October 2016 to July 2020 in the laboratories of Prof. Dr. Karl-Peter Hopfner at the Gene Center of the Ludwig-Maximilians-Universität München and of PD Dr. Philipp Korber at the Biomedical Center of the Ludwig-Maximilians-Universität München.

This is a cumulative thesis based on the following publications:

Knoll, K.R.*, Eustermann, S.*, Niebauer, V., Oberbeckmann E., Stoehr G., Schall K., Tosi A., Schwarz M., Buchfellner A., Korber P., Hopfner KP. The nuclear actin-containing Arp8 module is a linker DNA sensor driving INO80 chromatin remodeling. *Nat Struct Mol Biol* **25**, 823–832 (2018). <https://doi.org/10.1038/s41594-018-0115-8>

Oberbeckmann E.*, Krietenstein N.*, **Niebauer V.**, Schall K., Moldt M., Straub T., Hopfner K.-P., Korber P., Eustermann S. (2020). Genome information processing by the INO80 chromatin remodeler positions nucleosomes. (under revision)

Oberbeckmann E.*, **Niebauer V.***, Watanabe S., Farnung L., Moldt M., Schmid A., Cramer P., Peterson C., Eustermann S., Hopfner K.-P., Korber P. (2020). Ruler elements in chromatin remodelers set nucleosome array spacing and phasing. (under revision)

*: These authors contributed equally.

Parts of this thesis have been presented at international conferences:

Poster presentation at the EMBO Conference: The Nucleosome – August 2017 in Heidelberg, Germany

Poster presentation at the 5th Munich Chromatin Symposium: Chromatin Dynamics – October 2017 in Munich, Germany

To my family.

Table of Contents

Abstract	1
1. Introduction	3
1.1 A glimpse into chromatin history	3
1.2 The nucleosome core particle	4
1.3 Architecture of chromatin	6
1.3.1 Modulation of chromatin architecture	9
1.3.2 Nucleosome spacing, phasing and positioning in a promoter-focused context	13
1.4 ATP-dependent chromatin remodelers	17
1.4.1 Phylogenetic classification of chromatin remodelers	17
1.4.2 Remodeler families and their function	18
1.4.3 Structural evidence for remodeler-nucleosome complexes	20
1.4.4 A unifying DNA translocation mechanism	23
1.5 The INO80 chromatin remodeler	25
1.5.1 INO80 function <i>in vivo</i> and <i>in vitro</i>	25
1.5.2 The modular architecture of the INO80 chromatin remodeling complex	26
1.5.3 Structural insights into the INO80 – nucleosome complex	27
1.5.4 The INO80 ARP module	30
1.6 Objectives	32
2. Publications	34
2.1 The nuclear actin-containing Arp8 module is a linker DNA sensor driving INO80 chromatin remodeling	34
2.2 Genome information processing by the INO80 chromatin remodeler positions nucleosomes	64
2.3 Ruler elements in chromatin remodelers set nucleosome array spacing and phasing	108
3. Discussion	130
3.1 The sequence-specific general regulatory factor Reb1 as well as double strand DNA ends are potent barriers to set nucleosome phasing distances independent of spacing distances	130
3.1.1 Density-independent setting of spacing and phasing distances by ISW1a and Chd1	130
3.1.2 Density-dependent setting of spacing and phasing distances by ISW2 and INO80	131
3.2 Nucleosome positioning driven by ATP-dependent chromatin remodelers is guided by a ruler-like functionality	132
3.3 The INO80 ruler element is multi-layered and hierarchically organized	135

3.3.1 Direct interaction between the Ino80 N-terminus and Reb1 governs nucleosome positioning	136
3.3.2 The INO80 ARP module ruler element evolved to read genomic information	137
3.3.3 The INO80 ruler feature hierarchically processes information	138
3.4 DNA shape profiles define a new type of positioning sequences	139
3.4.1 DNA shape read-out as a common mechanism for genome-wide operating machineries	140
3.6 Function of the ARP module in genomic information processing	141
3.6.1 A general perspective on the ARP module in chromatin remodeler function based on recent structural data	143
3.6.2 DNA length sensing and DNA shape read-out by the ARP module	146
4. References	152
5. Acknowledgements	166

Abstract

Knowing the explicit locations of nucleosomes in a genome is a pre-requisite for understanding the regulation of genes. Predominantly at regulatory active promoter sites, regular spaced arrays phased at reference points shape the chromatin landscape. In eukaryotic cells ATP-dependent chromatin remodeler align nucleosomes at reference points and are pivotal in the formation of the stereotyped promoter pattern. Chromatin remodeler of the ISWI, CHD, SWI/SNF and INO80 family convert energy derived from ATP hydrolysis to operate on their nucleosomal substrates to accomplish nucleosome spacing, eviction and editing reactions. Recent structural elucidations provided mechanistic insights into how chromatin remodelers engage their nucleosomal substrates (Eustermann *et al.*, 2018, Aramayo *et al.*, 2018, Willhoft *et al.*, 2018, Ayala *et al.*, 2018, Farnung *et al.*, 2017, Wagner *et al.*, 2020, Yan *et al.*, 2019, He *et al.*, 2020, Han *et al.*, 2020) and brought about a unifying DNA wave mechanism underpinning ATP-dependent DNA translocation by chromatin remodeling complexes (Yan and Chen, 2020). Understanding how phased arrays of equally spaced nucleosomes are generated by chromatin remodelers represents an ultimate long-term goal in chromatin biology.

What remains unclear is the underlying mechanism that directs nucleosome positioning by chromatin remodelers in absolute terms. How do ATP-dependent chromatin remodelers generate phased arrays of regularly spaced nucleosomes? How are the distances between nucleosomes and phasing sites and between adjacent nucleosomes set? Is DNA shape read-out part of nucleosome positioning driven by chromatin remodelers? Do remodelers have intrinsic ruler-like elements that set spacing and phasing distances? The aim of this thesis was to delineate whether, and if so, what type of genomic information is read by a remodeler in the stereotypic placement of nucleosomes at physiological sites, and how the remodeler activities fit into the unifying framework of ATP-dependent DNA translocation mechanism of chromatin remodelers.

To gain an insight into nucleosome positioning driven by *Saccharomyces cerevisiae* (S.c.) ATP-dependent chromatin remodelers, a combination of a minimalistic genome-wide *in vitro* reconstitution system, biochemical analysis, high-resolution structures and structure-guided mutagenesis of the S.c. INO80 model system was applied.

Findings of this work would have an impact on the mechanistic understanding of nucleosome positioning driven by ATP dependent chromatin remodelers based on the ruler concept that has been described earlier for the ISW1a chromatin remodeler (Yamada *et al.*, 2011). The ISW1a, Chd1 and ISW2 remodelers demonstrated “clamping” activity and used ruler elements to set

Abstract

distances with a defined linker length (21-26 bp at all densities, 12-13bp at all densities, 54-58 bp at low/medium densities, respectively). Mutagenesis of the INO80 model system identified and tuned the INO80 ruler element, which is comprised of the Ino80_HSA domain of the ARP module, the NHP10 module and Ino80 N-terminal residues. Regularly spaced symmetrical arrays were generated at the Reb1 reference point sites as well as at BamHI-introduced dsDNA break sites. Nucleosome positioning on the genomic sequences of *S. c.*, *Schizosaccharomyces pombe* (*S.p.*) as well as *Escherichia coli* (*E.coli*) showed no significant differences. Mutagenesis of residues located within the Ino80_HSA domain established a causal link between nucleosome positioning by INO80 and DNA shape read-out by the INO80_HSA domain.

The spacing and phasing distances generated by ATP-dependent chromatin remodelers point towards a remodeler-intrinsic ruler activity that is independent of underlying DNA sequences and can be sensitive to nucleosome density. This study measured linker lengths set by remodeler-intrinsic ruler-like functionalities in absolute terms, which will be instrumental to dissect contributions from individual remodelers in nucleosome positioning *in vivo*. This provides the starting point to understand how remodeler-driven nucleosome dynamics direct stable steady-state nucleosome positions relative to DNA bound factors, DNA ends and DNA sequence elements. Sequence-dependent DNA shape features have been mainly associated with binding of transcription factors as well as general regulatory factors and more static DNA binding events. This study augments the general description of nucleosome positioning sequences for chromatin remodelers by establishing nucleosome positioning motifs based on DNA shape analysis. This study provides an intriguing framework to implement DNA shape read-out in the tracking mechanism of DNA-translocating machineries.

1. Introduction

1.1 A glimpse into chromatin history

The first definition of a cellular nucleus was introduced by W. Flemming as a part of the pioneer work on cell division and mitosis in 1882. The term “chromatin” originates from the ancient Greek word “chrôma”, meaning “color”, and refers to the stainable feature within a cellular nucleus. In 1871, the DNA molecule itself was discovered by F. Miescher and in 1884 A. Kossel and colleagues discovered the histone proteins. Based on X-ray diffraction patterns and other pioneering works of P. Levene and E. Chargaff, J. Watson and F. Crick (as well as M. Wilkins, R. Franklin and R. Gosling) made the groundbreaking conclusion in 1953 that a 3D double-helical model thoroughly describes the structural arrangement of the DNA molecule within the nucleus (Watson and Crick, 1953). Starting with Flemming’s discovery in 1882, chromatin research mainly focused on deciphering the molecular structure of chromatin and its impact on gene regulation. It required almost a hundred years of research until in 1974, D. and A. Olins published the first structure of chromatin fibers isolated from chicken erythrocytes visualized by electron microscopy (EM) (Olins and Olins, 1974, Woodcock *et al.*, 1976). Chromatin was described as repetitive protein-DNA complexes of ~10 nm in diameter and a dyad axis, so called “v-bodies”, that formed a “beads-on-a-string”-like structure. D. and A. Olins proposed a model for the structure of chromatin in which two copies of each histone protein form a central octameric symmetric unit wrapped by double stranded B-DNA. Non-covalent interactions between the v-bodies were proposed to stabilize additional layers of helical packing (Olins and Olins, 1974).

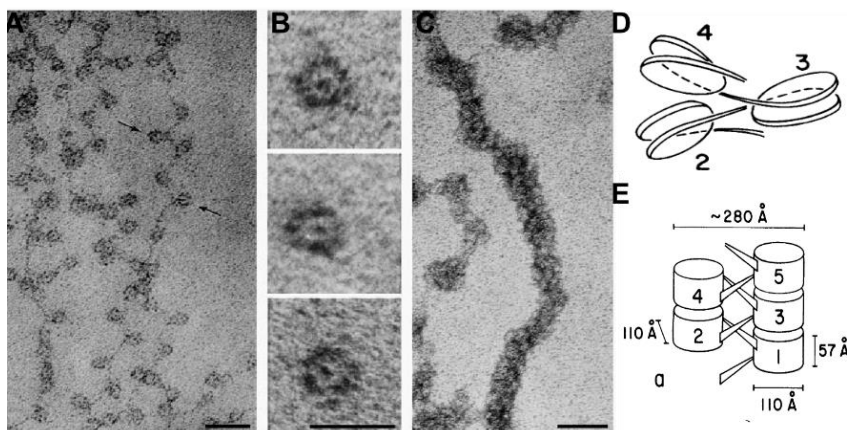


Figure 1: The first electron microscopy structure and folding model of chromatin (A) An electron micrograph of the “beads-on-a-string” structure of chromatin (size marker: 30 nm). (B) A close-up view of the nucleosome core particle (NCP) or v-bodies (size marker: 10 nm). (C) A close-up view of the 30 nm solenoid structure of chromatin (size marker: 50 nm). From (Olins and Olins,

Introduction

2003). (D) An Early chromatin fiber folding model. (E) Helical ribbon model with nucleosomes drawn as flat cylinder and the path of DNA from nucleosomes 2, 3 and 4 depicted. Adapted from (Worcel *et al.*, 1981).

Nuclease digest and histone crosslinking data generated by J. Thomas and colleagues, together with X-ray diffraction patterns of M. Wilkins and colleagues built the groundwork for R. Kornberg's model of chromatin structure published only months later ((Kornberg, 1974, Kornberg and Thomas, 1974). A 146 bp double stranded DNA (dsDNA) wrapped around a central histone octameric complex consisting of four histone dimers represents the central "repeating subunit of chromatin" (Kornberg, 1974). The protein-DNA complex comprised a dyad axis, 11nm in diameter and 5.5nm in height that enabled a 6-fold compaction in length of the DNA molecule. The discovery of the heart of chromatin structure, coined "nucleosome" in 1975, led to a fundamental change in perspective on all eukaryotic DNA- and chromatin-dependent processes, such as DNA replication, transcription and repair.

1.2 The nucleosome core particle

Elucidating the structural characteristics of nucleosome core particle (NCP) represents a cornerstone in our understanding of not only chromatin biology, but also the fundamental basis of eukaryotic life itself. Low-resolution structures already showed that approximately 200bp of DNA are wrapped around a central histone octamer (Kornberg, 1974, Woodcock *et al.*, 1976). G. Bunick and colleagues published a low-resolution X-ray structure of the NCP, showing that the B-DNA superhelix wrapped around the central histone octamer exhibits several local distortions due to histone-DNA contacts located predominantly in the DNA minor groove. Histone protein fold shared by all four histone types, as well as the H2B tail extending between the two DNA gyres and the H4 in close proximity to the dyad added knowledge to the, until then, less understood structure of the NCP itself (Uberbacher and Bunick, 1985, Finch *et al.*, 1977, Klug *et al.*, 1980). The tripartite assembly of the histone octamer, meaning a central H3/H4 tetramer bound by two H2A/H2B dimers, resulting in a "flat disk"-like shape of the octamer, was suggested by E. Moudrianakis and colleagues in 1991 (Arents *et al.*, 1991). The structure of the so called, "histone fold" was described as a "handshake" motif, consisting of a helix-loop-helix structure that is highly conserved, shared by all four histone proteins and integral for heterodimerization (Figure 2A) (Arents *et al.*, 1991, Cutter and Hayes, 2015). The gap in structural knowledge of the particle central to all eukaryotic DNA-dependent processes was filled by K. Luger in 1997, publishing the first high-resolution X-ray structure of the nucleosome core particle at 2.8 Å. A 146 bp of 1.6 left-handed super-helical turns of B-DNA are wrapped around a central spool-like structure, consisting of two copies of each histone type forming the histone octamer (Figure 2A, PDB:1AOI). The DNA superhelix within the core particle is not uniformly shaped and exhibits a double helix twist value

Introduction

of 10.2bp per turn and forms a generally flat, disk-like structure. A central DNA base pair is located at the pseudo-two-fold axis of the particle, where the major groove of the DNA faces the octamer, referred to as super helix location zero (SHL 0) or dyad axis (Figure 2B), causing an asymmetric disposition of 72 bp and 73 bp in each gyre or half along the two-fold axis. As a consequence, nucleosomal DNA is overwound by 1 bp, meaning one additional base pair can easily be accommodated within the NCP (Luger *et al.*, 1997). Years later, the resulting defect in DNA twist was found to be pivotal for DNA translocation and nucleosome movement by ATP-driven chromatin remodelers based on stepwise disruption of histone-DNA contacts (Luger *et al.*, 1997, Davey *et al.*, 2002, Richmond and Davey, 2003, Yan and Chen, 2020). For every successive turn of the DNA helix, the numbering of SHLs increases with the distance from the dyad axis (Figure 2B, from SHL+/-1 to 7).

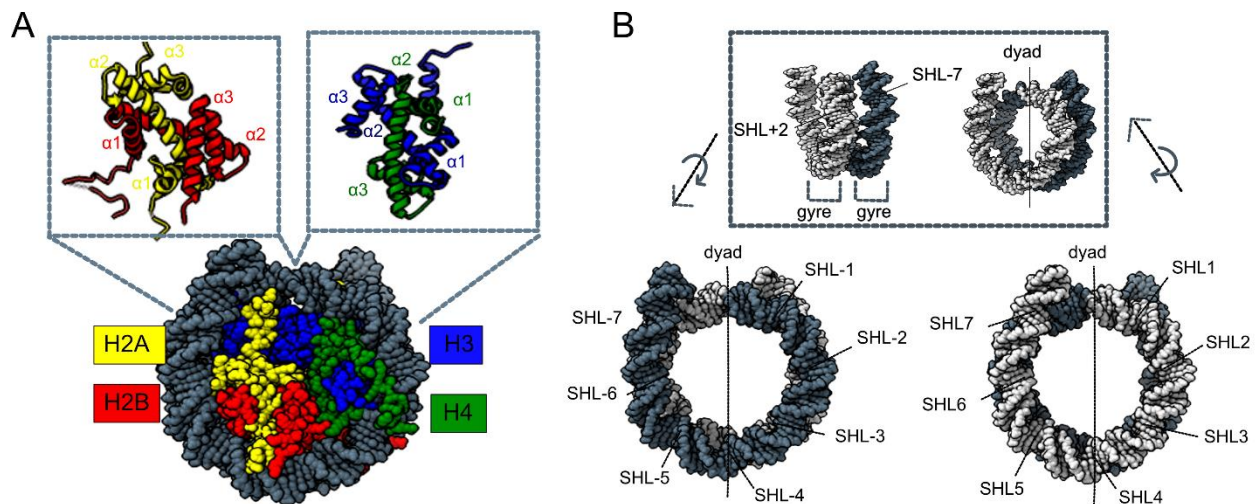


*Figure 2: The nucleosome core particle structure. (A) Bottom: “disk-view” of the nucleosome core particle (top view perpendicular to the two-fold axis) shown in cartoon representation, adapted from (Schalch *et al.*, 2005) (PDB: 1ZBB). The color scheme used for histone proteins is green (H4), blue (H3), red (H2B) and yellow (H2A). The dsDNA is shown in dark grey. Top left: H2A/H2B, top right: H3/H4 histone fold dimers. Conserved histone fold domains are labeled $\alpha 1$, $\alpha 2$ and $\alpha 3$, respectively (starting from the N-terminus). (B) Arrangement of the nucleosomal DNA (PDB: 1ZBB). Top Box: right panel shows the nucleosomal DNA along the dyad axis, indicated as black solid lines. Left panel shows the side view of the DNA highlighting the two DNA gyres. Bottom: dyad refers to the center of nucleosomal DNA and is denoted as super helix location zero (SHL 0). SHL 1-7 denote repetitive locations where the DNA major groove is facing inwards. Beyond SHL-/+7, DNA is referred to as extranucleosomal DNA. Numbering of SHLs increases with the distance from the dyad. + and - indicate on which DNA gyre the respective SHLs are located. Related to chromatin remodeling on a single nucleosome substrate, the directionality of the SHL prefix is defined by the location of extranucleosomal DNA and the direction of DNA translocation by the remodeler. The site with extranucleosomal DNA that is translocated towards the dyad by the chromatin remodeler ATPase domain is denoted the “entry site” and SHL numbering starts with negative prefix. After the nucleosomal dyad SHL numbering carries on with positive SHL prefix.*

The bending of the DNA superhelix reaches its maximum at SHL +/- 1.5 and SHL +/- 4 to 5. The DNA sequence itself dictates its flexibility, and therefore histone-induced bendability. GC base pairs are preferentially found where the major groove faces the central octamer, whereas the AT

Introduction

base pairs show a preference for the minor groove, due to base pair-specific twist and tiltability (Luger *et al.*, 1997, Cutter and Hayes, 2015). Histone proteins are highly conserved among the eukaryotic species, mainly within their histone fold domains (Figure 2A). Three α -helices (α 1, α 2 and α 3 starting from the N-terminus of the sequence) connected by two loops (L1 and L2) make up the central structural element of the histone fold. The histone fold is crucial for H3/H4 and H2A/H2B heterodimer formation in anti-parallel arrangement and exclusive histone-histone contacts (Luger *et al.*, 1997, Richmond and Davey, 2003). The N-terminus of the α 1 helices of H3, H4 and H2B specifically point towards deoxyribose and phosphate groups of the DNA superhelix at SHL 1.5 in H3/H4 and SHL4.5 in H2B (Luger *et al.*, 1997, Zhou *et al.*, 2019). The histone N- and C-terminal regions are less conserved than the core histone fold and supposedly adopt a random coil conformation. Nonetheless, N- and C-termini of histones contribute remarkably to the overall stability of the NCP (Smith and Rill, 1989). The random coils of the N-terminal part of the histone H2B and H3 pass through a channel formed by two adjacent DNA minor grooves, creating a periodicity of histone tails in the DNA minor grooves of about 20bp. The N-terminal part of H2A exits the core in the minor groove of the DNA on the bottom and top faces of the particle. The H4 tail binds to an acidic patch within the H2A/H2B dimer interface of an adjacent nucleosome, suggesting a role in higher order chromatin structure formation (Zheng and Hayes, 2003). In summary, the core histone fold and histone tails both contribute to create a strong platform for DNA interaction, binding and bending. The investigation of DNA sequence-dependent positioning of nucleosomes and the intrinsic sequence determinants have been investigated for decades, but the underlying biochemical principles are not completely understood. An in depth understanding of an artificial nucleosome positioning sequence was provided by the Widom 601 sequence (Lowary and Widom, 1998), generated via systematic evolution of ligands by exponential enrichment (SELEX) (Irvine *et al.*, 1991). The strong nucleosome positioning sequence is characterized by a 10bp periodicity of “TA” steps across one gyre at the H3/H4 interface. Periodic “TA” steps increase nucleosome stability in dimer exchange and unwrapping reactions (McGinty and Tan, 2015, Ngo *et al.*, 2015). The Widom 601 sequence is defined by an asymmetric architecture comprised of a TA-rich gyre and a TA-poor gyre separated by the dyad axis.

1.3 Architecture of chromatin

The genomic organization in eukaryotes involves multiple nested levels. The primary structure of chromatin, the first level of organization, arises from the arrangement of nucleosomes into one-

Introduction

dimensional arrays envisioned in the 1974 “beads on a string” structure obtained using electron microscopy by D. and A. Olins and R. Kornberg. (Figure 1A) (Olins and Olins, 1974, Kornberg, 1974). Nucleosome positioning and histone modifications are understood in great detail at this level of chromatin organization. The second layer of organization is the formation of the chromatosome (Simpson, 1978), consisting of 147bp wrapped around the central histone octamer accompanied by a linker histone binding to the nucleosome dyad symmetry axis, covering in total 165bp of superhelical DNA. Evolutionarily less conserved than their respective core histones, the linker histones consist of an 80 residue central globular domain flanked by a short N- terminal and longer C-terminal extensions (Widom, 1998). The globular domain can interact with entry and exit DNA of one or two adjacent NCPs simultaneously and the C-terminal domain dictates linker DNA conformation and consequently chromatin condensation (Zlatanova and van Holde, 1996, Robinson and Rhodes, 2006, Sivolob and Prunell, 2003). Formation of the chromatosome leads to a more inactive state, due to preferred formation of higher-order chromatin structures and hinderance of transcription factor binding to nucleosomal or extranucleosomal DNA (Routh *et al.*, 2008, Robinson and Rhodes, 2006). Additionally, linker histones interact with the core histone tails. Removal or hyperacetylation of core histone tails (especially H3 and H4 tails) or the C-terminal part of linker histones leads to loss of salt-induced fiber formation, underscoring the essential role of histone tails in this process (Clayton *et al.*, 1993, Zlatanova and van Holde, 1996). Linker histones are not essential and gene knockout leads to viable cells with only minor gene expression modifications despite their decisive contribution to chromatin fiber formation (Widom, 1998).

Early views on chromatin structure suggested that the linear nucleosomal arrangement undergoes a further round of compaction, forming fiber-like higher order chromatin structures. Over the next few decades, several models based on structural, biochemical, biophysical and also computational modelling data have been proposed.

Introduction

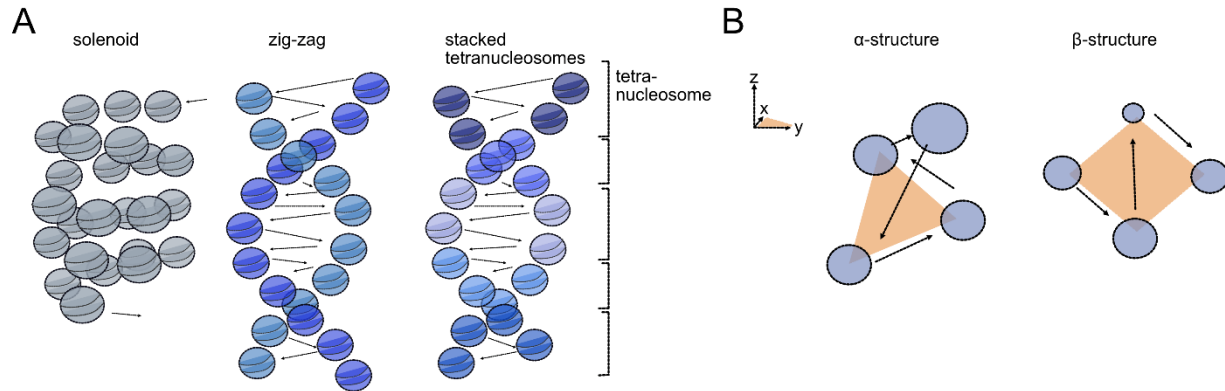


Figure 3: Chromatin fiber folding motifs. Cartoon representation of chromatin fiber folding motifs, adapted from (Krietenstein and Rando, 2020). (A) Schematic depiction of a one-start solenoidal helix proposed by J. Finch and A. Klug. Two-start zig-zag arrangement of the chromatin fiber as proposed by A. Worcel and colleagues. Stacked tetra-nucleosome model based on (Maeshima *et al.*, 2010). (B) Tetranucleosomal folding motifs. Left panel shown as a cartoon representation of the α -motif mainly found in gene bodies. Right panel shows the β -motif located at gene ends. Adapted and modified from (Ohno *et al.*, 2019).

Using native chromatin fibers, J. Finch and A. Klug proposed the “solenoidal model” in 1976 in which a ‘one-start’ solenoidal helix formed by a single protein-DNA polymer chain and ~5-6 nucleosomes per turn describes the conformation of the 30 nm fiber (Figure 3A, left panel) (Finch and Klug, 1976). Five years on, A. Worcel and colleagues, and C. Woodcock and colleagues proposed a “zig-zag” arrangement model, in which a ‘two-start’ helical ribbon describes chromatin fiber formation (Figure 3A, middle panel) (Worcel *et al.*, 1981). A third model proposed by J. Daban and colleagues in 1998 describes planes of nucleosomes as the building block of the fiber. These planes of adjacent nucleosomes turn crisscross to each other to form fiber-like structures (Daban and Bermudez, 1998, Grigoryev and Woodcock, 2012). Subsequent experiments done by T. Richmond and colleagues, and also D. Rhodes and colleagues focused on nucleosomal arrays based on the Widom 601 sequence (refer to 1.2) (Lowary and Widom, 1998) and recombinant histones. Studies of crosslinks between H4 and H2A/H2B acidic interface at a high salt concentration (Dorigo *et al.*, 2004) and the crystal structure of a tetranucleosome with 167bp repeat length (Schalch *et al.*, 2005) supported the zig-zag model of A. Worcel and colleagues (Figure 3A). In contrast, cryo-EM studies of Widom 601 repeat fibers by D. Rhodes and colleagues (Robinson and Rhodes, 2006) and single molecule force microscopy studies by C. Bustamante and colleagues (Cui and Bustamante, 2000) supported the solenoid model. *In vitro* experiments of chemically fixed nucleosomes showed highly ordered 30 nm fibers (McGinty and Tan, 2015) for which *in vivo* evidence is lacking (Cai *et al.*, 2018, Ou *et al.*, 2017). Recent experiments highlight the role of linker DNA sequence and length in determining the exit and entry DNA angle and linker DNA bendability in chromatin fiber folding (Grigoryev, 2018, Hsieh *et al.*, 2015). As a result of the intrinsic heterogeneity of native chromatin fibers, such as linker histone levels, histone

modifications, histone variants and DNA linker lengths, detailed structural information is highly challenging to generate. Accumulating evidence over time has generally favored the ‘zig-zag’ model, but the exact organization above first level nucleosomal arrays *in situ* remains unknown (Hansen *et al.*, 2018).

Recent technical advances including super-resolution light microscopy and genome-wide mapping approaches allowed a remarkable gain in knowledge of chromosomal compartments, topologically associating domains (TADS) and loop domains (Krietenstein and Rando, 2020, Ciabrelli and Cavalli, 2015, Franke *et al.*, 2016, Dixon *et al.*, 2016, Hansen *et al.*, 2017). Super-resolution fluorescence imaging as well as electron microscopy analysis *in vivo* provide clear and consistent evidence for the presence of “clutches” of about ~2-10 nucleosomes without evidence for extended, organized fibers (Ricci *et al.*, 2015, Ou *et al.*, 2017, Chen *et al.*, 2016, Eltsov *et al.*, 2008). Growing reports favor a dynamic, liquid-like structure of chromatin that allows long-distance interactions and constant restructuring *in vivo*, summarized in the “liquid drop” or “polymer melt” model (Dubochet *et al.*, 1986, Brangwynne *et al.*, 2009, Eltsov *et al.*, 2008, Fussner *et al.*, 2011, Nishino *et al.*, 2012). Phase separation was reported to play a pivotal role in self-organization of subcellular compartments, such as P bodies and nucleoli (Chen *et al.*, 2016). Two landmark studies within the field of chromatin research by G. Narlikar and colleagues and G. Karpen and colleagues *in vivo* and *in vitro* showed that heterochromatin self-association is based on droplet formation of the heterochromatin protein 1 (HP1) (Larson *et al.*, 2017, Strom *et al.*, 2017). This suggested a possible link between phase separation and chromatin self-organization within the genome. Phase-separation *in vitro* is regulated by nucleosome array length, divalent salt concentrations, histone tail modifications and the nucleosome repeat length (Krietenstein and Rando, 2020). Tetranucleosome motifs located in gene bodies (α structure) or at regulatory regions at gene ends (β structure) have been recently discovered (Figure 3B) (Maeshima *et al.*, 2010, Ohno *et al.*, 2019, Moraru and Schalch, 2019)). Future work is required to define the specific location of tetranucleosome motifs, and therefore their distinct role in regulating DNA-dependent processes. It will be of great interest to see how nucleosome positioning influences the formation of tetranucleosome motifs.

1.3.1 Modulation of chromatin architecture

Chromatin is a highly dynamic entity reacting to and processing a myriad of stimuli that demand a highly specific regulation of accessibility. While improving a cytological staining method in 1928, E. Heitz coined terms for certain regions of mitotic chromosomes that are less densely stained and for regions that are densely stained throughout the cell cycle (euchromatin and

Introduction

heterochromatin, respectively). This observation led to the proposition that protein coding genes are mainly found in euchromatin whereas heterochromatin is mainly genetically inert. Recent studies define heterochromatin as a highly conserved and structurally distinct nuclear domain of eukaryotic genomes (Janssen *et al.*, 2018, Allshire and Madhani, 2018, Berger, 2019). Constitutive heterochromatin is typically established at pericentromeric and telomeric domains of chromosomes and is essential for many cellular processes such as chromosome segregation and transcription (Janssen *et al.*, 2018, Allshire and Madhani, 2018). In contrast to the gene-rich euchromatin domain, the heterochromatin domain is densely organized throughout interphase, is enriched in repetitive sequences and is associated with comparatively low transcriptional levels (Allshire and Madhani, 2018). Polycomb-based facultative heterochromatin is, in contrast with constitutive heterochromatin, mainly associated with the transcriptional regulation of developmental genes and is characterized by distinct post-translational histone marks. The nuclear domain of constitutive heterochromatin is enriched in di- and trimethylation marks on histone H3 lysine residue 9 (H3K9(me)₂ and H2K9(me)₃, respectively) and its binding protein heterochromatin protein-1 (HP-1) which guide the overall architecture of the nuclear domain. (Janssen *et al.*, 2018).

1.3.1.1 Histone modifications

To gain access to DNA histones are post-translationally modified, in every species from yeast to human, which alters their chemical properties to relax or compact chromatin or to label it for chromatin remodeling. Covalent histone modifications have been discovered in the 1960s with histone hyperacetylation at highly transcribed genes being the first one (Allfrey *et al.*, 1964). A variety of known histone modifications exists which occur in distinct patterns and are read by effector proteins that in turn have distinct downstream functions (Turner, 2000, Strahl and Allis, 2000, Latham and Dent, 2007). The interplay of “writer”, “reader” and “eraser” factors of post-translational modifications (PTMs) leads to changes in the chromatin structure and dynamics, therefor impacting all underlying cellular processes (Venne *et al.*, 2014). The permutational complexity and the cross-regulatory potential of histone tail modification patterns partially govern chromatin dynamics by influencing nucleosome mobility (occupancy and positioning), turnover rates and composition (Strahl and Allis, 2000, Latham and Dent, 2007). Covalent modifications have been mostly associated with the histone N-terminal residues. A recent mass spectrometry analysis revealed that covalent modifications are additionally located at histone core and C-terminal residues affecting the core nucleosome structure itself (Hyland *et al.*, 2005). Among others, histone acetylation, methylation, phosphorylation and monoubiquitination (Ac, Me, P and Ub1, respectively) have been described each assigned to a specific function in gene regulation

(Latham and Dent, 2007). The regulatory cross-talk between covalent histone modifications is of many folds and can either be in “cis” (a covalent modification of a histone residue influences the modification of additional residues on the same histone) or in “trans” (on an adjacent histone). The regulatory unit of histone methylation is unique among covalent histone modifications in that it includes mono-, di- or trimethylation of lysine and arginine residues (Latham and Dent, 2007). Histone acetylation is generally associated with an increase in gene expression whereas histone methylation is associated with both gene activation as observed with H3K4 (at promoter sites) and H3K36 (within gene bodies) (Zentner and Henikoff, 2013) and gene repression as observed with H3K9 and H3K27 methylation (Latham and Dent, 2007, Zentner and Henikoff, 2013). Phosphorylations of histone tail threonine and serine residues introduce negative charges, opening up the chromatin structure by charge repulsion with the DNA backbone phosphates (North *et al.*, 2011). The cross-regulatory mechanisms of other histone modifications, such as ADP-ribosylation, glycosylation, and sumoylation and their impact on chromatin structure (Zentner and Henikoff, 2013) are outside the scope of this thesis.

1.3.1.2 Histone variants

Histone variants are less conserved than their canonical counterparts and can be grouped into universal variants, found in almost all eukaryotes, and lineage-specific variants (Talbert and Henikoff, 2010). Focusing on universal histone variants, CenP-A, H3.3, H2A.Z and H2A.X are relatively better characterized. CenP-A is specialized in centromeric regions with its tail preferring AT-rich centromeric DNA where it provides a platform for the kinetochore assembly. H3.3 is placed on transcribed genes, promoter sites and gene regulatory elements and drives transcription initiation and elongation (Talbert and Henikoff, 2010). H2A.X shares the histone fold with H2A and differs in the C-terminus where the serine residue 139 (H2A.XS139) gets highly phosphorylated provoked by DNA double strand breaks (Scully and Xie, 2013). H2A.X phosphorylation and the recruitment of chromatin remodeler to the sites of dsDNA breaks are essential in the DNA double strand break repair (Talbert and Henikoff, 2010, van Attikum and Gasser, 2009). The histone variant H2A.Z shares 60% sequence identity with canonical H2A (Zlatanova and Thakar, 2008, Talbert and Henikoff, 2010), its incorporation into the nucleosome leads to destabilization (Adam *et al.*, 2001) and the H2A.Z/H2B dimer is characterized by an extended acidic patch (Zlatanova and Thakar, 2008). *In vitro* studies showed that incorporation of H2A.Z into nucleosomes inhibits highly compact chromatin fiber formation (Fan *et al.*, 2002). Genome-wide mapping data show higher enrichment of H2A.Z at promoter than non-promoter and intergenic regions (Zanton and Pugh, 2006). Indeed, two-thirds of nucleosomes flanking the NDR of promoters are H2A.Z-containing nucleosomes (Raisner *et al.*, 2005, Chereji *et al.*, 2018).

Introduction

1.3.1.3 Non-histone proteins

The chromatin fiber is a highly heterogeneous protein filament covered with multiple non-histone proteins, such as high mobility group-1 (HMGI) proteins, transcription factors (TF) or general regulatory factors (GRF) that influence chromatin fiber architecture (Horn and Peterson, 2002). HMGI-type proteins are characterized by two DNA-binding domains that belong to the HMG-box family and their ability to induce bends and kinks into a linear DNA template (Falciola *et al.*, 1997). The HMGI-type proteins have been proposed to act similarly to linker histone H1, for which binding subsequently induces a bend into nucleosomal linker DNA (Varga-Weisz *et al.*, 1993, Schroter and Bode, 1982). Some HMGI-type proteins mark active chromosomal regions, such as HMG14 and HMG17 (Hock *et al.*, 1998). The presence and binding of these non-histone proteins influence chromatin dynamics and potentially prevents higher order fiber folding.

1.3.1.4 Chromatin modifying machineries

A DNaseI digestion experiment led to the identification of two types of multi-subunit protein complexes that maintain a fluid and dynamic chromatin state through two distinct mechanisms, overcoming the barrier chromatin structure established on all DNA-dependent processes (Wu and Grunstein, 2000). Histone acetyltransferases (HATs) or histone deacetylase complexes (HDACs) are chromatin-dependent counteracting factors that accomplish covalent modifications of histones. HATs catalyze the transfer of acetyl groups taken from acetyl-CoA to the ϵ -amino groups of lysine residues located on the N-termini of histones (Barnes *et al.*, 2019, Carrozza *et al.*, 2003). Early observations by Allfrey and colleagues already suggested a role of HATs in transcription regulation (Allfrey *et al.*, 1964). A direct link between HATs and transcription regulation was established when the yeast transcription activator Gcn5 was found to acetylate histones (Brownell and Allis, 1996). HATs are divided into 5 families and exist as multi-subunit complexes with additional subunits defining substrate preference and gene-specific targeting (Carrozza *et al.*, 2003). The recruitment of HATs to promoters is directed by the cross-regulatory interplay of PTMs. Phosphorylation of histone H3 serine 10 was shown to increase Gcn5 targeting to the INO1 promoter in yeast (Lo *et al.*, 2001). HDACs, similar to HATs, are multi-subunit complexes that are targeted to specific gene loci through complex-associated, sequence-specific DNA binding proteins as well as histone acetylation. HDACs catalyze the inverse reaction of HATs by deacetylation of acetyl-lysines through zinc-catalyzed hydrolysis of the amide bond or through transferring it to a sugar moiety of nicotinamide adenine dinucleotide (NAD). In earlier studies deacetylation was associated with transcription repression by two mechanisms. The removal of the acetyl group increases the charge density on the N-terminus of histones, which blocks the access

of the transcription machinery to DNA by strengthened histone-DNA interactions. Additionally, deacetylation primes the histone tails for subsequent histone methylation of the respective lysine residues that are recognized by chromodomain containing proteins such as CHD family remodeler or HP-1 (Gallinari *et al.*, 2007). Recent studies show that active gene transcription requires repeating synchronized cycles of HATs mediated acetylation and HDAC mediated histone deacetylation (Barnes *et al.*, 2019).

Nucleosome formation is pivotal for the packaging of genomic DNA into chromatin although it thoroughly restricts the accessibility to genomic DNA, and therefore regulates genomic DNA functions (Luger *et al.*, 2012). To ensure proper genomic DNA function the nucleosome structure must be adaptable and dynamic (Kobayashi and Kurumizaka, 2019). ATP-dependent chromatin remodelers alter the structure and/or positioning of nucleosomes. Chromatin remodeling complexes belong to the RNA/DNA helicase superfamily 2 proteins that use energy provided by ATP hydrolysis to remodel nucleosome patterns across the genome (refer to section 1.4) (Flaus *et al.*, 2006, Clapier *et al.*, 2017). The re-configuration of histone-DNA contacts through chromatin remodeler-mediated DNA translocation re-positions nucleosomes and provides access to genomic DNA for the binding of diverse factors including TFs, GRFs, transcription activators, transcription repressors or the transcription machinery itself (Narlikar *et al.*, 2002, Vignali *et al.*, 2000, Pazin and Kadonaga, 1997, Kobayashi and Kurumizaka, 2019). Chromatin remodelers have been shown re-organize the chromatin structure after replication and in the wake of transcription (Langst and Becker, 2001, Schnitzler *et al.*, 2001, Kingston and Narlikar, 1999). An extraordinary example illustrating the intense interplay to maintain a dynamic chromatin landscape is the yeast nucleosome remodeling deacetylase (NURD) complex, which combines a histone deacetylase activity with a chromatin remodeling factor in a single multi-subunit complex (Tong *et al.*, 1998, Narlikar *et al.*, 2002, Bornelov *et al.*, 2018, Feng and Zhang, 2003).

1.3.2 Nucleosome spacing, phasing and positioning in a promoter-focused context

Starting from Micrococcus Nuclease (MNase) digestion data and electron microscopy data generated by various labs including R. Kornberg, M. Noll, D. and A. Olins, R. Thomson, J. Miller and K. Luger, the simple “beads on a string” picture evolved into one of a highly dynamic “sea of nucleosomes” shaped by a variety of factors. Advancing from the new high throughput sequencing technologies, genome-wide approaches showed that nucleosomes are organized in regular arrays interrupted by regions with lower uniformity. The DNA linker length that defines the number of DNA base pairs that reside between two adjacent NCPs (Figure 4A, top) varies between

Introduction

species and cell types (Struhl and Segal, 2013, Moraru and Schalch, 2019). The nucleosome repeat length (NRL), which is the average distance between the dyads of two neighboring nucleosomes, and the array regularity are related to the transcriptional activity, incorporation of linker histones, heterochromatin formation and chromatin fiber folding (Baldi *et al.*, 2018, Lai *et al.*, 2018, Chereji *et al.*, 2016, Routh *et al.*, 2008, Beshnova *et al.*, 2014). Focusing on the model organism *S. cerevisiae* (*S.c.*), nucleosomes are generally well-positioned and regularly spaced with an average NRL of 165bp. More highly expressed genes in yeast tend to show shorter NRLs (Baldi *et al.*, 2020, Chereji *et al.*, 2018). Promoter regions of expressed genes are distinguished by a unique nucleosome array pattern. Visualization of genome-wide sequence reads aligned at the transcription start site (TSS) or the canonical *in vivo* +1 nucleosome position (refer to Figure 4B) revealed a stereotypical pattern, which consists of a nucleosome-free or nucleosome-depleted region (NFR or NDR) upstream of the TSS, well-positioned +1 and -1 nucleosomes flanking the NDR, followed by a regularly spaced nucleosomal array relative to the +1 hallmark downstream of the TSS (Figure 4B) (Krietenstein *et al.*, 2016, Mavrich *et al.*, 2008b, Yuan *et al.*, 2005, Struhl and Segal, 2013, Jiang and Pugh, 2009b)).

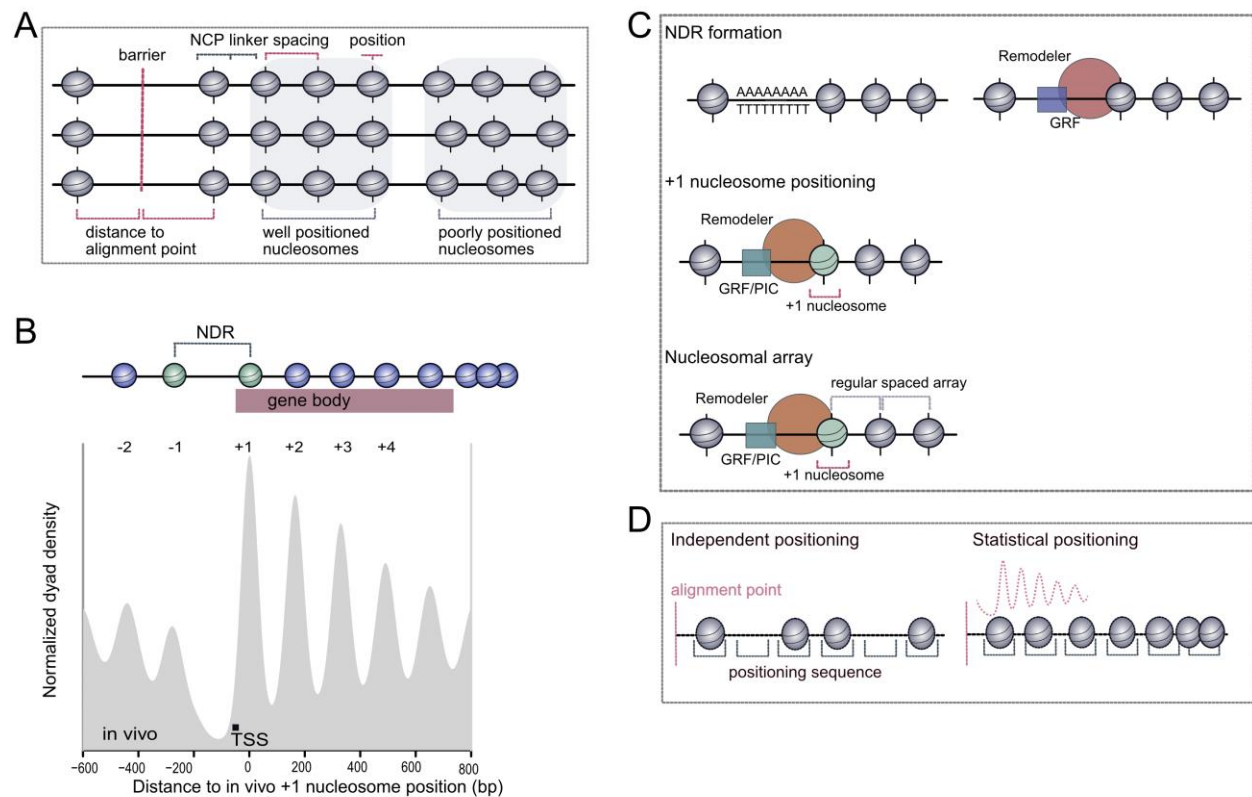


Figure 4: Stereotypical promoter organization. (A) Definition of Terms. Depicted are definitions of nucleosome alignment to reference points (phasing), NCP, linker DNA, nucleosome spacing and positioning as well as the difference between well- and

Introduction

poorly-positioned nucleosomes within a population. Adapted from (Baldi *et al.*, 2020). (B) Composite plot of MNase sequencing data. Sequencing reads are aligned at the +1 nucleosome position mapped *in vivo* in wild type yeast (BY4741) cells. Adapted from (Knoll *et al.*, 2018). The +/-1 nucleosomes flanking the NDR and prone to H2A.Z incorporation are highlighted in green. (C) Features defining the archetypical promoter architecture. NDR formation: Poly(dT):poly(dA) tracks and GRF binding sites (in blue and green) are located in NDRs. Poly(dT):poly(dA) tracks *per se* tend to exclude the formation of nucleosomes owing to the rigidity of the DNA sequence. Nucleosome displacement to form NDRs is directed by poly(dT):poly(dA)-mediated and/or GRF-mediated RSC (depicted in red) action. The +1 nucleosome positioning (+1 nucleosome positioning), as well as the nucleosome array formation (Nucleosomal array) is facilitated by distinct ATP-dependent chromatin remodelers. Adapted from (Krietenstein *et al.*, 2016). (D) Models for nucleosome positioning. Independent positioning: Sequence-based packing of nucleosomes is guided by the underlying DNA sequence which assigns a specific “slot” to every individual nucleosome. This model implies that positions of adjacent nucleosomes are independently controlled. Statistical positioning: Statistical nucleosome positioning relative to a barrier or an alignment point (red) arises from the closed packing of nucleosomes into arrays. The position of one nucleosome in the array forces the position of all other nucleosomes which can be described by a probabilistic density trace shown in red dashed line. Adapted from (Jiang and Pugh, 2009a, Jiang and Pugh, 2009b).

Phased arrays radiating from the NDR, which is on average 150bp in length, are also present in human cells (Valouev *et al.*, 2011). In contrast with yeast, *Drosophila melanogaster* (*D.m.*) TSSs are not buried within the +1 nucleosome, but located in the NDR, and H2A.Z is not enriched in the +1 nucleosome (Mavrich *et al.*, 2008b, Fan *et al.*, 2002, Raisner *et al.*, 2005, Zlatanova and Thakar, 2008). The NDR is evolutionarily conserved and in budding yeast and worms often enriched in poly-(dA):(dT) sequences (Figure 4C, top). Combinatorial effects of DNA sequence, DNA binding proteins, the RNA polymerase II (Pol II) transcription machinery and ATP-dependent chromatin remodeler play a pivotal role in shaping the stereotypic nucleosome pattern at regulatory regions (Figure 4B and C) (Struhl and Segal, 2013, Krietenstein *et al.*, 2016, Clapier *et al.*, 2017, Jiang and Pugh, 2009a, Rossi *et al.*, 2018, Yen *et al.*, 2012)).

Physical parameters determining the arrangement of nucleosomes on chromosomal DNA are shown in Figure 4. ATP-dependent chromatin remodelers are the central machineries facilitating the adjustment of nucleosome spacing between the dyads of two adjacent nucleosomes, as well as nucleosome positioning and phasing, which is the alignment of a nucleosome relative to a genomic reference point or a barrier (Baldi *et al.*, 2020). Accordingly, the term ‘regular spaced array’ refers to a constant nucleosome repeat length. Well-positioned nucleosomes, such as the +1 and -1 nucleosomes flanking the NDR, are nucleosomes that cover identical DNA sequences among different cells. Spacing and positioning of nucleosomes are two independent qualities, because regularly spaced nucleosomes do not need to be accurately-positioned (Baldi *et al.*, 2020). To gain knowledge about the distinct location of a nucleosome in the genomic context, its significant task and also the mechanistic background guiding its location is a time-honored subject in the chromatin research field (Lu *et al.*, 1994, Kornberg, 1981, Kornberg and Stryer, 1988, Yuan *et al.*, 2005). Relying on comparative genomics, a model for nucleosome positioning based on statistics was introduced (Ioshikhes *et al.*, 2006, Jiang and Pugh, 2009a). Potentially fixed barriers, meaning the bendability of the underlying DNA directed through its sequence (Simpson

and Stafford, 1983), poly-(dA):(dT) tracks precluding nucleosome formation (Iyer and Struhl, 1995, Nelson *et al.*, 1987), and intrinsic barriers formed by DNA bound factors (Fedor *et al.*, 1988), create adjacent ordered nucleosomal arrays that can be described by a probabilistic density trace (Figure 4D) (Jiang and Pugh, 2009b). Here, the number of positions a nucleosome can potentially occupy adjacent to a barrier is statistically restricted. This also holds true for the subsequent nucleosome for which the number of positions is statistically limited by the preceding nucleosome (Figure 4D). Statistical limitations introduce a decay in positioning precision depending on nucleosome density and the distance to the barrier (Figure 4D) (Kornberg and Stryer, 1988, Mavrich *et al.*, 2008a, Jiang and Pugh, 2009b, Ioshikhes *et al.*, 2006)).

GRFs, such as Rap1, Reb1 or Abf1, control the expression of several genes in yeast with their binding sites generally located in the NDRs at promoter sites. GRFs are often indispensable for cell viability and transcription / replication regulation (Challal *et al.*, 2018). Genome-wide *in vitro* assays showed that Abf1 and Reb1 binding sites were less occupied by nucleosomes *in vivo* than *in vitro*, suggesting a mechanism by which the presence of respective factors influences the local chromatin environment keeping their respective binding sites nucleosome-depleted (Kaplan *et al.*, 2009). A study focusing on finding transcription factor binding sites and their position relative to regulatory regions, such as TSSs using a microarray approach by G. Badis and colleagues showed that, compared with genic regions, binding motifs for Abf1 and Reb1 are 16-fold enriched in NDRs located closely to TSSs. Mutation or deletion of Abf1 or Reb1 caused increases in the nucleosome occupancy over potential binding sites located within the NDR (Badis *et al.*, 2008). Additionally, D. Challal and colleagues show that dramatic changes in transcription initiation induced by GRF deletion correlate strongly with a modified nucleosomal array architecture at GRF binding sites and downstream TSSs. GRFs may apply either steric hindrance or a recruitment function for chromatin remodeler or TFIID to orchestrate proper NDR formation and maintenance to prevent ectopic transcription initiation (Figure 4C) (Challal *et al.*, 2018). Generally, GRFs represent a reference point or barrier for nucleosome alignment both *in vivo* (Li *et al.*, 2015) and *in vitro* (Krietenstein *et al.*, 2016).

A very elegant study by BF. Pugh and colleagues analyzing genome-wide nucleosome positioning *in vivo* elucidated that AA dinucleotides located towards the 5'- and TT dinucleotides towards the 3' -end of nucleosomal DNA, a 10 bp repeating AT and TA dinucleotide pattern, as well as transcription factor binding sequences are central in orchestrating the exact positioning of the -1/+1 nucleosome hallmark for downstream nucleosomal array alignment (Mavrich *et al.*, 2008a, Jiang and Pugh, 2009b). Limitations of the statistical positioning model based on DNA sequence

preferences of the histone octamer became obvious when attempts to re-generate physiological promoter NDR array patterns by salt gradient dialysis (SGD) and purified components failed *in vitro*. DNA sequence alone akin with statistical mechanisms is insufficient to recapitulate the physiological nucleosome positions *in vitro* (Struhl and Segal, 2013, Zhang *et al.*, 2009). No evidence was found *in vivo* as well as *in vitro* for the correlation of inter-nucleosomal distances and the overall nucleosome density, which is a prerequisite for statistical positioning (van Bakel *et al.*, 2013, Lieleg *et al.*, 2015a). The addition of yeast cell-free extract to the *in vitro* reconstitution system above recovered for the first time physiological nucleosome positioning patterns *in vitro* in an ATP-dependent manner (Zhang *et al.*, 2011). An even more minimalistic setting for genome wide *in vitro* reconstitution with individually purified components (Krietenstein *et al.*, 2016, Lieleg *et al.*, 2015b) showed that ATP-dependent chromatin remodelers are at the center of NDR array pattern formation and nucleosome positioning. ATP-dependent remodelers have been shown to not only co-determine nucleosome positioning, but also carry out an active nucleosome positioning mechanism (Lorch *et al.*, 2014, Lieleg *et al.*, 2015a).

1.4 ATP-dependent chromatin remodelers

1.4.1 Phylogenetic classification of chromatin remodelers

ATP-dependent chromatin remodelers (“chromatin remodelers” or simply “remodelers”) are conserved from yeast to human and phylogenetically and functionally belong to the superfamily2 (SF2) of helicase and nucleoside triphosphate- (NTP-) driven nucleic acid translocases (Flaus *et al.*, 2006, Durr *et al.*, 2006, Hopfner *et al.*, 2012, Singleton *et al.*, 2007, Koonin, 1993, Byrd and Raney, 2012, Sirinakis *et al.*, 2011, Clapier *et al.*, 2017). Their comprehensive range of tasks include the packaging of the genome, (following the DNA replication or RNA polymerase II transcription), the organization of specialized nucleosomal architectures at regulatory regions, (occluding or providing access to regulatory regions for transcription factor binding mainly at promoter sites), and the establishment of long-range nucleosome-free DNA stretches needed for the DNA repair machineries. Although differing in subunit composition and capacities, chromatin remodelers share a central split Swi2/Snf2-type ATPase (Snf2 ATPase) characterized by two RecA-like lobes (DExx: N-lobe/lobe1 and HELICc: C-lobe/lobe2) that make up the catalytic core mechanically coupling ATP hydrolysis to DNA translocation (Pazin and Kadonaga, 1997, Clapier and Cairns, 2009, Saha *et al.*, 2002, Clapier *et al.*, 2017, Whitehouse *et al.*, 1999, Sirinakis *et al.*, 2011, Flaus *et al.*, 2006, Cote *et al.*, 1994). Earlier work on monomeric DNA/RNA helicases that track along the phosphate backbone of one DNA strand while ATP-dependently translocating

Introduction

DNA was fundamental for the understanding of ATP-dependent DNA translocation by chromatin remodelers (Singleton *et al.*, 2007). The central Swi2/Snf2-type ATPase harbors several highly conserved motifs, such as the walker A and B motifs, a DNA binding cleft and an ATP binding site, which are accompanied by subfamily-specific regulatory motifs based on which chromatin remodelers are classified into four families (refer to section 1.4.2 Remodeler families and their function). Chromatin remodeling complexes use energy generated by ATP-hydrolysis to mechano-chemically reconstruct histone-DNA contacts within the substrate nucleosome, tailoring nucleosome occupancy and composition in a genome-wide manner. Chromatin remodelers are pivotal regulators of nearly every chromatin-dependent process, such as DNA replication, transcription and repair, actively providing access to DNA regulatory sequences for cognate binding factors. De-regulation of chromatin remodelers causes severe effects on development (Ho and Crabtree, 2010) and potentially leads to extensive disease development, including a disposition for cancer (Wilson and Roberts, 2011, Lai and Wade, 2011, Byrd and Raney, 2012).

1.4.2 Remodeler families and their function

The SWI/SNF family of chromatin remodelers was first discovered in yeast and typically facilitates chromatin access through nucleosome sliding, disassembly and eviction reactions (Lorch *et al.*, 2014). Two classes of SWI/SNF remodelers are present in yeast, the switch/sucrose non-fermentable (SWI/SNF) and the remodel the structure of chromatin (RSC) remodelers with only the latter being essential for cell viability. SWI/SNF remodelers are comprised of 8-14 subunits and are referred to as master regulators of transcription and development (Clapier *et al.*, 2017). Their central Snf2-type ATPase domain is characterized by two RecA-like lobes flanking a short conserved insertion domain, a N-terminal helicase-SANT associated (HSA) and post-HSA domain and C-terminal bromodomains (Figure 5A). The C-terminal bromodomains of *S.c.* RSC (in the Rsc1, 2, 4 and 10 subunits) bind to acetylated histone N-terminal lysines which enhances RSC binding to nucleosomes *in vitro* (VanDemark *et al.*, 2007). Two actin-related proteins (Arp) Arp7 and Arp9 are associated with the HSA domain of SWI/SNF remodelers in fungi (Clapier and Cairns, 2009, Clapier *et al.*, 2017, Lorch *et al.*, 2014, Wagner *et al.*, 2020). *In vitro* as well as *in vivo* data linked SWI/SNF DNA translocation activity to the Sth1^{HSA}-Arp7-Arp9 module (Clapier *et al.*, 2016).

The only remodeler family capable of catalyzing nucleosome editing reactions, meaning the replication-independent incorporation of histone variants into canonical nucleosomes and *vice versa*, is the INO80 chromatin remodeler family (Mizuguchi *et al.*, 2004, Clapier and Cairns, 2009, Clapier *et al.*, 2017, Brahma *et al.*, 2017). The INO80 family was initially identified as transcription

regulator, but also participates in DNA repair to a large extent (Shen *et al.*, 2000, Gerhold and Gasser, 2014, Shen *et al.*, 2003b). The INO80 family member *S.c.* SWI2/SNF2-Related 1 (SWR1) remodeling complex is involved in nucleosome editing reactions, incorporating the H2A.Z histone variant into canonical histone octamers (Ranjan *et al.*, 2015, Luk *et al.*, 2010, Mizuguchi *et al.*, 2004). C. Wu and colleagues showed in an elegant study that heterotypic nucleosomes, comprised of one canonical and one variant H2A(.Z)/B dimer, are existing *in vivo*. They also demonstrated that the incorporation of H2A.Z/B dimers is a step-wise process *in vitro* (Luk *et al.*, 2010). Whether INO80 is a histone exchange factor and indeed catalyzes the reverse reaction by exchanging H2A.Z with H2A is still under debate (Watanabe *et al.*, 2015, Brahma *et al.*, 2017, Clapier *et al.*, 2017). The INO80 family members are comprised of more than 10 subunits and are unique in their “split” main ATPase (Clapier *et al.*, 2017, Chen *et al.*, 2011). The main ATPase harbors a long insertion domain between the DExx (N-lobe) and the HELICc (C-lobe) domain, which recruits the Rvb1/2 heterohexamer that is thought to drive the assembly of full INO80 complex (Figure 5A, refer to section 1.5 The INO80 chromatin remodeler) (Clapier and Cairns, 2009, Clapier *et al.*, 2017, Chen *et al.*, 2011, Tosi *et al.*, 2013).

Imitation switch (ISWI) and chromodomain helicase DNA-binding (CHD) family remodelers function in vicinity of the replication and also transcription machineries, facing the major task of nucleosome assembly and organization. Assembly and organization of nucleosomes involve the maturation of pre-nucleosomes into canonical, octameric nucleosomes, as well as the formation of regularly spaced nucleosome arrays *in vivo* as well as *in vitro* (Ito *et al.*, 1997, Lusser *et al.*, 2005, Fei *et al.*, 2015, Lieleg *et al.*, 2015a, Krietenstein *et al.*, 2016). The CHD family of chromatin remodelers can be categorized into three subfamilies according to the presence or absence of up to 10 auxiliary subunits and is typically characterized by the chromodomains in tandem on the N-terminus of the main ATPase and a DNA binding domain (DBD) at the C-terminus (Figure 5A). The two tandem chromodomains of human Chd1 bind and recognize specifically H3K4(me)₂ or H3K4(me)₃ histone tail modifications. Chd1 is the founding member of the CHD family of remodelers and is capable of nucleosome assembly and sliding reactions mainly within coding regions to promote transcription, or in case of Mi-1/NURD, to repress transcription (Bornelov *et al.*, 2018, Feng and Zhang, 2003, Clapier *et al.*, 2017). Chd1 reassembles and stabilizes nucleosomes in the wake of transcription, putatively in cooperation with histone chaperones (Fei *et al.*, 2015, Farnung *et al.*, 2017). Yeast Chd1 typically operates as a single polypeptide, providing a model system to study the mechanistic background of nucleosome sliding reactions. The loss of Chd1 leads to severe effects on nucleosome occupancy as well as nucleosome

Introduction

spacing (Gkikopoulos *et al.*, 2011, Sundaramoorthy *et al.*, 2018). Structural work suggested that the N-terminal chromodomains negatively regulate the ATPase N- and C-lobes by limiting the conformations of both lobes to the inactive state (Hauk *et al.*, 2010)

ISWI remodelers are comprised of 2-4 subunits and were first discovered in *D. melanogaster*. Two distinct ISWI genes are present in *S. cerevisiae*, ISW1 and ISW2. ISWI family remodelers share a C-terminal SANT-domain adjacent to a SLIDE domain, which are involved in extranucleosomal DNA binding (Figure 5B). HAND-SANT-SLIDE domains are structurally related to c-Myb DNA binding domains and are reported to interact with the entry site and linker DNA of the NCP, driving nucleosome recognition and regulating the activity of the main ATPase (Zofall *et al.*, 2004). The two conserved AutoN and NegC domains are located adjacent to the N- and C-lobes of the main ATPase and direct the ISWI activity through a well-characterized regulatory cycle (refer to section 3.2) (Sundaramoorthy, 2019, Clapier *et al.*, 2001, Clapier and Cairns, 2012).

1.4.3 Structural evidence for remodeler-nucleosome complexes

Recent advances in structural biology shed light on the long-standing question of where ATP-dependent chromatin remodelers engage their nucleosomal substrate and where and how DNA translocation is carried out (Figure 5A and B) (Eustermann *et al.*, 2018, Ayala *et al.*, 2018, Farnung *et al.*, 2017, Liu *et al.*, 2017, Li *et al.*, 2019, Sundaramoorthy *et al.*, 2018, Wagner *et al.*, 2020, Han *et al.*, 2020, He *et al.*, 2020, Yan *et al.*, 2019).

Introduction

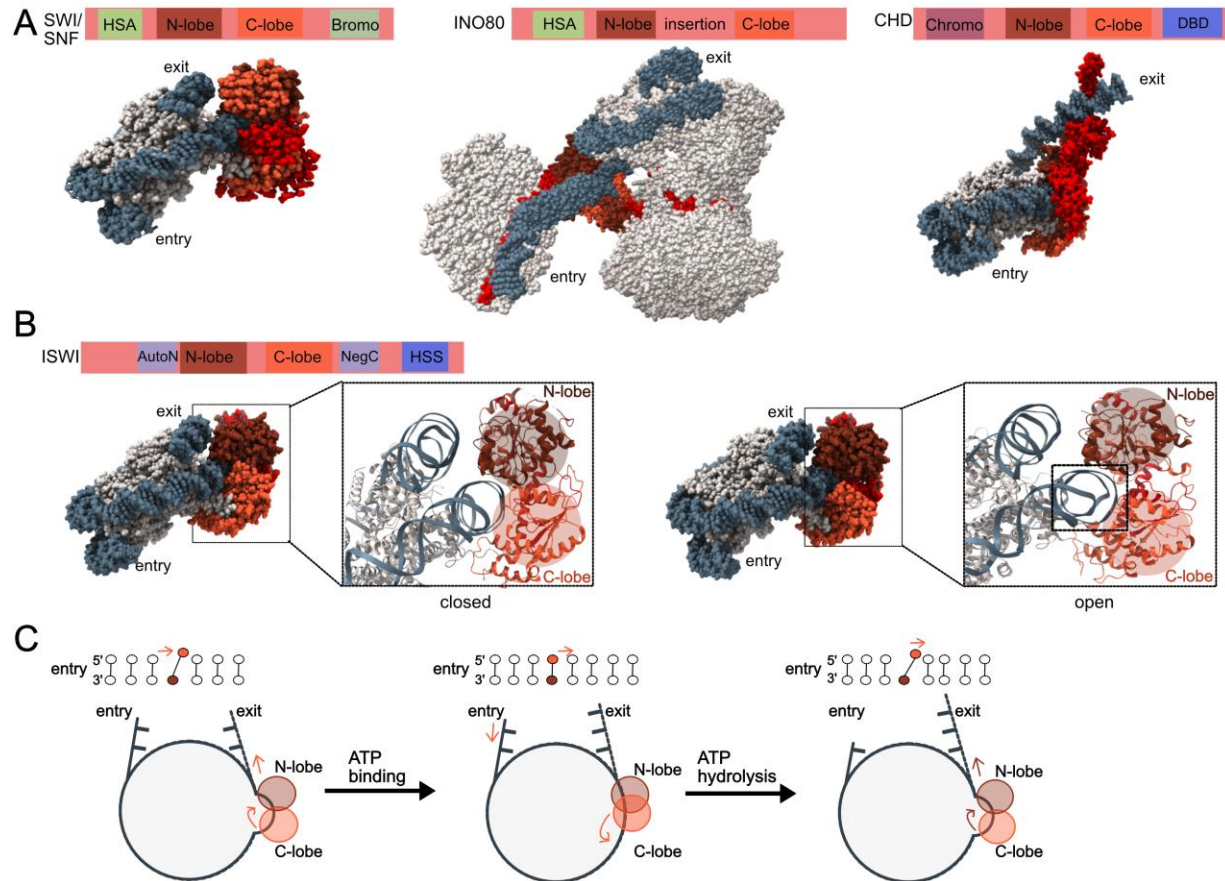


Figure 5: Chromatin remodeler and the central DNA translocation mechanism. (A) Schematic illustration of the SWI/SNF, INO80 and CHD main ATPase domain organization. The HSA domains of SWI/SNF and INO80 are highlighted in green, the SWI/SNF bromodomain is shown in light green and the CHD tandem chromodomain is shown in purple and the DNA binding domain (DBD) in blue. INO80 main ATPase is shown with the long insertion domain between the N- and C-lobe. (Structures: SWI/SNF PDB: 5Z3U, CHD PDB: 5O9G, INO80 PDB: 6FHS). Scheme adapted from (Clapier *et al.*, 2017). (B) The closed and open states of the N- and C-lobe exemplified by the ISWI chromatin remodeler in the closed (ADP-Befx bound, PDB: 6K1P) and the open (ADP-bound, PDB: 6IRO) state (Yan *et al.*, 2019). The N- and C-lobes of the ATPase motor domain are highlighted in dark (N-lobe) and light (C-lobe) red. The ATPase domain is shown in red. The ISWI main ATPase organization is schematically depicted with the C-terminal SANT-SLIDE (HSS) domain highlighted in blue and the regulatory AutoN and NegC domains shown in light blue, adapted from (Clapier *et al.*, 2017). (C) Model of the DNA translocation mechanism of chromatin remodelers, adapted from (Yan and Chen, 2020). DNA translocation starts with the binding of the ATPase motor domain (N-lobe and C-lobe) to SHL2 or SHL6, respectively, in the open conformation (apo state), stabilizing a 1bp DNA bulge. After ATP binding and transition into the closed state, the 1bp bulge translocates towards the dyad and reaches the DNA exit site (ATP state). Following the ATP hydrolysis (ADP state), 1bp DNA from the entry site is pulled in during transition into the open conformation, creating a 1bp bulge at SHL2 (SHL6).

An earlier model based on high resolution structural data suggested that the catalytic ATPase domain resides on the extranucleosomal DNA outside the NCP. It was proposed that “screw motion of DNA” at the ATPase domain could move DNA towards and away from the nucleosomal substrate while creating rotational torque for a remodeling reaction (Durr *et al.*, 2005, Clapier *et al.*, 2017). Biochemical studies including hydroxyl-radical foot-printing, crosslinking, DNaseI hypersensitivity, comparative analysis of nucleosomes containing strand-specific DNA gaps and FRET (Clapier *et al.*, 2017) brought about an important shift in thinking by supporting a model in

Introduction

which two RecA-like lobes (N-lobe and C-lobe) of the Snf2-type remodeler ATPase motor domains bind within the NCP at SHL+/-2 and SHL+/-6, respectively, *in lieu* of binding to DNA entry/exit sites or linker DNA outside the NCP (Langst and Becker, 2001, Zofall *et al.*, 2006, Brahma *et al.*, 2017, Schwanbeck *et al.*, 2004, Saha *et al.*, 2002, Saha *et al.*, 2005). These pioneering findings already suggested a strategically important role for SHL2/SHL6 in chromatin remodeling and placed the main ATPase binding site within the NCP (Saha *et al.*, 2002, Saha *et al.*, 2005, Langst and Becker, 2001, Havas *et al.*, 2000, Flaus and Owen-Hughes, 2003, Lorch *et al.*, 2001, Narlikar *et al.*, 2001).

Indeed, recent electron cryo-microscopy (cryo-EM) data of the *S.c.* remodeler Snf2 bound to the nucleosome in the presence of various nucleotides verified earlier biochemical data (Liu *et al.*, 2017, Li *et al.*, 2019). The Snf2 ATPase DNA binding cleft formed by the two RecA-like lobes binds to the DNA phosphate backbone at the aforementioned SHL+2 location. CryoEM data also showed Snf2 occupying the SHL+6 location, but the physiological relevance of this additional binding site for the Snf2 remodeler remains unclear. *Apo* as well as ADP-bound state show Snf2 in an “open” conformation, in which a 1bp DNA bulge distortion at SHL+2 is stabilized (Figure 5C). A highly similar structural arrangement of the main ATPase lobes at SHL2 was resolved for the ISWI remodeler (Figure 5B) (Yan *et al.*, 2019) and was also suggested for the Chd1 remodeler in a study using site-specific crosslinking (Winger *et al.*, 2018).

The binding of the ATP analogue (ADP-BeF_x) to Snf2 triggered a transition into the closed state of the two RecA-like lobes, leaving the nucleosomal DNA in an unstrained state (Figure 5C) (Li *et al.*, 2019, Yan *et al.*, 2019). Structures verified that the two RecA-like lobes of ISWI as well as CHD remodeler in the ADP-BeF_x-bound state are in the closed conformation (Figure 5A and B) (Farnung *et al.*, 2017, Winger *et al.*, 2018, Yan *et al.*, 2019). Interestingly, the Chd1 motor domain was anchored to the nucleosome via the DNA-binding domain (DBD) interacting with the exit DNA, leading to a partial unwrapping of 20bp that has not been observed before in the ISWI nor the Snf2 remodeler (Figure 5A, right panel) (Farnung *et al.*, 2017).

In contrast to ISWI, Snf2 and Chd1 (Farnung *et al.*, 2017, Yan *et al.*, 2019, Liu *et al.*, 2017), earlier biochemical data suggested (Udugama *et al.*, 2011, Brahma *et al.*, 2017) and two recent cryo-EM structures of the *Chaetomium thermophilum* (*C.t.*) INO80 core complex (Eustermann *et al.*, 2018) and the human INO80 core complex (Ayala *et al.*, 2018) subsequently verified the binding of the Ino80 main ATPase near the nucleosomal entry site, at SHL+/-6 and SHL+/-7, with an Arp5/les6 counter-grip located at SHL+/-2 (Figure 5A, middle panel). In the apo state the two RecA-like lobes

Introduction

of Ino80 were in a rather “open” state, lacking a detectable 1bp DNA deformation at the binding site (Figure 5A, Figure 6) (Aramayo *et al.*, 2018, Eustermann *et al.*, 2018). Ino80 binding on the entry side DNA disrupts histone-DNA contacts and leads to a partial unwrapping of DNA. Recent structural data revealed the interaction mode of another INO80 family member SWR1 and its nucleosomal substrate (Willhoft *et al.*, 2018). SWR1 grips the nucleosome at SHL \pm 2 with the Swr1 motor domain and at SHL+6 with the ARP6 module. This leads to partial unwrapping of the entry DNA and the introduction of a 1bp DNA bulge by the Swr1 motor domain bound at SHL \pm 2 as seen for ISWI, SWI/SNF and CHD family remodelers. Interestingly, both the guide and the tracking strands of the DNA are locally distorted in the ADP-BeF_x bound, closed conformation (Willhoft *et al.*, 2018). Accumulating biochemical and structural data suggested that the open conformation of the N- and C-lobes of the respective main ATPases introduce DNA torsion by creating a 1 bp DNA bulge, independent of the binding site location (Li *et al.*, 2019, Yan *et al.*, 2019, Farnung *et al.*, 2017, Yan and Chen, 2020).

1.4.4 A unifying DNA translocation mechanism

In general, the current mechanistic understanding of DNA translocation carried out by ATP-dependent chromatin remodelers involves binding of the two RecA-like lobes simultaneously on one DNA strand, followed by an ATP-dependent ratchet-like cycle of DNA binding and release carried out by both lobes. This results in a DNA net-movement of 1-2bp per ATP-hydrolysis cycle (Figure 5C) (Deindl *et al.*, 2013, Harada *et al.*, 2016, Singleton *et al.*, 2007, Velankar *et al.*, 1999, Sirinakis *et al.*, 2011, Yan and Chen, 2020). Earlier structures of the NCP already suggested the accommodation of variable DNA length within the NCP, meaning the stretching of DNA by 1bp is possible at SHL \pm 2 and/or \pm 5 (refer to section 1.2) (Luger *et al.*, 1997, Luger and Richmond, 1998, Tan and Davey, 2011). The core issue in DNA translocation by chromatin remodelers is how those enzymes overcome the energy barrier built up by the extensive histone-DNA contacts within the nucleosome. Earlier models of DNA translocation by remodelers suggested a ‘polymerase-like’ mechanism, meaning DNA peeling from the octamer in a processive movement along the histone octamer (Lorch *et al.*, 1999). The high-resolution crystal structure of the *Sulfolobus sulfataricus* SWI2/SNF2 core ATPase bound to a dsDNA suggested superhelical torsion of the dsDNA generated by ATP-driven “screw motion” of DNA along the histone octamer as the basis for DNA translocation, and that SWI2/SNF2 ATPases track along the phosphate backbone of the dsDNA minor groove without strand separation activity (Durr *et al.*, 2005).

Introduction

Over time, several models for chromatin remodeling have been proposed, including the “DNA loop formation” model, the “DNA twist diffusion” model, as well as the “octamer deformation” model (Mueller-Planitz *et al.*, 2013, Narlikar *et al.*, 2001, Havas *et al.*, 2000, Flaus and Owen-Hughes, 2003, Saha *et al.*, 2002, Lorch *et al.*, 2001, Langst and Becker, 2001). A clear data provided by recent cryo-EM as well as single molecule fluorescence resonance energy transfer (smFRET) studies (Armache *et al.*, 2019, Nodelman *et al.*, 2017, Yan *et al.*, 2016, Yan *et al.*, 2019, Winger *et al.*, 2018, Qiu *et al.*, 2017, Sabantsev *et al.*, 2019, Farnung *et al.*, 2017, Sundaramoorthy *et al.*, 2018, Aramayo *et al.*, 2018, Willhoft *et al.*, 2018, Eustermann *et al.*, 2018, Wagner *et al.*, 2020, Han *et al.*, 2020, He *et al.*, 2020) clarified where and how the DNA translocase core of ATP-dependent chromatin remodelers engages its substrate and how the DNA translocation is carried out mechanistically, favoring the “DNA wave” model as a general model (Yan and Chen, 2020).

The ATPase motor domain engages the phosphate backbone of one DNA gyre at SHL \pm 2 by a grip composed of the two RecA-like lobes (Figure 5C). A secondary DNA binding surface anchors the remodeler at this site in a fixed orientation (Liu *et al.*, 2017). Within the stabilized 1bp DNA bulge in the apo- and ADP-bound “open” conformation of the ATPase motor, the tracking strand showed greater distortion than the guide strand. This created force to pull in DNA in 1bp step size from the entry site (Figure 5C). A large conformational rotation occurs upon ATP binding and the two RecA-like lobes transition into the “closed” conformation. During this massive rotation the C-lobe (“torsion sub-domain”) tightly binds the tracking strand and moves the DNA bulge towards the exit site *in lieu* of the N-lobe (“tracking sub-domain”), which remains at a fixed position (Figure 5C, middle panel). This implicates a DNA net-movement relative to the octamer of 1bp DNA. The re-opening of the complex after ATP-hydrolysis and phosphate release again introduces a 1bp bulge, restarting the cycle (Figure 5C, right panel) (Yan and Chen, 2020). Distortion of the DNA upon ATP binding and bulge formation prime the nucleosome for the following remodeling reaction. The ATP motor domain movement relative to DNA is, in and of itself, an “inchworm-like” mechanism, reflecting again the homology of chromatin remodelers to SF2 helicases. Ratchet-like DNA movement is guided by a “gating helix”, protrusion-II, in the C-lobe that hinders backslippage of the DNA bulge in entry site direction (Eustermann *et al.*, 2018, Wagner *et al.*, 2020, Han *et al.*, 2020). Propagation of 1bp distortions from the entry to the exit site reflects a wave-like behavior and was therefore termed “wave-model” (Richmond and Davey, 2003, Flaus and Owen-Hughes, 2003, Yan and Chen, 2020). The tracking strand showed intact DNA-histone contacts with an altered register of DNA, whereas the guide strand kept its canonical DNA-histone register

(Figure 5C). Additionally, recent three-color smFRET data verifies the “wave model” showing that entry DNA movement clearly precedes exit DNA movement (Sabantsev *et al.*, 2019). The aforementioned strand-specific DNA translocation was also seen for ISWI and CHD family remodelers (Yan *et al.*, 2019, Winger *et al.*, 2018). This difference in distortion between guide and tracking strands are in line with chromatin remodelers being phylogenetically classified as SF2 DNA/RNA helicases/translocases (Singleton *et al.*, 2007, Byrd and Raney, 2012, Koonin, 1993, Hopfner *et al.*, 2012). The closed state of the ATPase motor domain resets the nucleosome in an unstrained state lacking a DNA bulge at SHL+/-2 (Figure 5C, right panel) (Winger *et al.*, 2018, Liu *et al.*, 2020, Yan *et al.*, 2019, Li *et al.*, 2019). Taken together, these findings suggest an open-closed conformational cycle of the two RecA-like domains of the main ATPase being the fundamental basis for DNA translocation by ATP-dependent chromatin remodelers.

A central question within the field of chromatin remodeler research is how ATP hydrolysis is coupled to a remodeling event and how, based on this shared translocation mechanism, remodeler specific, genome-wide phased arrays of regular spaced nucleosomes are generated. The current understanding includes the regulation of the ATPase motor domain by histone tails, for example the H4 tail acetylation lowers ATPase activity for yeast ISW2 and yeast Chd1 in contrast with the yeast RSC, which is activated upon H4 tail acetylation (Clapier *et al.*, 2017). The best examined regulatory interplay by far is the multi-layered regulation of the ISWI remodeler main ATPase by auxiliary domains, where AutoN and NegC are antagonized by histone modification, histone H4 tail and DNA linker length (refer to section).

1.5 The INO80 chromatin remodeler

1.5.1 INO80 function *in vivo* and *in vitro*

Regulation of DNA replication, transcription and damage repair are functions assigned to INO80 *in vivo* (Shen *et al.*, 2000). INO80 has been originally discovered as a co-regulator of transcription in yeast (Shen *et al.*, 2000, Ebbert *et al.*, 1999) and was shown to influence the expression of various genes by up as well as downregulation. The repression of non-coding transcripts and ectopic transcription initiation by INO80 might be related to its +1 nucleosome positioning activity, establishing a hallmark for the downstream alignment of nucleosomal arrays (Ebbert *et al.*, 1999, van Attikum *et al.*, 2004, Poli *et al.*, 2017, Klopff *et al.*, 2017, Krietenstein *et al.*, 2016, Challal *et al.*, 2018, Kubik *et al.*, 2019). In DNA repair and homologous recombination INO80 was associated with the incorporation of H2A into H2A.Z-containing nucleosomes (Alatwi and Downs,

2015, Lademann *et al.*, 2017). INO80 is enriched in vicinity of dsDNA breaks in yeast and co-localizes with phosphorylated H2A.X that represents a hallmark for dsDNA breaks and DNA repair. The INO80 complex was therefore proposed to function in dsDNA break repair (van Attikum *et al.*, 2004, Morrison *et al.*, 2004, Andreev *et al.*, 2019). A third function attributed to INO80 is the recovery of stalled replication forks in yeast and human cells (Papamichos-Chronakis and Peterson, 2008, Vassileva *et al.*, 2014). INO80 was shown to release RNA polymerase II (RNAPII), stalled by interference with the replication machinery, from chromatin (Lafon *et al.*, 2015, Poli *et al.*, 2017, Poli *et al.*, 2016), which provides evidence for an involvement of INO80 in DNA replication *in vivo*.

In vitro INO80 was capable of centering end-positioned mononucleosomes, as well as regular spacing of trinucleosomes with a sufficient extranucleosomal DNA length of 50bp (Udugama *et al.*, 2011, Zhou *et al.*, 2018). Both *in vivo* as well as *in vitro* genome-wide studies have proven a pivotal role for INO80 in shaping the stereotyped architecture of regulatory promoter regions (Figure 4B). Genome-wide *in vitro* reconstitution assays elucidated that the yeast INO80 complex is so far, the only remodeler known to be capable of autonomously and precisely positioning the +1 nucleosome flanking the NDRs that harbors the TSS (refer to section 1.3.2) (Krietenstein *et al.*, 2016, Zhang *et al.*, 2011). Positioning of the +1 nucleosome is consistent with earlier data mapping several INO80 subunits specifically to the +1 nucleosome or to the proximal sequences located within the NDR (Yen *et al.*, 2012, Yen *et al.*, 2013, Brahma *et al.*, 2017).

1.5.2 The modular architecture of the INO80 chromatin remodeling complex

Structural, biochemical and crosslinking studies verified that INO80 is characterized by a modular architecture with the main ATPase motor functioning as a scaffolding backbone protein for the complex assembly (Figure 6) (Tosi *et al.*, 2013, Chen *et al.*, 2011, Watanabe *et al.*, 2015). In yeast, INO80 is assembled by three main architectural modules: INO80^{core}, the actin related proteins (ARP) module and the NHP10 module (Figure 6). Nucleosome sliding by INO80 requires INO80^{core} and the ARP module (Figure 6A). The ARP module is assembled by Arp8 and Arp4, with the latter in conserved association with nuclear actin (N-actin), bound to the N-terminal helicase SANT associated (HSA) domain of the Ino80 main ATPase (Figure 6A, Figure 8). The IATA-binding protein-associated factor 14 (Taf14) and the INO eighty subunit 4 (Ies4) complete the functional unit of the ARP module in yeast (Chen *et al.*, 2011, Szerlong *et al.*, 2008, Gerhold *et al.*, 2012, Tosi *et al.*, 2013). Deletion of Arp8 or the Ino80_HSA domain abolishes the INO80 chromatin

remodeling activity, suggesting an integral role for this module in this mechano-chemical reaction (Tosi *et al.*, 2013, Chen *et al.*, 2013, Kapoor *et al.*, 2013, Shen *et al.*, 2003a). The RuvB-like 1/2(Rvb1/2) heterohexamer is recruited by the Ino80 ATPase insertion domain and connects Arp5/les6 with the Ino80 ATPase (refer to Figure 6A and C) (Tosi *et al.*, 2013, Chen *et al.*, 2011, Eustermann *et al.*, 2018). In yeast, the species-specific NHP10 module consists of les1, les3, les5 and the non-histone protein 10 (Nhp10) containing an HMG-box like domain, and associates with the N-terminus of the Ino80 ATPase (Figure 6A) (Tosi *et al.*, 2013, Chen *et al.*, 2011, Zhou *et al.*, 2018)). With its strong intrinsic DNA and nucleosome binding affinity, the NHP10 module is integral for nucleosome binding (Tosi *et al.*, 2013, Shen *et al.*, 2003b), but not essential for INO80 ATPase activity nor nucleosome sliding (Tosi *et al.*, 2013, Zhou *et al.*, 2018). In addition, crosslinking studies mapped the les5 subunit of the NHP10 module to the NDR at promoter sites (Yen *et al.*, 2013, Badis *et al.*, 2008). Taken together, these findings proposed a more regulatory role for the NHP10 module by targeting INO80 to promoter sites (Yen *et al.*, 2013). Intriguingly, in a recent study based on single molecule enzymology, the NHP10 module was shown to be pivotal in DNA length sensing by INO80 by setting a sufficient extranucleosomal DNA length requirements (minimum 40bp) without a sequence preference (Zhou *et al.*, 2018) By applying ensemble and single-molecule enzymology, C. Zhou and colleagues could show that INO80 sliding activity and thus the DNA translocation rate strongly depends on the length of DNA flanking the nucleosome, and indeed nucleosome sliding increased 100-fold by increasing flanking DNA from 40 bp to 60 bp. These findings suggested an ISWI-like mechanism for INO80, in which length sensing of linker DNA is directly coupled to the central ATPase motor (Yang *et al.*, 2006). Unexpectedly, the inability to slide nucleosomes was unrelated to a robust ATPase activity (Zhou *et al.*, 2018).

1.5.3 Structural insights into the INO80 – nucleosome complex

Recent cryo-EM structures of the human (Aramayo *et al.*, 2018) and the *Chaetomium thermophilum* (C.t.) INO80-nucleosome complex (Figure 6C and D) (Eustermann *et al.*, 2018, Ayala *et al.*, 2018) clarified how INO80 engages its nucleosomal substrates. Comparing the substrate binding mode, INO80 clearly differs from ISWI and CHD remodelers, but shows similarities to the isolated Snf2 motor domain of SWI/SNF remodeler that binds at SHL+2 and SHL+6 (refer to Figure 5 and Figure 6) (Farnung *et al.*, 2017, Yan *et al.*, 2019, Liu *et al.*, 2017, Li *et al.*, 2019).

Introduction

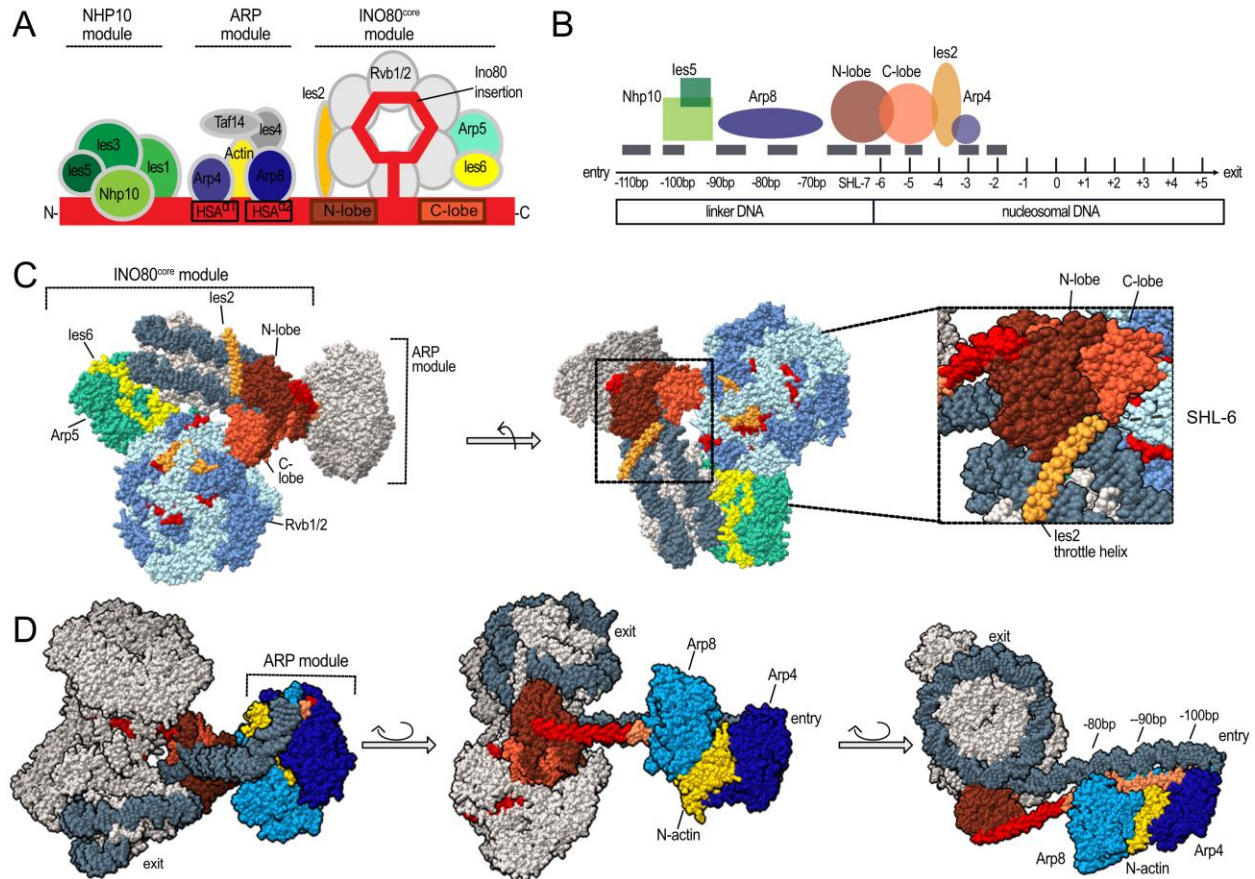


Figure 6: The INO80 chromatin remodeler. (A) Modular architecture of the INO80 chromatin remodeler. Schematic representation of the NHP10 module in green comprised of Nhp10, les1, les3, les5, the ARP module with Taf14, les4 (grey), Arp8 (dark blue), N-actin (gold) and Arp4 (blue), as well as the INO80^{core} comprised of Ino80 (red), Arp5 (turquoise), les6 (yellow), les2 (orange) and the Rvb1/2 heterohexamers (light grey). Location of the N- (dark red) and C-lobes (light red) of the main ATPase as well as the $\alpha 1$ and $\alpha 2$ helices of the HSA domain are indicated. (B) Schematic depiction of INO80 crosslink data adapted from (Brahma *et al.*, 2017). SHL locations as well as extranucleosomal DNA with respective distance to the dyad are indicated. Strong crosslink signals are represented by bars in dark grey. Color coding for the INO80 subunits is consistent with (A). (C) Cryo-EM structure of the INO80 complex bound to the nucleosome highlighting the INO80^{core} conformation. A close up into the arrangement of the les2 throttle helix relative to the N- and C-lobes of the main ATPase. Color coding is consistent with (A). (D) Cryo-EM structure of the INO80 complex focusing on the ARP module binding to extranucleosomal DNA. Entry and exit sites of the DNA are indicated as well as the extranucleosomal DNA with relative distance to the dyad bound by the HSA domain of the INO80 ARP module. (C) and (D) are adapted from (Knoll *et al.*, 2018, Eustermann *et al.*, 2018) (PDB:6FML).

The human INO80 full complex as well as conserved subunits of *C.t.* INO80^{core} (Ino80, Rvb1/2, les6, Arp5 and les2) engage the nucleosome at SHL-6 (Figure 6C). Both studies found that the nucleosome is grasped from two opposite sites by the two RecA-like lobes of the Ino80 ATPase bound to nucleosomal DNA at SHL-6 and SHL-7, and Arp5/les6 at SHL-2 and SHL-3 forming a counter grip, which is clearly in line with the former biochemical data (Figure 6B and C) (Brahma *et al.*, 2017, Eustermann *et al.*, 2018, Ayala *et al.*, 2018)). The N- and C-lobes, harboring the conserved Snf2 binding motifs (I, Ia, II, and III for the N-lobe, and IV, V and VI for the C-lobe), bind and engage nucleosomal DNA at SHL-6 in a conformation stabilized by the brace helix I

(Eustermann *et al.*, 2018). As a consequence, approx. 15bp of entry side DNA are unwrapped and the DNA minor groove at SHL-6 is widened, leading to the proposition that DNA shape may be potentially involved in nucleosome positioning by INO80 (Eustermann *et al.*, 2018). The insertion domain of the Ino80 ATPase C-lobe nucleates alternating Rvb1/2 subunits into a heterohexamer and contacts all six subunits (Figure 6A and C). The “Ino80 insertion - Rvb1/2 complex” is then proposed to recruit and arrange the INO80 nucleosome-clamping elements: The Ino80 main ATPase-les2 motor element and the Arp5-les6 stator element. The Ino80 insertion is characterized by the insertion “plug” and the insertion “latch”, which both directly or indirectly (by orienting the Rvb1/2 heterohexamer) rearrange les2, Arp5 and les6 architecturally. The Ino80 insertion “latch” provides a binding site for Arp5/les6 to the Rvb1/2 heterohexamer. The insertion “plug” binds les2, which then pins the N-lobe of Ino80 to SHL+/-2. The les2 contacts nucleosomal DNA through the les2 “throttle helix” and interacts with the acidic patch at the H2A/B interface on the octamer surface (Figure 6C). The les2 is the proposed throttle of INO80 remodeling (Willhoft *et al.*, 2016, Eustermann *et al.*, 2018, Ayala *et al.*, 2018). Secondary contacts are made by les2 and the Ino80 main ATPase at SHL2, by Arp5 through the Arp5 “grappler” element (Arp5^{grappler}) at the nucleosomal dyad and by Arp5^{grappler}, les2 and les6 at histone core residues (Eustermann *et al.*, 2018, Ayala *et al.*, 2018). The post-HSA and HSA domains of the Ino80 ATPase arrange in an extended helical conformation with the Ino80_HSA domain nucleating Arp8, N-Actin and Arp4.

1.5.3.1 ATP-dependent DNA translocation by INO80

The INO80 ATPase motor domain anchored at SHL-6 is primed for the pumping of entry DNA from the proximal site towards the nucleosomal dyad (Figure 6D, Figure 7A). The Arp5-les6 element binds about 7-8 bp at SHL-2/SHL-3 and carries out, in complex with the Rvb1/2 heterohexamer that acts as a “stator” keeping the Ino80 C-lobe in a fixed position, ratchet-like, unidirectional DNA translocation. Binding of the two RecA-like lobes deforms nucleosomal DNA located at the H2A/B dimer interface (Eustermann *et al.*, 2018). Entry DNA of the proximal, ATPase motor domain binding site, is pumped towards the dyad against the Arp5-les6 stator. Elementary steps of 1-2bp per ATP hydrolysis are pumped towards the dyad, creating a DNA loop of approximately 10bp between the motor and the stator elements (Figure 7A). This solves the conundrum of small 1-2bp step sizes characteristic of Snf2-type ATPases (Clapier *et al.*, 2017, Yan and Chen, 2020) and the contradictory observation of large 10-15bp step sizes for DNA translocation by INO80 (Zhou *et al.*, 2018, Brahma *et al.*, 2017, Schwarz *et al.*, 2018). After the DNA loop collapse, the histone octamer is repositioned relative to DNA. Deletion or mutation of the conserved Arp5 DBD

decouples INO80 ATPase activity from the sliding ability, underlining its integral role as “counter grip” in DNA translocation (Tosi *et al.*, 2013, Eustermann *et al.*, 2018). The Arp5^{grapppler} as well as les2 bind to the acidic patch on each site of the nucleosome with the first mentioned ensuring octamer integrity and the latter regulating the Ino80 ATPase activity (Eustermann *et al.*, 2018, Ayala *et al.*, 2018).

1.5.4 The INO80 ARP module

The family of actin-related proteins (Arp) belongs to the superfamily of actin-fold proteins, but is not able to build filamentous structures in contrast to actin-fold proteins (Schafer and Schroer, 1999). Arps are in principle conserved from yeast to higher eukaryotes, except for Arp7/Arp9 that have not been detected in higher eukaryotes (Olave *et al.*, 2002). The INO80 ARP module is assembled by Taf14, les4, Arp4-N-Actin and Arp8. The latter three are nucleated by the Ino80 N-terminal HSA and post-HSA domains. In yeast, N-actin and Arps are indispensable subunits of the remodelers INO80, SWR1, SWI/SNF and RSC (Olave *et al.*, 2002). Structural data showed that Arps as well as N-Actin bind through hydrophobic residues to the helical HSA domain of Snf2 (Arp7-Arp9), Sth1 (Arp7-Arp9) and Swr1 (N-actin-Arp4) (Cao *et al.*, 2016, Schubert *et al.*, 2013, Wagner *et al.*, 2020). The ARP module is pivotal for the SWI/SNF remodeler RSC, since it directly interacts with the Sth1 main ATPase and regulates nucleosome sliding as well as ejection in the RSC complex (Turegun *et al.*, 2018, Clapier *et al.*, 2016). Given the importance of SWI/SNF remodeler, it is likely that the ARP module functions similarly in the INO80 chromatin remodeler. Earlier studies suggested that Arps and N-actin putatively function as chaperones or DNA binding subunits (Gerhold *et al.*, 2012, Kapoor *et al.*, 2013, Shen *et al.*, 2003a). In case of INO80, the HSA domain of the Ino80 ATPase (Ino80_HSA) and Arp8 are pivotal for the recruitment of ARP module components (Szerlong *et al.*, 2008, Tosi *et al.*, 2013), since deletion of Arp8 or Ino80_HSA lead to the loss of the entire ARP module (Shen *et al.*, 2003a, Tosi *et al.*, 2013, Shen *et al.*, 2003b). Nucleosome binding as well as nucleosome-stimulated ATPase activity of INO80 lacking the ARP module is comparable to the wild type INO80, whereas the nucleosome sliding ability is strongly impaired (Shen *et al.*, 2003a, Tosi *et al.*, 2013). ChiP-Exo data mapped the INO80 Arp8 subunit to extranucleosomal DNA upstream of the +1 nucleosome within the NDR (Figure 6B), (Brahma *et al.*, 2017). Indeed, recent cryo-EM data provided low-resolution density for the ARP module located at extranucleosomal entry DNA proximal to the Ino80 ATPase motor (Eustermann *et al.*, 2018, Knoll *et al.*, 2018). Crystal structures of ARP7-Arp9-Snf2^{HSA} and N-actin-Arp4-Swr1^{HSA} (Cao *et al.*, 2016, Schubert *et al.*, 2013), structures of individual Arp4 and Arp8 (Gerhold *et al.*, 2012, Fenn *et al.*, 2011), as well as a recent cryo-EM structure of the RSC complex

Introduction

(Arp7-Arp9-Sth1^{HSA}) are limited in deducing the ARP module contribution to nucleosome sliding by INO80. Although clear data built the foundation to establish a model of the DNA translocation mechanisms, we still lack in-depth understanding of biochemical and regulatory mechanisms guiding the molecular interplay between the INO80^{core} and its accessory ARP and NHP10 modules.

Objectives

1.6 Objectives

The combination of precise nucleosome positions and their respective post-translational modifications and compositions are integral to genome regulation. The chromatin landscape of active promoter sites is characterized by an archetypical pattern of phased arrays of regularly spaced nucleosomes. ATP-dependent remodelers of the CHD, ISWI, SWI/SNF and INO80 families are pivotal in the formation of the archetypical promoter architecture. Clear structural evidence elucidated how ATP-dependent remodelers engage their nucleosomal substrates. The mechanistic understanding of how ATP-dependent chromatin remodelers position equally spaced nucleosomes from a given reference point and what type of information is read by these macromolecular machineries is still highly limited.

In vitro genome-wide reconstitution assays were performed to probe the nucleosome positioning mechanisms of (*S.c.*) remodelers with regard to spacing of adjacent nucleosomes, phasing at GRF sites and phasing at dsDNA break sites. The author expanded the genome-wide *in vitro* experimental set up to attempt answering several questions. The general regulatory factor Reb1 was used as a reference point to test if remodelers generate phased arrays radiating from the Reb1 binding sites. Additionally, dsDNA break reference points were introduced by BamHI to test if chromatin remodelers align phased nucleosomal arrays at simple dsDNA breaks that lack a promoter sequence context.

The remodeler ruler concept was first described for the ISW1a chromatin remodeler and refers to spacing of nucleosomes guided by a remodeler ruler element (Yamada *et al.*, 2011). To determine if nucleosome positioning driven by *S.c.* chromatin remodelers is directed by a ruler-like functionality, we tested different nucleosomal densities as well as *S.c.*, *S. p.* and *E. coli* genomic sequences in a genome-wide reconstitution assay.

Based on these findings, structure-guided mutagenic studies in the INO80 model system including Ino80_HSA constructs, Ino80_ΔN, INO80_ΔNHP10 and INO80_HMG constructs were performed to dissect the role of respective sub-modules in INO80-mediated nucleosome positioning. All mutant constructs were tested in genome-wide *in vitro* reconstitution assays. In order to probe if INO80 is capable of direct transduction of Reb1 phasing information into nucleosome positioning, mononucleosome sliding assays were performed. The yeast YGL167c promoter sequence was selected according to the degree of +1 nucleosome positioning by INO80 on its own (Krietenstein *et al.*, 2016) well as high Reb1 occupancy *in vivo* (Brahma *et al.*, 2017). The +1 nucleosome positioning sequence was replaced with the Widom 601 sequence (Lowary and Widom, 1998).

Objectives

The effect of the presence and absence of Reb1 on INO80 nucleosome sliding kinetics was tested in mononucleosome sliding assays. INO80 wild type and mutant constructs in presence and absence of Reb1 were tested in NADH-based ATPase assays to see if Reb1 affected the overall ATP hydrolysis rates of the ATPase domain.

INO80 nucleosome positioning through DNA shape read-out has been suggested by previous studies. To directly test this proposition, genome-wide assays were applied to characterize if, in case DNA shape is read by INO80, mutant constructs impact DNA shape read-out by INO80. If INO80 mutants generate different clusters of nucleosome positions than the wild type INO80 was tested by independent principal component analysis (PCA) clustering.

2. Publications

2.1 The nuclear actin-containing Arp8 module is a linker DNA sensor driving INO80 chromatin remodeling

Kilian R Knoll*, Sebastian Eustermann*, Vanessa Niebauer, Elisa Oberbeckmann, Gabriele Stoehr, Kevin Schall, Alessandro Tosi, Marianne Schwarz, Andrea Buchfellner, Philipp Korber, Karl-Peter Hopfner (2018). The nuclear actin-containing Arp8 module is a linker DNA sensor driving INO80 chromatin remodeling. *Nat Struct Mol Biol.* 2018; 25(9):823-832.

*: equal contribution

DOI:10.1038/s41594-018-0115-8

URL: <https://www.nature.com/articles/s41594-018-0115-8#Sec1>

This publication reports the crystal structure of the *S.c.* INO80 ARP module in the ATP bound state along with a functional study of ARP module mutations targeting DNA binding residues of the Ino80_HSA domain. Actin related proteins (Arps) are integral components of large mega-Dalton chromatin-modifying and chromatin-remodeling machineries. What was not evident is the molecular function of Arps within these complexes that operate genome-wide. This study shows that the Arp8 subunit of the *S.c.* remodeler INO80 recruits Arp4 and N-actin to the Ino80_HSA domain which itself is organized in a segmented helix. The extended conformation of the Ino80_HSA domain forms a binding platform for entry side extranucleosomal DNA. A causal link between the Ino80_HSA domain and the extranucleosomal DNA-sensing activity could be established by mutagenesis of Ino80_HSA–DNA contact residues. Mutations of the INO80_HSA domain abolished INO80-mediated sliding in mononucleosome assays, while maintaining a robust and wild type-like ATPase and +1 nucleosome positioning activities tested using NADH-based ATPase assays and genome-wide reconstitution assays. The ARP module is proposed to sense 40bp of extranucleosomal entry side DNA, which is allosterically coupled to the main Ino80 ATPase and influences processive nucleosome remodeling by the INO80.

Author contribution

Publications

The author of this thesis contributed to this publication by cloning, expressing and purifying S.c. INO80 wild type and Ino80_HSA domain mutant complex constructs for *in vitro* characterization of DNA binding, sliding and nucleosome positioning. The author performed electro-mobility shift assays (EMSA) to evaluate binding affinities for nucleosomes with varying extranucleosomal DNA for the wild type and mutant INO80 constructs. The author performed *in vitro* mononucleosome sliding assays to characterize sliding kinetics for both wild type and mutant constructs. The author also performed fluorescence-based ATPase assays using to test the ATPase activity of the wild type and mutant constructs in presence of varying mononucleosomes and double-strand DNA. The author analyzed nucleosomal DNA accessibility in restriction enzyme accessibility assays (REA) and nucleosome positioning of wild type and mutant constructs in genome-wide *in vitro* reconstitution assays in the laboratory of PD Dr. Philipp Korber.

The nuclear actin-containing Arp8 module is a linker DNA sensor driving INO80 chromatin remodeling

Kilian R. Knoll^{1,2,9}, Sebastian Eustermann^{1,2,9}, Vanessa Niebauer^{1,2}, Elisa Oberbeckmann³, Gabriele Stoehr^{1,2,7}, Kevin Schall^{1,2}, Alessandro Tosi^{1,2,8}, Marianne Schwarz^{1,2,4}, Andrea Buchfellner⁵, Philipp Korber³ and Karl-Peter Hopfner^{1,2,6*}

Nuclear actin (N-actin) and actin-related proteins (Arps) are critical components of several chromatin modulating complexes, including the chromatin remodeler INO80, but their function is largely elusive. Here, we report the crystal structure of the 180-kDa Arp8 module of *Saccharomyces cerevisiae* INO80 and establish its role in recognition of extranucleosomal linker DNA. Arp8 engages N-actin in a manner distinct from that of other actin-fold proteins and thereby specifies recruitment of the Arp4-N-actin heterodimer to a segmented scaffold of the helicase-SANT-associated (HSA) domain of Ino80. The helical HSA domain spans over 120 Å and provides an extended binding platform for extranucleosomal entry DNA that is required for nucleosome sliding and genome-wide nucleosome positioning. Together with the recent cryo-electron microscopy structure of INO80^{Core}-nucleosome complex, our findings suggest an allosteric mechanism by which INO80 senses 40-bp linker DNA to conduct highly processive chromatin remodeling.

ATP-dependent chromatin remodelers shape the spatial and temporal organization of chromatin and generate hallmark features such as regularly spaced nucleosomal arrays flanking nucleosome-depleted regions at promoters^{1,2}. Remodelers are generally grouped into four families, INO80, SWI/SNF, ISWI, and CHD, according to sequence similarities within their common Snf2-type ATPase motor domain. They use ATP-dependent DNA translocation to catalyze different types of large-scale nucleosome remodeling reactions—sliding, eviction/assembly, positioning, and editing (histone exchange)^{3,4}.

INO80 and SWI/SNF family remodelers are mega-Dalton complexes comprising typically more than 15 different protein subunits⁴. A unifying but poorly understood key feature of these two multi-subunit remodeler families is the presence of N-actin and Arps. *Saccharomyces cerevisiae* possesses altogether ten Arps. Arp4–9 localize to the nucleus as integral, functionally important subunits of INO80 and SWI/SNF remodelers and of the histone acetyl transferase NuA4/TIP60^{4–8}. Arp4 and N-actin form an evolutionarily conserved pair in all of these enzymes, except yeast SWI/SNF and RSC, where the Arp4–N-actin pair is replaced by the diverged, but structurally related, Arp7–Arp9 pair. Structural studies of Arp4–N-actin or Arp7–Arp9 revealed binding via their barbed ends to a helical helicase-SANT-associated (HSA) domain N-terminal to the Snf2-type ATPase domain of Swr1 and Sth1, respectively^{9–11}. N-actin and nuclear Arps play an essential role in cellular stress response as well as during development^{12,13}, and respective genes, encoding, for example, the human Arp4 homolog BAF53, are frequently mutated in cancer^{13,14}. However, the precise molecular mechanism explaining the functional importance of N-actin and nuclear Arps remains still largely elusive.

The INO80 complex is particularly intriguing for studying the functional role of actin-fold proteins in the nucleus^{6,15}. In addition to N-actin and Arp4, INO80 contains with Arp5 and Arp8 in total four actin-fold proteins and is conserved in this respect from yeast to man^{6,16}. INO80 has pivotal functions in gene regulation, replication, and genome maintenance^{16,17}, as it slides¹⁵, edits¹⁸, and positions^{2,19} nucleosomes including the +1 nucleosome at promoter regions². INO80 has a modular architecture^{11,16,20,21}. The Ino80 protein subunit, harboring the Snf2-type ATPase motor, is an assembly platform for the other subunits: its N-terminal region interacts in yeast with the species-specific ‘Nhp10 module’ (a subcomplex of INO80 subunits Ies1, Ies3, Ies5, and Nhp10), which regulates the switch-like stimulation of INO80’s nucleosome sliding efficiency by extranucleosomal DNA >40 bp²². The middle region of Ino80 contains the HSA domain (Ino80^{HSA}), which binds the highly conserved ‘Arp8 module’ composed of N-actin, Arp4, Arp8, Ies4, and Taf14^{11,16}. Deletion of Arp8 or the HSA-domain leads to the loss of the whole Arp8 module and results in a remodeling defective INO80 complex^{15,16,23}. The C-terminal region of Ino80 forms the equally conserved INO80 core module (INO80^{Core}), containing the Snf2-type ATPase, Ies2, the Arp5–Ies6 complex, and the Rvb1–Rvb2 heterohexameric AAA-type ATPases. The structure and unified mechanism by which INO80^{Core} recognizes and remodels the nucleosome core particle (NCP) has been recently revealed at high resolution by cryo-electron microscopy (cryoEM)^{24,25}. We uncovered also that the function of INO80^{Core} as a macromolecular ratchet depends critically on a direct interaction of Arp5 with nucleosomal DNA²⁴. It has been proposed that other nuclear Arps could be involved in DNA or nucleosome interactions^{23,26,27}.

¹Department of Biochemistry, Ludwig-Maximilians-Universität München, Munich, Germany. ²Gene Center, Ludwig-Maximilians-Universität München, Munich, Germany. ³Chair of Molecular Biology, Biomedical Center, Faculty of Medicine, Ludwig-Maximilians-Universität München, Munich, Germany. ⁴Institute of Biophysics, Ulm University, Ulm, Germany. ⁵ChromoTek GmbH, Planegg, Germany. ⁶Center for Integrated Protein Science, Ludwig-Maximilians-Universität München, Munich, Germany. ⁷Present address: OmicScouts GmbH, Freising, Germany. ⁸Present address: Vossius & Partner, Munich, Germany. ⁹These authors contributed equally: K.R. Knoll, S. Eustermann. *e-mail: hopfner@genzentrum.lmu.de

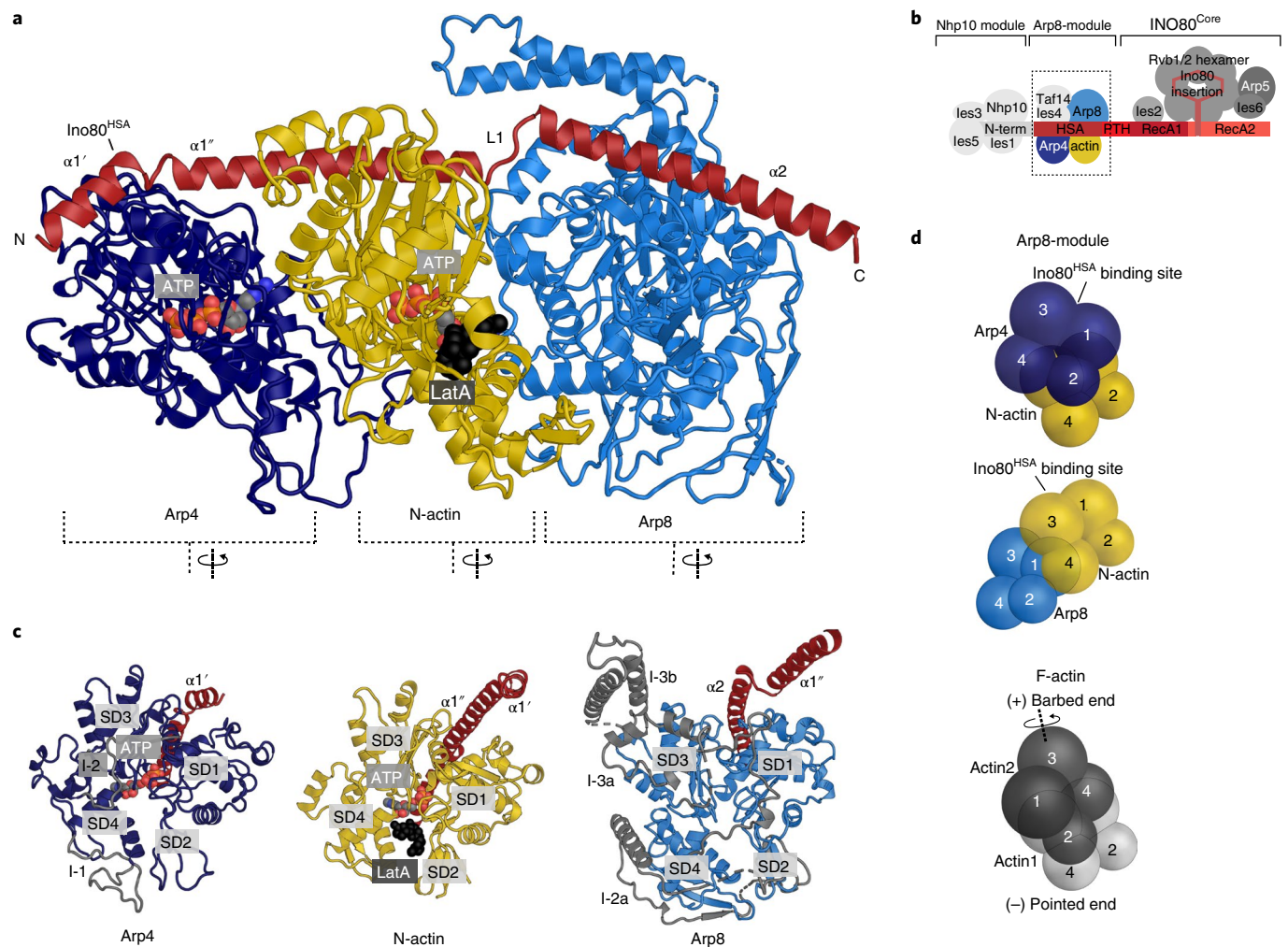


Fig. 1 | Crystal structure of the 180-kDa Ino80^{HSA}-Arp4-N-Actin-Arp8 complex. **a**, Crystal structure of the INO80 Arp8 module comprising Arp4, N-actin, Arp8, and Ino80^{HSA}. Arp4 and N-actin are ATP-bound (colored spheres), whereas Arp8 is nucleotide-free. LatA (black spheres) is bound next to ATP in the N-actin nucleotide binding cleft. **b**, Schematic overview of the *S. cerevisiae* INO80 complex illustrating its modular architecture. N-term, N-terminal region of the Ino80 polypeptide; HSA, HSA domain of Ino80; PTH, post-HSA domain of Ino80. **c**, Front views of the actin-fold proteins Arp4, N-actin, and Arp8. The Ino80^{HSA} binds to the barbed end of each of the actin folds. Actin fold insertions of Arp4 and Arp8 are shown in gray. **d**, Arrangement of actin-fold proteins. Schematics of actin folds with the individual subdomains shown as spheres. Interaction of Arp4 with N-actin, and N-actin with Arp8 in the Arp8 module is compared with two laterally interacting actin molecules in F-actin.

Indeed, our cryoEM analysis of a fungal INO80 complex, which included all evolutionarily conserved subunits, located the Arp8 module near extranucleosomal entry DNA, but its analysis was, unlike the NCP-INO80^{Core} region of the complex, limited by lower resolution. Until now, high-resolution structural information on the functionally critical architecture of the Arp8 module is missing.

Here, we report the crystal structure of the INO80 Arp8 module and identify it as an allosteric sensor of linker DNA. Strikingly, the Ino80^{HSA} adopts a segmented conformation comprising three helices that bind to the barbed ends of Arp4, N-actin, and Arp8. The Arp8 module binds extranucleosomal DNA, and we identified a conserved positively charged patch on the solvent-accessible site of the Ino80^{HSA} as responsible for DNA binding. Structure-based mutagenesis showed that binding of extranucleosomal, linker DNA by Ino80^{HSA} is critical for INO80 nucleosome sliding, but not for INO80 nucleosome binding and ATP hydrolysis. Thus, linker DNA sensing by the Arp8 module drives remodeling by INO80 via coupling motor activity to nucleosome repositioning.

Results

Crystal structure of the 180-kDa Ino80^{HSA}-Arp4-N-actin-Arp8 complex. To gain molecular and functional insights into the evolutionarily conserved Arp8 module of INO80, we determined its crystal structure (Fig. 1). N-actin, Arp4, Arp8 (residues 255–881, excluding the non-conserved N-terminal region²⁷), and Ino80^{HSA} (residues 461–598) from *S. cerevisiae* were produced in insect cells as a stoichiometric 180-kDa complex (Supplementary Fig. 1a). Initial crystallization attempts failed, most probably due to structural flexibility. In a recent study, N-actin adopted a nucleotide-free state⁹ bound to Arp4 and Swr1^{HSA}, whereas early biochemical analysis of N-actin in the human BAF complex²⁸, as well as our own structural analysis using a cameloid nanobody (see below), indicated ATP binding of N-actin. Consequently, we sought to limit the structural heterogeneity of the Arp8 module by using latrunculin A (LatA), a small molecule, sea sponge toxin that inhibits nucleotide exchange of monomeric actin²⁹. Addition of LatA yielded crystals of the complex diffracting to 4 Å, and the structure was determined by molecular replacement (see Table 1 for refinement and model statistics).

Table 1 | Data collection and refinement statistics

	NactNB-Arp4-N-actin(ATP) (PDB 5NBM)	NactNB-Arp4-N-actin(apo) (PDB 5NBL)	Ino80 ^{HSA} -Arp4-N-Actin-Arp8 (PDB 5NBN)
Data collection			
Space group	P 6 ₅	P 6 ₅	C 222 ₁
Cell dimensions			
<i>a</i> , <i>b</i> , <i>c</i> (Å)	190.58, 190.58, 220.62	191.22, 191.22, 221.97	172.29, 263.91, 241.40
α , β , γ (°)	90.00, 90.00, 120.00	90.00, 90.00, 120.00	90.00, 90.00, 90.00
Resolution (Å)	47.73–3.40 (3.50–3.40) ^a	49.43–2.80 (2.90–2.80)	49.40–4.00 (4.10–4.00)
<i>R</i> _{merge}	0.160 (1.081)	0.146 (1.107)	0.236 (1.336)
<i>I</i> / σ (<i>I</i>)	12.61 (2.19)	12.08 (2.09)	8.71 (1.87)
<i>CC</i> _{1/2}	0.996 (0.719)	0.995 (0.617)	0.996 (0.605)
Completeness (%)	100 (100)	100 (100)	100 (100)
Redundancy	6.5 (6.8)	5.9 (5.4)	9.6 (10.0)
Refinement			
Resolution (Å)	47.73–3.40 (3.50–3.40)	49.43–2.80 (2.90–2.80)	49.40–4.00 (4.10–4.00)
No. reflections	62,264 (6,206)	112,476 (11,263)	46,675 (4,625)
<i>R</i> _{work} / <i>R</i> _{free}	0.152 (0.231)/0.193 (0.281)	0.171 (0.276)/0.204 (0.316)	0.193 (0.254)/0.242 (0.288)
No. atoms			
Protein	13,949	14,000	23,029
Ligand/ion	128 ^b	64 ^c	186 ^d
Water	-	119	-
<i>B</i> factors			
Protein	92.30	58.50	121.87
Ligand/ion	85.97	38.80	101.03
Water	-	48.77	-
R.m.s. deviations			
Bond lengths (Å)	0.004	0.004	0.002
Bond angles (°)	0.66	0.70	0.68

Diffraction data from one NactNB-Arp4-N-actin(ATP), one NactNB-Arp4-N-actin(apo) and one Ino80^{HSA}-Arp4-N-Actin-Arp8 crystal were used to solve the structures. ^aValues in parentheses are for highest-resolution shell. ^bBound ligands are four ATP and four calcium ions. ^cBound ligands are two ATP and two calcium ions. ^dBound ligands are two LatA, four ATP, and four calcium ions.

Figure 1 shows the elongated architecture of the Arp8 module. Ino80^{HSA} forms a markedly segmented α -helix with helical elements $\alpha 1'$, $\alpha 1''$, and $\alpha 2$, spanning a distance of in total 120 Å (Fig. 1a). All three actin-fold proteins bind via their barbed ends to the different HSA helical elements in a similar and serial fashion, while pointed ends remain accessible (Fig. 1c). From Ino80^{HSA}'s N to C terminus, the order of binding is Arp4 (to $\alpha 1''$), N-actin (to $\alpha 1''$), and Arp8 (to $\alpha 2$). The segmentation of the HSA helix enables N-actin to form multiple contacts to both Arp4 and Arp8. Arp4 engages N-actin in a 'front-to-back' orientation in contrast to the classical fibrous (F) actin 'front to front' interaction³⁰ (Fig. 1d). However, the staggered packing of their subdomains (SDs) as well as local contacts between Arp4 and N-actin resemble lateral interactions of two F-actin subunits in a filament. In contrast, Arp8 packs against the lateral face of N-actin opposite Arp4 by using a fundamentally different 'side-to-front' type of interaction, unlike any other seen so far between actin-fold proteins. Interestingly, we observed unambiguous density for ATP in the nucleotide binding pocket of Arp4 and N-actin, whereas Arp8 remains nucleotide-free (Supplementary Fig. 1b,c). Constitutive ATP binding by Arp4 is consistent with our previous observations suggesting that Arp4 is catalytically inactive²⁶. However, N-actin may still retain its activity as part of chromatin remodelers²⁸ and was captured here in its ATP state by LatA. Of note, ATP must have been copurified with the complex from the cellular environment, as we did not add any nucleotides and LatA was added after purification.

N-actin and Arp4: a conserved heterodimer in distinct chromatin complexes. Arp4-N-actin within the Arp8 module has an overall configuration similar to Arp4-N-actin bound to Swr1^{HSA} and Arp7-Arp9 bound to Snf2^{HSA9,10}, suggesting that the Arp4-N-actin heterodimer is a structurally conserved module within the INO80 and SWI/SNF families.

To probe the Arp4-N-actin heterodimer in its native environment, we capitalized on a nanobody (denoted NactNB) that we generated from an alpaca immunized with the endogenous *S. cerevisiae* INO80 complex. Nanobodies emerged as a valuable technology to reveal physiologically important states of cellular key components^{31,32}. NactNB is highly selective for the endogenous Arp4-N-actin heterodimer. Affinity enrichment mass spectrometry of yeast whole-cell lysate using NactNB showed all 35 subunits of chromatin-associated yeast complexes containing the Arp4-N-actin heterodimer (INO80, SWR1, and NuA4) (Fig. 2a,b), suggesting that NactNB recognizes a solvent-exposed and conserved feature in all of these complexes. To reveal this binding epitope, we determined crystal structures of the Arp4-N-actin-NactNB ternary complex (Fig. 2c, Supplementary Fig. 2a, and Table 1). NactNB binds into a crevice jointly formed by the pointed ends of the two actin-folds opposite the Ino80^{HSA} binding site (Supplementary Fig. 2b). Satisfyingly, NactNB recognizes the same staggered configuration of N-actin and Arp4, as present in the structure of the Arp8 module (Arp4-N-actin heterodimers align with a backbone r.m.s.d. of 0.68 Å; number of aligned residues

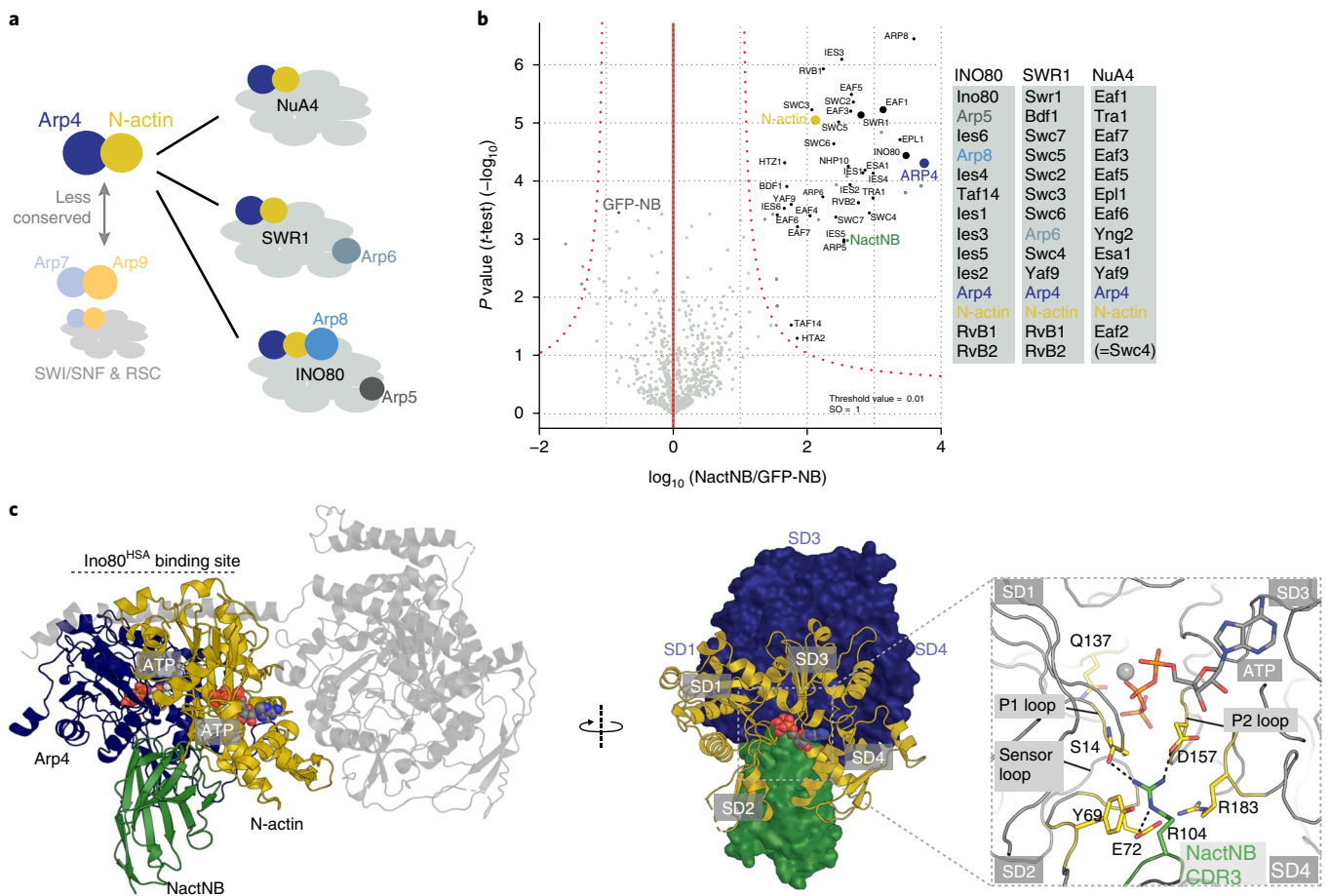


Fig. 2 | The Arp4-N-actin heterodimer is a conserved structural module of chromatin complexes. **a**, Arp4 and N-actin are conserved core components of all INO80 and SWI/SNF chromatin remodeler families, except for the *S. cerevisiae* SWI/SNF and RSC remodelers, which instead contain the sequence-divergent Arp7 and Arp9 proteins. INO80 and SWR1 contain the additional Arp5, Arp6, and Arp8 subunits. **b**, NactNB captures endogenous Arp4-N-actin heterodimer. Yeast whole-cell extract was subjected to affinity enrichment mass spectrometry experiments using NactNB and a GFP-binding nanobody as a control. Assays were performed in triplicate, and a two-sided and two-sampled *t*-test shows (in a volcano plot representation) significant enrichment of all 34 subunits of INO80, SWR1, and NuA4 complexes (see Methods for details). **c**, Structure of the Arp4-N-actin-NactNB complex in two orientations shown as cartoon and surface representations (left panel: the Arp8 module structure aligned on the Arp4-N-actin dimer is shown in light gray). N-actin and Arp4 are ATP-bound (colored spheres). Boxed 'zoom' image shows that Arg104 of NactNB binds the nucleotide binding cleft of N-actin.

(N_{align} 753 using Secondary Structure Matching³³ in COOT³⁴) and in complex with Swr1^{HSA} (Arp4-N-actin heterodimers align with an r.m.s.d. of 0.96 Å and N_{align} 724). Moreover, residual density in the nucleotide binding pocket in absence of added nucleotide as well as cocrystallization with ATP showed that NactNB recognizes the ATP state of N-actin (Supplementary Fig. 2c–e). NactNB detects the relative orientation of the two N-actin lobes and inserts Arg104 in between SD2 and SD4, where it makes hydrogen bonds to the ATP-bound conformation of Ser14 and Asp157 of the phosphate binding loop P1 and P2, respectively, as well as Glu72 of the ATP sensor loop (Fig. 2c).

Taken together, our data provide direct evidence for a conserved configuration of the Arp4-N-actin heterodimer in the complete endogenous INO80, SWR1, and NuA4 complexes and suggest that N-actin can adopt an ATP-bound state in its native environment, as previously also suggested for the human BAF complex²⁸. The conserved nature of the Arp4-N-actin heterodimer may point towards a common, yet so far unknown, functional role of this module in distinct chromatin complexes.

Arp8 recruits Arp4-N-actin to a segmented 'two-plug' scaffold of Ino80^{HSA}. Deletion of Arp8 resulted in partially assembled INO80 lacking also Arp4 and N-actin^{15,16}. It rendered yeast cells highly

sensitive to metabolic and genotoxic stress¹⁵. A similar phenotype was observed on partial removal of the Ino80^{HSA} and post-HSA domain (Ino80^{post-HSA}) (residues 531–598)²³. The structure of the Arp8 module provides a framework for rationalizing the importance of Arp8 and the Ino80^{HSA} for recruitment of the Arp4-N-actin heterodimer to the INO80 complex (Fig. 3a). Arp8 directly engages N-actin through contacts between SD1 and SD2 of Arp8 with SD3 and SD4 of N-actin. In addition, we identify a function for long insertion element I-3a of Arp8. I-3a covers the lateral surface of the Arp8 actin-fold and forms thereby a latch that consolidates the interaction with N-actin. Overall, this bipartite interaction of Arp8 recognizes a 1,392 Å² large area of the N-actin lateral face opposite Arp4 and thus specifically helps to recruit and retain the interaction of Arp4-N-actin with Ino80^{HSA}.

Previous models proposed that N-actin and Arps are recruited to chromatin remodelers by a long, continuous HSA helix that provides a binding platform for barbed ends of actin-fold proteins^{9,10}. While the general helical structure and serial binding of Arp4 and N-actin barbed ends are consistent with this model, Ino80^{HSA} adopts a distinct segmented structure (Fig. 3b and Supplementary Fig. 3a,b). The N-terminal helix α 1 (residues 472–518), bound to the barbed ends of Arp4 and N-actin, has a pronounced kink at position 483–485 that divides it into segments α 1' and α 1". The C-terminal

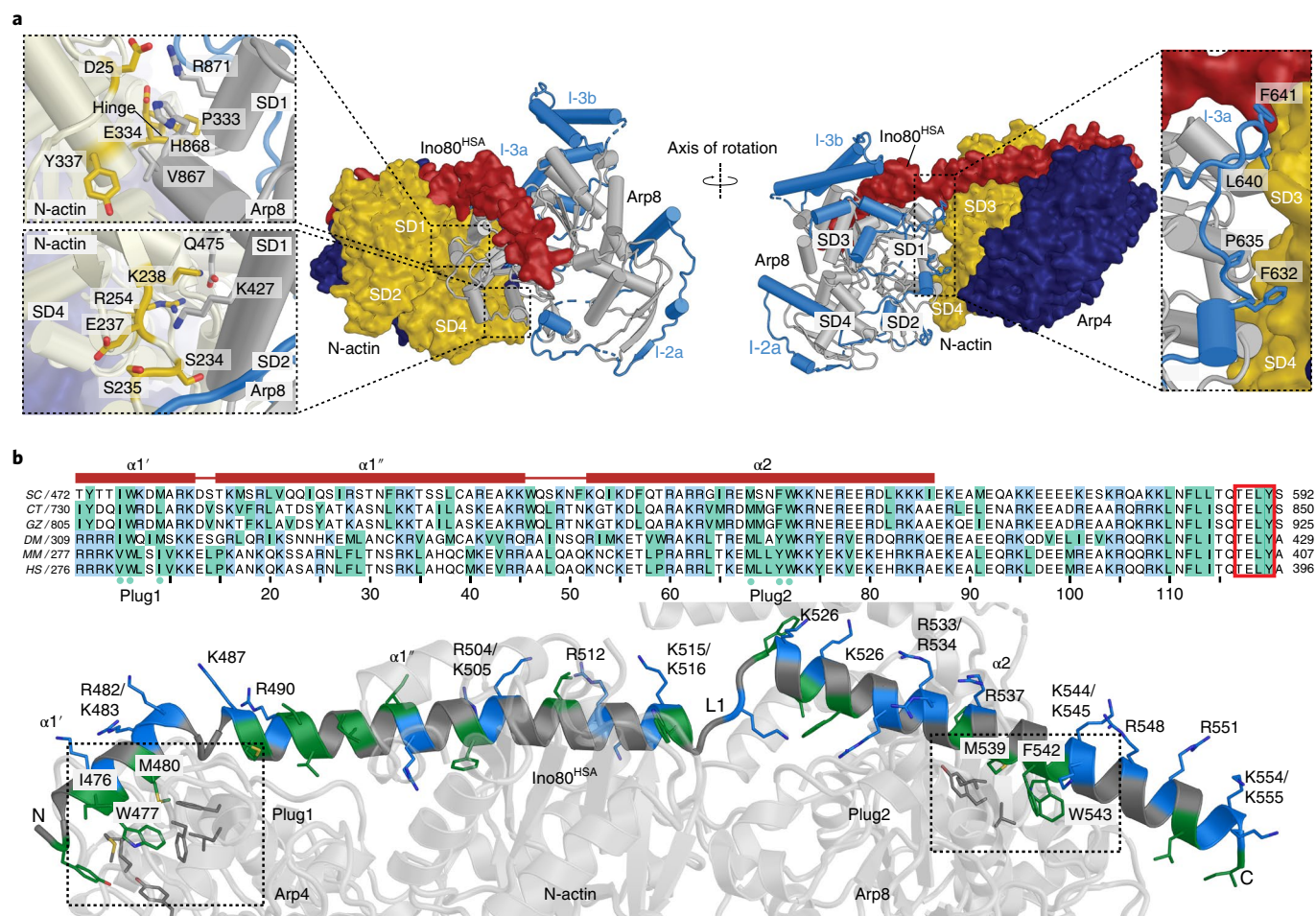


Fig. 3 | Arp8 recruits Arp4-N-actin to a segmented 'two-plug' scaffold of Ino80^{HSA}. **a**, Cartoon and surface representations of the Arp8 module displaying interaction sites between Arp8 and N-actin. The Arp8 actin core fold is colored in gray and the insertions in blue. Arp8 contacts N-actin SD3 and -4 via its actin core fold, with SD1 and -2 (boxed close-ups in the left panel), and its actin fold insertion 3a (close-up in the right panel). **b**, Sequence alignment of Ino80^{HSA} from different species, with positively charged residues (Arg and Lys) colored in blue and hydrophobic residues (Ile, Leu, Trp, Val, Phe, Tyr, and Met) in green. The region visualized in the crystal structure is indicated by red lines above the sequences. The highly conserved TELY motif is highlighted by a red rectangle. Green dots below the sequences emphasize conserved hydrophobic residues in Plug1 and Plug2 that bind Arp4 and Arp8, respectively. Below, cartoon representation of the Arp8 module. The Ino80^{HSA} domain is shown, with hydrophobic residues colored in green and positively charged residues colored in blue.

helix $\alpha 2$ (residues 522–557) forms the third segment, bound to the barbed end of Arp8. We identified two hydrophobic residue clusters (Plug 1 and Plug 2) that define the register and contain each an anchoring tryptophan residue. A structural shift resulting from segmentation of $\alpha 1$ enables Plug 1 (Ile476, Trp477, and Met480) to insert into a hydrophobic pocket of the barbed end of Arp4 (Fig. 3b and Supplementary Fig. 3c), while well-defined loop L1 in between $\alpha 1''$ and $\alpha 2$ shifts $\alpha 2$, enabling insertion of Plug 2 (Met539, Phe542, and Trp543) into a hydrophobic pocket of the barbed end of Arp8. The latter interaction appears to be critical not only for recruitment of Arp8 but also of the Arp4-N-actin dimer. The previously reported partial removal of the Ino80^{HSA} and Ino80^{post-HSA} includes Plug2 of $\alpha 2$ and leads to loss of the entire Arp8 module *in vivo*²³, although the Arp4-N-actin binding site of the Ino80^{HSA} is still intact. The distance between the two hydrophobic plugs in conjunction with the asymmetry of Ino80^{HSA} segmentation matches the unique arrangement of actin-folds within the sandwich-like structure of Arp4, N-actin, and Arp8. In addition, loop L1 and the resulting translational and rotational shift of $\alpha 2$ enable formation of the extensive contacts between N-actin and Arp8 that would not be

possible for a continuous HSA helix. Thus, our structure shows how Arp8 specifies recruitment of the Arp4-N-actin heterodimer to the segmented, 'two-plug' scaffold of the helical Ino80^{HSA}.

Ino80^{HSA} of the Arp8 module binds extranucleosomal DNA.

Our recent cryoEM study of the INO80^{Core}-nucleosome complex revealed density of the Arp8 module adjacent to the well resolved nucleosomal DNA entry site, where the Ino80 Snf2-motor domain pumps DNA into the nucleosome²⁴ (Fig. 4a). To test for binding of the Arp8 module to nucleosomal and extranucleosomal DNA, we performed electro mobility shift assays (EMSA) where nucleosomes with (0N80) and without (0N0) 80 bp extranucleosomal DNA on one side compete for binding the Arp8 module (Fig. 4b). In such competition assays, the Arp8 module showed a clear binding preference for the 0N80 over the 0N0 nucleosome, showing that the Arp8 module binds extranucleosomal DNA.

Combination of the INO80^{Core}-nucleosome complex cryoEM structure²⁴ and the Arp8 module crystal structure leads directly to a structural model of how the Arp8 module might be located at extranucleosomal DNA, as discussed further below. In this

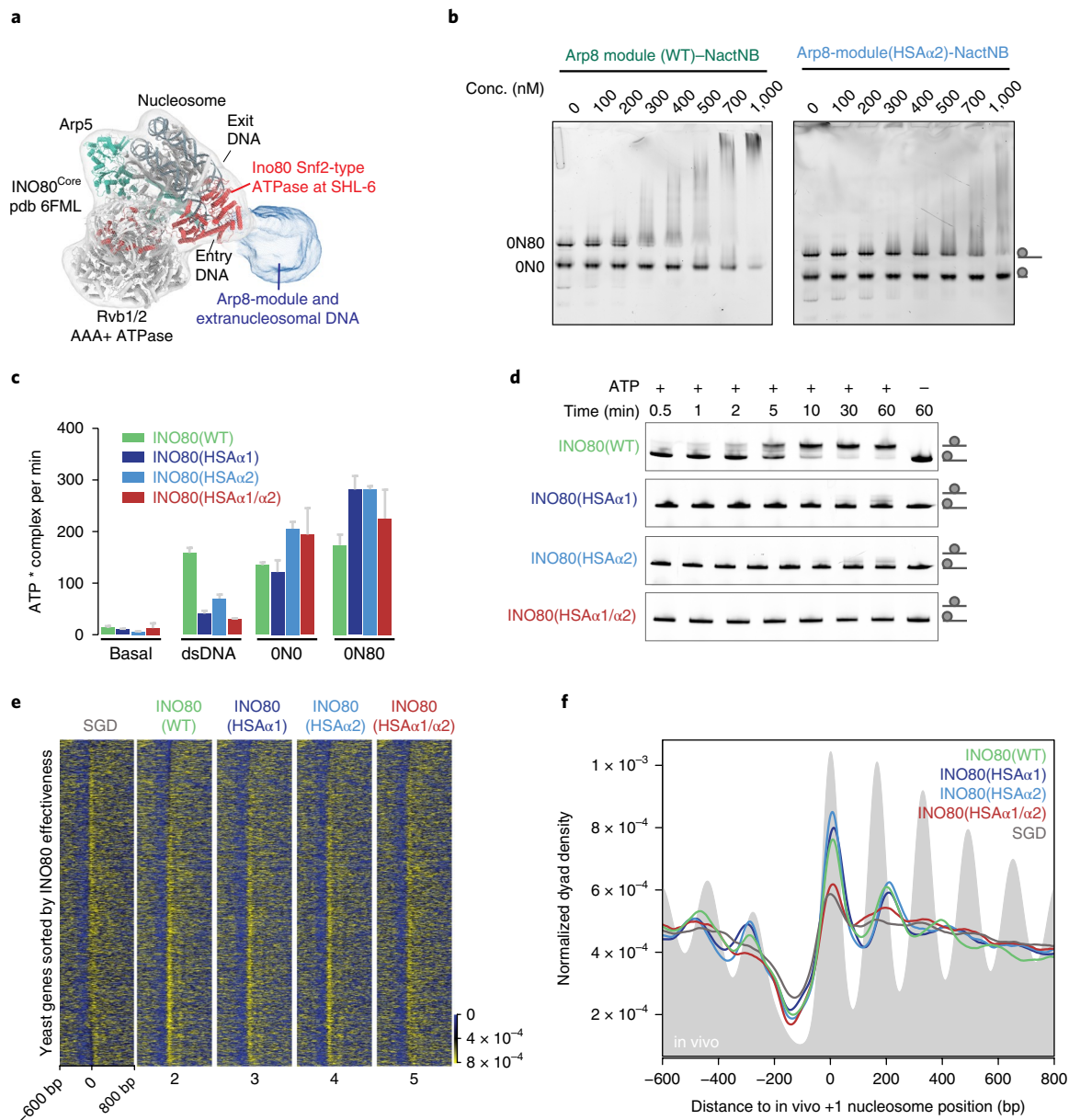


Fig. 4 | Extranucleosomal DNA binding by the Arp8 module is critical for INO80 nucleosome sliding and genome-wide nucleosome positioning.

a, CryoEM density of the INO80-nucleosome complex²⁴, with a structural model for Ino80^{Motor}, les2, Arp5, les6, and the Rvb1-Rvb2 heterohexamer bound to an NCP. Density next to the nucleosomal DNA entry site could be assigned to the Arp8 module (colored in blue). **b**, Competition EMSAs with two nucleosome species (20 nM each; one with (ON80) and one without (ON0) an 80-bp extranucleosomal DNA overhang), showing a clear binding preference of the Arp8 module for ON80 nucleosomes. Mutation of solvent-exposed basic residues on helix α 2 of Ino80^{HSA} (HSA α 2) decreases ON80 binding by the Arp8 module. Assays were performed in triplicate. Conc., molar concentration in nM; WT, wild type. **c**, INO80 (27 nM) ATPase activity, basal or stimulated with 223-bp dsDNA (100 nM), ON0 (100 nM), and ON80 (50 nM) nucleosomes. Error bars represent the mean \pm s.d. from three independent experiments. **d**, Time course of ATP-dependent INO80 nucleosome (ON80) sliding on a single mononucleosome substrate (with 18 nM IN80 and 90 nM ON80). Reaction product (end-positioned nucleosome) and product (center-positioned nucleosome) were resolved by NativePAGE. Assays were performed in triplicate. **e**, Genome-wide nucleosome positioning by INO80 (18 nM). Heat map displaying color-coded nucleosome dyad density of YCp50 plasmid library yeast genes aligned on the in vivo-defined +1 nucleosome dyad (0 bp) position, after sequence-intrinsic nucleosome positioning by salt gradient dialysis (SGD), or after additional incubation with indicated wild-type or mutant INO80 complexes. Rows are sorted according to INO80 effectiveness. **f**, Composite plots of heat maps shown in **e**. Grey background displays in vivo nucleosome positioning. Genome-wide nucleosome positioning assays were performed in duplicate. Uncropped gel images are shown in Supplementary Data Set 1.

model, Ino80^{HSA} mediates direct binding of extranucleosomal DNA along the barbed ends of Arp8, N-actin, and Arp4. In isolation, neither actin and Arp4 nor human Arp8 bind double-stranded DNA (dsDNA) with considerable affinity²⁶, while the Ino80^{HSA} was proposed from sequence analysis to be part of a dsDNA binding

domain of Ino80³⁵. Having the crystal structure for Ino80^{HSA}, we noticed a set of highly conserved, solvent-accessible lysine and arginine residues that may account for binding of extranucleosomal DNA (Fig. 3b and Supplementary Fig. 4a). To test this hypothesis, we mutated several of these lysine and arginine residues

in the Ino80^{HSA} $\alpha 2$ helix to glutamines (HSA $\alpha 2$). We observed lower expression yields of the mutated minimal Arp8 module, indicating perhaps destabilizing effects of the mutations by lowering the helix propensity of Ino80^{HSA}. However, using complex-stabilizing NactNB for purification provided sufficient quantities of stable material for DNA binding studies (Supplementary Fig. 4b). Fluorescence anisotropy analysis on binding of generic 40bp dsDNA and competition EMSAs with 0N0 and 0N80 nucleosomes showed that binding of NactNB at the pointed end of N-actin only slightly reduced dsDNA binding (around twofold; Supplementary Fig. 4c,d). So, we used NactNB to rule out that any loss of DNA binding is induced by weakening of the complex. Importantly, the $\alpha 2$ mutations substantially reduced binding of the Arp8 module both to dsDNA (Supplementary Fig. 4c) and nucleosomes (Fig. 4b and Supplementary Fig. 4d). Thus, we conclude that the positively charged HSA domain of Ino80 provides a binding site for extra-nucleosomal DNA.

Arp8 module is important for nucleosome sliding and genome-wide nucleosome positioning. To assess the mechanistic impact of DNA binding by the Arp8 module on nucleosome remodeling by INO80 (Fig. 4), we mutated Ino80^{HSA} in the context of the entire INO80 complex (Supplementary Fig. 4e). Parallel to this study, we established an insect cell co-expression approach for expression and purification of the entire *S. cerevisiae* 15-subunit INO80 complex. Such recombinant INO80 retains the activity of the endogenous complex, but is fully amenable to site-directed mutagenesis (to be published elsewhere by: Krietenstein Nils, Oberbeckmann Elisa, Niebauer Vanessa, Schall Kevin, Schwarz Marianne, Moldt Manuela, Tobias Straub, Korber Philipp, Hopfner Karl-Peter, and Eustermann Sebastian). Using this system, we were able to purify stable INO80 complexes with wild-type-like stoichiometry of all subunits, and also if full-length Ino80 with mutated HSA was co-expressed together with all other 14 subunits of INO80 (Supplementary Fig. 4f). EMSAs with 0N80 nucleosomes showed homogenous complex formation at similar concentrations for wild-type as well as for mutant INO80 (Supplementary Fig. 4g). This was in contrast to the decreased binding affinity of Ino80–HSA $\alpha 2$ in context of the isolated Arp8 module and suggests that binding of the entire complex to nucleosomes is mostly dominated by subunits other than the minimal Arp8 module; for example, subunits of the INO80 core that interact directly with the nucleosome, or other DNA binding subunits such as the Nhp10 module. Of note, Arp8 in the recombinant 15-subunit INO80 complex contains the full N-terminal tail in contrast to the construct used for crystallization. Although the N-terminal region of Arp8 is not well conserved among species, it might additionally contribute to nucleosome interactions, DNA binding, or complex stability.

However, despite retaining high-affinity nucleosome interactions, mutations of the Ino80^{HSA} domain markedly affected dsDNA-stimulated ATPase and ATP-dependent nucleosome sliding activity of INO80. ATP hydrolysis by wild-type INO80 is robustly stimulated on addition of dsDNA or 0N80 nucleosomes (Fig. 4c). Mutations of the helix $\alpha 1$ or $\alpha 2$ of Ino80^{HSA} impaired ATPase stimulation by dsDNA, while the same mutants showed similar or even moderately faster ATP hydrolysis rates than wild-type complex if stimulated by 0N80 nucleosomes. Despite this similar or increased ATP turnover, HSA mutations substantially decreased INO80's activity to slide 0N80 nucleosomes towards the center of a 225-bp DNA substrate (Fig. 4d). Mutations of either helix $\alpha 1$ or $\alpha 2$ reduced nucleosome centering to residual levels, while mutations targeting both helices abrogated this remodeling activity completely.

Given this mechanistic impact on sliding activity in a specialized mononucleosome context, we asked whether Ino80^{HSA} is also more generally important to mobilize and position nucleosomes across the whole yeast genome. To this end, we employed a genome-wide

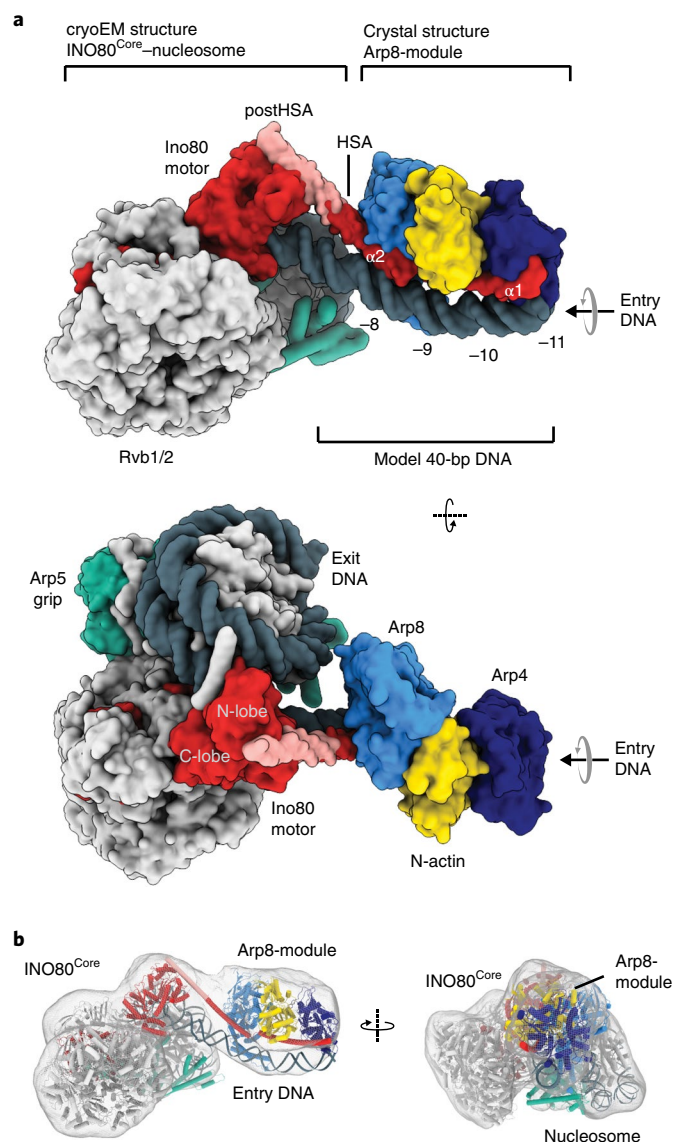


Fig. 5 | Structural model of the INO80^{Core+Arp}-nucleosome complex.

a, Model of the INO80^{Core+Arp}-nucleosome complex (shown as surface representation) based on the INO80^{Core}-nucleosome cryoEM structure²⁴ and the Arp8 module crystal structure (this study). **b**, Previously published cryoEM density map of the INO80^{Core+Arp}-nucleosome complex²⁴ with the model of the INO80^{Core+Arp}-nucleosome complex fitted into the density.

reconstitution approach, where it was shown previously that purified INO80 on its own is able to properly position +1 nucleosomes on a genomic plasmid library². A similarly direct analysis of INO80's nucleosome positioning activity would be inherently difficult in vivo, given the complex interplay between different remodeler families as well as other factors such as the transcription and replication machinery^{3,36}. Micrococcal nuclease digestion and next generation DNA sequencing (MNase-seq) was used as read out for nucleosome positions across the genomic plasmid library before and after incubation with INO80 and ATP. In contrast to the strongly decreased sliding activity with a mononucleosomal substrate based on the 'Widom 601' sequence (Fig. 4d), INO80 mutations targeting HSA helix $\alpha 1$ or $\alpha 2$ individually did not compromise average patterns of genomic +1 nucleosome positioning (Fig. 4e,f). This finding is intriguing as it suggests that nucleosomes on genomic DNA in plasmids may be a less demanding substrate for translocation and positioning than a 'Widom 601' mononucleosome. This could be,

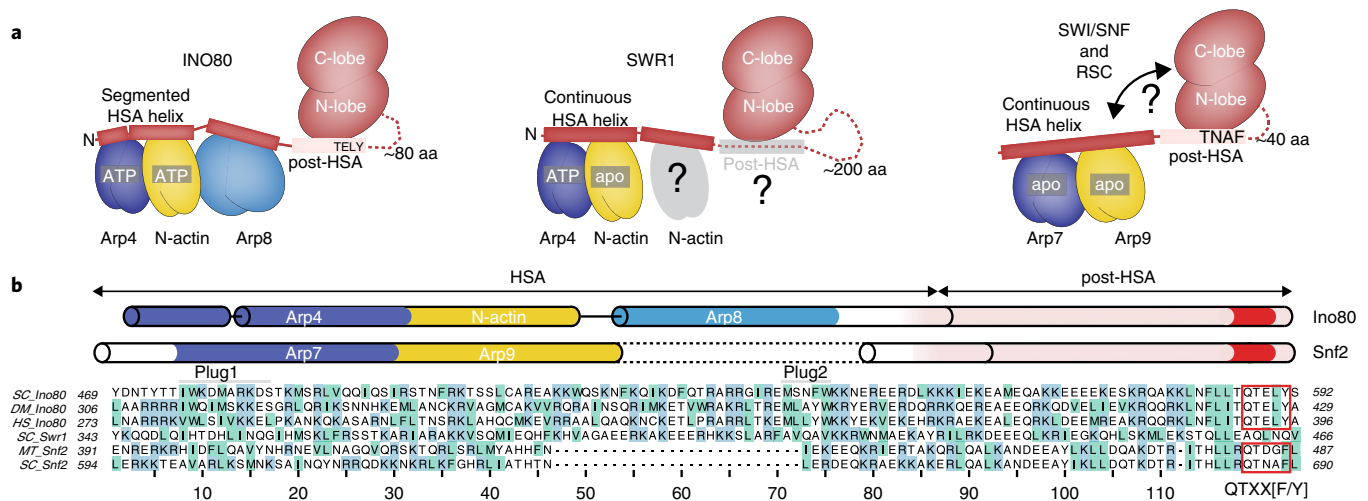


Fig. 6 | Conserved architecture of N-actin-Arp modules in INO80/SWR1 and SWI/SNF family chromatin remodelers. **a**, Organization of the N-actin-Arp modules in INO80, SWR1, and RSC remodelers with respect to the Snf2-type ATPase. The schematic representation is based on our Ino80^{Core+Arp}-nucleosome model (shown in Fig. 5a), the structure-based sequence alignment shown in **b**, and the crystal structures of Arp4-N-actin-Swr1^{HSA} (PDB 519E), Arp7-Arp9-Snf2^{HSA} (PDB 416M), Arp4-N-actin-Arp8-Ino80^{HSA}, and Snf2 in complex with a nucleosome (PDB 5HZR). Conformation of the respective HSA domains (red) is illustrated by a continuous or segmented helix. The post-HSA of Ino80 and Snf2 (pink) interacts directly with N-lobe of the Snf2-type ATPase (red) and is connected via a linker region (dotted line). The nucleotide state of the actin-fold proteins is indicated according to the respective crystal structure. Interestingly, recent biochemical analysis suggested that the Swr1^{HSA} is bound by Arp4 and two N-actin molecules⁴⁹. Our structure-based alignment shown in **b** reveals that the Arp8 binding site of Ino80^{HSA} corresponds to the second N-actin site in Swr1^{HSA}. aa, amino acids. **b**, Structure-based sequence alignment of the HSA and post-HSA domains of Ino80, Snf2, and Swr1 (basic and hydrophobic residues are highlighted in blue and light green, respectively). Binding sites for Arps and N-actin are conserved between the INO80 and SWI/SNF remodeler families. Our structure-based alignment reveals that the Ino80^{post-HSA} (Q)TELY motif is related to the Snf2^{post-HSA} QTXX[F/Y] motif.

for example, due to the presence of multiple nucleosomes, extranucleosomal DNA on both sides, the absence of DNA ends, or due to lower intrinsic nucleosome stabilities. The former three possibilities seemed unlikely as remodeling an internal nucleosome within an array of 601 sequences separated by 50 bp extranucleosomal DNA³⁷ was also strongly impaired by mutations targeting either HSA helix individually (Supplementary Fig. 4h,i). Importantly, however, mutation of both HSA helices $\alpha 1$ and $\alpha 2$ at the same time abolished INO80 nucleosome remodeling on all tested substrates including genome-wide nucleosome positioning (Fig. 4d-f and Supplementary Fig. 4j).

Taken together, our biochemical results identify a critical role for binding extranucleosomal DNA by the Arp8 module in coupling the energy derived from ATP hydrolysis to productive nucleosome sliding by INO80. Such chemo-mechanical coupling may be particularly important to mobilize nucleosomes in the context of sequences that strongly bind the histone octamer, such as the 601 sequence. Positioning of +1 nucleosomes guided by promoter sequences is likely to involve also other parts of the INO80 complex, such as the Nhp10 module.

A structural model of the INO80-nucleosome complex including its Arp8 module. Combination of the 4.3-Å cryoEM structure of the *C. thermophilum* INO80^{Core}-nucleosome complex²⁴ with the 4-Å *S. cerevisiae* crystal structure of the 180-kDa Arp8 module leads directly to a composite model of the evolutionarily conserved INO80^{Core+Arp} complex bound to a nucleosome with a molecular weight of approximately 1 MDa (Fig. 5a). The two structures can be joined in silico by the highly conserved post-HSA and HSA domains of Ino80: helix $\alpha 2$ of the HSA domain crystal structure needs to be extended by only 35 C-terminal residues to include the post-HSA helix that is present in the cryoEM structure²⁴. This structural model is consistent with the mapping of INO80 subunits onto nucleosomal substrates in vivo³⁸, in vitro³⁹, and with our previous cryoEM

data²⁴ as it places the Arp8 module into the large unassigned density patch (Figs. 4a and 5b) and at the same time maintains a continuous HSA and post-HSA helical structure. In particular, we observed cryoEM density for an extended post-HSA-HSA helix pointing from the N-terminal lobe of the Snf2-type ATPase domain at SHL-6 towards entry DNA at SHL-8²⁴. Moreover, the elongated architecture of the Arp8 module accommodates approximately 40 bp extranucleosomal entry DNA and fits thereby into the low-resolution reconstruction obtained for the entire 11-subunit INO80^{Core+Arp}-nucleosome complex²⁴. The 120-Å HSA domain is positioned along the dsDNA with conserved arginine and lysine residues contacting the phosphate backbone as probed by our biochemical experiments described above. Helix $\alpha 2$ contacts the DNA around SHL-8 while the N-terminal helix $\alpha 1$ reaches SHL-10 to -11. Consequently, Arp8 resides on the extranucleosomal DNA proximal to the Snf2-type ATPase of Ino80, while the Arp4-N-actin heterodimer binds in a distal position. The model is therefore consistent with promoter binding of Arp8 proximal to the +1 nucleosome in vivo³⁸, as well as cross-linking of Arp4-N-actin heterodimer to extranucleosomal DNA at position -110 nt (SHL-11) in vitro³⁹. However, given the flexibility of the Arp8 module in the cryoEM reconstructions, we do not rule out the presence of other conformations and positions of this module during the functional cycle of INO80 in nucleosome remodeling.

Discussion

Here, we provide a structure and function for the enigmatic, evolutionarily conserved actin-fold subunits Arp4, N-actin, and Arp8 in the INO80 chromatin remodeler. We show that the three actin-fold proteins in complex with the Ino80^{HSA} form an extended structural element that recognizes extranucleosomal, linker DNA, a critical feature of INO80 mechanism and function.

INO80 is a highly processive chromatin remodeler^{22,40} and we recently proposed a mechanism by which INO80 core subunits

function as a macromolecular ratchet²⁴: minor groove tracking by the Ino80 Snf2-type ATPase motor at SHL-6 pumps DNA in multiple 1–2 bp steps against a grip formed by Arp5–Ies6 at SHL-2/-3 until DNA propagates around the histone octamer and translocates nucleosomes by a large step size. Indeed, 10–20 bp translocation steps are observed^{22,41}, and a kinetic model has been proposed describing the dependency of INO80 on extranucleosomal DNA²²: the activity of the ATPase motor does not result in efficient DNA translocation unless more than 40 bp of entry DNA are available; the pumped DNA might otherwise collapse backwards²². Intriguingly, the footprint of the Arp8 module matches this limiting length of 40 bp DNA (Fig. 5a). If less than 40 bp extranucleosomal, linker DNA are available, pumping an additional 10–20 bp DNA into the nucleosome would substantially shorten the entry DNA beyond this limit; that is, pull away the DNA and thereby abrogate the contacts between DNA and the distal part of the HSA domain, where the Arp4–N-actin heterodimer binds. Consequently, this scenario recapitulates the impact of HSA mutations that also lead to loss of extranucleosomal DNA binding and reduce nucleosome sliding to residual levels, most probably caused by ‘back-slippage’ of DNA. By combining our structural and biochemical data with previous kinetic insights²², we thus propose that the Arp8 module within INO80 functions as sensor of extranucleosomal DNA, mechanistically coupling ATP-dependent DNA pumping to processive nucleosome translocation.

Biochemical and genetic evidence for the SWI/SNF chromatin remodeler family suggests that the yeast Arp7–Arp9 module of RSC has a role similar to that proposed here for the Arp8 module of INO80, as it also couples ATP-dependent DNA translocation of the Snf2-type Sth1 motor domain to nucleosome remodeling such as translocation and ejection⁴². It was proposed that the post-HSA domain of Sth1 acts as a ‘throttle’ controlling ATPase activity⁴². Indeed, our structural study shows that the post-HSA domain interacts with the N-lobe of Ino80²⁴ in a homologous manner as previously observed for Snf2⁴³ and Sth1⁴⁴. A structure-based alignment reveals that the highly conserved (Q)TELY motif⁵ of the Ino80^{post-HSA} domain is related to the QTXX[F/Y] motif of Snf2 (Fig. 6a,b), while the interaction with protrusion-I provides, together with brace helix-I, a key allosteric site for controlling DNA groove tracking by the ATPase motor^{42,43}. Despite recent progress^{10,42,44,45}, it is still elusive how the Arp7–Arp9 module of RSC functions at a molecular level. It was suggested that the module folds back onto the Sth1 motor domain acting as ‘clutch’ to promote nucleosome remodeling. While INO80 might adopt a closed conformation in absence of a nucleosome^{46,47}, our structural and biochemical data suggest an extended conformation of the Arp8 module which enables extranucleosomal DNA binding. The interplay between the HSA and post-HSA domains may thus link sensing of extranucleosomal DNA to allosteric control of the Snf2-like motor domain of Ino80.

Sensing of linker DNA is a hallmark of chromatin remodelers since it provides mechano-chemical means to conduct higher order remodeling reactions such as spacing and phasing of nucleosomes in genic arrays^{4,48}. Future studies will use the mechanistic insights discovered here as a framework to dissect such functions and will show whether they may provide unifying principles for regulation of the INO80 and SWI/SNF families of multi-subunit chromatin remodelers.

Methods

Methods, including statements of data availability and any associated accession codes and references, are available at <https://doi.org/10.1038/s41594-018-0115-8>.

Received: 24 April 2018; Accepted: 17 July 2018;
Published online: 3 September 2018

References

- Jiang, C. & Pugh, B. F. Nucleosome positioning and gene regulation: advances through genomics. *Nat. Rev. Genet.* **10**, 161–172 (2009).
- Krietenstein, N. et al. Genomic nucleosome organization reconstituted with pure proteins. *Cell* **167**, 709–721.e12 (2016).
- Hopfner, K. P., Gerhold, C. B., Lakomek, K. & Wollmann, P. Swi2/Snf2 remodelers: hybrid views on hybrid molecular machines. *Curr. Opin. Struct. Biol.* **22**, 225–233 (2012).
- Clapier, C. R., Iwasa, J., Cairns, B. R. & Peterson, C. L. Mechanisms of action and regulation of ATP-dependent chromatin-remodelling complexes. *Nat. Rev. Mol. Cell Biol.* **18**, 407–422 (2017).
- Dion, V., Shimada, K. & Gasser, S. M. Actin-related proteins in the nucleus: life beyond chromatin remodelers. *Curr. Opin. Cell Biol.* **22**, 383–391 (2010).
- Shen, X., Mizuguchi, G., Hamiche, A. & Wu, C. A chromatin remodelling complex involved in transcription and DNA processing. *Nature* **406**, 541–544 (2000).
- Peterson, C. L., Zhao, Y. & Chait, B. T. Subunits of the yeast SWI/SNF complex are members of the actin-related protein (ARP) family. *J. Biol. Chem.* **273**, 23641–23644 (1998).
- Cairns, B. R., Erdjument-Bromage, H., Tempst, P., Winston, F. & Kornberg, R. D. Two actin-related proteins are shared functional components of the chromatin-remodeling complexes RSC and SWI/SNF. *Mol. Cell* **2**, 639–651 (1998).
- Cao, T. et al. Crystal structure of a nuclear actin ternary complex. *Proc. Natl Acad. Sci. USA* **113**, 8985–8990 (2016).
- Schubert, H. L. et al. Structure of an actin-related subcomplex of the SWI/SNF chromatin remodeler. *Proc. Natl Acad. Sci. USA* **110**, 3345–3350 (2013).
- Szerlong, H. et al. The HSA domain binds nuclear actin-related proteins to regulate chromatin-remodeling ATPases. *Nat. Struct. Mol. Biol.* **15**, 469–476 (2008).
- Meagher, R. B., Kandasamy, M. K., Smith, A. P. & McKinney, E. C. Nuclear actin-related proteins at the core of epigenetic control. *Plant Signal. Behav.* **5**, 518–522 (2010).
- Son, E. Y. & Crabtree, G. R. The role of BAF (mSWI/SNF) complexes in mammalian neural development. *Am. J. Med. Genet. C* **166C**, 333–349 (2014).
- Hodges, C., Kirkland, J.G. & Crabtree, G.R. The many roles of BAF (mSWI/SNF) and PBAF complexes in cancer. *Cold Spring Harb. Perspect. Med.* **6**, (2016).
- Shen, X., Ranallo, R., Choi, E. & Wu, C. Involvement of actin-related proteins in ATP-dependent chromatin remodeling. *Mol. Cell* **12**, 147–155 (2003).
- Tosi, A. et al. Structure and subunit topology of the INO80 chromatin remodeler and its nucleosome complex. *Cell* **154**, 1207–1219 (2013).
- Gerhold, C. B. & Gasser, S. M. INO80 and SWR complexes: relating structure to function in chromatin remodeling. *Trends Cell Biol.* **24**, 619–631 (2014).
- Papamichos-Chronakis, M., Watanabe, S., Rando, O. J. & Peterson, C. L. Global regulation of H2A.Z localization by the INO80 chromatin-remodeling enzyme is essential for genome integrity. *Cell* **144**, 200–213 (2011).
- Udugama, M., Sabri, A. & Bartholomew, B. The INO80 ATP-dependent chromatin remodeling complex is a nucleosome spacing factor. *Mol. Cell Biol.* **31**, 662–673 (2011).
- Chen, L. et al. Subunit organization of the human INO80 chromatin remodeling complex: an evolutionarily conserved core complex catalyzes ATP-dependent nucleosome remodeling. *J. Biol. Chem.* **286**, 11283–11289 (2011).
- Jonsson, Z. O., Jha, S., Wohlschlegel, J. A. & Dutta, A. Rvb1p/Rvb2p recruit Arp5p and assemble a functional Ino80 chromatin remodeling complex. *Mol. Cell* **16**, 465–477 (2004).
- Zhou, C. Y. et al. The yeast INO80 complex operates as a tunable DNA length-sensitive switch to regulate nucleosome sliding. *Mol. Cell* **69**, 677–688.e9 (2018).
- Kapoor, P., Chen, M., Winkler, D. D., Luger, K. & Shen, X. Evidence for monomeric actin function in INO80 chromatin remodeling. *Nat. Struct. Mol. Biol.* **20**, 426–432 (2013).
- Eustermann, S. et al. Structural basis for ATP-dependent chromatin remodelling by the INO80 complex. *Nature* **556**, 386–390 (2018).
- Ayala, R. et al. Structure and regulation of the human INO80–nucleosome complex. *Nature* **556**, 391–395 (2018).
- Gerhold, C. B. et al. Structure of Actin-related protein 8 and its contribution to nucleosome binding. *Nucleic Acids Res.* **40**, 11036–11046 (2012).
- Saravanan, M. et al. Interactions between the nucleosome histone core and Arp8 in the INO80 chromatin remodeling complex. *Proc. Natl Acad. Sci. USA* **109**, 20883–20888 (2012).
- Zhao, K. et al. Rapid and phosphoinositol-dependent binding of the SWI/SNF-like BAF complex to chromatin after T lymphocyte receptor signaling. *Cell* **95**, 625–636 (1998).
- Dominguez, R. & Holmes, K. C. Actin structure and function. *Annu. Rev. Biophys.* **40**, 169–186 (2011).

30. von der Ecken, J. et al. Structure of the F-actin-tropomyosin complex. *Nature* **519**, 114–117 (2015).
31. Huang, W. et al. Structural insights into micro-opioid receptor activation. *Nature* **524**, 315–321 (2015).
32. Rasmussen, S. G. et al. Crystal structure of the beta2 adrenergic receptor-Gs protein complex. *Nature* **477**, 549–555 (2011).
33. Krissinel, E. & Henrick, K. Secondary-structure matching (SSM), a new tool for fast protein structure alignment in three dimensions. *Acta Crystallogr. D Biol. Crystallogr.* **60**, 2256–2268 (2004).
34. Emsley, P., Lohkamp, B., Scott, W. G. & Cowtan, K. Features and development of Coot. *Acta Crystallogr. D Biol. Crystallogr.* **66**, 486–501 (2010).
35. Bakshi, R., Prakash, T., Dash, D. & Brahmachari, V. In silico characterization of the INO80 subfamily of SWI2/SNF2 chromatin remodeling proteins. *Biochem. Biophys. Res. Commun.* **320**, 197–204 (2004).
36. Yen, K., Vinayachandran, V., Batta, K., Koerber, R. T. & Pugh, B. F. Genome-wide nucleosome specificity and directionality of chromatin remodelers. *Cell* **149**, 1461–1473 (2012).
37. Mueller-Planitz, F., Klinker, H., Ludwigsen, J. & Becker, P. B. The ATPase domain of ISWI is an autonomous nucleosome remodeling machine. *Nat. Struct. Mol. Biol.* **20**, 82–89 (2013).
38. Yen, K., Vinayachandran, V. & Pugh, B. F. SWR-C and INO80 chromatin remodelers recognize nucleosome-free regions near +1 nucleosomes. *Cell* **154**, 1246–1256 (2013).
39. Brahma, S., Ngubo, M., Paul, S., Udugama, M. & Bartholomew, B. The Arp8 and Arp4 module acts as a DNA sensor controlling INO80 chromatin remodeling. *Nat. Commun.* <https://doi.org/10.1038/s41467-018-05710-7> (2018).
40. Schwarz, M. et al. Single-molecule nucleosome remodeling by INO80 and effects of histone tails. *FEBS Lett.* **592**, 318–331 (2018).
41. Brahma, S. et al. INO80 exchanges H2A.Z for H2A by translocating on DNA proximal to histone dimers. *Nat. Commun.* **8**, 15616 (2017).
42. Clapier, C. R. et al. Regulation of DNA translocation efficiency within the chromatin remodeler RSC/Sth1 potentiates nucleosome sliding and ejection. *Mol. Cell* **62**, 453–461 (2016).
43. Liu, X., Li, M., Xia, X., Li, X. & Chen, Z. Mechanism of chromatin remodelling revealed by the Snf2-nucleosome structure. *Nature* **544**, 440 (2017).
44. Turegun, B., Baker, R. W., Leschziner, A. E. & Dominguez, R. Actin-related proteins regulate the RSC chromatin remodeler by weakening intramolecular interactions of the Sth1 ATPase. *Commun. Biol.* **1**, 1 (2018).
45. Turegun, B., Kast, D.J. & Dominguez, R. Subunit Rtt102 controls the conformation of the Arp7/9 heterodimer and its interactions with nucleotide and the catalytic subunit of SWI/SNF remodelers. *J. Biol. Chem.* (2013).
46. Aramayo, R. J. et al. Cryo-EM structures of the human INO80 chromatin-remodeling complex. *Nat. Struct. Mol. Biol.* **25**, 37–44 (2018).
47. Watanabe, S. et al. Structural analyses of the chromatin remodelling enzymes INO80-C and SWR-C. *Nat. Commun.* **6**, 7108 (2015).
48. Yamada, K. et al. Structure and mechanism of the chromatin remodelling factor ISW1a. *Nature* **472**, 448–453 (2011).
49. Lin, C.-L. et al. Functional characterization and architecture of recombinant yeast SWR1 histone exchange complex. *Nucleic Acids Res.* **45**, 7249–7260 (2017).

Acknowledgements

We are grateful to M. Moldt for technical support and J. Michaelis, Gregor Witte, Katja Lames, and Robert Byrne for discussion and technical help. We thank the Max-Planck Crystallization Facility (Martinsried, Germany), the staff of the Swiss Light Source (Villingen, Switzerland), and the European-Molecular-Biology-Laboratory/Deutsches-Elektronen-Synchrotron (Hamburg, Germany) for support and measurement time. We thank S. Krebs and H. Blum at the Laboratory of Functional Genome Analysis (Gene Center, LMU Munich) for high-throughput sequencing. We thank T. Straub (Bioinformatics Core Unit, Biomedical Center, LMU Munich) for advice on bioinformatics. This work is supported by the Deutsche Forschungsgemeinschaft CRC1064 (to K.-P.H. and P.K.) and the European Research Council (ERC Advanced Grant ATMMACHINE), the Gottfried-Wilhelm-Leibniz Prize, and the Center for Integrated Protein Sciences Munich to K.-P.H. K.R.K. is supported by GRK1721. S.E. acknowledges an EMBO long-term fellowship. V.N., K.S., and M.S. acknowledge funding by Quantitative Biosciences Munich.

Author contributions

K.R.K. and S.E. determined the structures and built atomic models. K.R.K. prepared samples for crystallization and performed biochemical analysis of the Arp8 module. S.E., A.T., M.S., and A.B. identified the Arp4–N-actin binding nanobody and performed its initial characterization. K.R.K. and G.S. performed affinity enrichment mass spectrometry analysis. S.E. and K.P.H. devised with a contribution of M.S. preparation and characterization of recombinant INO80 complex. V.N. prepared mutant complexes and performed their biochemical analysis. V.N. and E.O. performed and analyzed genome-wide remodeling assays under supervision by P.K. K.S. prepared nucleosomes. S.E. and K.-P.H. designed the overall study, analyzed the results, and wrote the paper with contributions from K.R.K., V.N., E.O., and P.K.

Competing interests

The authors declare no competing interests.

Additional information

Supplementary information is available for this paper at <https://doi.org/10.1038/s41594-018-0115-8>.

Reprints and permissions information is available at www.nature.com/reprints.

Correspondence and requests for materials should be addressed to K.-P.H.

Publisher's note: Springer Nature remains neutral with regard to jurisdictional claims in published maps and institutional affiliations.

Methods

Nanobody generation. For generation of the Arp4–N-actin binding nanobody (NactNB), an alpaca was immunized with purified and cross-linked endogenous INO80 complex. INO80 complex for immunization was prepared as earlier described¹⁶. Alpaca immunization, nanobody library generation, and selection of INO80 binding nanobodies were performed as previously published³⁰ by ChromoTek GmbH.

Cloning, protein expression, and purification. *Nanobody (NactNB).* The DNA sequence coding NactNB carrying a C-terminal Twin-Strep-Tag was cloned into a pHEN6 vector upstream of the pelB leader sequence⁵¹. *Escherichia coli* Rosetta (DE3) cells (Merck Millipore) were transformed with the pHEN6–NactNB vector. Freshly transformed cells were cultured at 37 °C in lysogeny broth containing 100 µg ml⁻¹ ampicillin. Protein was expressed for 2 h at 22 °C after induction with 0.3 mM isopropyl β-D-1-thiogalactopyranoside at an optical density at 600 nm of 0.6. All protein purification steps were performed at 4 °C. Cells were collected by centrifugation and subsequently incubated for 30 min in lysis buffer (50 mM Tris pH 8.0, 300 mM NaCl, 1× protease inhibitor cocktail (Sigma-Aldrich), 1 mg ml⁻¹ lysozyme (Carl Roth), and 12.5 units ml⁻¹ benzonase (unit is a measure for the amount of the enzyme and defined by the vendor Sigma-Aldrich)) for periplasmic lysis. The cell debris were separated by centrifugation. NactNB was purified from the soluble extract via the C-terminal Twin-Strep-Tag using Strep-Tactin Sepharose (IBA) in 50 mM Tris pH 8.0 and 300 mM NaCl. NactNB bound to Strep-Tactin Sepharose was stored at 4 °C and used within 2 d for pull-down assays or eluted with buffer containing 2.5 mM D-desthiobiotin.

Arp4–N-actin–NactNB complex. *S. cerevisiae* genes coding for Arp4, Arp8, actin, Taf14, Ies1, Ies2, Ies3, Ies4, Ies5, and Nhp10 were combined in a single pFBDM vector using the MultiBac system⁵². Integration of genes from the pFBDM vector into the baculoviral genome was performed in DH10MultiBac cells (GenevaBiotech), baculovirus generation in *Spodoptera frugiperda* Sf21 insect cells (IPLB-Sf21AE Invitrogen), and protein co-expression in *Trichoplusia ni* High Five insect cells (BTI-TN-5B1-4 Invitrogen) according to a published protocol⁵². High Five cells were transfected 1/100 (v/v) with baculovirus. Cells were cultured for 60 h at 27 °C until they were collected by centrifugation. Cells were lysed by sonication in 50 mM Tris pH 8, 300 mM NaCl, 5% glycerol, and 1× protease inhibitor cocktail (Sigma-Aldrich). The raw cell lysate was cleared by centrifugation. NactNB-bound Strep-Tactin Sepharose was used to isolate the Arp4–N-actin heterodimer from the soluble cell extract. The Arp4–N-actin–NactNB complex was washed with 50 mM Tris pH 8, 300 mM NaCl, and 5% glycerol and eluted with 50 mM Tris pH 8, 300 mM NaCl, 5% glycerol, and 2.5 mM D-desthiobiotin. The ternary complex was further purified by ion-exchange chromatography with a HiTrapQ HP column (GE Healthcare; linear gradient 100 mM to 1 M NaCl) and gel filtration with a Superdex 200 column (GE Healthcare) equilibrated with 20 mM HEPES pH 8 and 200 mM NaCl. Pure protein was concentrated to a final concentration of 16–20 mg ml⁻¹, flash frozen in liquid nitrogen, and stored at –80 °C.

Arp8 module. Genes encoding *S. cerevisiae* Arp4 and actin were cloned into one pFBDM vector and those coding for *S. cerevisiae* Arp8 (residues 255–881; the non-conserved N-terminal residues 1–254 were deleted²⁷) and Ino80^{HSA} (residues 462–598) carrying a C-terminal StrepTag II were combined on a second pFBDM vector⁵². Baculoviruses for the respective vectors were generated in Sf21 insect cells as described above. For the co-expression of the four proteins, High Five insect cells (BTI-TN-5B1-4 Invitrogen) were co-infected with the two viruses (1/100 (v/v) each), cultivated for 60 h at 27 °C, and collected by centrifugation. High Five cells were lysed by sonication in 20 mM HEPES pH 7.8, 100 mM KCl, 2.5% glycerol, and 1× protease inhibitor cocktail (Sigma-Aldrich). The complex was purified from the cleared cell lysate by affinity chromatography using Strep-Tactin Sepharose (IBA), ion exchange chromatography with a HiTrapQ HP column (GE Healthcare; linear gradient 100–800 mM NaCl), and gel filtration with a Superdex 200 column (GE Healthcare) equilibrated with 20 mM HEPES pH 8, 150 mM KCl, 2.5% glycerol, and 1 mM dithiothreitol. Peak fractions containing homogenous Arp8 module complex were pooled, concentrated, flash frozen, and stored at –80 °C.

For the Arp8 module Ino80–HSAα2 mutant (see Supplementary Table 1 for the mutated sequence range), a single pACE–Bac vector encoding expression cassettes for *S. cerevisiae* Arp4, actin, Arp8 (residues 255–881), and Ino80–HSAα2 (residues 462–598 + C-terminal StrepTag II) was generated by using the latest MultiBac system⁵². Generation of the baculovirus, expression in High Five insect cells, and purification of the wild-type and the HSAα2 mutant Arp8 module in complex with NactNB were performed in principle as described above. Prior purification of the respective complex 1 mg of purified NactNB (purification of NactNB is described above) was added directly to 20 ml of cleared insect cell lysate. Further purification followed the procedure described before for the wild-type Arp8 module.

INO80 complex. Purification of recombinant expressed *S. cerevisiae* INO80 complex from insect cells will be published elsewhere (unpublished data by: Krietenstein Nils, Oberbeckmann Elisa, Niebauer Vanessa, Schall Kevin, Schwarz Marianne, Moldt Manuela, Korber Philipp, Hopfner Karl-Peter, and Eustermann Sebastian). Briefly, two Baculoviruses were generated by MultiBac technology⁵² using coding sequences for *S. cerevisiae* Ino80(2x Flag), Rvb1, Rvb2, Arp4,

Arp5-His, Arp8, Actin, Taf14, Ies1, Ies2, Ies3, Ies4, Ies5, Ies6, and Nhp10 subcloned into pFBDM vectors. For expression, High Five insect cells (BTI-TN-5B1-4 Invitrogen) were co-infected with the two baculoviruses 1/100 (v/v) each. INO80 complex was purified from the insect cells according to a previous published protocol¹⁶ which resulted in a pure and monodisperse sample.

INO80 complex HSA mutants were prepared as described for wild-type INO80. Three Ino80(2x Flag) HSA mutants (HSAα1, HSAα2, or HSAα1/α2) were generated using standard cloning techniques and integrated into above-described Baculovirus using MultiBac technology⁵² (mutated residues are shown in Supplementary Fig. 4e and Supplementary Table 1).

Preparation of human mononucleosomes. Canonical human histones were essentially purified as described previously⁵³.

Briefly, *E. Coli* BL21 (DE3) cells (Novagen) were used to express histones for 2 h at 37 °C. Cells were disrupted using non-denaturing conditions and inclusion bodies were washed using 1% Triton X-100. Guanidinium chloride (7 M) was used for resuspension and inclusion bodies were dialyzed in urea (8 M). Cation exchange chromatography was applied to purify histones. After refolding of histones under low-salt conditions, an anion exchange chromatography step was used as a final purification step. Histones were lyophilized for long-time storage. To assemble histone octamers, single histones were resuspended in 7 M guanidinium chloride, mixed at a 1.2-fold excess of H2A/ H2B, and dialyzed against 2 M NaCl for 16 h. Size exclusion chromatography (Superdex 200 16/600 column; GE Healthcare) was used to purify histone octamers, which were then stored in 50% glycerol at –20 °C. For the purpose of mononucleosome reconstitution we used fluorescein-labeled Widom 601 DNA⁵⁴ with 80 bp extranucleosomal DNA in the ON80 orientation⁵⁵ or without extranucleosomal DNA (ON0). After amplification by PCR, the DNA was purified using anion exchange chromatography and concentrated by applying vacuum. Histone octamers and DNA were mixed at 1.1-fold excess of DNA at 2 M NaCl. The sodium chloride concentration was then decreased to a final concentration of 50 mM over 17 h at 4 °C. In a final step, NCPs were purified using anion exchange chromatography. After dialysis to 50 mM NaCl, NCPs were concentrated to 1 mg ml⁻¹ and stored at 4 °C.

Crystallization. *Arp4–N-actin–NactNB.* Before crystallization the Arp4–N-actin–NactNB complex (16 mg ml⁻¹) was mixed with subtilisin (1:6,000 (w/protease)/w(complex)) for in-drop proteolysis, 0.2 mM CaCl₂, and either 1 mM ATP (buffered at pH 7.5 in 100 mM Tris) for the N-actin ATP-bound structure or with 1 mM ADP (buffered at pH 7.5 in 100 mM Tris) for the nucleotide-free (apo) structure. Crystals were grown by hanging-drop vapor diffusion at 20 °C in 1.4–1.5 M sodium malonate at pH 6.0. The best diffracting crystals were harvested after 4–8 d and cryo-protected with 23% glycerol.

Ino80^{HSA}–Arp4–N-actin–Arp8. For the crystallization of the Ino80^{HSA}–Arp4–N-actin–Arp8 complex, protein solution (13 mg ml⁻¹) was mixed with LatA (for the LatA stock solution LatA was dissolved in 100% dimethylsulfoxide to a final concentration of 10 mM) at a molar ratio of 1:1.5 (complex/LatA). Crystals were grown by hanging-drop vapor diffusion at 4 °C against 0.1 M sodium citrate tribasic dihydrate and 18% w/v polyethylene glycol 3,350. The crystals were collected after 30 d and cryo-protected with 20% glycerol.

Data collection and processing, structure determination, and refinement.

Diffraction data from all crystals were collected at 100 K with a wavelength of 1.0 Å at the Swiss Light Source beamline X06SA. Data were processed with XDS⁵⁶ and scaled with POINTLESS and AIMLESS within the CCP4 suite⁵⁷.

Arp4–N-actin–NactNB. The two structures of the Arp4–N-actin–NactNB complex with N-actin ATP bound (Protein Data Bank (PDB) 5NBM) and nucleotide-free (apo) (PDB 5NBL) were determined by molecular replacement with Phaser⁵⁸. For a first model, structures of *S. cerevisiae* actin (PDB 1YAG) and Arp4 (PDB 3QB0) were used as search models following the removal of any nucleotides, water molecules, or metal atoms. A homology model of NactNB was generated using the PHYRE server⁵⁹ and the three complementarity-determining region loops were deleted before its use as a search model. Sequential search analyses with two copies of each of the search models for Arp4, actin, and NactNB resulted in a unique solution for two copies of the ternary complex per asymmetric unit. The initial model was used as search model for the analysis of the diffraction data sets from crystals grown in presence of ATP or ADP giving immediately a single solution with two complexes per asymmetric unit for both structures. In crystals grown with ATP, N-actin was clearly ATP bound. In contrast, in crystals grown in presence of ADP, N-actin was nucleotide-free. First models were then improved by iterative rounds of model refinement with *phenix.refine*⁶⁰ and manual model building with COOT⁶¹. Both electron density maps contain density for a peptide of unknown source that we could not assign to any sequence of the expressed proteins. This density was therefore modeled as a poly-UNK (unknown amino acid) peptide. The final model of the N-actin(ATP)–Arp4–NactNB complex (PDB 5NBM) at 3.4 Å resolution has $R_{\text{work}}/R_{\text{free}}$ values of 15.2%/19.3% and the model of the N-actin(apo)–Arp4–NactNB complex (PDB 5NBL) at 2.8 Å resolution has $R_{\text{work}}/R_{\text{free}}$ values of 17.1%/20.4% (Table 1).

Ino80^{HSA}-Arp4-N-Actin-Arp8. The Ino80^{HSA}-Arp4-N-Actin-Arp8 structure (PDB 5NBN) was determined by molecular replacement with Phaser⁵⁸. The Arp4-N-actin-NactNB structure (PDB 5NBM) without NactNB and the yeast Arp8CTD structure (PDB 4AM6) were used as search models following the removal of any ligands or waters molecules. A single solution containing two copies of the Arp4-N-actin-Arp8 complex per asymmetric unit was found. Clear difference density for the Ino80^{HSA} domain was visible in the initial map after molecular replacement. The model was improved through iterative rounds of refinement with *phenix.refine*⁶⁰, applying secondary structure restraints and NCS restraints, and manual model building with COOT³⁴. The Ino80^{HSA} domain was built manually with COOT³⁴ using B-factor sharpening and feature-enhanced maps⁶¹ (calculated by *phenix.fem*) for model building. Density for bound nucleotides at the canonical nucleotide binding sites of Arp4 and N-actin could be identified as ATP. Building and refinement of ADP into the unbiased density map showed in both cases clear difference density for a missing gamma-phosphate. Subsequent refinement shows similar B-factors for the alpha, beta, and gamma phosphate of each ATP molecule. The final model of the Ino80^{HSA}-Arp4-N-Actin-Arp8 complex at 4.0 Å resolution has $R_{\text{work}}/R_{\text{free}}$ values of 19.3%/24.2% (Table 1).

Structures were analyzed using COOT³⁴ and PISA⁶². Superposition of structures was performed by using the Secondary Structure Matching³³ algorithm in COOT³⁴. Figures of structures were prepared with PyMOL⁶³ and ChimeraX⁶⁴.

Affinity enrichment mass spectrometry. Yeast with a double FLAG-tagged INO80 (Genotype: MATa INO80-FLAG₂ his3Δ200 leu2Δ0 met15Δ0 trp1Δ63 ura3Δ0; kindly provided by X. Shen⁶) were grown for 2 d in YPD medium at 30 °C. Cells were collected by centrifugation. Pellets were re-suspended 5:1 (w/yeast)/w(buffer) in 20 mM HEPES pH 7.8. The cell suspension was dripped into liquid nitrogen and the frozen cells were lysed using a freezer mill (SPEX SamplePrep). The frozen cell powder was stored at -80 °C until usage.

Frozen yeast cell powder (20 g) was thawed in 20 ml lysis buffer (25 mM HEPES pH 8.0, 500 mM KCl, 10% glycerol, 0.05% NP40, 1 mM EDTA, 4 mM MgCl₂, and 1× protease inhibitor cocktail (Sigma-Aldrich)). Chromatin was fragmented with a polytron homogenizer (Kinematica; Fisher Scientific) and by sonication (Branson). The raw cell lysate was cleared by centrifugation and 250 μg ml⁻¹ avidin (IBA) was added.

The specific-binder nanobody (NactNB) and the control nanobody (enhancer GFP nanobody; eGFP-NB)⁶⁵ both had a C-terminal Twin-Strep-Tag and were expressed and purified as described for above for NactNB. NactNB or eGFP-NB immobilized on Strep-Tactin Sepharose were incubated with equal amounts of cleared yeast cell lysate. Unbound protein was removed by washing with buffer W1 (25 mM HEPES pH 8.0, 500 mM KCl, 10% glycerol, 0.05% NP40, 1 mM EDTA, and 4 mM MgCl₂) followed by buffer W2 (25 mM HEPES pH 8.0, 200 mM KCl, 10% glycerol, 1 mM EDTA, and 4 mM MgCl₂).

Samples for liquid chromatography-tandem mass spectrometry measurement were in principle prepared as published before⁶⁶. Briefly, equal amounts of the nanobody Strep-Tactin Sepharose beads from each pull-down were incubated in buffer E1 (50 mM Tris-HCl pH 7.5, 2 M urea, 5 μg ml⁻¹ trypsin (Promega), and 1 mM dithiothreitol) for 30 min at 30 °C for on-bead digest. Any remaining peptides were eluted from the beads and alkylated with buffer E2 (50 mM Tris-HCl pH 7.5, 2 M urea, 5 mM iodoacetamide). Elution fractions were pooled and incubated in the dark overnight at 32 °C. The digestion was stopped by the addition of 1% trifluoroacetic acid. Samples were loaded on self-made C18 reversed-phase StageTips for purification and enrichment following a standard protocol⁶⁷. Peptides were eluted with 2 × 20 μl buffer B (80% ACN and 0.5% AcOH) and concentrated using a SpeedVac concentrator to a final volume of 5–10 μl. Finally, 2.5 μl buffer A* (2% ACN, 1% TFA) and 2.5 μl buffer A (0.5% AcOH) were added to the sample.

Peptide samples were measured on a liquid chromatography-tandem mass spectrometry system using an ultra-high performance liquid chromatography system (EASY-nLC 1000) coupled to an LTQ Orbitrap Elite (both Thermo Scientific) equipped with a standard nanoelectrospray source. Peptides were loaded onto a 15-cm × 0.050-mm inner diameter reversed phase column packed with 2 μm C18 beads (Acclaim PepMap RSLC analytical column, Thermo Scientific) and subsequently separated using a 90-min gradient of solvent B (98% ACN, 0.1% FA) from 2% to 35% at a flow rate of 250 nL min⁻¹.

*.RAW files from the eGFP-NB (mock) and NactNB triplicate experiments were analyzed together using the MaxQuant software suite (version 1.5.2.18) including the label-free algorithm for label-free quantification intensity calculation⁶⁸. Downstream data analysis was performed in the Perseus environment (version 1.5.0.9)⁶⁹. Briefly, label-free quantification intensity values were log₁₀ transformed, the data were filtered for at least two valid values in at least one of the two conditions, and missing values were imputed using a normal distribution at the noise level (width: 0.3 s.d. of the data; down shift: 1.8 s.d. of the valid data). To reveal significant outliers, a two-sample *t*-test was performed and data were visualized using an in-house R script.

Fluorescence anisotropy. Arp8 module in solution 40 bp dsDNA binding affinity was measured by fluorescence anisotropy in principle as described before⁷⁰.

Equimolar amounts of the two complementary DNA strands (forward 5'-3': fluorescein-CCCTGGCGACTTCGCCTCGTTTTGGCGATTTCCTAGCAAA TATTCTTTC and reverse 5'-3': GAAAGAATATTGCTAAGAAAATCGCCA

AAACGAGGCGAAGTCGCCAGGG), solved in water, were heated to 95 °C for 10 min and slowly cooled at room temperature to anneal the two DNA strands. Arp8 module was diluted to the respective working concentration and incubated with 20 nM dsDNA on ice for 30 min in 20 mM Tris pH 7.8, 50 mM KCl, and 2.5% glycerol in a total volume of 100 μl. Fluorescence anisotropy was measured in a black flat-bottomed non-binding 96-well plate (Greiner-Bio) on a Tecan Infinite M1000 plate reader (excitation wavelength 470 nm, emission wavelength 520 nm).

Data were analyzed and fitted to a non-linear, non-cooperative 1:1 binding model ($y = Af - (Af - Ab) \times (x / (Kd + x))$); *y* anisotropy; *Af* anisotropy of free ligand; *Ab* Anisotropy of bound ligand; *Kd* dissociation constant; *x* receptor concentration) with the program Prism (GraphPad) to calculate the dissociation constants for the respective complex. Experiments were performed in triplicate.

EMSAs. The Arp8 module binding preference for mononucleosomes with or without extranucleosomal DNA was examined with competition EMSAs.

Increasing amounts of Arp8 module were titrated against a 1:1 mixture of 0N0 and 0N80 (20 nM each) mononucleosomes in 10 mM HEPES pH 8.0, 2 mM MgCl₂, 60 mM NaCl, 8% glycerol, and incubated for 20 min on ice. Then, 15 μl of each titration step were loaded on a precast native polyacrylamide gel (NativePAGE Novex 4–16% Bis-Tris Protein Gels; Invitrogen). Arp8 module bound and unbound nucleosomes were resolved by Native-PAGE in 1× NativePAGE Running Buffer (Invitrogen; according to the manufacturer protocol) at 120 V for 120 min at 4 °C. Gels were analyzed on a Typhoon FLA 9000 plate reader (GE Healthcare) with 25 μm pixel size, using FITC fluorescence scan.

To test the binding capability of INO80 to nucleosomes, a titration of the complex was carried out. Increasing amounts of the protein in 25 mM Hepes, pH 8.0, 60 mM KCl, 7% glycerol, and 1 mM CaCl₂ were incubated with 20 nM 0N80 nucleosomes for 30 min on ice. INO80 bound and unbound nucleosomes were resolved by NativePAGE (Novex 4–16% Bis-Tris Protein Gels; Invitrogen) and subsequently visualized on a Typhoon FLA 9000 plate reader as described above.

Nucleosome sliding assays. The nucleosome sliding activity of INO80 was monitored on 0N80 mononucleosomes.

INO80 (18 nM) was incubated with 90 nM 0N80 nucleosomes in sliding buffer (25 mM Hepes, pH 8.0, 60 mM KCl, 7% glycerol, 0.10 mg ml⁻¹ BSA, 0.25 mM dithiothreitol, 2 mM MgCl₂) at 26 °C. The sliding reaction was started by the addition of ATP and MgCl₂ (final concentrations: 1 mM ATP and 2 mM MgCl₂). At the respective time points (30, 60, 120, 300, 600, 1,800, and 3,600 s), the reaction was stopped by adding lambda DNA (NEB) to a final concentration of 0.2 mg ml⁻¹. NativePAGE (NativePAGE Novex 4–16% Bis-Tris Protein Gels; Invitrogen) was used to separate distinct nucleosome species. Gels were visualized on a Typhoon FLA 9000 plate reader as described above.

ATPase assays. In order to determine the ATPase rate of INO80, we applied an NADH-based ATPase assay in principle as described in^{24,71}.

Briefly, 27 nM INO80 was incubated in assay buffer (25 mM Hepes, pH 8.0, 50 mM KCl, 5 mM MgCl₂, 0.1 mg ml⁻¹ BSA) with 0.5 mM phosphoenolpyruvate, 2 mM ATP, 0.2 mM NADH, and 25 units ml⁻¹ lactate dehydrogenase/pyruvate kinase (unit is a measure for the amount of the enzymes and defined by the vendor Sigma-Aldrich) in a final volume of 50 μl at 30 °C. The Tecan Infinite M100 (Tecan) was used to monitor the NADH dependent fluorescence signal in non-binding, black, 384-well plates (Greiner) at an excitation wavelength of 340 nm and an emission wavelength of 460 nm over a time course of 40 min. ATPase activity for all samples was determined at conditions of maximum INO80 wild-type ATPase activity. Stimulation was performed with 50 nM 0N80 nucleosome, 100 nM 0N0 nucleosome, or 100 nM 223 bp DNA (DNA template used to reconstitute 0N80 nucleosomes). The final ATP turnover rate was calculated using maximal initial linear rates, which were corrected for a buffer blank.

The genome-wide in vitro reconstitution assay and the restriction enzyme accessibility assay are described in the Supplementary Note.

Reporting Summary. Further information on research design is available in the Nature Research Reporting Summary linked to this article.

Data availability. Coordinates and structure factors have been deposited in the PDB under accession codes 5NBM for the N-actin(ATP)-Arp4-NactNB module, 5NBL for the N-actin(apo)-Arp4-NactNB module, and 5NBN for the Ino80^{HSA}-Arp4-N-actin-Arp8 structures. Data for the genome-wide nucleosome positioning experiments reported in this paper have been deposited in the Gene Expression Omnibus under accession number GSE113401. All other data and materials are available from the corresponding author on reasonable request.

References

- Rothbauer, U. et al. Targeting and tracing antigens in live cells with fluorescent nanobodies. *Nat. Methods* **3**, 887–889 (2006).
- Conrath, K. E. et al. Beta-lactamase inhibitors derived from single-domain antibody fragments elicited in the camelidae. *Antimicrob. Agents Chemother.* **45**, 2807–2812 (2001).

52. Trowitzsch, S., Bieniossek, C., Nie, Y., Garzoni, F. & Berger, I. New baculovirus expression tools for recombinant protein complex production. *J. Struct. Biol.* **172**, 45–54 (2010).
53. Dyer, P. N. et al. Reconstitution of nucleosome core particles from recombinant histones and DNA. *Methods Enzymol.* **375**, 23–44 (2004).
54. Lowary, P. T. & Widom, J. New DNA sequence rules for high affinity binding to histone octamer and sequence-directed nucleosome positioning. *J. Mol. Biol.* **276**, 19–42 (1998).
55. Levendosky, R.F., Sabantsev, A., Deindl, S. & Bowman, G.D. The Chd1 chromatin remodeler shifts hexasomes unidirectionally. *eLife* **5** (2016).
56. Kabsch, W. XDS. *Acta Crystallogr. D Biol. Crystallogr.* **66**, 125–132 (2010).
57. Winn, M. D. et al. Overview of the CCP4 suite and current developments. *Acta Crystallogr. D Biol. Crystallogr.* **67**, 235–242 (2011).
58. McCoy, A. J. et al. Phaser crystallographic software. *J. Appl. Crystallogr.* **40**, 658–674 (2007).
59. Kelley, L. A., Mezulis, S., Yates, C. M., Wass, M. N. & Sternberg, M. J. The Phyre2 web portal for protein modeling, prediction and analysis. *Nat. Protoc.* **10**, 845–858 (2015).
60. Adams, P. D. et al. PHENIX: a comprehensive Python-based system for macromolecular structure solution. *Acta Crystallogr. D Biol. Crystallogr.* **66**, 213–221 (2010).
61. Afonine, P. V. et al. FEM: feature-enhanced map. *Acta Crystallogr. D Biol. Crystallogr.* **71**, 646–666 (2015).
62. Krissinel, E. & Henrick, K. Inference of macromolecular assemblies from crystalline state. *J. Mol. Biol.* **372**, 774–797 (2007).
63. *The PyMOL Molecular Graphics System, Version 1.8.* (Schrodinger, LLC, 2015).
64. Goddard, T. D. et al. UCSF ChimeraX: meeting modern challenges in visualization and analysis. *Protein Sci.* **27**, 14–25 (2018).
65. Kirchhofer, A. et al. Modulation of protein properties in living cells using nanobodies. *Nat. Struct. Mol. Biol.* **17**, 133–138 (2010).
66. Keilhauer, E. C., Hein, M. Y. & Mann, M. Accurate protein complex retrieval by affinity enrichment mass spectrometry (AE-MS) rather than affinity purification mass spectrometry (AP-MS). *Mol. Cell. Proteomics* **14**, 120–135 (2015).
67. Rappsilber, J., Mann, M. & Ishihama, Y. Protocol for micro-purification, enrichment, pre-fractionation and storage of peptides for proteomics using StageTips. *Nat. Protoc.* **2**, 1896–1906 (2007).
68. Cox, J. et al. Accurate proteome-wide label-free quantification by delayed normalization and maximal peptide ratio extraction, termed MaxLFQ. *Mol. Cell. Proteomics* **13**, 2513–2526 (2014).
69. Tyanova, S. et al. The Perseus computational platform for comprehensive analysis of (prote)omics data. *Nat. Methods* **13**, 731–740 (2016).
70. Favicchio, R., Dragan, A. I., Kneale, G. G. & Read, C. M. Fluorescence spectroscopy and anisotropy in the analysis of DNA-protein interactions. *Methods Mol. Biol.* **543**, 589–611 (2009).
71. Kiiianitsa, K., Solinger, J. A. & Heyer, W.-D. NADH-coupled microplate photometric assay for kinetic studies of ATP-hydrolyzing enzymes with low and high specific activities. *Anal. Biochem.* **321**, 266–271 (2003).

Reporting Summary

Nature Research wishes to improve the reproducibility of the work that we publish. This form provides structure for consistency and transparency in reporting. For further information on Nature Research policies, see [Authors & Referees](#) and the [Editorial Policy Checklist](#).

Statistical parameters

When statistical analyses are reported, confirm that the following items are present in the relevant location (e.g. figure legend, table legend, main text, or Methods section).

n/a Confirmed

- The exact sample size (n) for each experimental group/condition, given as a discrete number and unit of measurement
- An indication of whether measurements were taken from distinct samples or whether the same sample was measured repeatedly
- The statistical test(s) used AND whether they are one- or two-sided
Only common tests should be described solely by name; describe more complex techniques in the Methods section.
- A description of all covariates tested
- A description of any assumptions or corrections, such as tests of normality and adjustment for multiple comparisons
- A full description of the statistics including central tendency (e.g. means) or other basic estimates (e.g. regression coefficient) AND variation (e.g. standard deviation) or associated estimates of uncertainty (e.g. confidence intervals)
- For null hypothesis testing, the test statistic (e.g. F , t , r) with confidence intervals, effect sizes, degrees of freedom and P value noted
Give P values as exact values whenever suitable.
- For Bayesian analysis, information on the choice of priors and Markov chain Monte Carlo settings
- For hierarchical and complex designs, identification of the appropriate level for tests and full reporting of outcomes
- Estimates of effect sizes (e.g. Cohen's d , Pearson's r), indicating how they were calculated
- Clearly defined error bars
State explicitly what error bars represent (e.g. SD, SE, CI)

Our web collection on [statistics for biologists](#) may be useful.

Software and code

Policy information about [availability of computer code](#)

Data collection

Data collection software at the Swiss Light Source (Villigen, Switzerland) MX beamlines (DA+ GUI).

Data analysis

XDS (version May 1, 2016 BUILT=20160617)
CCP4 Suite (version 7.0.017) including Pointless version 1.10.26; Aimless version 0.5.27; Phaser (version 2.6.1)
PHENIX (version 1.11.1_2575)
COOT (version 0.8.8)
MaxQuant software suite (version 1.5.2.18)
Perseus (1.5.0.9)
Bowtie
DANPOS

For manuscripts utilizing custom algorithms or software that are central to the research but not yet described in published literature, software must be made available to editors/reviewers upon request. We strongly encourage code deposition in a community repository (e.g. GitHub). See the Nature Research [guidelines for submitting code & software](#) for further information.

Data

Policy information about [availability of data](#)

All manuscripts must include a [data availability statement](#). This statement should provide the following information, where applicable:

- Accession codes, unique identifiers, or web links for publicly available datasets
- A list of figures that have associated raw data
- A description of any restrictions on data availability

Coordinates and structure factors have been deposited in the Protein Data Bank under PDB ID accession codes 5NBM for the N-actin(ATP)-Arp4-NactNB, 5NBL for the N-actin(apo)-Arp4-NactNB and 5NBN for the Ino80HSA-Arp4-N-Actin-Arp8-module structures.

Data of the genome-wide nucleosome positioning experiments reported in this paper have been deposited on the NCBI Gene Expression Omnibus (accession number GSE113401).

All other data and material are available from the corresponding author upon reasonable request.

Field-specific reporting

Please select the best fit for your research. If you are not sure, read the appropriate sections before making your selection.

Life sciences Behavioural & social sciences Ecological, evolutionary & environmental sciences

For a reference copy of the document with all sections, see [nature.com/authors/policies/ReportingSummary-flat.pdf](https://www.nature.com/authors/policies/ReportingSummary-flat.pdf)

Life sciences study design

All studies must disclose on these points even when the disclosure is negative.

Sample size	not applicable for x-ray structure determination (PDB validation report is attached). Affinity enrichment mass spectrometry (AE MS) using the nanobody (Figure 2b) was performed in triplicates and statistically evaluated as previously described by Keilhauer et al. Mol Cell Proteomics 14, 120-35 (2015). All biochemical experiments with Arp8-module or INO80 were performed in triplicates. INO80 genome-wide in vitro reconstitution assay were performed in duplicates.
Data exclusions	no data were excluded
Replication	all attempts of replication were successful
Randomization	no randomization
Blinding	no blinding

Reporting for specific materials, systems and methods

Materials & experimental systems

n/a	Involvement in the study
<input checked="" type="checkbox"/>	<input type="checkbox"/> Unique biological materials
<input type="checkbox"/>	<input checked="" type="checkbox"/> Antibodies
<input type="checkbox"/>	<input checked="" type="checkbox"/> Eukaryotic cell lines
<input checked="" type="checkbox"/>	<input type="checkbox"/> Palaeontology
<input checked="" type="checkbox"/>	<input type="checkbox"/> Animals and other organisms
<input checked="" type="checkbox"/>	<input type="checkbox"/> Human research participants

Methods

n/a	Involvement in the study
<input checked="" type="checkbox"/>	<input type="checkbox"/> ChIP-seq
<input checked="" type="checkbox"/>	<input type="checkbox"/> Flow cytometry
<input checked="" type="checkbox"/>	<input type="checkbox"/> MRI-based neuroimaging

Antibodies

Antibodies used Arp4-N-actin binding nanobody (identified in this study).

Validation The specificity of the nanobody has been evaluated by AE MS experiments (Figure 2B) and by using x-ray crystallography.

Eukaryotic cell lines

Policy information about [cell lines](#)

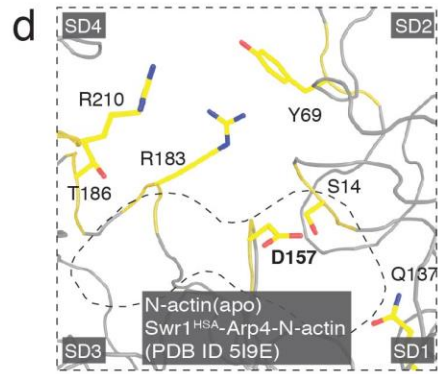
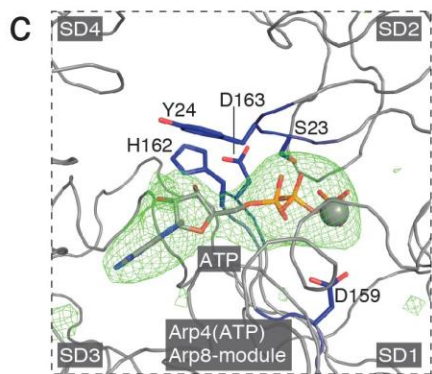
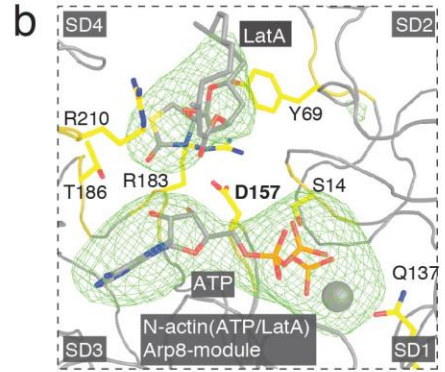
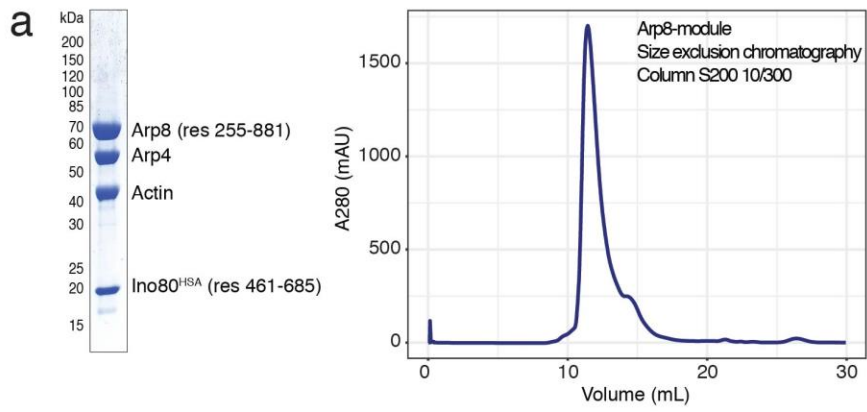
Cell line source(s)	Yeast with a double FLAG-tagged INO80 (Genotype: MATa INO80-FLAG2 his3Δ200 leu2Δ0 met15Δ0 trp1Δ63 ura3Δ0) were kindly provided by X. Shen (The University of Texas MD Anderson Cancer Center, Smithville, Texas, USA) and has been previously described in Shen et al. Nature 406, 541-4 (2000). Spodoptera frugipeda Sf21 insect cells (Invitrogen; 11497013) Trichoplusia ni High Five insect cells (Invitrogen; B85502)
Authentication	INO80 purifications described in Shen et al. Nature 406, 541-4 (2000) were successfully repeated. Insect cells lines from Invitrogen were not further authenticated.
Mycoplasma contamination	Protein expression cell lines were not tested.
Commonly misidentified lines (See ICLAC register)	not applicable

In the format provided by the authors and unedited.

The nuclear actin-containing Arp8 module is a linker DNA sensor driving INO80 chromatin remodeling

Kilian R. Knoll^{1,2,9}, Sebastian Eustermann^{1,2,9}, Vanessa Niebauer^{1,2}, Elisa Oberbeckmann³, Gabriele Stoehr^{1,2,7}, Kevin Schall^{1,2}, Alessandro Tosi^{1,2,8}, Marianne Schwarz^{1,2,4}, Andrea Buchfellner⁵, Philipp Korber³ and Karl-Peter Hopfner^{1,2,6*}

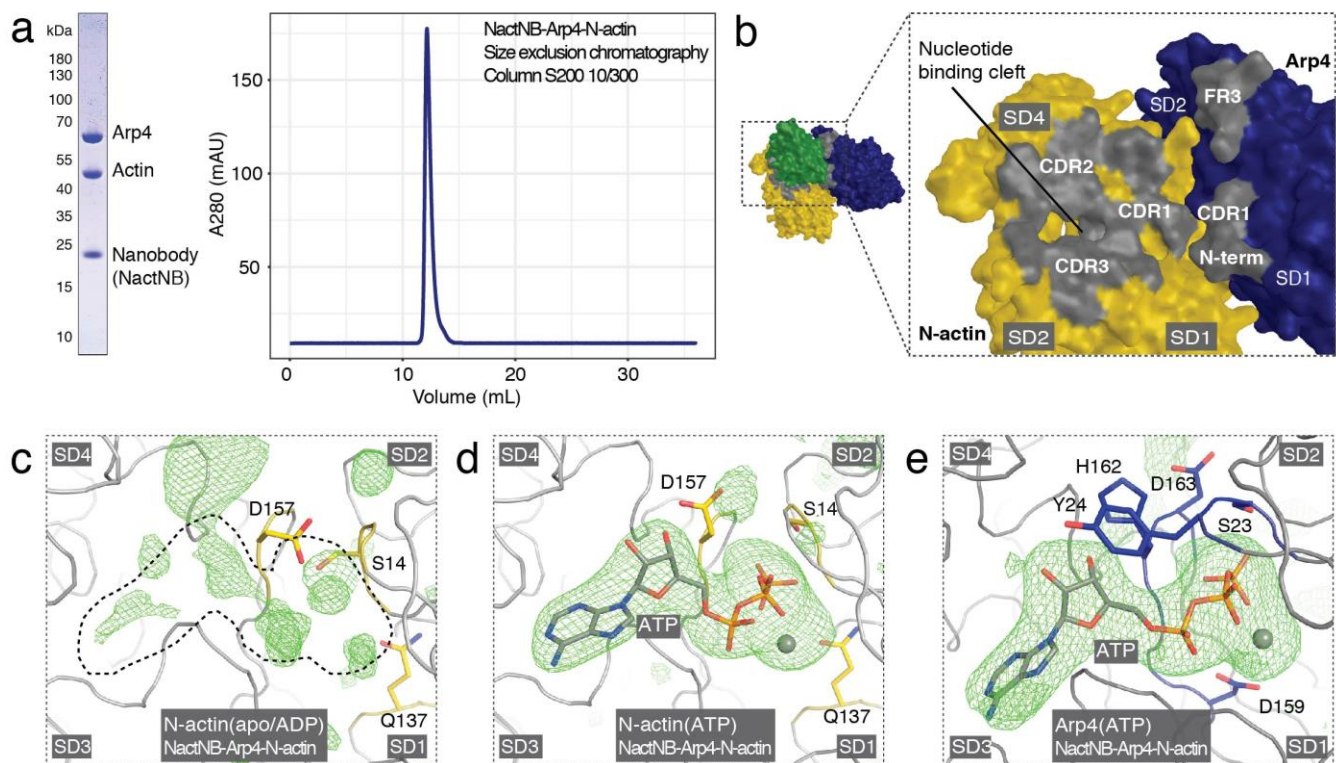
¹Department of Biochemistry, Ludwig-Maximilians-Universität München, Munich, Germany. ²Gene Center, Ludwig-Maximilians-Universität München, Munich, Germany. ³Chair of Molecular Biology, Biomedical Center, Faculty of Medicine, Ludwig-Maximilians-Universität München, Munich, Germany. ⁴Institute of Biophysics, Ulm University, Ulm, Germany. ⁵ChromoTek GmbH, Planegg, Germany. ⁶Center for Integrated Protein Science, Ludwig-Maximilians-Universität München, Munich, Germany. ⁷Present address: OmicScouts GmbH, Freising, Germany. ⁸Present address: Vossius & Partner, Munich, Germany. ⁹These authors contributed equally: K.R. Knoll, S. Eustermann. *e-mail: hopfner@genzentrum.lmu.de



Supplementary Figure 1

Crystal structure of the 180 kDa Arp4–N-actin–Arp8–Ino80^{HSA} module.

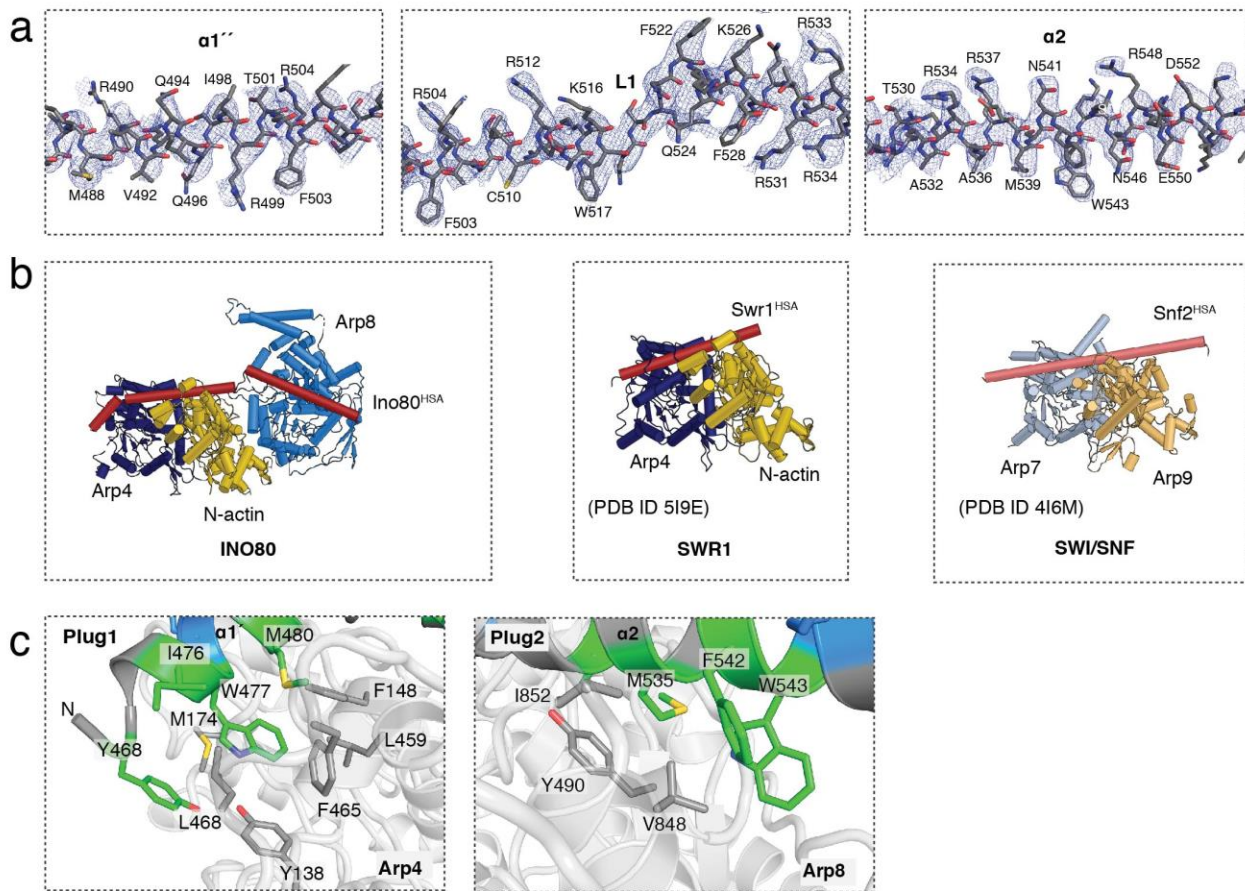
a, SDS–PAGE and Coomassie brilliant blue staining of the Arp8 module and the size-exclusion chromatography elution profile of the Arp8 module on a S200 10/300 column. Uncropped gel images are shown in Supplementary Dataset 1. **b,c**, Close-ups of the Arp8 module structure showing the N-actin(ATP/LAR) and Arp4(ATP) nucleotide-binding pockets with electron density (green mesh) for the bound ligands ($mF_o - DF_c$ difference map with a carving radius of 20 Å around each ligand; contoured at 3σ , resulting from structure refinement with phenix.refine lacking ligands). **d**, Close-up of the Arp4–N-actin–Swr1^{HSA} crystal structure N-actin(apo) nucleotide-binding pocket (PDB 5I9E). The dotted line illustrates the canonical ATP-binding site of actin. Interestingly, Asp157 would block ATP binding in the apo N-actin structure, while it is moved outward in the ATP-bound N-actin structure in **b**.



Supplementary Figure 2

Arp4-N-actin heterodimer: a conserved structural subunit in chromatin complexes.

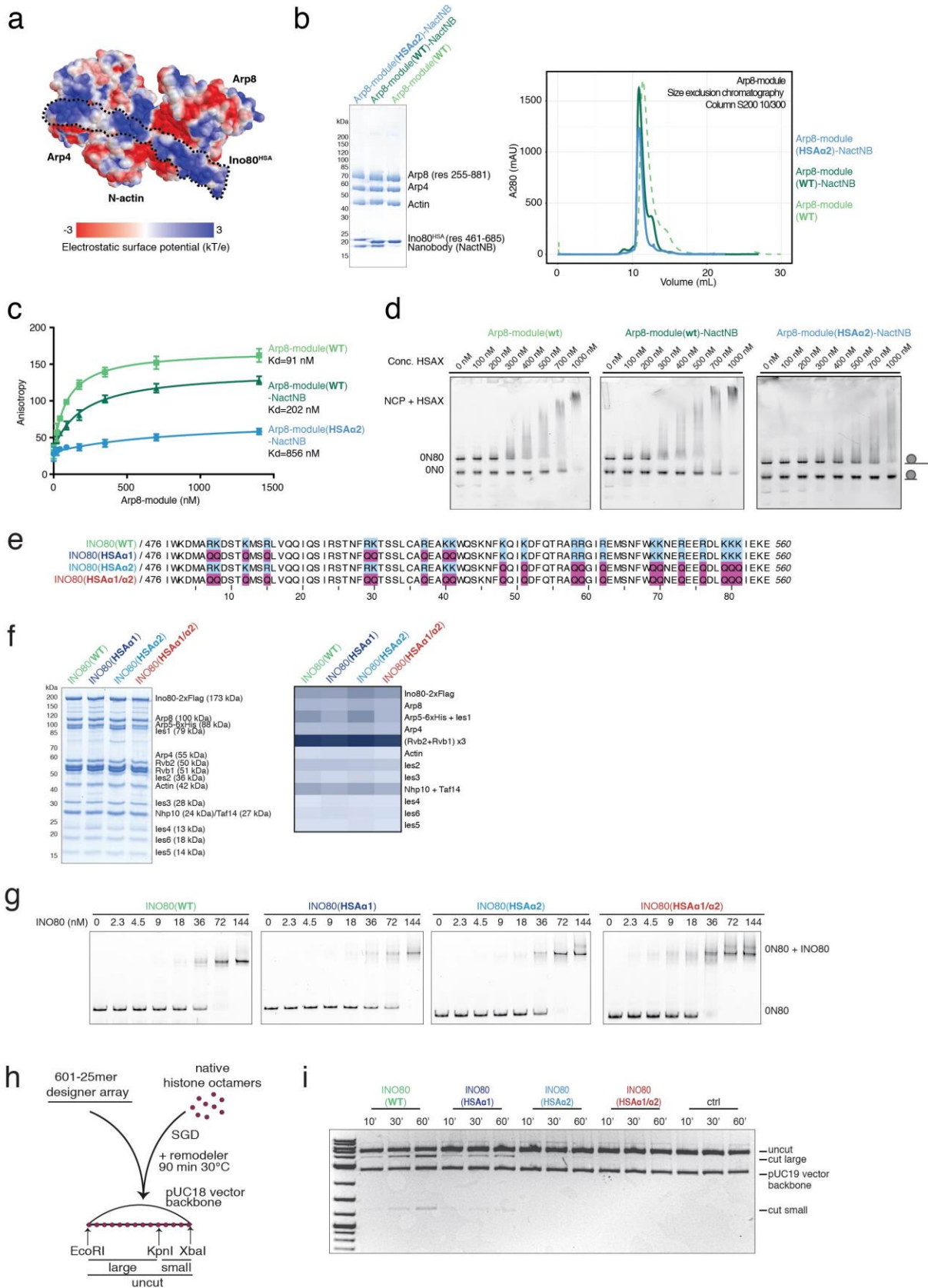
a, SDS-PAGE and Coomassie brilliant blue staining of the NactNB-Arp4-N-actin complex and the size-exclusion chromatography elution profile of the NactNB-Arp4-N-actin complex on a S200 10/300 column. Uncropped gel images are shown in Supplementary Dataset 1. **b**, Surface representation of the NactNB-Arp4-N-actin complex displaying the NactNB-binding epitope on the Arp4-N-actin dimer. Gray regions indicate recognition sites of the respective labeled NactNB-binding element. **c**, Close-up of the NactNB-Arp4-N-actin(apo) structure N-actin nucleotide-binding pocket, with the green mesh displaying electron density in the $mF_o - DF_c$ difference electron density map (contoured at 3σ with a carving radius of 20 Å around ATP-binding residues Asp157, Ser14 and Gln137). The dotted line illustrate the canonical ATP-binding site of actin. **d**, **e**, Close-ups of the NactNB-Arp4-N-actin structure N-actin(ATP) and Arp4(ATP) nucleotide-binding pockets with electron density (green mesh) for the bound ligands ($mF_o - DF_c$ difference map with a carving radius of 20 Å around each ligand; contoured at 3σ , resulting from structure refinement with phenix.refine lacking ligands).



Supplementary Figure 3

Arp8 recruits Arp4–N-actin to a segmented ‘two-plug’ scaffold of Ino80^{HSA}.

a, Electron density for Ino80^{HSA}. Shown is a feature-enhanced map (FEM) calculated by phenix.fem at a contour level of 1σ (blue mesh). Ino80^{HSA} is shown in stick representation. **b**, Structures of the Arp4–N-actin–Arp8–Ino80^{HSA} complex, the Arp4–N-actin–Swr1^{HSA} complex (PDB 5I9E) and the Arp9–Arp7–Snf2^{HSA} complex (PDB 4I6M) shown as cartoon representations. **c**, Close-ups display binding of Ino80^{HSA} plug 1 to a hydrophobic pocket at the barbed end of Arp4 and plug 2 to a hydrophobic pocket at the barbed end of Arp8.



Supplementary Figure 4

Extranucleosomal DNA binding by the Arp8 module is important for nucleosome sliding and genome-wide nucleosome positioning.

a, Electrostatic surface potential of the Arp8 module (calculated with the APBS PyMol plugin; *Proc. Natl. Acad. Sci. USA* **98**, 10037–10041, 2001) shown as surface representation. Ino80^{HSA} is outlined by a dotted line. **b**, SDS–PAGE and Coomassie brilliant blue staining of the Arp8 module (WT) and the Arp8 module in complex with NactNB (WT and Ino80^{HSA} mutant HSA α 2). Size-exclusion chromatography elution profiles are shown of the different Arp8 module complexes on an S200 10/300 column. **c**, Arp8 module 40-bp dsDNA binding affinity measured by fluorescence anisotropy (with 20 nM dsDNA). Anisotropy is plotted against Arp8 module protein concentration and fitted to a non-linear non-cooperative 1:1 binding model (Methods). Data points and error bars represent the means \pm s.d. from three independent experiments. **d**, Competition electrophoretic mobility shift assays with two nucleosome species (20 nM each), one with 80 bp (ON80) and one without DNA overhang (ON0), and increasing concentration of the indicated Arp8 module complexes. For Arp8 module(wt)-NactNB and Arp8 module(HSA α 2)-NactNB, the same gels are shown in Fig. 4b. Experiments were performed in triplicates. **e**, Sequence alignment of WT Ino80^{HSA} (residues 476–560) and the three Ino80^{HSA} mutants. Mutated residues are highlighted in purple. **f**, Left, SDS–PAGE and SimplyBlue (Thermo Scientific) staining of the INO80 WT, HSA α 1, HSA α 2 and HSA α 1/ α 2 complexes. Right, heat map showing color-coded quantification of the respective protein band intensity for the SDS gel in the left panel. Band intensity was determined using the profile plot implementation of ImageJ (*Nat. Methods* **9**, 671–675, 2012). **g**, Electrophoretic mobility shift assays with ON80 nucleosomes (20 nM) and increasing concentrations of the indicated INO80 complexes. Experiments were performed in triplicate. **h**, Graphical description of the restriction enzyme accessibility assay shown in **i** (adopted from *Cell* **167**, 709–721, 2016). **i**, Restriction enzyme accessibility assay displaying the INO80 (18 nM) nucleosome-remodeling activity of arrays of 601-based nucleosomes under conditions identical to those in the genome-wide remodeling assays shown in Fig. 4e,f. Experiments were performed in triplicate. (Uncropped gel images are shown in Supplementary Dataset 1.)

Supplementary Table 1. Ino80 HSA domain mutant sequences.

Name	Mutated <i>S. cerevisiae</i> Ino80 region (residue 481 to 557)
HSA α 1	481-QQDSTQMSQLVQQIQSIRSTNFQQTSSLCAQEAQQWQSKNFKQIKDFQTRARRGIREMSNFWKKNEREERDLKKK-557
HSA α 2	481-RKDSTKMSRLVQQIQSIRSTNFRKTSSLCAREAKKWQSKNFQQIQDFQTRAQQGIQEMSNFWQQNEQEEQDLQQQ-557
HSA α 1/ α 2	481-QQDSTQMSQLVQQIQSIRSTNFQQTSSLCAQEAQQWQSKNFQQIQDFQTRAQQGIQEMSNFWQQNEQEEQDLQQQ-557

Supplementary Notes

Genome-wide *in vitro* reconstitution assay

Salt gradient dialysis (SGD)

For detailed procedures of the following refer to ¹. The yeast genome plasmid library used was originally described in ² and derived from 10-30 kb partial Sau3A digested yeast genome fragments and ligated via BamHI into the YCp50 plasmid. Library expansion was carried out as described in ¹.

The preparation of embryonic *D. melanogaster* histone octamers was carried out as described in ^{1,3}.

For reconstitution reactions, 10 µg of YCp50 library DNA in high salt buffer (10 mM Tris-HCl, pH 7.6, 2 M NaCl, 1 mM EDTA, 0.05 % IGEPAL CA630) was mixed with 20 µg BSA and *Drosophila* embryo histones in Slide-A-lyzer mini dialysis devices. The amount of histones was determined for each histone octamer preparation by titration and MNase ladder assays as read out for assembly extent. An assembly extent similar to the one chosen in ¹ was used. Samples were placed in a 3 L beaker containing 300 mL of high salt buffer and 300 µL β-mercaptoethanol at room temperature and dialyzed against a total of 3 L low salt buffer (10 mM Tris-HCl, pH 7.6, 50 mM NaCl, 1 mM EDTA, 0.05% IGEPAL CA630) containing 300 µL β-mercaptoethanol. The low salt buffer with β-mercaptoethanol was added continuously via a peristaltic pump over a time course of 16 h under stirring conditions. After complete transfer of low salt buffer, samples were additionally dialyzed against 1 L low salt buffer for 1 h at room temperature. DNA concentration of the SGD chromatin preparations was estimated with a NanoDrop 100 spectrophotometer (Thermo Scientific) and preparations were used directly or stored at 4°C.

Remodeling reactions

All remodeling reactions were performed at 30°C in 100 µL with final buffer conditions of 26.6 mM HEPES-NaOH pH 7.5, 1 mM Tris-HCl pH 7.6, 85.5 mM NaCl, 8 mM KCl, 10 mM ammonium sulfate, 10 mM creatine phosphate (Sigma), 3 mM MgCl₂, 2.5 mM ATP, 0.1 mM EDTA, 0.6 mM EGTA, 0.05 mM DTT, 14 % glycerol, 20 ng/µL creatine kinase (Roche Applied Science). Analogous to previous estimates using the same methodology¹ 1 µg DNA assembled by SGD and used in a 100 µl reaction volume was assumed to correspond to a nucleosome concentration of about 80 nM. Remodeling reactions contained 18 nM of WT or mutant INO80, were started by addition of SGD chromatin, and terminated after 1 h by adding 0.8 U apyrase (NEB) and incubation at 30°C for 10 min.

MNase digestion

After incubation with apyrase, remodeling reactions were supplemented with CaCl_2 to a final concentration of 1.5 mM and digested with 200 U MNase (SIGMA Aldrich, N3755-500UN) to generate mostly mononucleosomal DNA. MNase digest was stopped with a final concentration of 10 mM EDTA and 0.5% SDS. After proteinase K treatment for 1 h at 37°C, samples were ethanol precipitated and electrophoresed for 1-2 h at 100 V using a 1.5% agarose gel in 1x Tris-acetate-EDTA (TAE) buffer. The mononucleosomal DNA fragments were isolated from the gel using Freeze N Squeeze DNA Gel Extraction Spin Columns (Biorad) or the PureLink kit (Invitrogen).

Preparation of sequencing libraries

The NEBNext Multiplex Oligos for Illumina were used to generate sequencing libraries. Approximately 50 ng of purified mononucleosomal DNA after MNase digest was incubated with 1.25 U Taq polymerase (NEB), 3.75 U T4 DNA polymerase (NEB) and 12.5 U T4-PNK (NEB) in 1x ligation buffer (B0202S, NEB) for 15 min at 12°C, 15 min at 37°C and 20 min at 72°C. To ligate NEBNext Adaptors (0.75 μM final concentration, NEB) to the DNA, samples were incubated with T4 DNA ligase (NEB) at 25°C for 10 min, followed by incubation with 2 U USER enzyme (NEB) for 10 min at 37°C. Fragments were purified using AMPure XP beads (Beckman Coulter) and amplified for 10-12 cycles using NEBNext Universal Primer and NEBnext Index Primer, Phusion High-Fidelity DNA Polymerase (1 U, NEB), deoxynucleotide solution mix (dNTP, 2.5 mM, NEB) and Phusion HF Buffer (1x, NEB). The following protocol was applied for amplification: 98°C for 30 s, 98°C for 10 s, 65°C for 30 s, 72°C for 30 s (repeated for 12 cycles) with a final amplification step at 72°C for 5 min. The Qubit dsDNA HS Assay Kit (Invitrogen) was used to assess the DNA content of 1 μL PCR reaction. Adaptor-ligated mono-nucleosomal DNA was purified from agarose gels via Freeze N Squeeze DNA Gel Extraction Spin Columns (Biorad), ethanol precipitated and resuspended in 15 μL 0.1x TE buffer. DNA was measured with Qubit dsDNA HS Assay Kit and diluted to final concentration of 10 nM (calculation based on the assumption that the DNA fragment length is 272 bp, i.e., 147 bp nucleosomal DNA and 122 bp sequencing adaptor). 10 nM samples were pooled according to sequencing lane requirements. The final pool was quantified by BioAnalyzer (Agilent) and analyzed on an Illumina HiSeq 1500 in the 50 bp single-end mode (Laboratory for Functional Genome Analysis, LAFUGA, LMU Munich).

Data processing

Data processing was performed according to a so far unpublished protocol (Krietenstein et al.)^{*}.

In brief, reads were mapped to the *S. cerevisiae* S288C genome (genome build R64-1-1, Ensembl) using Bowtie⁴ and shifted by 48 bp to plot an extended nucleosome dyad of ± 25 bp. In vivo +1 nucleosome dyad positions were defined as the first DANPOS⁵ called nucleosomes downstream of transcription start sites⁶ (Krietenstein et al.)^{*}. Tags were normalized by dividing each tag count by the sum of all tags in a 2000 bp window around the in vivo +1 nucleosome dyad positions. Tags were smoothed using a 25 bp rolling mean.

For generation of heatmaps, rows / genes were sorted according to INO80 effectiveness⁷. Briefly, nucleosome dyad density levels within a 20 bp window centered on the in vivo +1 nucleosome dyad position were summed up, and ratios between this sum for SGD+INO80 and this sum for corresponding SGD only samples were calculated and used for sorting.

Restriction enzyme accessibility assay

SGD and remodeling reaction were essentially performed as described above. Instead of the *S. cerevisiae* plasmid library the pUC18-601-25-mer plasmid (pFMP233) as described in⁸ was used. The pUC18-601-25-mer plasmid contains a 25-mer of 197 bp Widom 601 sequence repeats, where some 601 sequences were engineered to contain unique restriction sites⁹.

To monitor the remodeling activity at a unique restriction site 50 U KpnI (NEB) was added. The INO80 (18 nM) remodeling reaction was started by adding 1 μ g of SGD-chromatinized pUC18-601-25-mer DNA (amounting to approximately 80 nM nucleosomes) and incubated at 30°C for 1 h. After stopping the reaction with 25 mM EDTA, the DNA was purified using proteinase K digestion followed by phenol-chloroform extraction and ethanol precipitation. A secondary cleavage reaction using 20 U XbaI and 20 U EcoRI was started for 1 h at 37°C. Samples were electrophoresed at 100 V for 3 h using a 1% agarose gel in 1x TAE. To address background KpnI accessibility, control reactions without remodeling enzymes were carried out in parallel.

^{*}Unpublished data by: Krietenstein Nils, Oberbeckmann Elisa, Niebauer Vanessa, Schall Kevin, Schwarz Marianne, Moldt Manuela, Straub Tobias, Korber Philipp, Hopfner Karl-Peter & Eustermann Sebastian

Supplementary references

1. Krietenstein, N., Wippo, C.J., Lieleg, C. & Korber, P. Genome-wide in vitro reconstitution of yeast chromatin with in vivo-like nucleosome positioning. *Methods Enzymol* **513**, 205-32 (2012).
2. Rose, M.D., Novick, P., Thomas, J.H., Botstein, D. & Fink, G.R. A *Saccharomyces cerevisiae* genomic plasmid bank based on a centromere-containing shuttle vector. *Gene* **60**, 237-43 (1987).
3. Simon, R.H. & Felsenfeld, G. A new procedure for purifying histone pairs H2A + H2B and H3 + H4 from chromatin using hydroxylapatite. *Nucleic Acids Res* **6**, 689-96 (1979).
4. Langmead, B., Trapnell, C., Pop, M. & Salzberg, S.L. Ultrafast and memory-efficient alignment of short DNA sequences to the human genome. *Genome Biol* **10**, R25 (2009).
5. Chen, K. et al. DANPOS: dynamic analysis of nucleosome position and occupancy by sequencing. *Genome Res* **23**, 341-51 (2013).
6. Xu, Z. et al. Bidirectional promoters generate pervasive transcription in yeast. *Nature* **457**, 1033-7 (2009).
7. Krietenstein, N. et al. Genomic Nucleosome Organization Reconstituted with Pure Proteins. *Cell* **167**, 709-721 e12 (2016).
8. Mueller-Planitz, F., Klinker, H., Ludwigsen, J. & Becker, P.B. The ATPase domain of ISWI is an autonomous nucleosome remodeling machine. *Nat Struct Mol Biol* **20**, 82-9 (2013).
9. Lowary, P.T. & Widom, J. New DNA sequence rules for high affinity binding to histone octamer and sequence-directed nucleosome positioning. *J Mol Biol* **276**, 19-42 (1998).

Publications

2.2 Genome information processing by the INO80 chromatin remodeler positions nucleosomes

Elisa Oberbeckmann*, Nils Krietenstein*, Vanessa Niebauer, Kevin Schall, Manuela Moldt, Tobias Straub, Karl-Peter Hopfner, Philipp Korber, Sebastian Eustermann (2020), Genome information processing by the INO80 chromatin remodeler positions nucleosomes. (under revision)

*: equal contribution

This publication addresses the central question of how ATP-dependent chromatin remodelers shape the genomic landscape by positioning nucleosomes flanking nucleosome depleted regions (NDR), which represent a reference point for subsequent downstream nucleosome array formation. To gain mechanistic insight into, on condition that information is read, what information is processed by chromatin remodelers, we applied a combination of purified remodeling enzymes and a minimalistic *in vitro* genome-wide reconstitution system. Based on the *S.c.* chromatin remodeler INO80 and mutagenesis of candidate target subunits based on high-resolution structures, we proposed that nucleosome positioning by INO80 integrates DNA sequence-related shape read-out as well as phasing activity on reference points, such as DNA binding proteins and dsDNA breaks. DNA shape read-out was mainly proposed for static DNA binding proteins, such as transcription factors and general regulatory factors as well as recently for RNA polymerases. The establishment of a causal link between DNA shape read-out and mutagenesis of the Ino80_HSA domain introduces firstly, a new concept for genome-wide operating machineries that scan DNA shape information while tracking along the DNA and secondly, points out a major role of the INO80 ARP module in this process.

Author contribution

The author of this thesis cloned, expressed and purified INO80 wild type and mutant constructs including Ino80_HSA, Ino80_ΔN, INO80ΔNHP10 and INO80_HMGII mutant constructs as well as double mutant constructs for *in vitro* characterization. The author cloned, expressed and purified wild type and mutant *S.c.* Reb1 constructs. The author assembled mononucleosomes using salt gradient dialysis. Wild type as well as mutant constructs were tested in mononucleosome sliding assays based on the YGL167c promoter DNA sequence with a Widom

Publications

601 positioning sequence and an introduced Reb1 binding site. The author tested ATPase activity of wild type and mutant constructs stimulated by mononucleosomes in presence and absence of Reb1.

Genome information processing by the INO80 chromatin remodeler positions nucleosomes

Elisa Oberbeckmann^{1,6}, Nils Krietenstein^{1,2,6}, Vanessa Niebauer³, Kevin Schall³, Manuela Moldt³, Tobias Straub⁴, Karl-Peter Hopfner^{3*}, Philipp Korber^{1*}, Sebastian Eustermann^{3,5*}

¹Division of Molecular Biology, Biomedical Center, Faculty of Medicine, Ludwig-Maximilians-Universität München, Martinsried near to Munich, Germany

²current address: Department of Biochemistry and Molecular Pharmacology, University of Massachusetts Medical School, Worcester, Massachusetts, USA

³Gene Center, Faculty of Chemistry and Pharmacy, Ludwig-Maximilians-Universität München, Munich, Germany

⁴Core Facility Bioinformatics, Biomedical Center, Faculty of Medicine, Ludwig-Maximilians-Universität München, Martinsried near to Munich, Germany

⁵current address: European Molecular Biology Laboratory (EMBL), Structural and Computational Biology Unit, Heidelberg, Germany

⁶These authors contributed equally.

*Corresponding authors:

sebastian.eustermann@embl.de, pkorber@lmu.de, hopfner@genzentrum.lmu.de

Abstract

The fundamental molecular determinants by which ATP-dependent chromatin remodelers organize nucleosomes remain largely elusive. Here, chromatin reconstitutions on physiological, whole-genome templates reveal how remodelers read and translate genomic information into nucleosome positions. Using the yeast genome and the multi-subunit INO80 remodeler as a paradigm, we identify DNA shape-encoded signature motifs as sufficient for nucleosome positioning and distinct from known DNA sequence preferences of histones. INO80 processes DNA shape information through an allosteric interplay between its core- and Arp8-modules that probes mechanical properties of nucleosomal and linker DNA. At promoters, INO80 integrates this direct DNA shape readout with an indirect readout of co-evolved sequence motifs via interaction with general regulatory factors bound to these motifs. Our findings establish a molecular mechanism for robust and yet adjustable +1 nucleosome positioning and, more generally, remodelers as information processing hubs that enable active organization and allosteric regulation of the first level of chromatin.

Introduction

The packaging of DNA with histones into nucleosomes underpins the maintenance and regulation of genome information in eukaryotes^{1,2}. Genome-wide mapping of chromatin revealed highly-defined patterns of nucleosomes carrying a combinatorial landscape of histone variants and modifications³⁻⁸. These patterns entail well-positioned nucleosomes, which occupy the same genomic position across a cell population and adopt even equivalent positions relative to genomic sites of equivalent function like transcription start sites (TSS)^{6,7}. Most prominently, nucleosome-depleted regions (NDRs) at promoters of active or poised genes are flanked by a well-positioned hallmark nucleosome (+1 nucleosome) that is the first in a regular nucleosome array over the transcribed region⁹. These stereotypic NDR-array patterns are conserved from yeast to man, and changes within their configuration play a pivotal role in transcriptional regulation, e.g., during cell differentiation and stress response^{10,11}. Understanding the fundamental molecular determinants of nucleosome positioning is likely to reveal core principles by which genome regulation occurs.

A nucleosome position is defined by the DNA sequence that is wrapped around the histone octamer¹². While this DNA sequence always answers the question “Where is this nucleosome?”, it may, but need not, answer the question “How was the nucleosome placed there?”. Histone octamers may form nucleosomes virtually at any DNA sequence position in the genome¹³. A molecular mechanism that consistently places a nucleosome at a particular genome position across a cell population must select this position against competing positions. This selection may be based on genetic information encoded within DNA sequence or epigenetic information like histone modifications and variants or other chromatin-associated factors. Regarding DNA sequence information, pioneering studies proposed two mechanisms (Figure 1A).

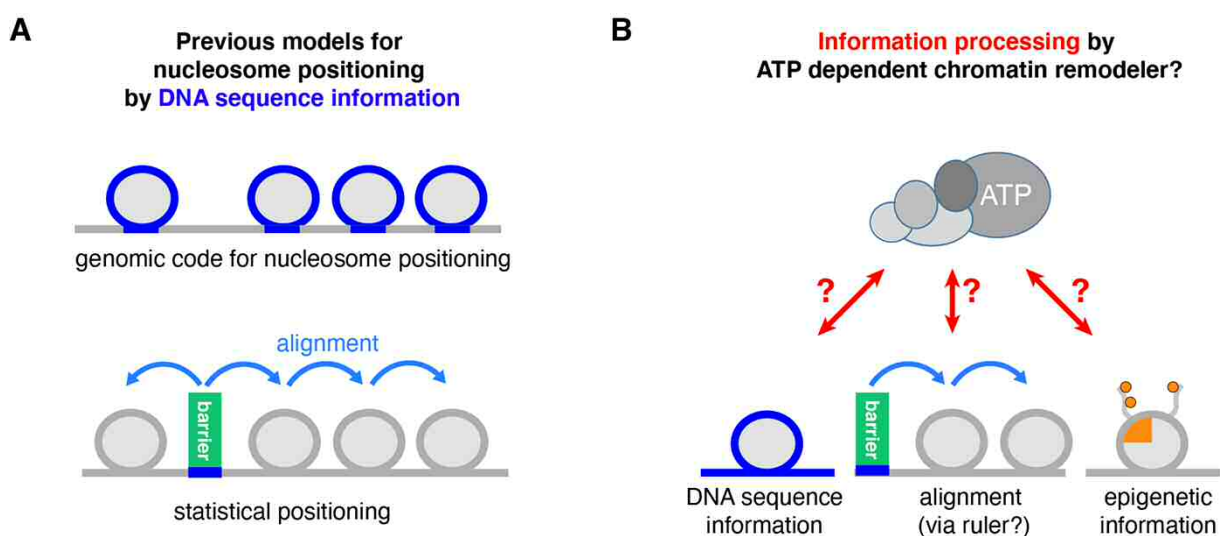


Figure 1: Models for nucleosome positioning mechanisms. (A) Genomic code for nucleosome positioning^{14,15} and statistical positioning¹⁶ are two previous models, which exemplify a direct versus indirect readout of DNA sequence information for nucleosome positioning, respectively. (B) In light of the decisive role of ATP-dependent

chromatin remodelers in nucleosome positioning^{24,28,29,60}, we asked if and how these large, macro-molecular machines actively process (epi)genetic information together with their own remodeler-specific information into stable nucleosome positioning.

One mechanism relies on the intrinsic specificity of nucleosomes to preferentially assemble on DNA sequences that favor the wrapping around the histone octamer (“genomic code for nucleosome positioning”)^{14,15}. In this case, the nucleosomal DNA sequence directly determines the position. The other mechanism requires DNA sequence-specific binding of a barrier factor, to which one or several histone octamers are aligned by statistical positioning regardless of the octamer-bound DNA sequences¹⁶. The principle difference between these two mechanisms illustrates two extremes, which pertain to the central question whether DNA sequence information directly or indirectly determines a nucleosome position. If directly, the nucleosome positioning mechanism directly reads out the DNA sequence information at the resulting nucleosome position itself. If indirectly, DNA sequence is read somewhere else, and the resulting positioning information is relayed by alignment mechanisms that position nucleosomes relative to barriers and other nucleosomes. In this case, the sequences underlying nucleosome positions would define, but not determine, these positions.

In recent years, it has become clear that the pure versions of these two mechanistic extremes fail to explain nucleosome positioning *in vivo*. Intrinsic histone octamer preferences, as operationally assessed by salt gradient dialysis (SGD) reconstitution from purified DNA and histones¹³, cannot recapitulate NDR-array patterns *in vitro*^{17,18}, and internucleosomal distances (spacing) are independent of nucleosome density *in vivo*^{19,20} and *in vitro*^{18,21} in contrast to predictions of the statistical positioning mechanism^{16,22}.

Instead, ATP-dependent chromatin remodelers have now been established as decisive nucleosome positioning factors by studies both *in vivo* and *in vitro*. Chromatin remodelers often form multisubunit macromolecular complexes and are grouped into four families: INO80, SWI/SNF, ISWI, CHD. By using energy derived from ATP hydrolysis, remodelers alter histone-DNA interactions resulting in nucleosome translocation (sliding), ejection, and reconfiguration²³. Mutations in genes encoding remodeler subunits, especially combined mutations, lead either to compromised nucleosome patterns and composition, or are lethal^{20,24-28}. Complementary to genetic studies, cell-free reconstitutions provided direct evidence for the critical role of chromatin remodelers in nucleosome positioning and allowed to distinguish remodeler contributions from those of other factors, like the transcription and replication machinery^{18,29}. Nucleosomes were assembled by SGD, even for an entire genome with yeast genomic DNA fragments or plasmid libraries^{17,18,29,30}. The largely non-physiological nucleosome positions generated by SGD were turned in an ATP-dependent manner into *in vivo*-like NDR-array patterns either by addition of

whole cell extracts¹⁸ or, remarkably, also by addition of remodelers purified from yeast²⁹. For example, the yeast INO80 or the SWI/SNF-type RSC remodeling complex, in the absence of other factors, generated hallmark features of *in vivo*-like nucleosome organization, +1 nucleosomes and NDRs at promoters, respectively²⁹. This argued for a remodeler-mediated direct readout of positioning information, possibly involving DNA sequence features^{29,31}. In contrast, the yeast ISW1a and ISW2 remodelers could not generate *in vivo*-like nucleosome positions on their own but required sequence information readout by other factors. So-called “general regulatory factors” (GRFs) are sequence-specific DNA binding proteins, often essential for viability and involved in transcription or replication regulation via their impact on chromatin organization³²⁻³⁴. Addition of purified GRFs, e.g., yeast Reb1 or Abf1, enabled the ISW1a and ISW2 remodelers to align regular nucleosome arrays relative to the GRF binding sites²⁹. This argued in turn for remodeler-mediated indirect readout of sequence information via processive alignment at GRFs as well as among nucleosomes, possibly involving a protein ruler³⁵.

Although genetic and cell-free reconstitution studies established the critical importance of remodelers in defining the genomic organization of nucleosomes, the dissection of their function at a molecular level has proven difficult. Recent structural work shed light onto the architecture of different remodelers and how they might act on mono-nucleosomes. However, it remains unclear how the activities of remodelers are regulated such that they determine genome-wide nucleosome positioning patterns. This poses the conundrum that the principal remodeler activity of mobilizing nucleosomes has to result in stable nucleosome positions relative to genomic sequence.

In this study, we directly addressed this fundamental conundrum by asking which kind of DNA sequence, histone, barrier or other epigenetic information provides the required input, and how remodelers turn this information input into stable nucleosome positioning (Figure 1B). We advanced whole genome reconstitutions into a fully recombinant, *de novo* approach. In this system full biochemical control is established by using recombinant components in conjunction with high resolution structural information enabling the bottom-up study of remodeling mechanisms. Not only the core mechanism of remodelers, as studied so far mainly in mono-nucleosome assays, but also the extended functions arising from remodeling of chromosomal multi-nucleosome substrates as well as the readout of physiological genomic DNA sequences and other nucleosome positioning information can be assessed at a detailed mechanistic level. We used the yeast genome and the multi-subunit structure of the INO80 complex as a paradigm to identify and probe the information and mechanism by which remodelers read information and translate it into stable nucleosome positions. In the accompanying study (Oberbeckmann & Niebauer et al.), we addressed how remodelers propagate nucleosome positioning information via an alignment mechanism to generate phased and regular nucleosomal arrays. Taken together, our data reveal

that and how remodelers are information processing hubs. Genome information is directly or indirectly read out by the remodelers and the allosteric interplay of their molecular machinery plays an active and decisive role in integrating this information and determining nucleosome positions.

Results

A fully recombinant approach for *de novo* whole-genome reconstitutions. To explore how ATP-dependent chromatin remodelers place nucleosomes at *in vivo*-like positions, we advanced whole-genome reconstitutions^{18,29,30} into a fully recombinant *de novo* approach (Figure 2A).

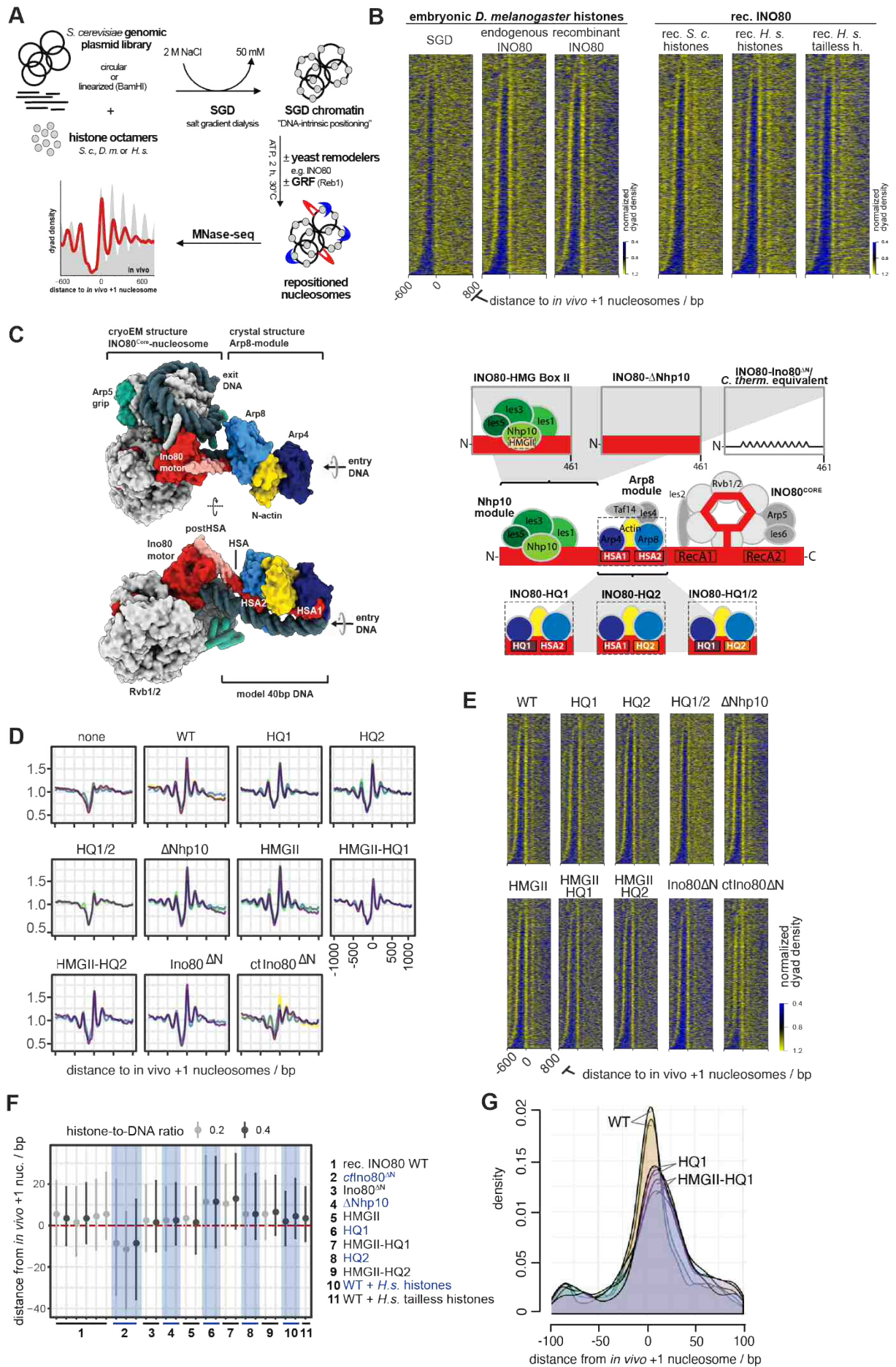


Figure 2: Fully recombinant genome-wide reconstitution of nucleosome positioning by INO80. (A) Overview of genome-wide *in vitro* chromatin reconstitution system. (B) Heat maps of MNase-seq data for SGD chromatin assembled with embryonic or recombinant (rec.) histones from the indicated species (“*H. s.*” abbreviates *Homo sapiens*, “*S. c.*” abbreviates *Saccharomyces cerevisiae*.) and remodeled with endogenous or recombinant *S. cerevisiae* INO80 complex as indicated. Heat maps are aligned at *in vivo* +1 nucleosome positions and sorted by NDR length. Single replicates are plotted, see Figure S1C for all replicates. (C) Left panel: Composite model of INO80 based on high resolution cryoEM structure of ctINO80 core in complex with a mono-nucleosome³⁷ and X-ray structure of Arp8 module modeled on 40bp linker DNA⁴². Images taken from Knoll et al. ⁴². Right panel: Schematic of INO80 complex submodule and subunit organization (middle) with zoom into Nhp10 (top) or Arp8 module (bottom) showing three mutant versions each. (D) Composite plots of MNase-seq data of individual replicates for SGD chromatin incubated with the indicated recombinant WT (WT) or mutant INO80 complexes (as in panel C) from *S. cerevisiae* or *C. thermophilum* (ctINO80^{ΔN}). (E) Heat maps of MNase-seq data for samples as in (D). (F) Distributions of distances between +1 nucleosome positions determined by paired-end sequencing after reconstitution by the indicated combinations of INO80 complexes and histones at the indicated histone-to-DNA mass ratio relative to *in vivo* +1 nucleosome positions. Dots mark the medians, vertical lines the interquartile distances. Alternating white and grey vertical zones group replicates of the indicated remodeler/histone combinations. (G) Density distributions of MNase-seq reads relative to *in vivo* +1 nucleosome positions of samples with INO80 WT, HQ1 and HMGII-HQ1 mutant complexes as in (F).

We established recombinant production of highly active and stoichiometric INO80 complex (Figure S1A,B) and performed whole-genome reconstitutions using recombinant histones. This leverages, compared to previously used endogenous fly embryo histones and endogenous purifications of remodelers²⁹, the full potential of biochemical systems: (1) A fully defined 15-subunit *S. cerevisiae* INO80 complex, amendable for structure-guided mutagenesis, (2) histones without posttranslational modifications (PTMs) and amendable for mutagenesis, and (3) defined DNA templates for chromatin assembly. We used MNase-seq to measure resulting nucleosome positions.

DNA sequence and globular histone octamer information is sufficient for *in vivo*-like +1 nucleosome positioning by INO80. This recombinant system enabled us to identify the minimal information for nucleosome positioning by INO80. Consistent with its localization and function *in vivo*³⁸, INO80 positions *in vivo*-like +1 nucleosomes adjacent to NDRs (Figure 2B,²⁹). As equally pronounced +1 nucleosome positioning activity was observed for recombinant as for endogenous INO80 (Figures 2B, left), we concluded that no yeast-specific PTMs were required and no co-purified yeast contaminant was responsible. To control the specificity of the highly pure INO80 complex (Figure 1SA), we assayed an INO80 complex with Ino80 Walker B motif mutation (Figure S1C) and excluded that nucleosome positioning activity was due to any co-purifying factor(s) from insect cells. Intriguingly, our recombinant whole-genome reconstitutions established conditions, under which INO80 generated extensive nucleosome arrays (e.g., upon addition of Reb1, see below). This served as starting point for the study of nucleosome spacing mechanisms (accompanying paper by Oberbeckmann & Niebauer et al.).

Next, we asked whether epigenetic information derived from histone modifications or variants was required for +1 nucleosome positioning. Histone variants, for example H2A.Z, may alter direct, sequence-dependent interactions of the histone octamer³⁹. However, compared to SGD

chromatin prepared with endogenous fly histones, using either recombinant human or yeast histones resulted in very similar nucleosome positioning by INO80 (Figure 2B, right). Patterns were less pronounced with yeast histones, which we attributed to their known propensity to form less stable nucleosomes⁴⁰. As the species-origin of the histones did not matter much, we went more minimalistic and asked if just the globular histone domains were sufficient. SGD chromatin with recombinant tailless human histones still allowed INO80 to position *in vivo*-like +1 nucleosome position (Figure 2B, right). We observed increased sliding rates with tailless compared to full-length histone nucleosomes (Figure S1D) consistent with previous studies^{36,37,41}. Nonetheless, this increased sliding rate did not alter the resulting steady state pattern.

We concluded that neither histone modifications nor histone variants nor histone tails nor yeast-specific INO80 modifications are essential for +1 nucleosome positioning by INO80. Thus, INO80 generates +1 nucleosome positioning solely by processing information from genomic DNA sequences and the globular histone octamer.

Structure-based site-directed mutagenesis probes nucleosome positioning by INO80.

Having identified a minimal set of components, from which INO80 derives nucleosome positioning information, we set out to specify this information and to dissect the molecular mechanism, by which it was processed. To this end, we leveraged high-resolution structures of INO80^{36,37,42} and asked which remodeler elements might function as reader of genome information.

Recent structural and biochemical studies revealed an extended configuration of the INO80 multi-subunit architecture on mono-nucleosomes (Figure S1F): the INO80 core module (Ino80 ATPase, Ies2, Ies6, Arp5, Rvb1, Rvb2) engages the nucleosome core particle^{36,37}, the nuclear-actin containing Arp8 module (Ino80-HSA domain, Arp8, Arp4, nuclear actin, Ies4 and Taf14) binds along 40-50 bp of linker DNA at the entry site^{36,37,43}, while the species-specific Nhp10 module (Nhp10, Ies1-3 and Ies5) bound to the Ino80 N-terminal region is located at the distal site of INO80's linker DNA footprint⁴³. Linker DNA binding by the Arp8 and Nhp10 modules was proposed to provide a DNA linker length dependent sensor that is allosterically coupled to processive nucleosome translocation catalyzed by the INO80 core⁴²⁻⁴⁴. *In vivo* ChIP-exo mapping suggested a highly similar INO80 configuration at +1 nucleosomes with the Arp8 or Nhp10 modules located at adjacent promoter regions³⁸. Thus, we reasoned that these INO80 modules are prime candidates for reading genomic DNA sequence information.

To test this hypothesis, we targeted candidate INO80-DNA interactions based on the high-resolution cryoEM and X-ray structures of the INO80 core and Arp8 module, respectively, as well as on homology modelling of the structurally less well characterized Nhp10 module. For the INO80 core, we tested the role of ATP hydrolysis by the hetero-hexameric AAA⁺-ATPase Rvb1/2

(Figures 2C, S1C), which structurally organizes the nucleosome core binding and remodeling unit of INO80^{36,37}. For the Arp8-module, we employed the Ino80-HSA helix mutants, which contain substitutions of highly conserved lysine/arginine to glutamine residues in the HSA1 and/or HSA2 domain (HQ1, HQ2 and combined HQ1/2 mutants, respectively) that are important for linker DNA binding⁴² (Figures 2C, S1E). For the Nhp10 module, we either mutated site-specifically the HMG box II in Nhp10 based on well-known DNA binding activity of HMG box proteins or removed the entire Nhp10 module by deleting Nhp10 or truncating Ino80's N-terminal 1-461 residues, to which this module binds (Figures 2C, S1E,G,H). This latter mutant corresponded to the *Chaetomium thermophilum* INO80 core complex used in the cryoEM structure³⁷, which we also employed here. Nhp10 module HMGII box and Arp8-module HQ1 or HQ2 mutations were also combined (HMGII-HQ1, HMGII-HQ2 mutants, respectively) (Figures 2C, S1E).

The INO80 Arp8 module is a reader of genomic sequence information. Comparison of nucleosome patterns in aligned heat map or composite plots suggested that most INO80 mutant complexes generated similar +1 nucleosome positioning as WT INO80 (Figures 2D,E, S1C). Rvb1/2 ATPase activity was not required (Figure S1C), consistent with the likely role of Rvb1/2 during INO80 biogenesis⁴⁵. Even the heterologous *C. thermophilum* INO80 core complex (ctINO80^{ΔN}) appeared to generate +1 nucleosomes on the *S. cerevisiae* genome to a remarkable extent, suggesting a conserved readout mechanism (Figure 2D,E). Only the HQ1/2 double mutant complex was substantially impaired in +1 nucleosome positioning (Figure 2D,E), consistent with its impaired nucleosome sliding and decoupled ATPase activity⁴². The apparent robustness of INO80 +1 nucleosome positioning activity was in contrast to the nucleosome spacing activity, which was affected for most of these INO80 mutants (accompanying paper by Oberbeckmann & Niebauer et al.).

However, quantification of distances between +1 nucleosome positions reconstituted *in vitro* and observed *in vivo* revealed a distinct impact of INO80 mutations (Figure 2F,G). Paired-end sequencing enabled accurate determination of nucleosome dyad positions, while we included also a lower histone-to-DNA mass ratio (~0.2, accompanying paper by Oberbeckmann & Niebauer et al.) than mostly used in this study (~0.4) to further reduce possible next-neighbor nucleosome effects. WT INO80 and Nhp10 module mutants generated *in vivo*-like +1 nucleosomes with remarkable precision (Figure 2F,G), whereas INO80 complexes bearing the HQ1 mutation and the ctINO80^{ΔN} complex generated +1 nucleosome positions that deviated more from the *in vivo* positions than those generated by the other complexes (Figure 2F). Compared to WT INO80, +1 nucleosome positioning by complexes with the HQ1 mutation was shifted by 10 bp downstream and reduced positioning precision was reflected in broadened distributions (Figure 2F,G). The downstream shifts observed here for individual INO80 points mutations were reminiscent of

similar effects resulting from INO80 depletion in the context of the interplay with other remodelers *in vivo*^{20,28,38}.

Taken together, our mutational analysis of candidate DNA contacts indicated robust processing of genomic sequence information by INO80 with a decisive role of the Arp8, but not the Nhp10 module, as direct reader of genome information at promoters.

DNA shape readout underlies INO80 nucleosome positioning Based on our mutational analysis, we sought to identify genomic DNA sequence features that provide positioning information. Previously, we proposed that *S. cerevisiae* INO80 might read DNA shape features of nucleosomal DNA²⁹. However, this hypothesis was based on correlation and the approach limited further interpretation, mainly because we used gene ranking by MNase-seq signal strength at pre-defined +1 to +3 nucleosome regions before and after remodeling as the discriminating category. This may introduce a bias towards the starting conditions, i.e. DNA sequence preferences of histones and variations in SGD assembly conditions. Moreover, the analysis was limited to pre-defined regions and numerous other DNA sequence motifs present at gene starts, e.g., evolved in the context of transcription regulation, may have convoluted the search for positioning information.

Here, we overcame these limitations and searched for the DNA sequence features of nucleosome positioning preferences by INO80 more globally, not only at promoters, and explored by a structure-based mutational analysis the direct and causal impact of altered INO80-DNA contacts on these preferences. We established a sensitive and unbiased Principal Component Analysis (PCA)/clustering approach solely on the basis of *de novo* generated nucleosome dyad positions determined by paired-end sequencing. This enabled unsupervised PCA/clustering of a large number of datasets (e.g. replicates, different assembly degrees, various INO80 WT and mutant complexes etc.) without prior assumptions (Figure S2A).

Nucleosomes remodeled by WT INO80 clearly clustered differently in PCA than those assembled during SGD without remodeling (Figure S2B), i.e. this approach could clearly distinguish positioning preferences under different conditions. The DNA sequences of different clusters did not differ in terms of sequence motifs assessed by motif search algorithms like Homer (data not shown) in contrast to previous studies of an isolated, truncated construct of human INO80 HSA domain that indicated sequence specific DNA binding⁴⁶.

However, DNA sequence information need not result in classical sequence motifs but may correspond to DNA shape features that are encoded in a more redundant way, i.e., rather disparate sequences may share similar shape features⁴⁷. A composite plot of propeller twist DNA shape feature of SGD-reconstituted versus INO80-remodeled nucleosomes revealed symmetrical but strikingly different profiles (Figure 3A), revealing distinct DNA sequence requirements for INO80

and SGD mediated positioning. Other shape features gave corresponding results (data not shown). The profile symmetry validated the shape information content as no nucleosome orientation was to be expected and symmetrical shape profiles are unlikely to occur by chance if no underlying shape feature were involved. Conversely, similar but asymmetrically distorted shape profiles were seen for nucleosomes reconstituted at positions close to *in vivo* +1 nucleosome positions and oriented relative to the direction of transcription (Figure S2C). This shows that the DNA shape information was also relevant for +1 nucleosome positioning.

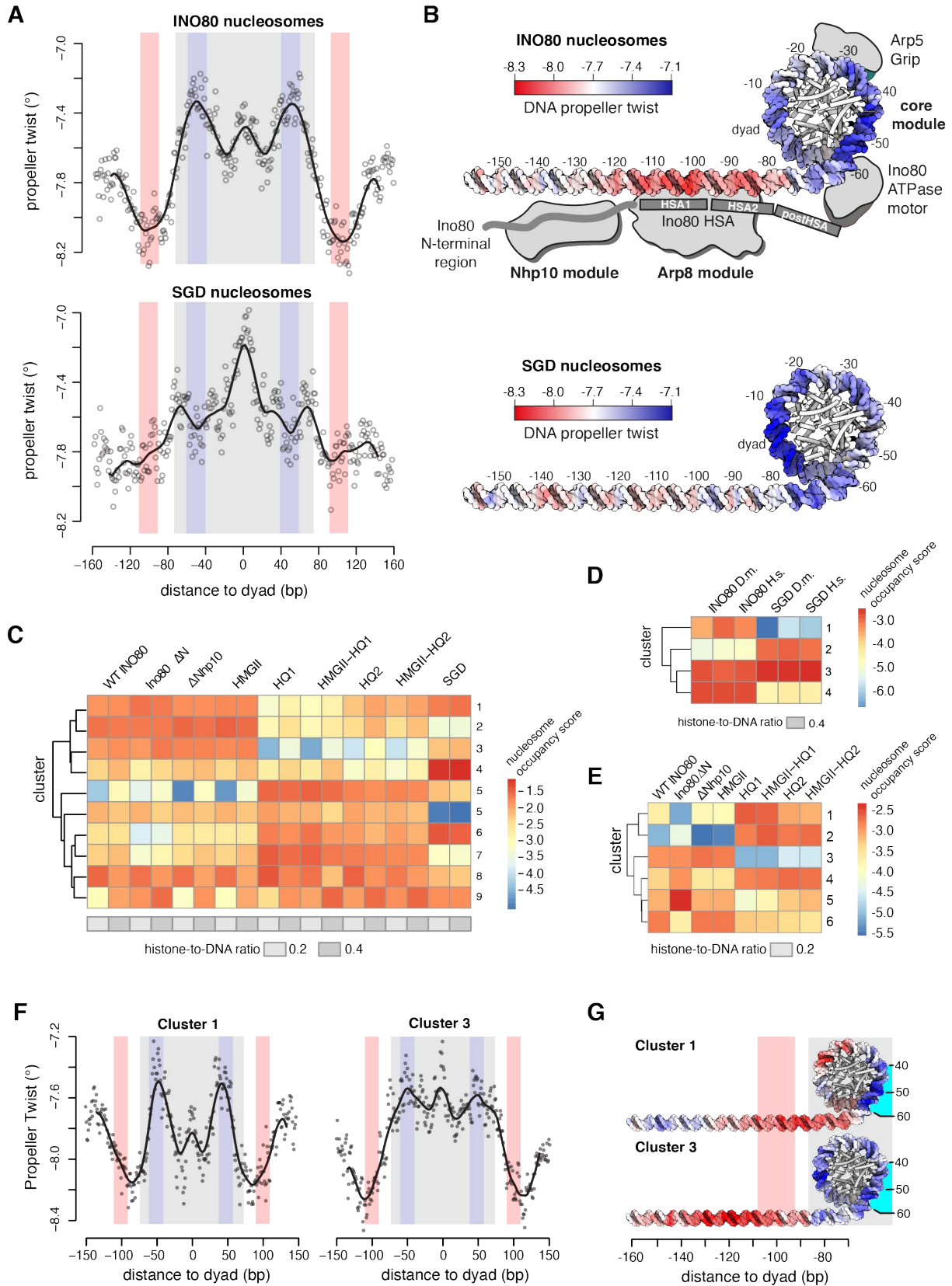


Figure 3: DNA shape readout underlies nucleosome positioning by INO80 and SGD. (A) Propeller twist DNA shape profiles for nucleosomal sequences of SGD chromatin with (INO80 nucleosomes) or without (SGD nucleosomes) remodeling by recombinant *S. cerevisiae* WT INO80 complex. Light red and light blue background indicate regions of major differences between SGD and INO80 profiles. Light grey background marks the location of the nucleosome core particle. **(B)** Red-white-blue color gradient mapping of propeller twist DNA shape profile

from A on model of linker and nucleosomal core DNA. Binding architecture of INO80 is shown schematically and based on structural data^{37,42} and biochemical mapping⁴³. **(C)** Nucleosome position clusters derived from principal component analysis (PCA) of nucleosome positions of SGD chromatin with embryonic *D. melanogaster* histones at the indicated histone-to-DNA mass ratio without (SGD) or after remodeling by the indicated recombinant *S. cerevisiae* WT and mutant INO80 complexes (as in Figure 2D,E) **(D)** As panel C but for SGD chromatin with embryonic *D. melanogaster* (*D. m.*) vs. recombinant *H. sapiens* (*H. s.*) histones at the indicated histone-to-DNA mass ratio without (SGD) or with remodeling by recombinant *S. cerevisiae* WT INO80 complex (INO80). **(E)** As panel C but only with the indicated subset of samples. **(F)** As panel A but only for nucleosomes from the indicated clusters of panel E. **(G)** Propeller twist DNA shape data from panel F mapped onto model of linker and nucleosomal DNA by using red-white-blue color gradient. See Supplementary Figure S3D for other clusters.

DNA shape profiles establish a new kind of nucleosome positioning information that is distinct from previously known DNA sequence preferences of histones. The relevance of DNA shape for remodeler-mediated nucleosome positioning was further underscored by a striking congruency between our PCA/clustering data and high-resolution structural information as well as *in vivo* mapping of INO80 subunits at gene promoters. The shape profiles of SGD-reconstituted versus INO80-remodeled nucleosomes differed mostly in the ± 55 bp and ± 100 bp regions relative to the dyad (color shaded areas in Figure 3A) where functionally important interactions with the INO80 complex are suggested by the biochemical and structural information available from INO80 in complex with mono-nucleosomes (Figure 3B). The HSA helix at the Ino80 N-terminus contacts linker DNA at about -100 bp from the dyad^{42,43}. The -55 bp region from the dyad lies between the Ino80 ATPase domain and the DNA contact point of Arp5. Both of these regions are critically important for nucleosome translocation. DNA strain build-up in the -55 bp region by successive rounds of DNA pumping by Ino80 ATPase motor is a central element of the proposed core mechanism of nucleosome translocation by INO80, while sensing of linker DNA by the Arp8 module ensures allosteric coupling of ATP hydrolysis to DNA translocation, which has been proposed to prevent back-slippage during DNA strain build up^{37,43}. This congruency immediately suggests a molecular mechanism by which a readout of shape encoded mechanical properties of DNA leads to the positioning of nucleosomes (see discussion). Notably, our findings provide thus also first insights into the hallmark mechanism of +1 nucleosome positioning; our data identify pronounced DNA shape signals in gene promoter regions upstream of INO80 positioned +1 nucleosomes. This direct readout is fully consistent with *in vivo* binding of INO80 subunits to gene promoter regions, as observed by ChIPexo mapping³⁸.

Altered Ino80-HSA-helix-DNA contacts affect DNA shape readout by INO80. To establish causality, we probed whether the INO80-DNA contacts and different histones would affect the shape readout. Nucleosomes positioned by WT INO80 clustered together with those positioned by mutant complexes where mutations affected the Nhp10 module, i.e., the Ino80 N-terminus or Nhp10 module subunits including the Nhp10 HMG Box (Figure 3C). This confirmed our results regarding nucleosome positioning in promoter regions (Figure 2D,E,F) and ruled out a major role for the Nhp10 HMG box in DNA shape readout by INO80. In contrast, all mutant complexes impaired in HSA helix-DNA contacts, either the HQ1 or HQ2 mutation and each also in combination

with the HMGII mutations, generated distinct clusters of nucleosome positions (Figure 3C). Overall shape preferences were not much affected if endogenous fly versus recombinant human histones were used (Figure 3D). This validated our use of fly histones for the comparisons among WT and mutant INO80 complexes in this approach.

In total, there were three major classes of nucleosome positions, those generated by i) SGD, ii) WT INO80/Nhp10 module mutant complexes or iii) HSA helix mutant complexes (Figure 3C). To investigate the differences in DNA sequence preferences only between the INO80 complexes and at minimal contribution of neighboring nucleosomes, we clustered only the respective samples with low assembly degree SGD chromatin (Figure 3E) and compared the resulting DNA shape profiles of clusters with clearly different occupancies among the INO80 complexes, e.g., cluster 1 versus 3 (Figure 3F,G, S3D). Propeller twist signal profiles clearly differed between clusters that contained nucleosome positions preferentially generated by the HSA helix-mutated INO80 versus WT or Nhp10 module mutated complexes. In particular, the ± 100 bp region of the linker DNA showed a distinct shift of the propeller twist signal by more than 20 bp between cluster 1 and 3 (Figure 3F). As this is the region where the Ino80 HSA domain contacts DNA (Figure 3B), these data directly showed that these HSA helix-DNA contacts contributed to the DNA shape readout during nucleosome positioning. Moreover, additional changes of propeller twist signals within the nucleosomal DNA region provides, in context of Ino80 HSA mutations, evidence for the allosteric interplay between the Arp8- and the core module of INO80^{42,43}. Taken together, we conclude that INO80 positions nucleosomes via a direct readout of DNA shape signature profiles. This information and its readout are distinct from known DNA sequence preferences of histones suggesting that remodelers play an active role in translating genomic information into nucleosome positions, i.e., determine nucleosome positions through their specific molecular mechanism of remodeling.

The DNA sequence-specific barrier Reb1 regulates nucleosome positioning by INO80.

Having established that INO80 directly reads DNA shape features and translates this information via specific modules into nucleosome positions, we asked next whether INO80 is also capable of processing nucleosome positioning information from DNA sequence-specific barrier factors (Figure 1B). Reb1 is a GRF important for promoter nucleosome organization *in vivo*²⁶. Sequence-specific GRFs serve, via an unknown mechanism, as nucleosome positioning alignment point for remodelers like ISW1a or ISW2²⁹.

To directly test whether Reb1 binding at cognate promoter sites controls +1 nucleosome positioning by INO80, we turned again to whole-genome reconstitutions. Increasing Reb1 concentrations clearly improved nucleosome positioning by INO80 at promoters with Reb1 sites in terms of +1 nucleosome occupancy (peak height), but also in array extent and NDR depth (Figures 4A,B, S3A). This Reb1 effect was again independent of the histone octamer species-origin

(Figure S3B). Detailed quantification of nucleosome spacing and array phasing at Reb1 sites and at different nucleosome densities was done in the accompanying paper (Oberbeckmann & Niebauer et al.). *In vivo* mapping of INO80 subunits by ChIPexo³⁸ indicated that INO80 adopts an extended conformation, which might bridge Reb1 binding sites and +1 nucleosomes.

To directly address whether INO80 relays positioning information from Reb1 to +1 nucleosomes, we turned to classical mononucleosome activity assay. We generated mononucleosomes with a long linker DNA on one side from a promoter (yGL167c) that was selected based on INO80 and Reb1 occupancy measured by ChIPexo *in vivo*³⁸ and clearly improved nucleosome positioning in whole-genome reconstitutions²⁹. *In vivo*, the Reb1 site is 145 bp upstream of the +1 nucleosome dyad. We replaced the +1 nucleosome sequence by a Widom-601 nucleosome positioning sequence (Lowary and Widom, 1998) and reconstituted with this construct (Figure 4C) via SGD the *in vivo* promoter nucleosome architecture.

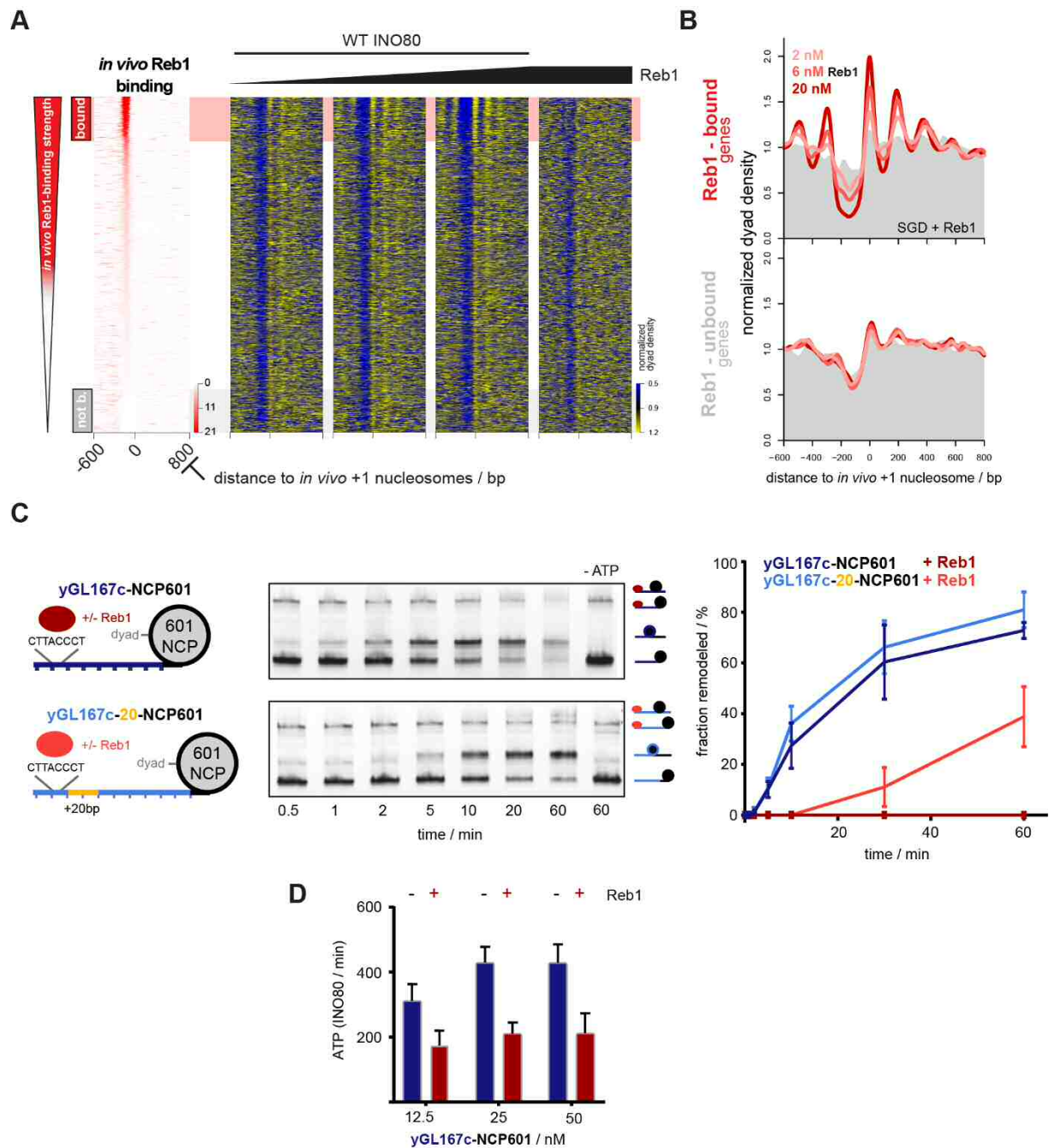


Figure 4: Reb1 regulates nucleosome positioning by INO80 and INO80's ATPase and sliding activity. (A) Heat maps of MNase-seq data for SGD chromatin assembled with recombinant *H. sapiens* histones at histone-to-DNA mass ratio 0.4, incubated with recombinant *S. cerevisiae* WT INO80 and increasing concentrations of recombinant Reb1 (ramp denotes 2, 6 and 20 nM Reb1). Right most panel shows sample prepared with embryonic *D. melanogaster* histones. Heat maps are aligned at *in vivo* +1 nucleosome positions and sorted according to decreasing (top to bottom) anti-Reb1 SLIM-ChIP score (*in vivo* Reb1 binding⁶¹) shown in leftmost heat map. Horizontal red or grey shading highlights genes with strong or weak *in vivo* Reb1 promotor-binding, respectively. Single replicates were plotted, see Figure S3A for all replicates. (B) Composite plots of MNase-seq data as in panel A averaged over genes highlighted in red (top) or grey (bottom) in panel A. (C) Left: mononucleosome substrate design with 80 bp (top) or 100 bp DNA overhang (bottom) taken from a promoter (yGL167c) with clear +1 nucleosome positioning by just INO80 *in vitro* and INO80 bound *in vivo*³⁸. Guided by its dyad positions, we replaced the genomic +1 nucleosome sequence of yGL167c with a 601-nucleosome positioning sequence. Middle: Native PAGE nucleosome sliding assay for indicated mononucleosome and Reb1 concentrations, and 10 nM recombinant *S. cerevisiae* WT INO80 for yGL16c-NCP601 (top) or yGL167c-20-NCP601 (bottom). "-ATP" denotes 60 min time point without ATP. Right: Quantification of sliding assays from the middle panel and two other replicates. Traces in red show data in the presence of Reb1. Error bar shows SD between

replicates. **(D)** NADH-based ATPase assay for the indicated mononucleosome concentrations and 10 nM recombinant *S. cerevisiae* WT INO80 alone or with Reb1 equimolar to mononucleosomes.

Reb1 was added substoichiometrically to reconstituted yGL167c-NCP601 mononucleosomes. As separation in native polyacrylamide gel electrophoresis could distinguish mononucleosomes with and without bound Reb1, we could compare remodeling kinetics with and without Reb1 in the same reaction (Figure 4C, middle). Kinetics of sliding the initially end-positioned nucleosome to the center were much slower, if at all detectable, in the presence of Reb1 (Figure 4C, middle and right). As the distance between bound Reb1 and the 601 nucleosome was as *in vivo* and therefore probably corresponded to the steady state distance set by INO80, we prepared and assayed in the same way a second construct (yGL167c-20-NCP601, Figure 4C) with additional 20 bp of DNA inserted in the yGL167c promoter. This end-positioned 601-nucleosome was clearly moved towards the Reb1 barrier by INO80 (Figure 4C, middle), but again at a slower rate compared to sliding this nucleosome to the center in the absence of Reb1 (Figure 4C, right).

We asked next, whether decreased sliding kinetics were caused by inhibition or by decoupling of ATPase activity. Notably, most INO80 mutations that abrogate nucleosome sliding, such as the HQ1/2 or Arp5 mutations, still showed robust ATPase activity^{37,42}. In contrast, INO80 ATPase assays in the presence of yGL167c-NCP601 mononucleosomes showed about twofold decreased ATPase activity upon addition of Reb1 compared to reactions without Reb1 (Figure 4D). This was not a general effect of Reb1 in this assay as Ino80^{ΔN} lacking the N-terminal region of Ino80 and the Nhp10-module did not show a reduction of ATPase activity upon Reb1 addition (see accompanying paper by Oberbeckmann & Niebauer et al.)

Taken together, we concluded that Reb1 binding to its cognate promoter sites regulates INO80 activity allosterically by inhibition through interaction via the N-terminal region of Ino80. The multi-subunit architecture of INO80 relays thereby positioning information between Reb1 and +1 nucleosomes and programs thereby such genes for formation of nucleosome arrays.

INO80 integrates information from DNA shape and Reb1 at promoters. A Reb1 site at a distance to a nucleosome position corresponds to an indirect input of DNA sequence information, mediated by its bound cognate factor Reb1, compared to the direct input of DNA shape features. Therefore, we asked if and how INO80 serves as an information processing hub and integrates such different information input into resulting nucleosome positions.

First, we asked if promoters with Reb1 sites at all contained DNA shape information leading to +1 nucleosome positioning by INO80 on its own in the absence of Reb1. Maybe promoter regions had evolved such that +1 nucleosome positions were either directly encoded via DNA shape or indirectly via GRF sites. We compared nucleosome positioning by INO80 in the absence of Reb1 at Reb1 site-containing promoters with positioning at an equal number of promoters lacking any

GRF sites. As INO80 was able to position *in vivo*-like +1 nucleosomes on its own at both types of promoter regions (Figure 5A), we concluded that both types contained +1 nucleosome position DNA shape information in their genomic sequence.

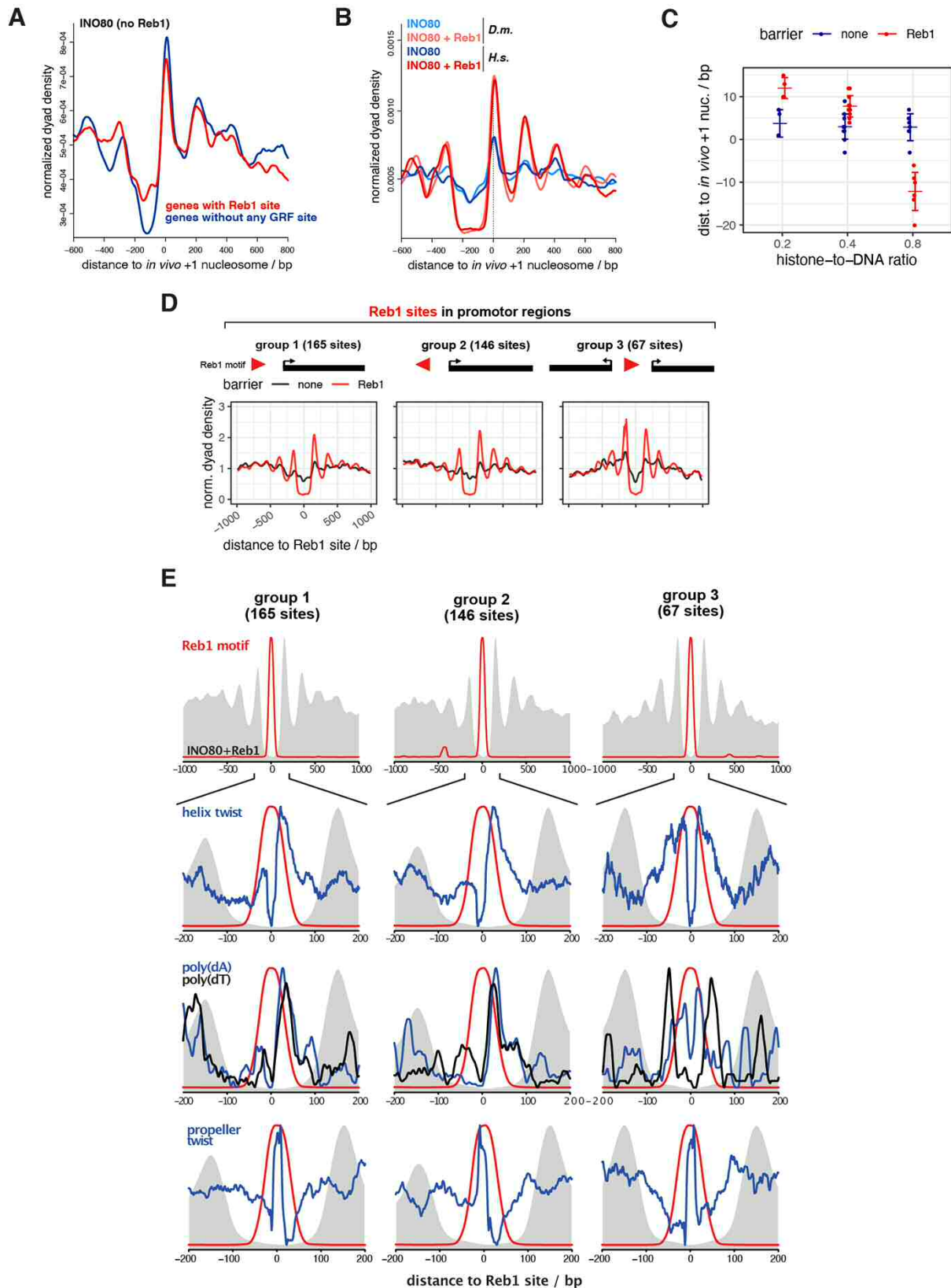


Figure 5: INO80 integrates nucleosome positioning information from DNA shape and Reb1 barriers. (A) Composite plots as in Figure 4B but for SGD chromatin with recombinant human histones at 0.4 histone-to-DNA mass ratio incubated with recombinant *S. cerevisiae* WT INO80 plotted for either genes with promoter Reb1 sites only (as red shading in Figure 4A) or for a randomly selected but similar number of genes with no GRF sites (Abf1, Rap1, Mcm1, Cbf1⁶²) in their promoters. **(B)** As panel A but for merged replicates comparing SGD chromatin with embryonic fly (*D. m.*) or recombinant human (*H. s.*) histones, \pm 20 nM Reb1 and only for genes with promoter Reb1 sites. **(C)** Distributions of distances between +1 nucleosome positions at Reb1-site containing promoters

reconstituted by incubation of SGD chromatin with the indicated histone-to-DNA mass ratio with recombinant *S. cerevisiae* WT INO80 in the presence (Reb1) or absence (none) of 20 nM Reb1. **(D)** As Figure 4B, but aligned at Reb1 sites of the indicated groups and with recombinant *S. cerevisiae* WT INO80 \pm 20 nM Reb1. **(E)** Reb1 site-aligned composite plots for genes groups as in panel D, from top to bottom: positions of Reb1 site PWM motifs, Reb1 site motifs and helix twist DNA shape features, Reb1 motifs and positions of poly(dA) or poly(dT) elements (> 6 homopolymeric stretches), Reb1 sites and propeller twist DNA shape features. Grey background in all panels shows composite plot of MNase-seq data as in panel D.

Second, we asked if the additional information of bound Reb1 at the promoters with Reb1 site was synergistic, antagonistic or neutral to the DNA shape-guided positioning by INO80. Comparing nucleosome positioning by INO80 at Reb1 site-containing promoters with versus without Reb1 showed that the Reb1 information mainly synergized with the DNA shape information and led to very similar positions but, in keeping with the outcome of the Reb1 titration (Figure 4A, B), to higher +1 nucleosome peaks (Figure 5B). Quantification of the differences in resulting peak positions with vs. without Reb1 showed that +1 nucleosome peaks differed on average only by 6 ± 3 bp for SGD chromatin with histone-to-DNA mass ratios of 0.2 or 0.4, which was within the experimental error of our reconstitutions (Figure 5C). For higher assembly degrees with a histone-to-DNA mass ratio of 0.8, the difference was 15 ± 5 bp, which was due to nucleosome positioning closer to Reb1 with increasing histone density, while the +1 nucleosome position as determined by INO80 on its own via DNA shape was hardly affected by variations in nucleosome density. Nonetheless, high density affected peak heights, which is discussed, together with the effects of density on nucleosome distance to barrier, in the accompanying paper (Oberbeckmann & Niebauer et al.) in the context of our remodeler ruler concept. Here, we concluded that genome sequence evolved a DNA shape signal downstream of a Reb1 site in direction of transcription so that nucleosome positioning by INO80 either guided by DNA shape or by Reb1 leads to very similar +1 nucleosome positions at low or medium nucleosome density. Note that promoter Reb1 sites are situated *in vivo* within NDRs⁴⁸, which by definition represent regions of locally low nucleosome density.

Third, we noted that the synergism between DNA shape- and Reb1-guided nucleosome positioning by INO80 only applied to the +1 nucleosome in direction of transcription, but not to the -1 nucleosome (Figure 5B). To assess this point more clearly and to ask if orientation of the intrinsically asymmetric Reb1 site further affected nucleosome positioning, we grouped Reb1 site-containing promoters according to the Reb1 site orientation relative to neighboring genes (groups 1 to 3, Figure 5D). Reb1 site-aligned MNase-seq data composite plots averaged over genes within these groups showed that peak heights and array generation were more pronounced in direction of transcription but independent of Reb1 site orientation. This further supported our conclusion that synergistic DNA shape information evolved next to Reb1 sites only in places where a +1 nucleosome becomes positioned that plays the well-known role in regulation of transcription initiation^{4,28}. Accordingly, promoters in groups 1 to 3 showed distinct asymmetrical DNA shape features and strand-specific poly(dA:dT) prevalence in the direction of transcription (Figure 5E).

Together, we concluded that INO80-mediated +1 nucleosome positioning is symmetrically guided by Reb1 as orientation of the Reb1 site did not matter (group 1 vs. 2, Figure 5D). Importantly, however, our analysis also revealed that Reb1 sites at promoters evolved synergistically with DNA shape features, which explains the observed asymmetry (groups 1 and 2) or symmetry (group 3) of nucleosome patterns depending on the DNA shape feature distribution in the genome (Figure 5E). The deviations in +1 nucleosome positions between DNA shape- versus Reb1-guided positioning (Figure 5C) in response to nucleosome density suggest that Reb1-guided positioning is either dominant or that Reb1-guided positioning is still possible at high density while DNA shape-guided positioning is not. In the accompanying paper (Oberbeckmann & Niebauer et al.) we show that the latter is the case.

DNA ends are potent barriers for INO80 nucleosome positioning. Having established a synergy between DNA shape and Reb1 sites at gene promoter regions, we asked whether we can uncouple barrier-mediated positioning from a promoter sequence context. To test this idea, we analyzed nucleosome positioning at all *in vivo* mapped genomic Reb1 sites (Figure 6A,B).

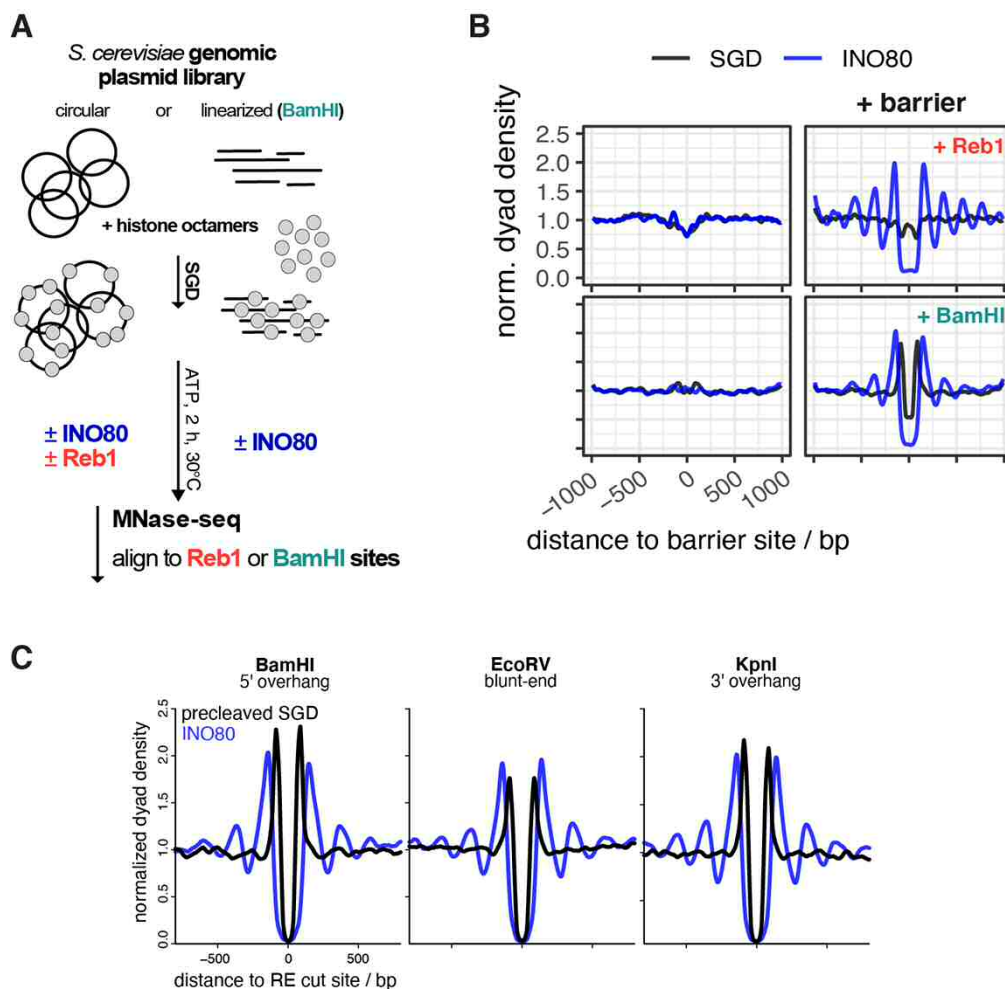


Figure 6: DNA ends are potent barriers for nucleosome positioning by INO80. (A) Overview (analogous to Figure 2A) of reconstitution with circular versus RE-precleaved plasmid libraries. (B) Composite plots of BamHI-site aligned versus anti-Reb1 SLIM-ChIP-defined Reb1 sites aligned MNase-seq data for: top, SGD prepared with

circular plasmid library and incubated without (SGD) or with recombinant *S. cerevisiae* WT INO80 (INO80), and bottom: as top but with BamHI-precleaved library if indicated (+ BamHI). **(C)** As panel B, but for SGD chromatin with plasmid libraries pre-cleaved with the indicated RE and data aligned at the indicated RE cut sites. Strong peaks flanking cut RE sites in SGD chromatin without INO80 remodeling reflected an MNase-seq bias. Due to the pre-cleavage, the probability that a mononucleosomal fragment flanking the cut site is released by MNase is increased.

Consistent with our findings above, we observed symmetrical nucleosome arrays around all Reb1 sites (Figure 6B, top right) suggesting that barrier-mediated positioning can occur independently of other DNA sequence features. In light of this, we considered that INO80 may align nucleosomes also to different barrier types as long as they represented a clear alignment point. In our search of the minimalistic system that provides nucleosome positioning information, we wondered if simply a DNA end could constitute a barrier. Notably, INO80 has been involved in DNA damage response signaling upon DNA double strand breaks (DSBs) *in vivo*⁴⁹. In principle, such as scenario was already tested in classical mononucleosome sliding assays as these automatically involve two DNA ends. However, effects there may have been due to the comparatively short length of template DNA and to the presence of two DNA ends at the same time. Our genome-wide system allowed us to test the effect of one-sided DNA ends in the context of very long DNA. We introduced double stranded DNA ends at fortuitous locations, i.e., without likely evolutionarily shaped context, throughout the *S. cerevisiae* genome via restriction enzyme (RE) digest of the plasmid library (Figure 6A). As expected, SGD chromatin neither with nor without remodeling by INO80 showed distinct nucleosome patterns at uncleaved BamHI sites (Figure 6B, bottom left). However, strong and symmetrical arrays were aligned at cut sites by INO80 (Figure 6B, bottom right). The same was true for other REs that generated different kinds of DNA ends (Figure 6C). We concluded that all three kinds of DNA ends (blunt, 3' or 5' overhang) were strong nucleosome positioning barriers for INO80.

Discussion

In this study, we identified and probed the fundamental molecular determinants by which ATP-dependent chromatin remodelers position nucleosomes across the genome. An integrated approach combining fully-recombinant, *de novo* whole-genome reconstitutions, high-resolution structural information, and PCA/clustering analysis revealed that the INO80 complex processes DNA sequence information, both directly, via readout of a distinct DNA shape signature motif, as well as indirectly, via alignment at a barrier like Reb1 or at DSBs. INO80's multi-subunit architecture integrates the readout of different positioning informations, contributes through its mechanism its own information and determines thereby how this is translated into nucleosome positions.

Although the pivotal role of remodelers in chromatin organization and their dependency on DNA sequences has been recognized^{29,31,50}, nucleosome positioning sequences (NPSs) were usually defined as sequences of "intrinsic" positioning by SGD driven solely by histone octamer-DNA interactions, as illustrated by the Widom 601 NPS⁵¹. PCA/clustering analysis enabled us now to reassess these classical SGD-NPSs and to identify a new kind of NPS. We find that SGD-NPSs correspond to distinct DNA-sequence dependent shape profiles, while nucleosome positioning by a remodeler like INO80 corresponds to a different shape profile. Therefore, we identified the latter as INO80-NPSs. Respective remodeler-NPSs are likely to exist for other remodelers and it will be interesting where they evolved in genomes. In analogy to the "genomic code for nucleosome positioning", i.e. the proposed evolution of SGD-NPSs, evolved remodeler-NPSs would implement a "remodeler code for nucleosome positioning" as proposed earlier⁵². We abstain from adding another "code" to the troubled epigenetics discussions but point out the conceptual analogy.

Importantly, we go here beyond a mere correlation between INO80-NPSs and DNA shape profiles. The causal mechanistic link was directly established by tuning the INO80 DNA shape readout via targeted INO80 mutations. Informed by high-resolution structures, we found independently that on the one hand mutation of Ino80-HSA-DNA contacts more than -100 bp away from the nucleosome dyad caused altered nucleosome positioning patterns, while on the other hand unbiased PCA/clustering analysis revealed also altered DNA shape features right in the same region. Together, our results provide strong evidence for a direct readout of these DNA shape features. Moreover, we observed altered processing of DNA shape features at the -55 bp region between the Ino80 core ATPase motor and the Arp5 grip, suggesting a critical role of DNA shape in regulating the build-up of DNA strain during the core mechanism of nucleosome translocation^{37,43,44}. Intriguingly, the effects at both regions are coupled via two allosteric communication pathways of possibly equal importance: on the protein side, linker DNA recognition by the Arp8 module is coupled to the activity of the Ino80 ATPase motor of the core module via the extended

helical configuration of the HSA and postHSA domains⁴². On the DNA side, DNA shape features at the histone-bound -55 bp region are most likely coupled to DNA shape features at the DNA linker -100 bp region in the context of over- and underwinding of DNA in front and behind the Ino80 ATPase motor. More generally, our data illustrates a regulatory circuitry comprising a two-way relationship between a protein factor working on DNA and DNA properties feeding back to the protein factor. Overall, INO80-NPSs represent the nucleosome positioning information that emerges from the combination of DNA, histones, and the active interpretation via the allosteric communication within the remodeler.

For these reasons, the DNA shape readout by INO80 importantly expands the scope of recently discussed DNA shape contributions. DNA shape was mostly studied in the context of “static” DNA binding, e.g., by transcription factors and GRFs⁵³⁻⁵⁵. In contrast, INO80 dynamically reads and interprets DNA shape while tracking along DNA in an ATP-dependent way. INO80 can be a role model for factors that translocate along DNA or also RNA, like other remodelers, helicases, cohesins or polymerases. For example, RNA polymerase I was suggested to read the DNA bend at its promoters⁵⁶ and RNA polymerase II may recognize its promoters via structural DNA features (bending, meltability, flexibility) rather than via classical consensus sequences⁵⁷. As these structural properties are redundantly linked to DNA sequence, we propose that readout of such DNA structural properties may be common if factors deal with a wide range of genomic regions.

As alternative DNA sequence signals, there is DNA sequence information of classical consensus motifs for specific binding by cognate factors. GRFs are well-known to program +1 nucleosome positioning and formation of genic nucleosome arrays *in vivo*^{26,32,58}. In light of our finding that DNA ends are also potent nucleosome positioning barriers, it is tempting to speculate that remodelers involved in DNA damage response, such as INO80⁴⁹, may generate regular nucleosome arrays as a licensing platform at DSBs *in vivo*.

The mechanism by which remodelers generate arrays at barriers, i.e., indirectly read positioning information via an alignment mechanism, remained largely unknown. This study reveals that nucleosome positioning by INO80 is actively regulated by Reb1 at promoter sites through an interaction with the N-terminal region of Ino80. Intriguingly, Reb1 decreased not only nucleosome sliding, but also inhibited ATPase activity of INO80, even at a distance of -145 bp between the cognate Reb1 site and the dyad of the +1 nucleosome. In contrast, DNA linker length sensing by INO80 uncouples a decrease in mononucleosome sliding from its robust stimulation of ATPase activity^{42,44}. Consequently, GRFs might represent “active barriers”, which regulate remodeler activity, whereas DSBs may correspond to “passive barriers”, at least in the absence of the DNA repair machinery. In the accompanying study, we identify the Arp8-module and the Nhp10 module as a multi-layered ruler element which measures and sets nucleosome arrays differently in respect to Reb1 sites, DNA ends and neighboring nucleosome. Taken together, we

conclude that the multi-subunit architecture of INO80 functions similar to a relay: INO80 receives barrier-specific input via its Arp8 and Nhp10 modules and communicates this information allosterically towards the ATPase of the INO80 core, where it is translated into a nucleosome position.

The exact +1 nucleosome position impacts transcription regulation, e.g., it differs between repressed and activated promoters and influences TSS selection^{4,11,28,59}. In this study, we show that these positions are robustly encoded in the genome in two ways, i.e., both by DNA shape features and corresponding distances to the Reb1 site. Nucleosome positioning next to Reb1 did not require DNA shape features as it also worked symmetrically on the other side even if there was no evolved promoter. Importantly, however, in context of promoter regions, we identify a co-evolved synergy between DNA shape signatures and Reb1 binding sites, leading to asymmetric +1 nucleosome positioning. This synergy provides not only robustness, but also an inroad to regulation. For example, we show that Reb1-mediated positioning is altered in response to nucleosome densities. Thus, we propose that regulation of nucleosome density at promoters, e.g., via the local activity of RSC, the major nucleosome-evicting remodeler in yeast²³, may result in regulation of +1 nucleosome positions. With high RSC activity, local promoter nucleosome density is low and +1 nucleosome positioning by INO80 coincides for DNA shape- and Reb1-information input. Upon low RSC activity, nucleosome density is high and INO80 disregards the shape signal and places the +1 nucleosome closer to Reb1, which corresponds to the more upstream +1 nucleosome position implicated in repressed promoter states.

By establishing genome wide biochemistry, this study reveals that a minimal set of information, comprising genomic DNA sequences, globular histones, and the molecular machinery of the remodeler, is sufficient to explain the placement and regulation of nucleosomes at their *in vivo* +1 positions for many promoters where appropriate DNA shape signatures evolved. The identified mechanism of active information processing provides allosteric control and versatile means for selective regulation, e.g., by epigenetic information such as histone modifications and variants as well as by the presence of sequence-specific factors such as transcription factors and pioneer factors. Signal integration of genome information from DNA shape and sequence specified GRF binding by the multi-subunit architecture of INO80 exemplifies such principles. In the accompanying paper (Oberbeckmann & Niebauer et al.), we show how information from GRFs, DNA ends and positioned nucleosomes can be propagated into regular nucleosome arrays and how this process is regulated by remodeler rulers and nucleosome density. Collectively, this makes ATP dependent remodelers the fundamental information processing hub for nucleosome positioning, which constitutes the first level of chromatin organization.

Acknowledgments

We thank Stefan Krebs and Helmut Blum at the Laboratory for Functional Genome Analysis (LAFUGA, Gene Center, LMU München) for high throughput sequencing, and Sigurd Braun for access to and help with the plating robot. This study was funded by the German Research Foundation (SFB1064 to P.K. and K.P.H. and Gottfried Wilhelm Leibniz-Prize to K.P.H.) and by the European Research Council (ERC Advanced Grant “INO3D” to K.P.H.). N.K. is supported by HFSP grant LT000631/2017-L.

Author contributions

Conceptualization: EO, NK, TS, KPH, PK, SE; Data curation: EO, NK, VN; Formal analysis: EO, NK, VN, TS; Funding acquisition, Project administration, Supervision: KPH, PK, SE; Investigation: EO, NK, VN, KS, MM, TS, SE; Methodology: EO, NK, VN, KS, TS, PK, SE; Validation: EO, NK, VN, KS, TS, PK, SE; Visualization: EO, NK, VN, TS, PK, SE; Writing original draft: EO, NK, PK, SE; Writing – review & editing: EO, NK, VN, TS, KPH, PK, SE

Competing interests

The authors declare no competing interest.

References

1. Bell, O., Tiwari, V.K., Thoma, N.H. & Schubeler, D. Determinants and dynamics of genome accessibility. *Nat Rev Genet* **12**, 554-64 (2011).
2. Lai, W.K.M. & Pugh, B.F. Understanding nucleosome dynamics and their links to gene expression and DNA replication. *Nat Rev Mol Cell Biol* **18**, 548-562 (2017).
3. Bannister, A.J. & Kouzarides, T. Regulation of chromatin by histone modifications. *Cell Res* **21**, 381-95 (2011).
4. Jiang, C. & Pugh, B.F. Nucleosome positioning and gene regulation: advances through genomics. *Nat Rev Genet* **10**, 161-72 (2009).
5. Lawrence, M., Daujat, S. & Schneider, R. Lateral Thinking: How Histone Modifications Regulate Gene Expression. *Trends Genet* **32**, 42-56 (2016).
6. Mavrich, T.N. et al. Nucleosome organization in the Drosophila genome. *Nature* **453**, 358-62 (2008).
7. Yuan, G.C. et al. Genome-scale identification of nucleosome positions in *S. cerevisiae*. *Science* **309**, 626-30 (2005).
8. Zink, L.M. & Hake, S.B. Histone variants: nuclear function and disease. *Curr Opin Genet Dev* **37**, 82-89 (2016).
9. Lieleg, C., Krietenstein, N., Walker, M. & Korber, P. Nucleosome positioning in yeasts: methods, maps, and mechanisms. *Chromosoma* **124**, 131-51 (2015).
10. Haberle, V. & Lenhard, B. Promoter architectures and developmental gene regulation. *Semin Cell Dev Biol* **57**, 11-23 (2016).
11. Shivaswamy, S. & Iyer, V.R. Stress-dependent dynamics of global chromatin remodeling in yeast: dual role for SWI/SNF in the heat shock stress response. *Mol Cell Biol* **28**, 2221-34 (2008).
12. Luger, K., Mader, A.W., Richmond, R.K., Sargent, D.F. & Richmond, T.J. Crystal structure of the nucleosome core particle at 2.8 Å resolution. *Nature* **389**, 251-60 (1997).
13. Widom, J. Role of DNA sequence in nucleosome stability and dynamics. *Q Rev Biophys* **34**, 269-324 (2001).
14. Satchwell, S.C., Drew, H.R. & Travers, A.A. Sequence periodicities in chicken nucleosome core DNA. *J Mol Biol* **191**, 659-75 (1986).
15. Kaplan, N. et al. The DNA-encoded nucleosome organization of a eukaryotic genome. *Nature* **458**, 362-6 (2009).
16. Kornberg, R.D. & Stryer, L. Statistical distributions of nucleosomes: nonrandom locations by a stochastic mechanism. *Nucleic Acids Res* **16**, 6677-90 (1988).
17. Zhang, Y. et al. Intrinsic histone-DNA interactions are not the major determinant of nucleosome positions in vivo. *Nat Struct Mol Biol* **16**, 847-52 (2009).
18. Zhang, Z. et al. A packing mechanism for nucleosome organization reconstituted across a eukaryotic genome. *Science* **332**, 977-80 (2011).
19. Gossett, A.J. & Lieb, J.D. In vivo effects of histone H3 depletion on nucleosome occupancy and position in *Saccharomyces cerevisiae*. *PLoS Genet* **8**, e1002771 (2012).
20. van Bakel, H. et al. A compendium of nucleosome and transcript profiles reveals determinants of chromatin architecture and transcription. *PLoS Genet* **9**, e1003479 (2013).
21. Lieleg, C. et al. Nucleosome spacing generated by ISWI and CHD1 remodelers is constant regardless of nucleosome density. *Mol Cell Biol* **35**, 1588-605 (2015).
22. Mobius, W. & Gerland, U. Quantitative test of the barrier nucleosome model for statistical positioning of nucleosomes up- and downstream of transcription start sites. *PLoS Comput Biol* **6**(2010).
23. Clapier, C.R., Iwasa, J., Cairns, B.R. & Peterson, C.L. Mechanisms of action and regulation of ATP-dependent chromatin-remodelling complexes. *Nat Rev Mol Cell Biol* **18**, 407-422 (2017).
24. Gkikopoulos, T. et al. A role for Snf2-related nucleosome-spacing enzymes in genome-wide nucleosome organization. *Science* **333**, 1758-60 (2011).
25. Cairns, B.R. et al. RSC, an essential, abundant chromatin-remodeling complex. *Cell* **87**, 1249-60 (1996).

26. Hartley, P.D. & Madhani, H.D. Mechanisms that specify promoter nucleosome location and identity. *Cell* **137**, 445-58 (2009).
27. Kubik, S. et al. Sequence-Directed Action of RSC Remodeler and General Regulatory Factors Modulates +1 Nucleosome Position to Facilitate Transcription. *Mol Cell* **71**, 89-102.e5 (2018).
28. Kubik, S. et al. Opposing chromatin remodelers control transcription initiation frequency and start site selection. *Nat Struct Mol Biol* **26**, 744-754 (2019).
29. Krietenstein, N. et al. Genomic Nucleosome Organization Reconstituted with Pure Proteins. *Cell* **167**, 709-721.e12 (2016).
30. Krietenstein, N., Wippo, C.J., Lieleg, C. & Korber, P. Genome-wide in vitro reconstitution of yeast chromatin with in vivo-like nucleosome positioning. *Methods Enzymol* **513**, 205-32 (2012).
31. Lorch, Y., Maier-Davis, B. & Kornberg, R.D. Role of DNA sequence in chromatin remodeling and the formation of nucleosome-free regions. *Genes Dev* **28**, 2492-7 (2014).
32. Challal, D. et al. General Regulatory Factors Control the Fidelity of Transcription by Restricting Non-coding and Ectopic Initiation. *Mol Cell* **72**, 955-969.e7 (2018).
33. Fourel, G., Miyake, T., Defossez, P.A., Li, R. & Gilson, E. General regulatory factors (GRFs) as genome partitioners. *J Biol Chem* **277**, 41736-43 (2002).
34. Tsankov, A., Yanagisawa, Y., Rhind, N., Regev, A. & Rando, O.J. Evolutionary divergence of intrinsic and trans-regulated nucleosome positioning sequences reveals plastic rules for chromatin organization. *Genome Res* **21**, 1851-62 (2011).
35. Yamada, K. et al. Structure and mechanism of the chromatin remodelling factor ISW1a. *Nature* **472**, 448-53 (2011).
36. Ayala, R. et al. Structure and regulation of the human INO80-nucleosome complex. *Nature* **556**, 391-395 (2018).
37. Eustermann, S. et al. Structural basis for ATP-dependent chromatin remodelling by the INO80 complex. *Nature* **556**, 386-390 (2018).
38. Yen, K., Vinayachandran, V. & Pugh, B.F. SWR-C and INO80 chromatin remodelers recognize nucleosome-free regions near +1 nucleosomes. *Cell* **154**, 1246-56 (2013).
39. Bonisch, C. & Hake, S.B. Histone H2A variants in nucleosomes and chromatin: more or less stable? *Nucleic Acids Res* **40**, 10719-41 (2012).
40. White, C.L., Suto, R.K. & Luger, K. Structure of the yeast nucleosome core particle reveals fundamental changes in internucleosome interactions. *Embo j* **20**, 5207-18 (2001).
41. Udugama, M., Sabri, A. & Bartholomew, B. The INO80 ATP-dependent chromatin remodeling complex is a nucleosome spacing factor. *Mol Cell Biol* **31**, 662-73 (2011).
42. Knoll, K.R. et al. The nuclear actin-containing Arp8 module is a linker DNA sensor driving INO80 chromatin remodeling. *Nat Struct Mol Biol* **25**, 823-832 (2018).
43. Brahma, S., Ngubo, M., Paul, S., Udugama, M. & Bartholomew, B. The Arp8 and Arp4 module acts as a DNA sensor controlling INO80 chromatin remodeling. *Nat Commun* **9**, 3309 (2018).
44. Zhou, C.Y. et al. The Yeast INO80 Complex Operates as a Tunable DNA Length-Sensitive Switch to Regulate Nucleosome Sliding. *Mol Cell* **69**, 677-688.e9 (2018).
45. Zhou, C.Y. et al. Regulation of Rvb1/Rvb2 by a Domain within the INO80 Chromatin Remodeling Complex Implicates the Yeast Rvbs as Protein Assembly Chaperones. *Cell Rep* **19**, 2033-2044 (2017).
46. Mendiratta, S., Bhatia, S., Jain, S., Kaur, T. & Brahmachari, V. Interaction of the Chromatin Remodeling Protein hINO80 with DNA. *PLoS One* **11**, e0159370 (2016).
47. Zhou, T. et al. DNashape: a method for the high-throughput prediction of DNA structural features on a genomic scale. *Nucleic Acids Res* **41**, W56-62 (2013).
48. Rhee, H.S. & Pugh, B.F. Comprehensive genome-wide protein-DNA interactions detected at single-nucleotide resolution. *Cell* **147**, 1408-19 (2011).
49. van Attikum, H., Fritsch, O., Hohn, B. & Gasser, S.M. Recruitment of the INO80 complex by H2A phosphorylation links ATP-dependent chromatin remodeling with DNA double-strand break repair. *Cell* **119**, 777-88 (2004).
50. Winger, J. & Bowman, G.D. The Sequence of Nucleosomal DNA Modulates Sliding by the Chd1 Chromatin Remodeler. *J Mol Biol* **429**, 808-822 (2017).

51. Lowary, P.T. & Widom, J. New DNA sequence rules for high affinity binding to histone octamer and sequence-directed nucleosome positioning. *J Mol Biol* **276**, 19-42 (1998).
52. Rippe, K. et al. DNA sequence- and conformation-directed positioning of nucleosomes by chromatin-remodeling complexes. *Proc Natl Acad Sci U S A* **104**, 15635-40 (2007).
53. Levo, M. et al. Unraveling determinants of transcription factor binding outside the core binding site. *Genome Res* **25**, 1018-29 (2015).
54. Rossi, M.J., Lai, W.K.M. & Pugh, B.F. Genome-wide determinants of sequence-specific DNA binding of general regulatory factors. *Genome Res* **28**, 497-508 (2018).
55. Zentner, G.E., Kasinathan, S., Xin, B., Rohs, R. & Henikoff, S. ChEC-seq kinetics discriminates transcription factor binding sites by DNA sequence and shape in vivo. *Nat Commun* **6**, 8733 (2015).
56. Engel, C. et al. Structural Basis of RNA Polymerase I Transcription Initiation. *Cell* **169**, 120-131.e22 (2017).
57. Dienemann, C., Schwalb, B., Schilbach, S. & Cramer, P. Promoter Distortion and Opening in the RNA Polymerase II Cleft. *Mol Cell* **73**, 97-106.e4 (2019).
58. Ganapathi, M. et al. Extensive role of the general regulatory factors, Abf1 and Rap1, in determining genome-wide chromatin structure in budding yeast. *Nucleic Acids Res* **39**, 2032-44 (2011).
59. Boeger, H., Griesenbeck, J., Strattan, J.S. & Kornberg, R.D. Nucleosomes unfold completely at a transcriptionally active promoter. *Mol Cell* **11**, 1587-98 (2003).
60. Ocampo, J., Chereji, R.V., Eriksson, P.R. & Clark, D.J. The ISW1 and CHD1 ATP-dependent chromatin remodelers compete to set nucleosome spacing in vivo. *Nucleic Acids Res* **44**, 4625-35 (2016).
61. Gutin, J. et al. Fine-Resolution Mapping of TF Binding and Chromatin Interactions. *Cell Rep* **22**, 2797-2807 (2018).
62. Yan, C., Chen, H. & Bai, L. Systematic Study of Nucleosome-Displacing Factors in Budding Yeast. *Mol Cell* **71**, 294-305.e4 (2018).

Methods

Organisms as source for materials used in experiments.

The pGP546 yeast genomic plasmid library was expanded from the clonal plates provided by Open Biosystems.

INO80 wild-type and mutant complexes were expressed in *Trichoplusia insect cells*. *Spodoptera frugiperda sf21* insect cells were used for virus production. Reb1 was purified from *E. coli* BL21 (DE3) cd+ cells. The *Drosophila* embryo histones were prepared from the *Drosophila melanogaster* strain OregonR.

Embryonic *D. melanogaster* histones, whole-genome plasmid libraries and salt gradient dialysis

Embryonic *D. melanogaster* histone purification. The preparation of embryonic *D. melanogaster* histones octamers was carried out as described before^{1,2}. In brief, 50 g of 0-12 hours old *D. melanogaster* embryos were dechorionated in 3 % sodium hypochlorite, washed with dH₂O and resuspended in 40 mL lysis-buffer (15 mM K-HEPES pH 7.5, 10 mM KCl, 5 mM MgCl₂, 0.1 mM EDTA, 0.5 mM EGTA, 1 mM DTT, 0.2 mM PMSF, 10 % glycerol). Embryos were homogenized (Yamamoto homogenizer), filtered through cloth and centrifuged at 6,500 *g* for 15 min. Nuclei (brownish light pellet) were washed 3 times with 50 mL sucrose-buffer (15 mM K-HEPES pH 7.5, 10 mM KCl, 5 mM MgCl₂, 0.05 mM EDTA, 0.25 mM EGTA, 1 mM DTT, 0.2 mM PMSF, 1.2 % sucrose) and resuspended in 30 mL sucrose-buffer containing 3 mM CaCl₂. To obtain mononucleosomes, nuclei were incubated for 10 min at 26 °C with 6250 Units MNase (Sigma-Aldrich). Reaction was stopped with 10 mM EDTA, nuclei were pelleted and resuspended in 6 mL TE (10 mM Tris-HCl pH 7.6, 1 mM EDTA) containing 1 mM DTT and 0.2 mM PMSF followed by 30 to 45 min of rotation at 4 °C. Nuclei were centrifuged for 30 min at 15,300 *g* at 4 °C. Solubilized mononucleosomes are found in the supernatant, which was applied to a pre-equilibrated hydroxyapatite column. After washing the hydroxyapatite column with 0.63 M KCl, histone octamers were eluted with 2 M KCl, concentrated and stored in 50 % glycerol and 1x Complete (Roche) protease inhibitors without EDTA at -20 °C.

Whole-genome plasmid library expansion. The *S. cerevisiae* genomic plasmid library (pGP546) was originally described in Jones et al., 2008 and purchased as a clonal glycerol stock collection from Open Biosystems. Library expansion was carried out via a Singer ROTOR plating machine (Singer Instruments) (8-12 rounds, 3 replicas). After 16 hours, colonies were combined into 3x2 L of LB medium containing 50 µg/mL kanamycin and grown for 4 hours. Cells were harvested and subjected to Plasmid Giga Preparation (PC 10 000 Kit, Macherey&Nagel).

Salt gradient dialysis (SGD). For low, medium and high assembly degrees, 10 µg of plasmid library DNA (*S. cerevisiae*, *S. pombe* or *E. coli*) was mixed with ~2, 4 or 8 µg of *Drosophila* embryo histone octamers, respectively, in 100 µl assembly buffer (10 mM Tris-HCl, pH 7.6, 2 M NaCl, 1 mM EDTA, 0.05 % IGEPAL CA630, 0.2 µg BSA). Samples were transferred to Slide-A-lyzer mini dialysis devices, which were placed in a 3 L beaker containing 300 mL of high salt buffer (10 mM Tris-HCl pH 7.6, 2 M NaCl, 1 mM EDTA, 0.05 % IGEPAL CA630, 14.3 mM β-mercaptoethanol), and dialyzed against a total of 3 L low salt buffer (10 mM Tris-HCl pH 7.6, 50 mM NaCl, 1 mM EDTA, 0.05 % IGEPAL CA630, 1.4 mM β-mercaptoethanol) added continuously via a peristaltic pump over a time course of 16 h while stirring. β-mercaptoethanol was added freshly to all buffers. After complete transfer of low salt buffer, samples were dialyzed against 1 L low salt buffer for 1 h at room temperature. DNA concentration of the SGD chromatin preparations was estimated with a DS-11+ spektrophotometer (Denovix) and could be stored at 4 °C for several weeks. To estimate the extent of the assembly degree, an aliquot of the sample was subjected to MNase digestion (as described below) for MNase-ladder read out.

Expression and purification of INO80 complex and respective mutants. Coding sequences for *S. cerevisiae* Ino80 (2xFlag), Rvb1, Rvb2, Arp5-His, Ies6 (pFBDM_1) and Actin, Arp4, Arp8, Taf14, Ies2, Ies4, Ies1, Ies3, Ies5 and Nhp10 (pFBDM_2) were subcloned into pFBDM vectors³ and sequence verified by Sanger Sequencing (GATC Services at Eurofins Genomics). Bacmids of both vectors were generated using DH10 multibac cells⁴. Baculoviruses were generated in *Spodoptera frugiperda* (SF21) insect cells (IPLB-Sf21AE). *Trichoplusia ni* High Five (Hi5) insect cells (BTI-TN-5B1-4 Invitrogen) were co-infected with two baculoviruses 1/100 each. After 60 h cultivation at 27 °C, cells were harvested by centrifugation. For purification of the INO80 complex, cells were resuspended in lysis buffer (50 mM Tris-HCl pH 7.9, 500 mM NaCl, 10 % glycerol, 1 mM DTT, SIGMAFAST™ protease inhibitor cocktail), sonified (Branson Sonifier, 3x 20 s with 40 % duty cycle and output control 3-4) and cleared by centrifugation (Sorvall Evolution RC, SS34 rotor, 15,000 g). The supernatant was incubated for 1 h with anti-Flag M2 Affinity Gel (Sigma-Aldrich) and centrifuged for 15 min at 1,000 g and 4 °C. The anti-Flag resin was washed with buffer A (25 mM K-HEPES pH 8.0, 500 mM KCl, 10 % glycerol, 0.025 mM IGEPAL CA630, 4 mM MgCl₂, 1 mM DTT) and buffer B (25 mM K-HEPES pH 8.0, 200 mM KCl, 10 % glycerol, 0.02 mM IGEPAL CA630, 4 mM MgCl₂, 1 mM DTT). Recombinant INO80 complex was eluted with buffer B containing 1.6 mg Flag Peptide (Sigma-Aldrich). Anion exchange chromatography (MonoQ 5/50 GL, GE Healthcare) was used for further purification which resulted in a monodisperse and clear INO80 complex (Figure S1A,B,E). Using standard cloning techniques, three INO80 (2xFlag) HSA domain mutants (HQ1, HQ2, HQ1/2; Figure 2C, S1E), one N-terminal deletion mutant (Ino80^{ΔN}, deletion of the first 461 amino acids of the N-terminus of Ino80) and two INO80 (2xFlag) Nhp10 module mutants (ΔNhp10 (INO80 complex without Ies1, Ies3, Ies5 and Nhp10 but with Ino80 N-terminus) and HMGII (Figure 2C, S1E) pFBDM vectors were generated and integrated into baculoviruses using MultiBac Technology as described above. Expression and purification of mutant INO80 complexes was essentially carried out as WT INO80 complex purification. The INO80 core complex from *Chaetomium thermophilum* (equivalent to the *S. cerevisiae* N-terminal deletion mutant) was essentially purified as described in ⁵.

Expression and purification of human tailless histone octamers. The genes for expression of tailless human histones H2A, H2B and H4 were cloned in pET21b vectors (Merck, Darmstadt, Germany) by blunt-end ligation of genes coding for full-length human histones. The gene coding for human tailless H3 was cloned in a pETM-11 vector (kindly provided by EMBL, Heidelberg, Germany) carrying a N-terminal SUMO-tag by Gibson assembly⁶. The SUMO-tag was removed during octamer assembly. Constructs of tailless histones were designed according to globular domains identified by tryptic digest of full-length histone⁷⁻⁹ and comprised the following amino acids: H2A: 13 – 118; H2B: 24 – 125; H3: 27 – 135; H4: 20 – 102. Histones were purified by a combination of inclusion body purification and ion-exchange chromatography, essentially as described previously^{10,11}. In brief, histones were expressed in *E. coli* BL21 (DE3) cells (Merck, Darmstadt, Germany) for 2 h after induction with 1 mM IPTG at 37 °C and disrupted under non-denaturing conditions to separate inclusion bodies from lysate. Inclusion bodies were first washed with 1% Triton-X100. Subsequently, inclusion bodies were resuspended in 7 M guanidinium chloride and dialyzed against 8 M urea. Individual histones were purified by cation-exchange chromatography, refolded under low-salt conditions and polished by anion-exchange chromatography. For long-time storage, histones were lyophilized overnight. For octamer reconstitution, histones were resuspended in 25 mM Tris, pH 7.5, 7 M guanidinium chloride, 0.25 mM DTT, mixed at 1.2-fold excess of H2A and H2B and dialyzed against 25 mM Tris-HCl pH 7.5, 2 M NaCl, 0.25 mM DTT overnight. 1 mg/mL SENP2 protease was added after 3 h. The octamer of tailless histones was purified by size-exclusion chromatography using a Superdex 200 16/60 column (GE Healthcare), which separated the octamer from aggregate, H2A/H2B dimers, the SENP2 protease and the SUMO-tag. The purification was analyzed on a 18 % polyacrylamide

SDS gel stained with Coomassie (data not shown). The octamer was concentrated to 3.0 mg/mL, mixed with 50 % glycerol and stored at -20°C.

Expression and purification of *S. cerevisiae* Reb1. Purification of *S. cerevisiae* Reb1 was essentially carried out as described in ¹². Briefly, using BY4741 genomic *S. cerevisiae* DNA the coding sequence for Reb1 was amplified by PCR and cloned into pET21b (Novagen) via InFusion cloning (Clontech) with a Streptavidin tag at the C terminus. Correct sequences were verified via Sanger sequencing (GATC Services at Eurofins Genomics). Expression plasmids were transformed into BL21 (DE3) cd⁺ cells. Three liters of LB medium supplemented with 600 mg/L ampicillin were inoculated with 200 mL pre-culture. Cells were grown at 37 °C to an OD₆₀₀ of 0.6 (WPA CO8000 cell density meter). Induction was carried out by addition of IPTG to a final concentration of 1 mM. Cells were grown overnight at 18 °C, harvested by centrifugation (3,500 rpm, Sorvall Evolution RC) and stored at -80 °C. Cells were resuspended in lysis buffer (50 mM Tris·HCl pH 7.9, 500 mM NaCl, 7 % glycerol, 1 mM DTT, 7 % sucrose and protease inhibitor 1:100), sonicated (Branson Sonifier 250, 5 min at 40-50 % duty cycle and output control 4) and cleared by centrifugation (Sorvall Evolution RC, SS34 rotor, 15,000 *g*). The supernatant was dialyzed over night against 2 L low salt buffer (25 mM K·HEPES pH 8.0, 150 mM KCl, 7 % glycerol, 4 mM MgCl₂, 1 mM DTT). Cation ion exchange chromatography (HiTrap SP HP 5 mL, elution buffer: 25 mM K·HEPES pH 8.0, 1 M KCl, 7 % glycerol, 4 mM MgCl₂, 1 mM DTT) followed by size exclusion chromatography (Superdex 200 10/300, buffer: 25 mM K·HEPES pH 8.0, 200 mM KCl, 7 % glycerol, 4 mM MgCl₂, 1 mM DTT) were used for purification. Peak fractions were analyzed by Coomassie SDS-PAGE. Fractions containing Reb1 were pooled, concentrated and stored at -80 °C.

Preparation of mononucleosomes with recombinant human octamers. Canonical human histones were provided by The Histone Source – Protein Expression and Purification (PEP) Facility at Colorado State University. Lyophilized individual human histones were resuspended in 7 M guanidinium chloride, mixed at a 1.2-fold molar excess of H2A/H2B and dialyzed against 2 M NaCl for 16 h. Histone octamers were purified by size exclusion chromatography (HILoad 16/600 Superdex 200 column, GE Healthcare) and stored at -20 °C in 50 % glycerol.

We used fluorescein-labeled Widom 601 DNA¹³ with 80 bp extranucleosomal DNA (ON80 orientation) harboring an in vivo ChIP-Exo verified Reb1 binding site¹⁴ of *S. cerevisiae* gene yGL167c (Reb1 binding motif: TTACCC) 64 or 84 bp distant to the 601 sequence. The DNA template (yGL267c_601) was amplified via PCR, purified by anion exchange chromatography (HiTrap DEAE FF, GE Healthcare) and vacuum concentrated. DNA and assembled histone octamer were mixed in 1.1-fold molar excess of DNA at 2 M NaCl. Over a time-period of 17 h at 4 °C the NaCl concentration was reduced to a final concentration of 50 mM NaCl. Again, anion exchange chromatography was used to purify reconstituted nucleosome core particle (NCP) which were then dialyzed to 50 mM NaCl. NCPs were concentrated to 1 mg/mL and stored at 4 °C.

ATPase Assay. As described previously¹⁵, we applied an NADH-based ATPase assay ¹⁶ to determine INO80's ATPase rate. 15 nM INO80 were incubated at 30 °C in a final volume of 50 µl assay buffer (25 mM K·HEPES pH 8.0, 50 mM KCl, 5 mM MgCl₂, 0.1 mg/mL BSA) with 0.5 mM phosphoenolpyruvate, 2 mM ATP, 0.2 mM NADH and 25 units/mL lactate dehydrogenase/pyruvate kinase (Sigma-Aldrich) to monitor the NADH dependent fluorescence signal in non-binding, black, 384-well plates (Greiner) at an excitation wavelength of 340 nm and an emission wavelength of 460 nm over a 40-min period. We used the Tecan Infinite M1000 (Tecan) plate reader for read out. For all samples, ATPase activity was determined at maximum INO80 WT ATPase activity. ATPase activity was stimulated with 50 nM, 25 nM and 12.5 nM Reb1 site-ON80 mononucleosomes with or without WT Reb1 at indicated concentrations. Using maximal initial linear rates corrected for the buffer blank, we calculated final ATP turnover rates.

Mononucleosome sliding assay. Nucleosome sliding activity of INO80 wild type and mutant complexes were monitored on Reb1 site-ON80 mononucleosomes in absence and presence of Reb1. INO80 at a concentration of 10 nM was incubated with 90 nM of Reb1 site-ON80 mononucleosomes in sliding buffer at 26 °C (sliding buffer: 25 mM Na·HEPES pH 8.0, 60 mM KCl, 7 % glycerol, 0.10 mg/mL BSA, 0.25 mM dithiothreitol and 2 mM MgCl₂). ATP and MgCl₂ at final concentrations of 1 mM and 2 mM, respectively, were added to start the sliding reaction. After 30 s, 60 s, 120 s, 300 s, 600 s, 1800 s and 3600 s the reaction was stopped by adding lambda DNA (NEB) to a final concentration of 0.2 mg/mL. To separate distinct nucleosome species, we applied NativePAGE (NativePAGE Novex 4-16 % Bis-Tris Protein Gels, Invitrogen). The Typhoon™ FLA 9000 was used for visualization.

Genome-wide remodeling reaction. All remodeling reactions were performed at 30 °C in 100 µL with final buffer conditions of 26.6 mM Na·HEPES pH 7.5, 1 mM Tris·HCl pH 7.6, 85.5 mM NaCl, 8 mM KCl, 10 mM ammonium sulfate, 10 mM creatine phosphate (Sigma-Aldrich), 3 mM MgCl₂, 2.5 mM ATP, 0.1 mM EDTA, 0.6 mM EGTA, 1 mM DTT, 14 % glycerol, 20 ng/µl creatine kinase (Roche Applied Science). Remodeling reactions were started by adding 10 µL SGD chromatin corresponding to ~ 1 µg DNA assembled into nucleosomes and terminated by adding 0.8 Units apyrase (NEB) followed by incubation at 30 °C for 30 min.

MNase-seq. After apyrase addition, remodeling reactions were supplemented with CaCl₂ to a final concentration of 1.5 mM and digested with 100 Units MNase to generate mostly mononucleosomal DNA. Chd1-reaction were incubated with 20 Units MNase to get the same extent of mononucleosomal DNA. 10 mM EDTA and 0.5 % SDS (final concentrations) were added to stop the MNase digest. After proteinase K treatment for 30 min at 37 °C, samples were ethanol precipitated and electrophoresed for 1.5 - 2 h at 100 V using a 1.5 % agarose gel in 1x Tris-acetate-EDTA (TAE) buffer. Mononucleosome bands were excised and purified with PureLink Quick Gel Extraction Kit (ThermoFisher Scientific).

For library preparation, 10-50 ng of mononucleosomal DNA was incubated with 1.25 Units Taq polymerase (NEB), 3.75 Units T4 DNA polymerase (NEB) and 12.5 Units T4-PNK (NEB) in 1x ligation buffer (B0202S, NEB) for 15 min at 12 °C, 15 min at 37 °C and 20 min at 72 °C. To ligate NEBNext Adaptors (0.75 µM final concentration, NEBNext Multiplex Oligos Kit) to the DNA, samples were incubated with T4 DNA ligase (NEB) at 25 °C for 15 min, followed by incubation with 2 Units USER enzyme (NEB) for 10 min at 37 °C. Fragments were purified using 2 volumes AMPure XP beads (Beckman Coulter) and amplified for 8-10 cycles using NEBNext Multiplex Oligos, Phusion High-Fidelity DNA Polymerase (1 U, NEB), deoxynucleotide solution mix (dNTP, 2.5 mM, NEB) and Phusion HF Buffer (1x, NEB). The following protocol was applied for amplification: 98 °C for 30 s, 98 °C for 10 s, 65 °C for 30 s, 72 °C for 30 s with a final amplification step at 72 °C for 5 min. DNA content was assessed by using Qubit dsDNA HS Assay Kit (Invitrogen). PCR reactions were applied to an 1.5 % agarose gel, needed fragment length (~270 bp) was excised and purified via PureLink Quick Gel Extraction Kit (ThermoFisher Scientific). DNA was measured again with Qubit dsDNA HS Assay Kit and diluted to a final concentration of 10 nM (calculation based on the assumption that the DNA fragment length is 272 bp, i.e., 147 bp nucleosomal DNA and 122 bp sequencing adaptor). Diluted samples were pooled according to sequencing reads (~6 Mio reads/ sample). The final pool was quantified with BioAnalyzer (Agilent) and analyzed on an Illumina HiSeq 1500 in 50 bp single-end mode (Laboratory for Functional Genome Analysis, LAFUGA, LMU Munich).

Data Processing. Sequencing data was mapped to the SacCer3 (R64) genome using *bowtie*¹⁷. Multiple matches were omitted. After mapping, data was imported into R Studio using *GenomicAlignments*¹⁸. Every read was shifted by 73 bp to cover the nucleosome dyad and extended to 50 bp. Genome coverage was calculated, and aligned to either *in vivo* +1 nucleosome

positions¹⁹, BamHI cut sites, Reb1 SLIM-ChIP hits²⁰ or Reb1 PWM hits²¹. Signal was normalized per gene in a 2001 bp window centered on the alignment point.

Heatmaps were sorted either by NFR length (distance between *in vivo* +1 and -1 nucleosome annotated by calling nucleosomes of *in vivo* MNase-seq data, see below) or by Reb1 binding score. For the latter, Reb1 SLIM-ChIP data (GSM2916407) was aligned to *in vivo* +1 nucleosome positions and sorted by signal strength in a 120 bp-window 160 bp upstream of every +1 nucleosome.

For promotor grouping according to Reb1 site orientation, Reb1 SLIM-ChIP hits which contain a PWM site (± 50 bp) and which are located within 400 bp upstream of *in vivo* +1 nucleosomes were used. Cluster 1 contains promoters where the Reb1 PWM motif is located on the sense strand and cluster 2, where the Reb1 PWM motif is located on the antisense strand. Cluster 3 contains Reb1 sites at bidirectional promoters.

DNA shape and poly(dA:dT) analysis surrounding Reb1 binding sites. The DNA sequence of the yeast genome (SacCer3) was downloaded from *Saccharomyces* Genome Database (SGD) and the DNA shape feature scores (DNA helix twist, propeller twist) were calculated for the entire genome using the R package *DNASHapeR* (v1.10.0). Similar to¹², the resulting DNA shape vectors were smoothed with a 5-bp rollmean. For composite analysis, DNA shape feature specific values were extracted in a window of -2000 to 2000 bp around Reb1 binding sites, oriented with respect to Reb1 motif directionality, and averaged by base pair. Plotted distance around Reb1 features are indicated in respective figures.

For the poly(dA:dT) analysis, stretches of 6 nucleotide long polyA (5'-AAAAAA-3') or polyT (5'-TTTTTT-3') were identified in the yeast genome using R package *Biostrings* (v2.52.0) and counted. For composite analysis, ploy(dA) or poly(dT) counts were extracted in a window of -2000 to 2000 bp around Reb1 binding sites, oriented with respect to Reb1 motif directionality, and averaged by base pair. Plotted distance around Reb1 features are indicated in respective figures.

Identification of TSS +1 nucleosomes. Plus 1 nucleosome positions were called according to²². In more detail, mono-nucleosomal fragments generated from BY4741 MNase digested chromatin were sequenced on an Illumina Genome analyzer, mapped to the SacCer3 genome with *bowtie*¹⁷ and shifted by 73 bp with respect to sequencing read directionality to obtain theoretical nucleosome dyads. The obtained dyad-density counts were smoothed with sliding Gaussian filter (width = 100, mean = 0, SD = 25) and resulting values were sorted by decreasing values. Iteratively, the position with the highest value was added to the list of "dyad centers" and all values for positions within +/-120 bp surrounding the position with the highest value were removed from further analysis. The top 90% of nucleosome dyad centers, by value, constituted the final list of nucleosome positions. Plus 1 nucleosome dyad positions were defined as the nearest nucleosome dyad position to TSS within a window 0 to +500 bp from the TSS, with respect to direction of transcription.

Genome-wide principal component and DNA shape analysis of nucleosomes. For PCA and DNA shape analysis, mononucleosomes were sequenced in 50 bp paired-end mode on an Illumina HiSeq1500. If not stated otherwise, functions were called with default parameters. Read pairs were aligned using *bowtie2* (version 2.2.9) with options "-X 250 --no-discordant --no-mixed --no-unal". Only unique matches were kept, and orphaned mates removed. Nucleosomes were called on each sample using *bioconductor/nucleR* (2.16.0) on nucleosomal fragments defined by paired reads as follows: fragments were processed with trimming to 40 bp around the dyads and their coverage was calculated. Noise was removed using FFT filtering with parameter *pcKeepComp*=0.02 and peak detection was carried out with threshold 99%.

For each sample in an analysis set, sample-specific dyad positions obtained by nucleosome calling were enlarged to 20 bp and all positions were merged across the samples. Overlapping regions were joined. We excluded regions locating closer than 250 bp to tile borders and those residing in a region with high artifactual signals (chr III, 91000-93000 bp).

On this joint set of nucleosome dyads, we counted the number of overlapping fragments (reduced to their center position) for each sample. With x being the number of counts of sample-specific fragment centers overlapping one dyad region of the joint set and $\text{sum}(x)$ being the sum of all counts across all dyad regions in the sample the data was normalized using the formula: normalized occupancy (dyad region) = $\log_2(((x/\text{sum}(x))*1000)+0.001)$. The resulting matrix was subjected to principal component analysis. K-means clustering was applied to the resulting principal components to group nucleosomes based on similar occupancy patterns across sample conditions.

DNA shape features in windows of 320 bp around dyad positions were calculated with bioconductor/DNAshapeR (version 1.14.0).

Data Availability

All raw and processed sequencing data generated in this study have been submitted to the NCBI Gene Expression Omnibus under accession number GSE145093.

References for Methods

1. Krietenstein, N., Wippo, C.J., Lieleg, C. & Korber, P. Genome-wide in vitro reconstitution of yeast chromatin with in vivo-like nucleosome positioning. *Methods Enzymol* **513**, 205-32 (2012).
2. Simon, R.H. & Felsenfeld, G. A new procedure for purifying histone pairs H2A + H2B and H3 + H4 from chromatin using hydroxylapatite. *Nucleic Acids Res* **6**, 689-96 (1979).
3. Trowitzsch, S., Bieniossek, C., Nie, Y., Garzoni, F. & Berger, I. New baculovirus expression tools for recombinant protein complex production. *J Struct Biol* **172**, 45-54 (2010).
4. Berger, I., Fitzgerald, D.J. & Richmond, T.J. Baculovirus expression system for heterologous multiprotein complexes. *Nat Biotechnol* **22**, 1583-7 (2004).
5. Eustermann, S. et al. Structural basis for ATP-dependent chromatin remodelling by the INO80 complex. *Nature* **556**, 386-390 (2018).
6. Gibson, D.G. Synthesis of DNA fragments in yeast by one-step assembly of overlapping oligonucleotides. *Nucleic Acids Res* **37**, 6984-90 (2009).
7. Bohm, L., Crane-Robinson, C. & Sautiere, P. Proteolytic digestion studies of chromatin core-histone structure. Identification of a limit peptide of histone H2A. *Eur J Biochem* **106**, 525-30 (1980).
8. Bohm, L., Briand, G., Sautiere, P. & Crane-Robinson, C. Proteolytic digestion studies of chromatin core-histone structure. Identification of the limit peptides of histones H3 and H4. *Eur J Biochem* **119**, 67-74 (1981).
9. Bohm, L., Briand, G., Sautiere, P. & Crane-Robinson, C. Proteolytic digestion studies of chromatin core-histone structure. Identification of limit peptides from histone H2B. *Eur J Biochem* **123**, 299-303 (1982).
10. Dyer, P.N. et al. Reconstitution of nucleosome core particles from recombinant histones and DNA. *Methods Enzymol* **375**, 23-44 (2004).
11. Klinker, H., Haas, C., Harrer, N., Becker, P.B. & Mueller-Planitz, F. Rapid purification of recombinant histones. *PLoS One* **9**, e104029 (2014).
12. Krietenstein, N. et al. Genomic Nucleosome Organization Reconstituted with Pure Proteins. *Cell* **167**, 709-721 e12 (2016).
13. Lowary, P.T. & Widom, J. New DNA sequence rules for high affinity binding to histone octamer and sequence-directed nucleosome positioning. *J Mol Biol* **276**, 19-42 (1998).
14. Rhee, H.S. & Pugh, B.F. ChIP-exo method for identifying genomic location of DNA-binding proteins with near-single-nucleotide accuracy. *Curr Protoc Mol Biol* **Chapter 21**, Unit 21 24 (2012).

15. Knoll, K.R. et al. The nuclear actin-containing Arp8 module is a linker DNA sensor driving INO80 chromatin remodeling. *Nat Struct Mol Biol* **25**, 823-832 (2018).
16. Kianitsa, K., Solinger, J.A. & Heyer, W.D. NADH-coupled microplate photometric assay for kinetic studies of ATP-hydrolyzing enzymes with low and high specific activities. *Anal Biochem* **321**, 266-71 (2003).
17. Langmead, B., Trapnell, C., Pop, M. & Salzberg, S.L. Ultrafast and memory-efficient alignment of short DNA sequences to the human genome. *Genome Biol* **10**, R25 (2009).
18. Lawrence, M. et al. Software for computing and annotating genomic ranges. *PLoS Comput Biol* **9**, e1003118 (2013).
19. Xu, Z. et al. Bidirectional promoters generate pervasive transcription in yeast. *Nature* **457**, 1033-7 (2009).
20. Gutin, J. et al. Fine-Resolution Mapping of TF Binding and Chromatin Interactions. *Cell Rep* **22**, 2797-2807 (2018).
21. Badis, G. et al. A library of yeast transcription factor motifs reveals a widespread function for Rsc3 in targeting nucleosome exclusion at promoters. *Mol Cell* **32**, 878-87 (2008).
22. Tirosh, I. Computational analysis of nucleosome positioning. *Methods Mol Biol* **833**, 443-9 (2012).

Supplementary Figures

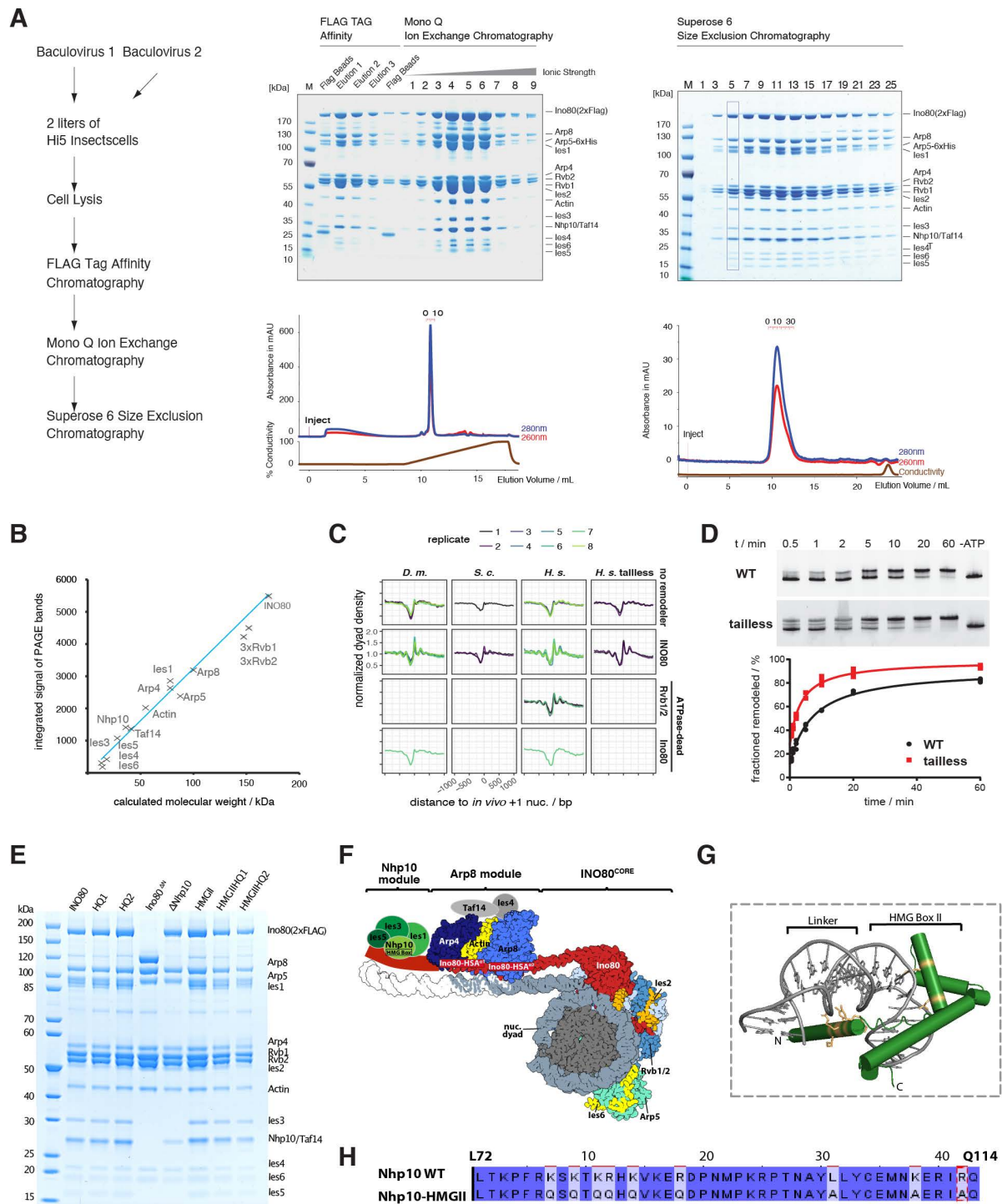


Figure S1. (A) Recombinant expression and purification of 15-subunit *S. cerevisiae* INO80 complex. Left: Schematic of expression and purification workflow. Two baculoviruses encoding five (Ino80, Arp5, les6, Rvb1 and Rvb2) and ten INO80 subunits (les1-5, Nhp10, Taf14, Actin, Arp4, Arp8), respectively, were used for insect cell expression. Middle and right: SDS-PAGE analysis of indicated chromatographies. Numbered lanes indicate elution fractions matching chromatograms below gels. Boxed lane represents a fraction used in this study. **(B)** Quantification of Coomassie-stained SDS PAGE bands shows stoichiometric assembly of recombinant *S. cerevisiae* INO80 complex. Note that AAA⁺ ATPase Rvb1 and Rvb2 form a hetero-hexameric. **(C)** Composite plots of MNase-seq data of individual replicates for the indicated combinations of histones (columns) and no (none), recombinant WT (INO80) or mutant (Rvb1/2 ATPase-dead, Ino80 ATPase-dead) *S. cerevisiae* INO80 complexes (rows). **(D)** top: Native gel electrophoresis analysis at indicated time points of mononucleosome sliding assay kinetics with wild type (WT) or tailless (tailless) recombinant *H. sapiens* histones and wild type

recombinant *S. cerevisiae* INO80 complex. “-ATP” denotes 60 min time point without ATP. bottom: Quantification of data from top. **(E)** SDS-PAGE of purified, recombinant WT (INO80) or indicated mutant complexes. **(F)** left: Structure-based^{5,15} model of a nucleosome bound by the INO80 complex with indicated subunits. Taf14, Ies4 and Nhp10 module organization is assumed. **(G)** Model of Nhp10 HMG box-like and Linker region (residues 62-172) based on TFAM structure (pdb 3tq6). **(H)** Sequence alignment showing mutated residues in Nhp10-HMGII mutant. Panels E-H are also shown in the accompanying paper Oberbeckmann & Niebauer et al.

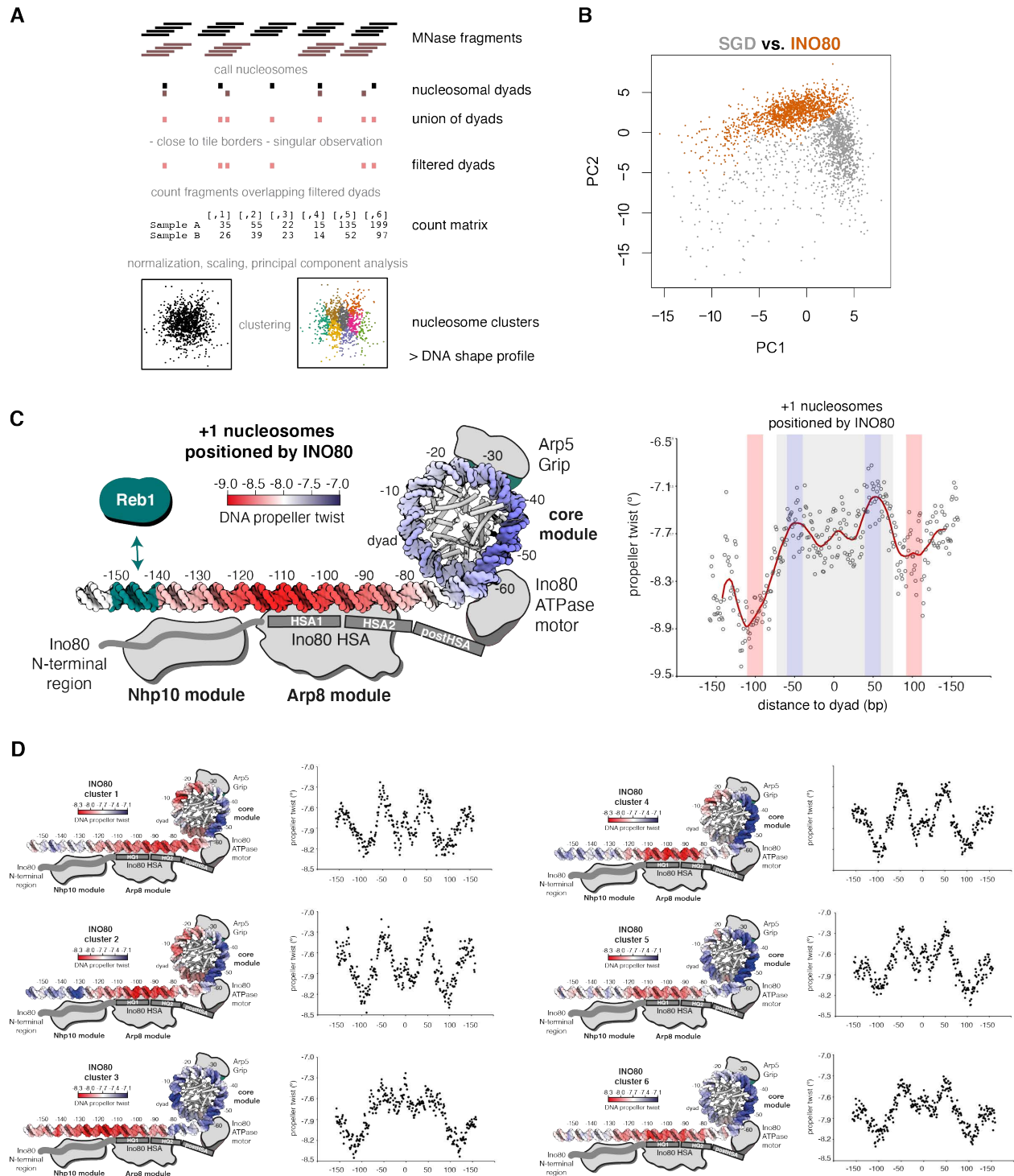


Figure S2. (A) Schematic of Principal Component Analysis (PCA)/clustering approach. For details see main text and Materials and Methods section. **(B)** Visualization of nucleosome clusters according to Principal Components 1 and 2 (PC1, PC2) for SGD chromatin (SGD) prepared with embryonic *D. melanogaster* histones at histone-to-DNA mass ratio of 0.4 alone (SGD) or after incubation with *S. cerevisiae* WT INO80 complex (INO80). **(C)** As Figure 3A and Figure 3B, but only for +1 nucleosomes and with same nucleosome orientation relative to direction of transcription. Reb1 cognate binding site in promoter regions is highlighted in teal. **(D)** Propeller twist DNA shape profiles and color-coded mapping for nucleosomal sequences of clusters shown in Figure 3E.

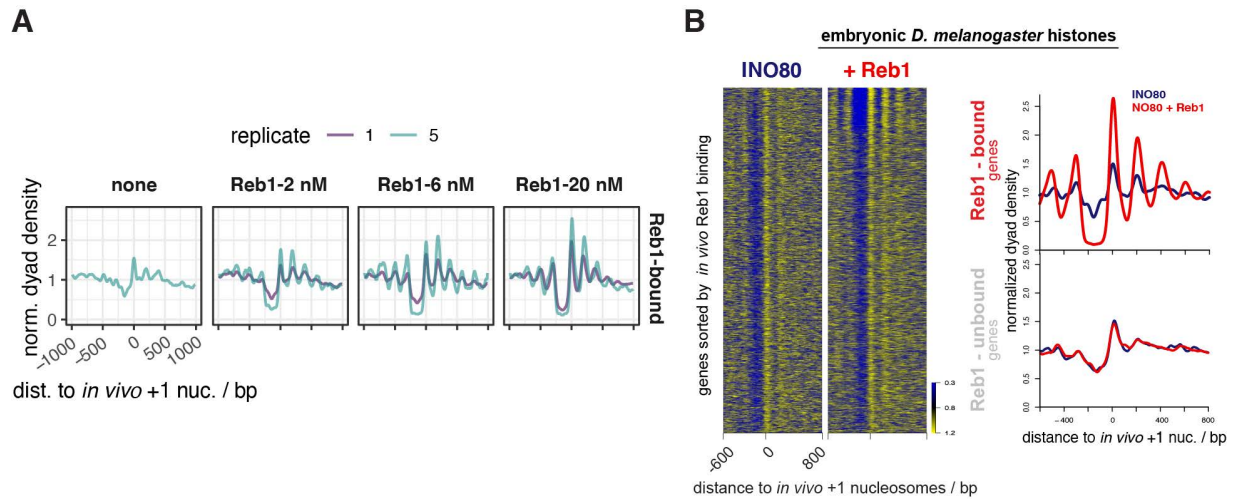


Figure S3. (A) Composite plots of MNase-seq data for individual replicates of samples as in Figure 3A, but only for genes with promoter Reb1 sites (Reb1-bound, same as red shading in Figure 4A) and also including SGD chromatin incubated with INO80 in the absence of Reb1 (none). **(B)** As Figure 4A,B but for the SGD chromatin with embryonic *D. melanogaster* histones at histone-to-DNA mass ratio of 0.4 and only 20 nM Reb1 (+ Reb1).

Publications

2.3 Ruler elements in chromatin remodelers set nucleosome array spacing and phasing

Elisa Oberbeckmann*, [Vanessa Niebauer](#)*, Shinya Watanabe, Lucas Farnung, Manuela Moldt, Andrea Schmid, Patrick Cramer, Craig L. Peterson, Sebastian Eustermann, Karl-Peter Hopfner, Philipp Korber (2020), Ruler elements in chromatin remodelers set nucleosome array spacing and phasing. (under revision) (online on bioRxiv: 2020.02.28.969618)

*: equal contribution

DOI: <https://doi.org/10.1101/2020.02.28.969618>

URL: <https://www.biorxiv.org/content/10.1101/2020.02.28.969618v1>

MNase ladders and the underlying regularly spaced nucleosomal arrays are one of the oldest observations in chromatin biology. Nucleosomal arrays are aligned to genomic reference points mainly located at regulatory regions, such as promoter sites. The exact distance setting of regular arrays by ATP-dependent chromatin remodelers is largely undefined. This publication advanced a minimalistic genome-wide *in vitro* reconstitution system to delineate the distance setting by chromatin remodelers in absolute terms between the adjacent nucleosomes (spacing) and between nucleosomes and reference points, such as GRFs and dsDNA breaks (phasing). To address this question, we tested all S.c. remodelers with known spacing activity in genome-wide assays. Based on our observations, we propose that all yeast remodelers with spacing activity including ISW1a, Chd1, ISW2 and INO80 bear intrinsic ruler features. The ruler feature is independent from the underlying DNA sequence, but, in some cases, shows nucleosome density sensitivity. A remodeler intrinsic ruler feature is at the heart of all chromatin remodeler-directed spacing and phasing processes. A remodeler intrinsic ruler is potent to set a sliding direction bias in response to its chromatin environment, integrating information regarding dsDNA breaks, DNA sequence elements and DNA-bound factors. Structure-directed mutagenesis of the S.c. INO80 chromatin remodeler enabled a dissection of its intrinsic ruler feature which is characterized by multi-layered cross-communications between the ARP and the NHP10 modules, as well as the Ino80 N-terminal residues.

Author contribution

Publications

The author of this thesis cloned, expressed and purified INO80 wild type and mutant constructs, including Ino80_HSA, Ino80_ΔN, INO80ΔNhp10 and INO80_HMGII mutant, as well as several double mutant constructs for *in vitro* characterization. The author cloned, expressed and purified wild type and mutant S.c. Reb1 constructs. The author assembled mononucleosomes via salt gradient dialysis. Wild type as well as mutant constructs were tested in mononucleosome sliding assays based on the yGL167c promoter DNA sequence with a Widom 601 positioning sequence and an inserted Reb1 binding sites. The author tested ATPase activity of wild type and mutant constructs stimulated by mononucleosomes in presence and absence of Reb1.

Ruler elements in chromatin remodelers set nucleosome array spacing and phasing

Elisa Oberbeckmann^{1,7}, Vanessa Niebauer^{2,7}, Shinya Watanabe³, Lucas Farnung⁴, Manuela Moldt², Andrea Schmid¹, Patrick Cramer^{4,6}, Craig L. Peterson^{3,6}, Sebastian Eustermann^{2,5,6*}, Karl-Peter Hopfner^{2,6*}, Philipp Korber^{1,6,8*}

¹Division of Molecular Biology, Biomedical Center, Faculty of Medicine, Ludwig-Maximilians-Universität München, Martinsried near to Munich, Germany; ²Gene Center, Faculty of Chemistry and Pharmacy, Ludwig-Maximilians-Universität München, Munich, Germany; ³Program of Molecular Medicine, University of Massachusetts, Worcester, USA; ⁴Department of Molecular Biology, Max Planck Institute for Biophysical Chemistry, Göttingen, Germany; ⁵current address: European Molecular Biology Laboratory (EMBL), Structural and Computational Biology Unit, Heidelberg, Germany

Arrays of regularly spaced nucleosomes dominate chromatin and are often phased by alignment to reference sites like active promoters. How the distances between nucleosomes (spacing) and between phasing sites and nucleosomes are determined remains unclear, and specifically, how ATP dependent chromatin remodelers impact these features. Here, we used genome-wide reconstitution to probe how *Saccharomyces cerevisiae* ATP dependent chromatin remodelers generate phased arrays of regularly spaced nucleosomes. We find that remodelers bear a functional element named the “ruler” that determines spacing and phasing in a remodeler-specific way. We use structure-based mutagenesis to identify and tune the ruler element in the INO80 remodeler complex. More generally, we propose that a remodeler ruler regulates the nucleosome sliding direction in response to nucleosome environment. This finally conceptualizes how remodeler-mediated nucleosome dynamics determine defined steady-state nucleosome positioning relative to other nucleosomes, DNA bound factors, DNA ends and DNA sequence elements.

Nuclear DNA is packaged into chromatin based on a repeating building block, the nucleosome core particle (NCP; (Kornberg, 1974; Olins and Olins, 1974)), where 147 base pairs (bp) of DNA are wound around a histone protein octamer (Kornberg and Lorch, 1999; Luger et al., 1997; Olins and Olins, 2003). Packaging by nucleosomes orchestrates all genomic processes (Lai and Pugh, 2017).

Nucleosomes mainly occur in regular arrays where they are aligned to each other such that the lengths of linker DNA between NCPs are about constant within an array. Linker lengths may vary among arrays in the same cell (Baldi et al., 2018b; Chereji et al., 2018; Ocampo et al., 2016; Valouev et al., 2011) and differ on average between cell types and species (van Holde, 1989). Arrays are often phased, i.e., aligned relative to a genomic reference point. A combination of both *in vivo* studies (Ganapathi et al., 2011; Hartley and Madhani, 2009; Kubik et al., 2018; Tsankov et al., 2011; van Bakel et al., 2013; Yan et al., 2018; Yarragudi et al., 2004) and *in vitro* reconstitutions (Krietenstein et al., 2016) indicated

that these genomic alignment points or “barriers” often reflect the binding of abundant, sequence-specific DNA binding proteins, like Reb1, Abf1, or Rap1 in budding yeast or other architectural factors like CTCF in mammals (Wiechens et al., 2016) or Phaser in flies (Baldi et al., 2018a).

Throughout eukaryotes, phased arrays are prominent at active promoters. Nucleosome-depleted regions (NDRs) at the core promoter are flanked by arrays that begin with the so called +1 nucleosome close to the transcription start site (TSS) and cover the gene body (Baldi et al., 2020; Lai and Pugh, 2017). This organization is important for transcription fidelity as mutants with impaired array phasing show aberrant transcription initiation (Challal et al., 2018; Hennig et al., 2012; Kubik et al., 2019; Pointner et al., 2012; Smolle et al., 2012). While nucleosome arrays are likely the most pervasive and longest known chromatin organization, their generation is still not explained. Specifically, regular spacing requires fixed distances between nucleosomes, and phasing requires a fixed distance

⁶ Senior author

⁷ These authors contributed equally.

⁸ Lead contact

* Correspondence: pkorber@lmu.de, hopfner@genzentrum.lmu.de, sebastian.eustermann@embl.de

between array and reference point. What sets these distances?

In vivo and *in vitro* data suggest that ATP dependent chromatin remodeling enzymes (remodelers) are key to the answer. Remodelers are conserved in eukaryotes (Flaus et al., 2006) and mobilize, reconfigure, or disassemble/reassemble nucleosomes upon ATP hydrolysis (Clapier and Cairns, 2009; Clapier et al., 2017). They are subdivided into the SWI/SNF, ISWI, CHD, and INO80 families, according to ATPase sequence features. Besides the core ATPase, remodelers often contain additional domains and subunits that bind the nucleosome, regulate activity and targeting, and convert their DNA tracking activity into the remodeler-specific chemo-mechanical reaction. For example, nucleosome disassembly is accomplished only by SWI/SNF family members and histone exchange only by INO80 family members, while nucleosome sliding is catalyzed by most remodelers.

Particularly relevant for array generation is an ATP-dependent nucleosome spacing activity, by which some remodelers convert irregular arrays into arrays of regularly spaced nucleosomes. Remodelers of the ISWI, CHD, and INO80 (Ito et al., 1997; Tsukiyama et al., 1999; Udugama et al., 2011; Varga-Weisz et al., 1997), but not of the SWI/SNF family, show spacing activity. This activity was suggested to rely on a length-sensor mechanism (Yang et al., 2006; Zhou et al., 2018) where nucleosome sliding rate is regulated by linker DNA length. For instance, sliding one nucleosome back and forth between two other nucleosomes, with a linker length-dependent velocity, would center a nucleosome at steady state when both flanking linkers have the same length.

While the length-sensor mechanism may equalize linker lengths and thereby generate spacing distance *regularity*, it does not by itself determine spacing distance *length* in absolute terms. This would reciprocally depend on nucleosome density. However, spacing *in vivo* (Gossett and Lieb, 2012; Hennig et al., 2012; van Bakel et al., 2013), as well as generated *in vitro* (Lieleg et al., 2015; Zhang et al., 2011), remains constant despite changes in nucleosome density. This has been called “active packing” (Zhang et al., 2011) or “clamping” (Lieleg et al., 2015), but it remained unclear if remodeler or nucleosome features led to such density-independent spacing.

Structural studies suggested that the yeast ISW1a remodeler appears to contact a neighboring nucleosome and may use thereby a “protein ruler” that sets the linker length (Yamada et al., 2011). *In vitro* studies found that two ISWI family remodelers, yeast ISW1a and ISW2, can each generate regular arrays aligned at DNA-bound Reb1 or Abf1, but with

different spacing at the same nucleosome density (Krietenstein et al., 2016). This points towards a remodeler-specific linker length determining ruler mechanism. Another indication for a built-in ruler, INO80 requires a minimum linker length for nucleosome sliding (Zhou et al., 2018) and recognizes linker DNA via a structural module that is important for sliding (Knoll et al., 2018).

The ruler metaphor may indeed be fit to describe a remodeler mechanism that measures and sets the phasing and spacing distances of arrays. However, so far it is mainly suggestive and has to be substantiated in molecular terms. This would be exceedingly convoluted *in vivo* but requires a defined system that allows to assay the generation of phased regular arrays by remodelers and to dissect if and how a ruler mechanism is at work. Are there rulers within some or all remodelers with spacing activity? Are linker length vs. distance to barrier determined in the same or different way? Are rulers autonomous or does the outcome depend on nucleosome density or underlying DNA sequence? Ultimately, is it possible to tune a ruler, i.e., can a remodeler be mutated to generate arrays with altered spacing and/or phasing distances?

Here, we use genome-wide *in vitro* chromatin reconstitution with purified remodelers ((Krietenstein et al., 2016), accompanying paper Krietenstein et al.) to answer these questions. All yeast remodelers with spacing activity, ISW1a, ISW2, Chd1, and INO80 have rulers that are largely autonomous regarding underlying DNA sequence but some may respond to nucleosome density. Remodeler-specific rulers mechanistically explain earlier *in vivo* observations. Structure-guided mutations in recombinant INO80 complexes (see also accompanying study Krietenstein et al.) led to shorter or longer spacing and phasing distances and showed that these quantities may be uncoupled. Finally, we propose a model how remodeler rulers position nucleosomes by regulating sliding direction according to nucleosome environment.

Results

Defined genome-wide chromatin reconstitution system with varying nucleosome densities. To assess array generation by remodelers in a biochemically defined way, we used our genome-wide chromatin reconstitution system with purified components (Figure 1A, (Krietenstein et al., 2016)) including recombinant INO80 complex (accompanying paper Krietenstein et al.) and recombinant Chd1 (Farnung et al., 2017). Briefly, genomic plasmid libraries were reconstituted with *Drosophila* embryo histone octamers into nucleosomes by salt gradient dialysis (SGD). SGD

chromatin was incubated with ATP, purified yeast remodelers (Figure S1A), and the barrier Reb1 or the restriction enzyme BamHI, which generates double strand breaks (DSBs) that also amount to nucleosome positioning barriers (accompanying paper Krietenstein et al.). Resulting nucleosome patterns were analyzed by MNase-seq. The effective histone-to-DNA mass ratio during SGD was varied from 0.2 to 0.8 yielding low, medium and high nucleosome densities reflected in increasingly extensive MNase-ladders at the same MNase digestion conditions (Figure 1B). Nucleosome density variation was instrumental to distinguish if linker lengths and phasing distances depended on nucleosome density and/or remodeler features.

INO80, ISW2, ISW1a and Chd1, but not Fun30 align regular arrays at the barrier Reb1. We tested all yeast remodelers with known spacing activity, INO80, ISW2, ISW1a and Chd1 (Krietenstein et al., 2016; Lusser et al., 2005; Stockdale et al., 2006; Torigoe et al., 2013; Tsukiyama et al., 1999; Udugama et al., 2011) as well as the Fun30 remodeler, for which it was unclear if it has spacing activity (Awad et al., 2010). INO80, ISW2, ISW1a and Chd1, each in combination with Reb1, generated phased regular arrays at promoters with Reb1 sites (red shaded top of heat maps in Figure 1C), while Fun30 did not (Figure S1B). This clarifies that Fun30 does not have regular array generation and alignment activity.

Previously, Chd1 purified from budding yeast did not show much effect in genome-wide reconstitutions (Krietenstein et al., 2016). This was maybe due to full-length Chd1 tending to aggregate *in vitro*, which is why truncated Chd1 constructs were often used (McKnight et al., 2011; Patel et al., 2011). Here, we leveraged our finding that recombinant full-length Chd1 is stabilized in complex with recombinant FACT complex (Farnung et al., 2017) and achieved *in vitro* array generation and alignment also by Chd1.

The heat map patterns (Figure 1C) and even more the corresponding composite plots for the Reb1-bound genes only (Figure 1D) suggested that the distance of arrays to the barrier Reb1 as well as the linker lengths varied with nucleosome density in a remodeler-specific way. For all remodelers with spacing activity, array extent increased with growing density, consistent with greater nucleosome availability and processive spacing activity. Array extent at high density was larger than in our previous reconstitutions (Krietenstein et al., 2016), i.e., we achieved higher densities here. Adding more remodeler after half of the incubation time did not change the array distances of resulting patterns confirming non-limiting remodeling activity and steady state conditions (Figure S1C).

Remodelers set phasing and spacing distances symmetrically around barriers. To better assess distances to barrier (phasing) and linker lengths (spacing), we aligned the MNase-seq data for each remodeler/barrier/density combination to either *in vivo* Reb1 sites or BamHI sites (Figure 2A). For each replicate (Figure S2A-C), we called nucleosome peaks and determined the distances to barrier and linker lengths as defined in Figure 2B.

All remodelers symmetrically aligned regular arrays to BamHI sites, which are palindromic and therefore inherently symmetrical, and most of them also to Reb1 sites (Figures 2A, S2A,B) regardless of site orientation and position relative to genes (groups 1 to 3; Figure S3A,B). However, if INO80 aligned arrays at promoter Reb1 sites (groups 1 to 3, Figure S3A, accompanying paper by Krietenstein et al.), nucleosome occupancy (peak height) was higher over genic versus non-genic regions at low and medium nucleosome density leading to asymmetric patterns with regard to peak heights in groups 1 and 2. Reb1 site orientation had no effect (group 1 vs. 2). This asymmetry in nucleosome occupancies reflected that positioning of +1 nucleosomes, per definition the first nucleosomes downstream of transcription start sites, i.e. at gene starts, is not only guided by Reb1 bound to promoter sites but also synergistically by underlying DNA shape features (accompanying paper Krietenstein et al.). We recapitulated here that INO80 was able to position *in vivo*-like +1 nucleosomes in the absence of a barrier at low and medium densities (Figure S2C,D). This synergism between Reb1- and DNA shape-guided +1 positioning at low and medium density resulted in higher occupancy at the +1 nucleosomes, which are alignment points for +2 nucleosomes and so on. Therefore, all array peaks over genes were higher than their counterparts over non-genic regions.

However, such synergism was not seen at high density where *in vivo*-like +1 nucleosomes positioning by INO80 alone was much less pronounced (Figure S3C,D). This inability could not be due to a general inability of INO80 to as INO80 could generate Reb1-aligned arrays at these high nucleosome densities, too (Figures 1C,D, 2A, S2A,B). Nonetheless, this activity was apparently incompatible with or dominant over DNA shape-guided nucleosome positioning (see Discussion). We note that the nucleosome density used previously (Krietenstein et al., 2016) must have been lower than our here generated high density, otherwise the positioning of *in vivo*-like +1 nucleosomes would not have been possible. In this context, we also tested if Fun30 positions *in vivo*-like +1/-1 nucleosomes on its own, but it did not (Figure S3D).

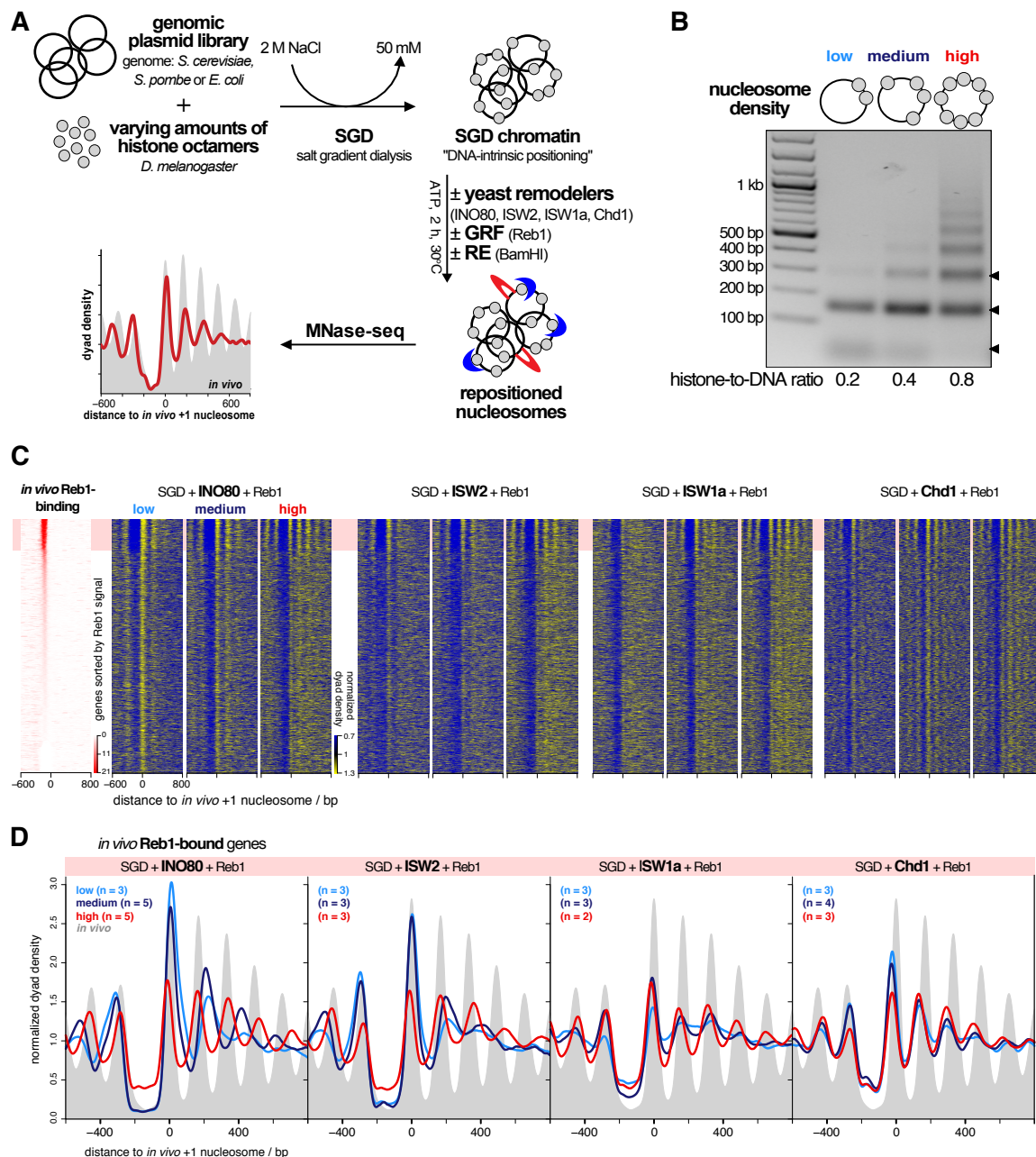


Figure 1. Reb1-guided nucleosome positioning *in vitro* by individual remodelers at varying nucleosome density. (A) Overview of genome-wide *in vitro* reconstitution system. **(B)** Comparison of SGD chromatin reconstituted at indicated histone-to-DNA ratios. DNA fragments after MNase-digest under the same conditions were resolved by agarose gel electrophoresis. Arrow heads on right point to subnucleosomal, mono- and dinucleosomal fragments (bottom to top). **(C)** Heat maps of MNase-seq data for SGD chromatin of the indicated nucleosome density and after incubation with indicated remodelers and Reb1. Chd1 refers to the Chd1/FACT complex. Heat maps are aligned at *in vivo* +1 nucleosome positions and sorted according to decreasing (top to bottom) anti-Reb1 SLIM-ChIP score (Gutin et al., 2018) shown in leftmost heat map. Horizontal red shading highlights genes with strong *in vivo* Reb1-binding in their promoters. Merged data of replicates are shown, individual replicates in Figure S1B,C. **(D)** Composite plots for MNase-seq data averaged over the indicated number of replicates (n) as in panel B but only for genes highlighted in red in panel B.

In contrast to nucleosome peak *heights*, nucleosome peak *positions* and therefore corresponding phasing and spacing distances were not significantly affected across groups 1 to 3, also not for INO80 (Figure S3B). Therefore, all remodelers symmetrically generated phasing and spacing distances at Reb1 and BamHI sites, which warranted averaging over the up- and downstream values. Resulting values were plotted in

different ways to facilitate multi-dimensional comparisons (Figure 2C-E). As all remodelers generated linker lengths independently of the barrier type, we combined linker length values for both barriers (Reb1 and BamHI, Figure 2C). Linker length determination relied on nucleosome peak calling, which was often not possible beyond the -1/+1 nucleosomes at low nucleosome density (Figure S2A),

so that linker length data for low density conditions were more sparse, even absent for ISW1a.

Remodeler-specific rulers set spacing in a density-independent or -dependent way. To compare spacing generated by different remodelers at different nucleosome densities, we focused on the averaged length of linker 1 (Figure 2B), which was most accessible across all nucleosome densities. Chd1 generated the shortest (12-13 bp) and ISW1a a bit longer (21-26 bp) linker 1 lengths without significant effects by nucleosome density (Figure 2D,E). ISW2 generated rather constant spacing (54-58 bp) at low and medium but tighter spacing (38 bp) at high density. For INO80, linker lengths steadily increased with decreasing density from 33 to 82 bp.

We concluded that linker lengths and their dependencies on nucleosome density were remodeler-specific and interpreted this as follows. Spacing activity of a remodeler has two aspects. On the one hand, the remodeler equalizes linker lengths leading to regularity in arrays, which is the classical definition of spacing activity (Ito et al., 1997; Varga-Weisz et al., 1997). On the other hand, the resulting linkers have a certain length. In our purified system, this may either be determined by nucleosome density and/or by a remodeler-intrinsic feature. Following (Yamada et al., 2011), we call a remodeler feature that sets nucleosome spacing a “ruler”. We use this term also for the feature that sets the distance to barriers (see below). Indicative for a remodeler ruler is remodeler-specific clamping, i.e., if constant spacing is generated at different nucleosome densities (=clamping) and different remodelers generate different spacing (=remodeler-specific), which shows that spacing depends on remodeler-intrinsic not nucleosome-intrinsic properties (Lieleg et al., 2015). We saw remodeler-specific clamping for Chd1 at all, for ISW1a at high versus medium and for ISW2 at medium versus low densities (Figure 2C-E). As none of the remodelers with spacing activity can disassemble nucleosomes (Clapier and Cairns, 2009) and thereby affect nucleosome density, their rulers can only set their respective linker lengths if these are shorter than or equal to the density-determined linker length at equidistant nucleosome distribution. Accordingly, Chd1 and ISW1a set their ruler-specified linker lengths at all and ISW2 at medium and low densities. ISW2 had to generate shorter linkers at high density and INO80 either did not have a ruler or the ruler responded to changes in nucleosome density.

In vitro mononucleosome assays suggested that INO80 requires at least 40 bp of nucleosome-free DNA for nucleosome sliding (Zhou et al., 2018), while it generated 30 bp linkers in trinucleosomes (Udugama et al., 2011). Here, at high nucleosome

density, INO80 generated linkers of about 33 bp consistent with previous observations. We tried to enforce even tighter spacing by increasing nucleosome density. This did not decrease spacing and phasing distances but peak heights (Figure S2B,C), probably due to increased aggregation without effective increase in nucleosome density of soluble chromatin.

Remodeler type, barrier type and nucleosome density determine distance to barrier. The findings for the distance to barrier were more complex than for lengths of linker 1 (Figure 2C-E). First, the distance to barrier is coupled to the barrier type (Figure 2C). It was always longer for Reb1 than for BamHI generated DNA ends, with the largest difference for ISW1a and the smallest for Chd1. The DNA footprint size of *S. cerevisiae* Reb1 is not known, possibly 20 bp as for the *S. pombe* Reb1 DNA binding domain (Jaiswal et al., 2016). This would contribute 10 bp to the distance to barrier (Figure 2B) and could explain the differences between distance to Reb1 vs. BamHI sites for Chd1, but not for the other remodelers. Therefore, INO80, ISW2 and ISW1a, but not Chd1, aligned nucleosomes differently at Reb1 versus at DSBs.

Second, the distance to DNA ends was mostly similar to linker lengths for INO80, ISW2 and ISW1a, arguing that these remodelers, but not Chd1, used a DNA end in a similar way as a neighboring nucleosome for nucleosome alignment.

Third, distances to barriers depended on nucleosome density in a similar way as linker lengths for all remodelers but INO80, where distances to both barriers varied less between low and medium density than linker length.

We concluded that there are remodeler-specific differences in how a nucleosome is positioned next to another nucleosome versus next to a barrier like Reb1 versus next to a DNA end and how this depends on nucleosome density. This is again a clear case of different remodelers generating different nucleosome positioning, although starting from the same SGD chromatin, which argues for remodeler-specific rulers governing nucleosome positioning.

Remodelers differ in processivity of nucleosome positioning. All remodelers generated similar lengths of linker 1 to linker 3 at high density (Figure 2D), which we interpreted as processive spacing activity along the arrays as long as nucleosomes were sufficiently provided. At low density, ISW2, Chd1 and especially INO80 still generated high +1/-1 nucleosome peaks (Figure S2A), in contrast to ISW1a, for which these peaks were less pronounced and +2/-2 nucleosome peaks could not be discerned. We

suggest that ISW1a is less processive than other remodelers in bringing nucleosomes next to barriers at low densities.

Remodelers generate similar arrays on all but more effectively on eukaryotic DNA sequences. The same linker lengths in arrays at BamHI and Reb1 sites (Figure 2C), at Reb1 sites in groups 1 to 3 and the symmetry of nucleosome distances to Reb1 sites in groups 1 to 3 (Figure S3A,B) suggested that

remodeler rulers position nucleosomes independently of DNA sequence flanking the barriers. Nonetheless, there are evolved DNA features at promoters, especially for INO80 (accompanying paper Krietenstein et al.), that affected occupancies (peak heights, not positions, Figure S3A), which may also be true for evolved nucleosome-favoring dinucleotide periodicities (Satchwell et al., 1986) in gene bodies.

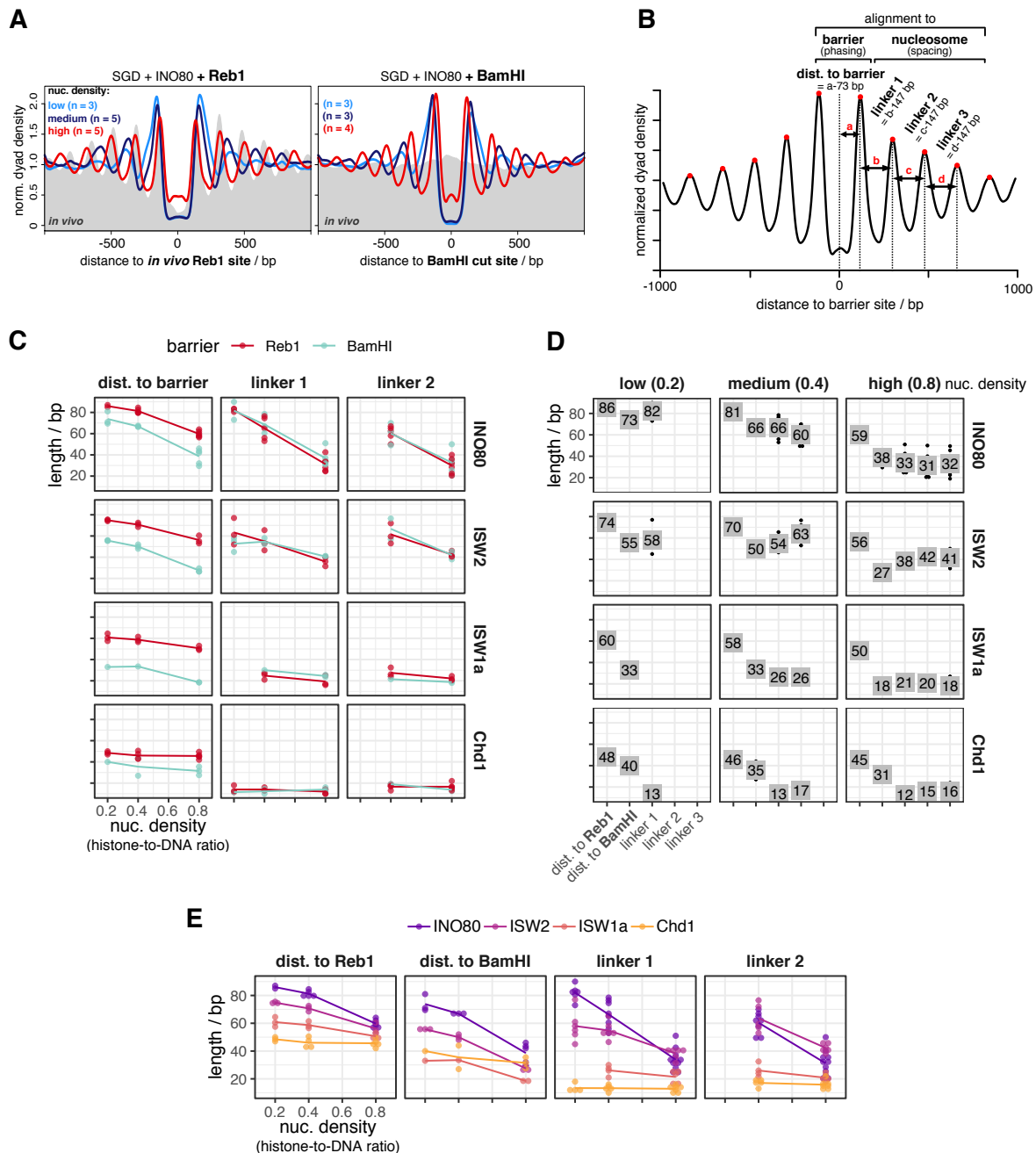


Figure 2. Quantification of barrier-aligned nucleosome array features depending on barrier, remodeler and nucleosome density. (A) Composite plots of same MNase-seq data for INO80 as in Figure 1D but aligned at anti-Reb1 SLIM-ChIP-defined Reb1 sites (left), or at BamHI sites (right) of SGD chromatin reconstituted at the indicated nucleosome densities and incubated with INO80 and BamHI. (B) Scheme defining array features quantified from barrier-aligned composite plots as in panel A. (C) – (D) Array feature values for the indicated combinations of barrier, remodeler and nucleosome density plotted in different ways allowing comparison between barriers (especially panel C), values (especially panel D) and remodelers (especially panel E). Chd1 refers to the Chd1/FACT complex. Panel D and Figure S2A-C show individual replicates, panels C and E replicate averages.

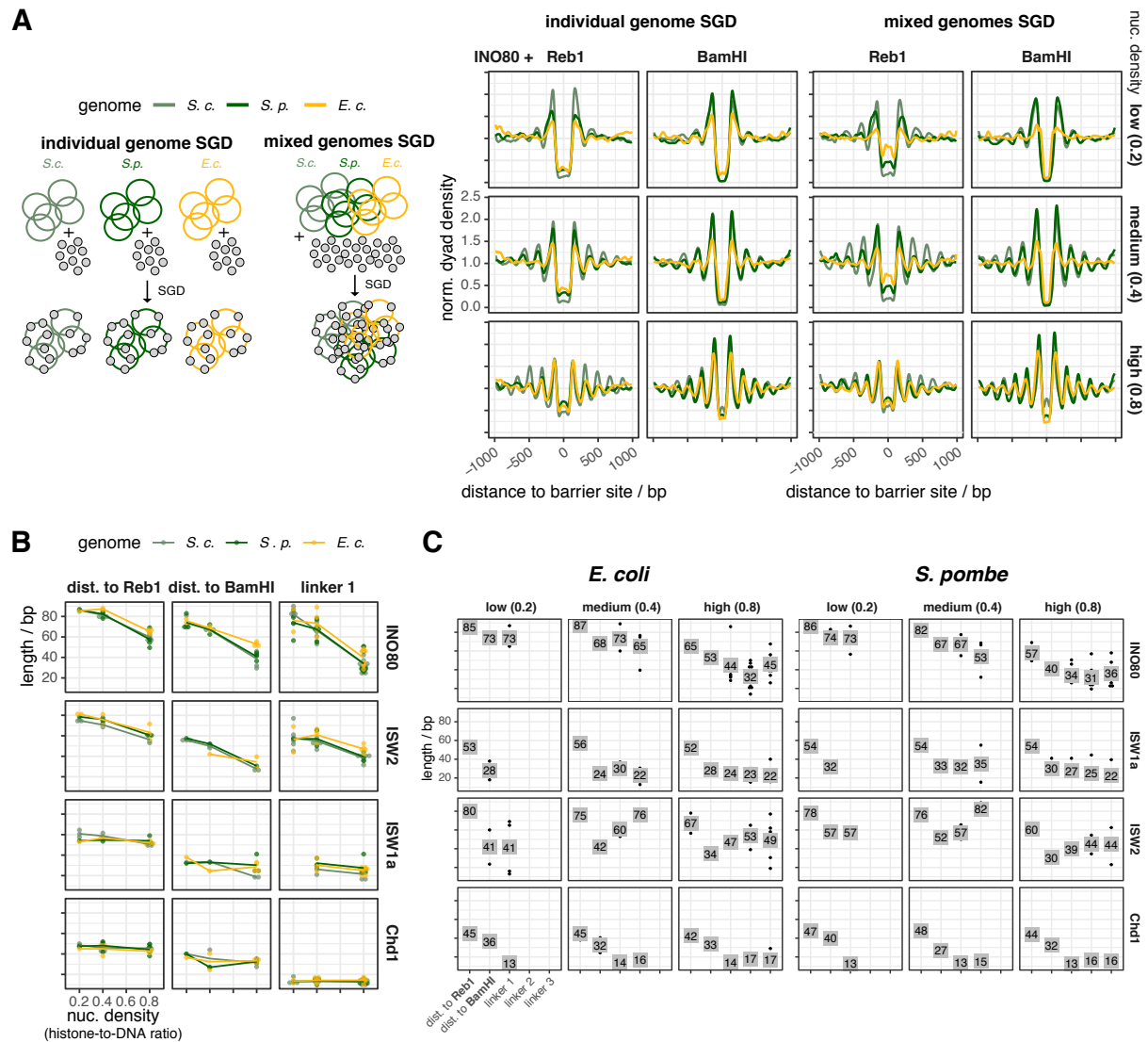


Figure 3. Yeast remodelers generate arrays on heterologous genomes with same spacing and phasing distances as on the yeast genome. (A) Left: Schematic showing SGD reconstitution with individual or mixed genomes. Right: Composite plots as Figure 2A but for the indicated barriers and either individual (left) or mixed (right) genomes. Reb1 sites were called by PWM. **(B)** and **(C)** As Figures 2C,D, respectively, but for the indicated genomes. Individual replicates in Figure S4.

To rigorously disentangle these contributions, we tested the remodeler/barrier/density combinations also with SGD chromatin of *S. pombe* and *E. coli* genomic plasmid libraries (Figures 1A, 3A,B, S4A), including the steady state control (Figure S4B). We did not observe substantial differences in spacing/phasing distances on these genomes for all remodelers, but some replicates, especially at medium and low density, showed lower relative occupancies for the *E. coli* genome.

We concluded that all remodelers align arrays at Reb1 or DSBs regardless of the underlying sequence. Nonetheless, they are more effective in terms of relative occupancies on eukaryotic genomes, likely due to dinucleotide periodicities (Zhang et al., 2009).

INO80 complexes mutated in the Arp8 and/or Nhp10 module. It was unexpected that the clamping

criterion did not clearly show a ruler for INO80 (Figure 2C-E), because the INO80 structure suggested modules that bind extranucleosomal DNA and could serve as ruler (Knoll et al., 2018). To clarify, we took advantage of the biochemical accessibility of our recombinant INO80 preparation, the modular INO80 composition and the high resolution structure (Eustermann et al., 2018, Knoll et al., 2018) to generate candidate mutations that may tune and thereby reveal INO80's ruler.

The INO80 complex has two modules with a likely role in ruler function. First, the Arp8 module consisting of N-Actin, Arp8, Arp4, Taf14 and Ies4 (Figure 4A). It binds to the HSA domain of the Ino80 subunit, which is structured as a long helix with a kink that subdivides it into the HSA α 1 and HSA α 2 part (Knoll et al., 2018). Both bind to extranucleosomal DNA, and mutating DNA contacting lysine residues in HSA α 1 or HSA α 2 to

glutamines (HQ1 and HQ2 mutant, respectively, Figure 4B,C,D) impaired, and combining both mutations (HQ1/2 mutant) abolished mononucleosome centering (Knoll et al., 2018).

The second, Nhp10 module, binds to the N-terminus part of the Ino80 subunit, and contains the HMG box-like Nhp10 subunit, along with Ies1, Ies3 and Ies5 (Figure 4A,E). This module is species-

specific and affects the processivity and extranucleosomal DNA requirements in mononucleosome sliding assays (Zhou et al., 2018). Calculating a homology model for Nhp10 based on another HMG box protein, TFAM (Ngo et al., 2014), we inferred and mutated amino acid residues putatively involved in Nhp10-DNA interactions (HMGII mutant, Figure 4F,G).

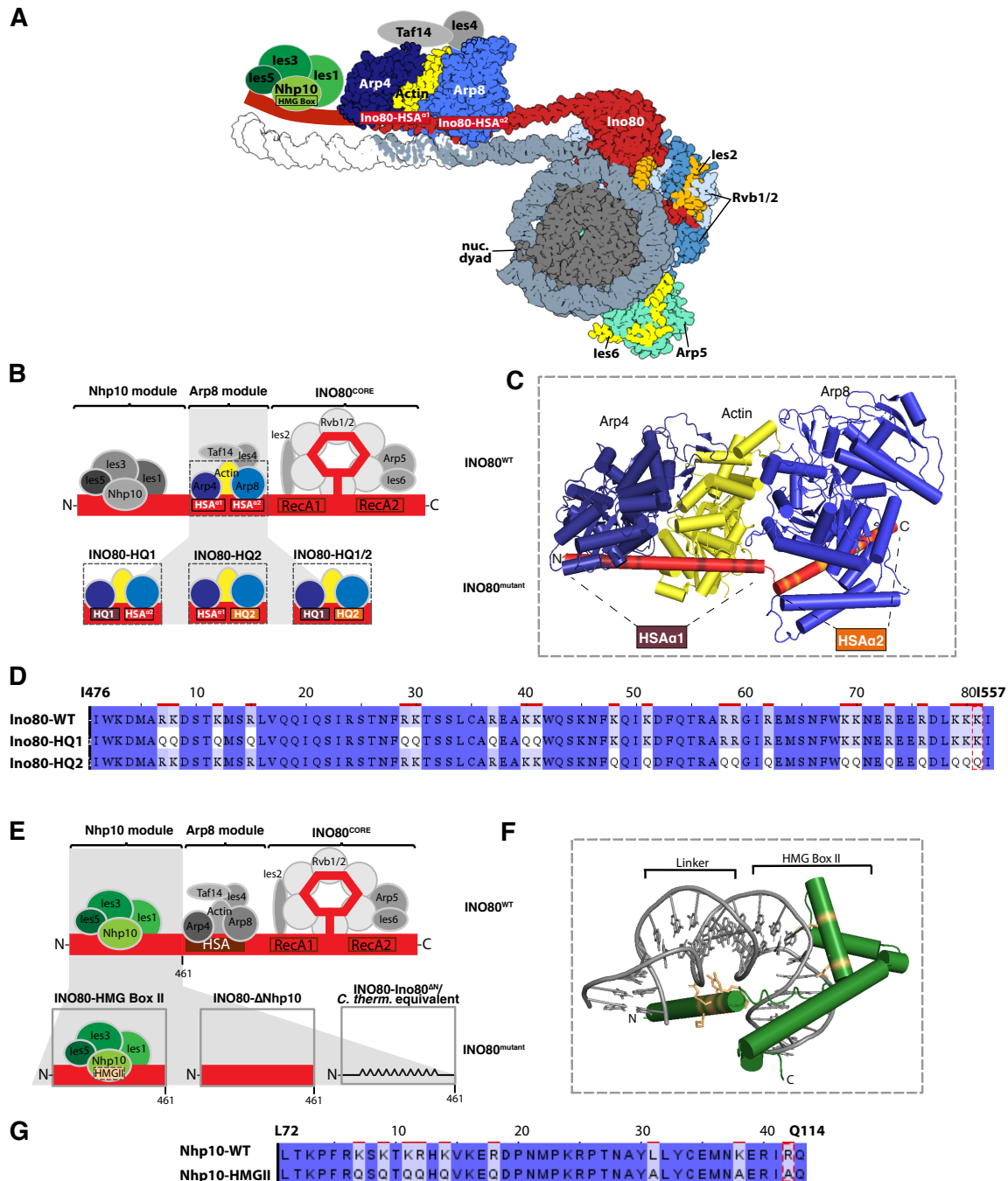


Figure 4. Construction of INO80 mutant complexes. (A) Structure-based (Eustermann et al., 2018; Knoll et al., 2018) model of a nucleosome bound by the INO80 complex with indicated subunits. Nhp10 module, Taf14 and Ies4 organization is assumed. **(B)** Schematic of INO80 complex submodule and subunit organization (top). Zoom into Arp8 module showing three mutant versions (bottom). **(C)** Cylindrical representation of the Arp8 module structure showing mutated residues of Ino80 HSA domain (highlighted in brown and orange). **(D)** Sequence alignment showing mutated residues in Ino80-HQ1 and -HQ2 mutants. **(E)** Schematic of INO80 complex organization as in panel B (top) but zoom into Nhp10 module (bottom) showing three mutant versions. **(F)** Model of Nhp10 HMG box-like and Linker region (residues 62-172) based on TFAM structure (pdb 3tq6). **(G)** Sequence alignment showing mutated residues in Nhp10-HMGII mutant.

These mutations were also combined with the HQ1 or HQ2 mutants (HMGII-HQ1 and HMGII-HQ2). Further, we prepared recombinant INO80 complex without any Nhp10 module subunits (Δ Nhp10 mutant, no truncation of the Ino80 ATPase N-terminus) or a version where the Ino80 ATPase lacked residues 1-461 (INO80 ^{Δ N} mutant), which removes the assembly platform for the Nhp10 module (Figure 4A).

INO80 mutant complexes reveal a multilayered ruler. All mutant complexes were assayed like the wild type (WT) INO80 complex (Figures 5A-E, 6A-D, S1A, S5A,B). WT INO80 was assayed again alongside with matching SGD chromatin. Comparing these replicates (Figure 5C) with

previous values for WT INO80 (Figure 2D) reflected variability in preparing SGD chromatin but at the same time the robustness of the overall effects as the average of absolute differences was 4.3 bp (standard deviation 1.5 bp). All tested INO80 mutants generated steady-state patterns (Figure S5B) and differed from WT INO80 in forming aligned arrays in the following ways.

First, all mutants, besides the HQ1/2 mutant, which was almost inactive (Figure S5A), as expected (Knoll et al., 2018), generated phased regular arrays, but with varying effectiveness and altered distance to one or both barrier types and/or linker lengths compared to WT INO80 (Figures 5D,E, 6D). This revealed that also INO80 has a ruler, to which both the Arp8 and the Nhp10 module contribute.

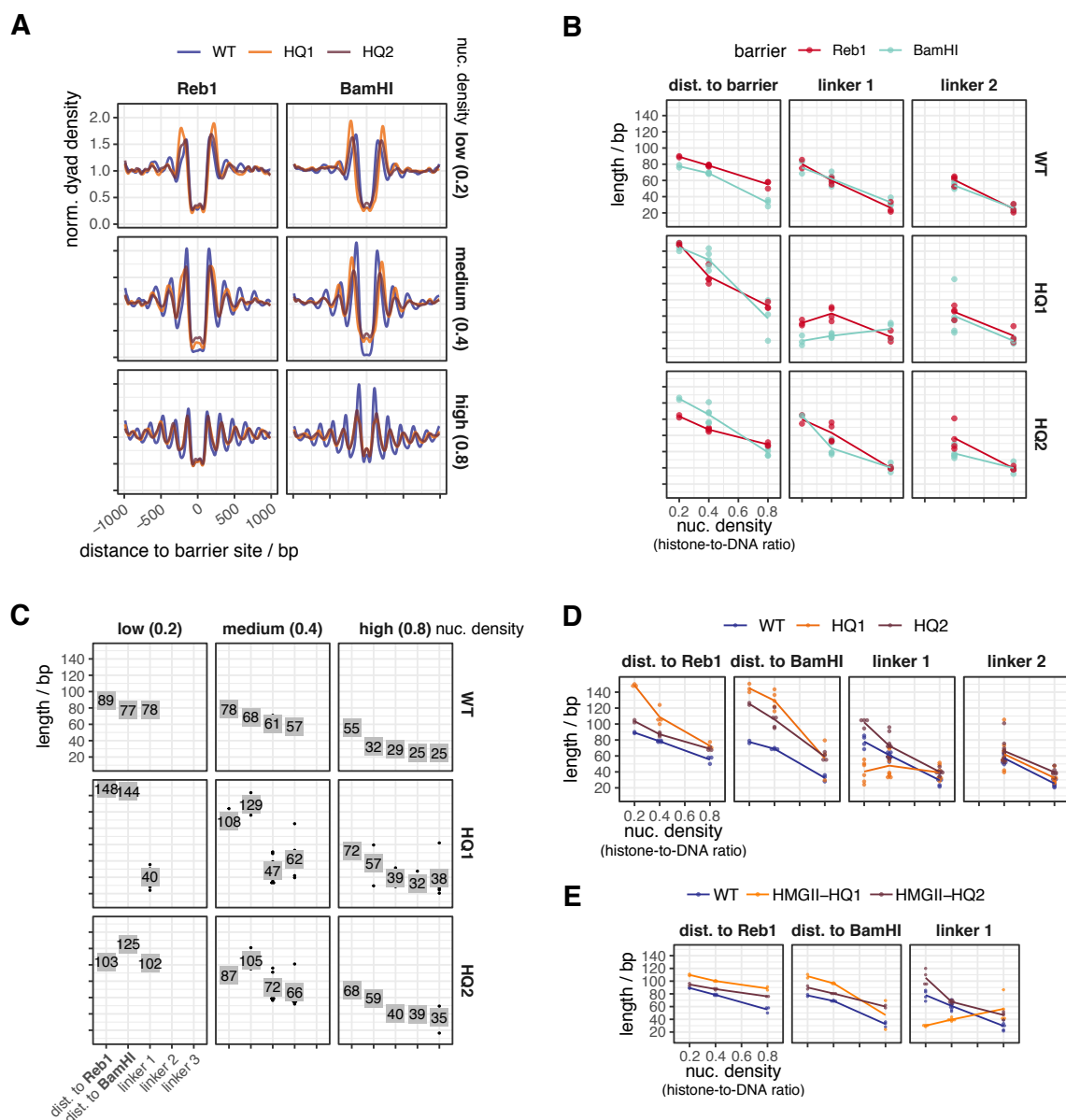


Figure 5. Mutations in the INO80 Arp8 module affect the generation of array features. (A) Composite plots as in Figure 2A but for the indicated WT and mutant INO80 complexes and nucleosome densities. (B) – (D) As Figure 2C-E, but comparing indicated WT and mutant INO80 complexes. Individual replicates in Figures S5A,B. (E) As Figure 2E, but for the indicated WT and mutant INO80 complexes.

Second, the HQ1 showed stronger effects than the HQ2 mutation (Figure 5D). Both increased the distances to both barriers. While HQ2 increased linker length at all densities, HQ1 gained clamping activity, i.e., linker length hardly depended on nucleosome density. Both mutations uncoupled distance to DNA ends from linker lengths, in

contrast to WT INO80 (Figure 2D,E). Only for HQ1, linker 1 length depended on barrier type (Figure 5B). We concluded that the Arp8 module, especially via HSA α 1 helix-DNA interactions, is threefold involved in spacing, alignment to barrier and responding to nucleosome density.

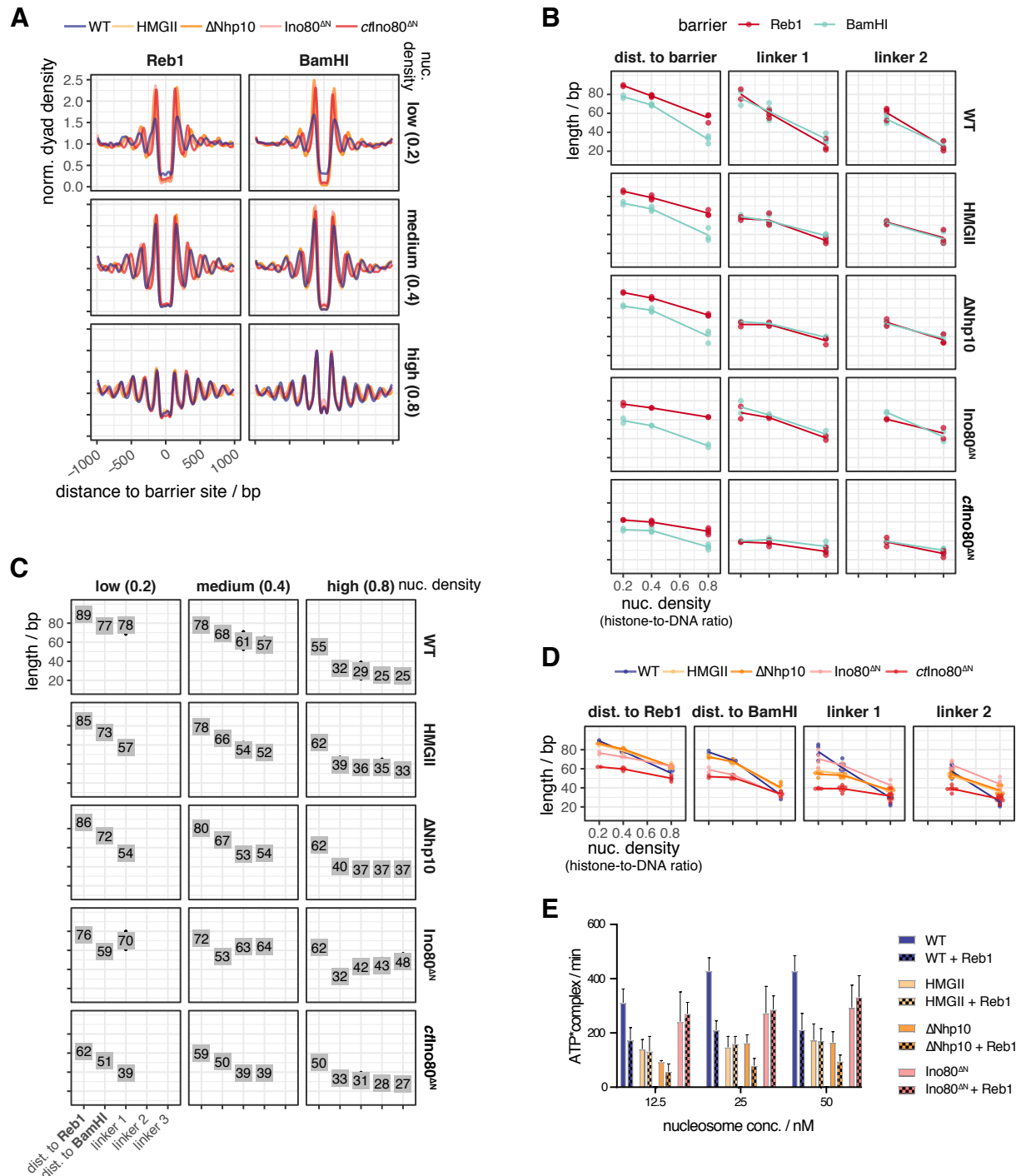


Figure 6. Mutations in the INO80 Nhp10 module affect the generation of array features. (A) – (D) As Figure 5A-D but for the indicated WT and mutant INO80 complexes. Individual replicates in Figure S5A. **(E)** Mononucleosome-stimulated ATPase activities for the indicated nucleosome concentrations and respective equimolar Reb1 concentrations, and INO80 complexes. The extranucleosomal DNA of the 601 mononucleosome contained a Reb1 site at 70 bp distance from the 601 sequence and Reb1 was included as indicated.

Third, the Nhp10 module subunits contributed to the ruler mainly through the HMG box of Nhp10 as the respective point mutations (HMGII mutant) mimicked the effects upon lack of all Nhp10 module subunits (Δ Nhp10 mutant) (Figure 6C,D). With these mutations, distances to both barriers were not much affected, but linker length depended less on density, i.e., clamping was gained, similar to the HQ1 mutation. Effects of the combined HMGII-HQ1 and -HQ2 mutations were dominated by the HQ mutations, but with reduced effects on distance to barriers (Figure 5E). Even though the Nhp10 HMG box was a prime candidate for sensing extranucleosomal DNA, its contribution was minor compared to the HSA helix contribution.

Fourth, the INO80^{AN} mutation affected the distance to Reb1 and even more to DNA ends, but gained clamping less strongly than the HMGII or Δ Nhp10 mutations (Figure 6D). The INO80^{AN} mutant lacked the complete Nhp10 module, but also the Ino80 ATPase N-terminus and Taf14 (Figure S1A), which may account for the differential effects.

Fifth, the INO80^{AN}, HQ1 and HQ2 mutations most drastically affected distance to BamHI sites, but in opposite ways (Figures 5C,D, 6C,D). Lack of the Ino80 N-terminus concomitant with lacking the Nhp10 module allowed INO80 to slide nucleosomes closer to DNA ends, maybe for steric reasons, while impaired DNA traction during remodeling due to compromised HSA helix-DNA interactions had the opposite effect.

Effects on nucleosome stimulated ATPase activity versus on ruler function are not strictly coupled.

The WT INO80 ATPase activity is stimulated by nucleosomes and inhibited about twofold in the presence of Reb1 (accompanying paper Krietenstein et al.). This relative inhibition by Reb1 was not seen or less pronounced for the mutated INO80 complexes (Figure 6E). The ATPase activity of HMGII and Δ Nhp10 mutants was similar to that of WT INO80 in the presence of Reb1. The INO80^{AN} mutant had intermediate activity. We concluded that all tested mutants were affected both with regard to ATPase activity and with regard to their ruler but that both effects were not strongly coupled.

***Chaetomium thermophilum* INO80 core complex suggests species-specific ruler.** The INO80 core complex of *C. thermophilum*, which we previously used for cryoEM studies (Eustermann et al., 2018), corresponds to the *S. cerevisiae* INO80^{AN} mutant as it also lacks its Ino80 ATPase N-terminus. It showed stronger clamping and generated shorter linkers and distances to Reb1 than INO80^{AN} at all densities, and much shorter linkers and distances to both barriers than *S. cerevisiae* WT INO80 at low and medium

densities (Figure 6B-D). This suggests that INO80's ruler may be species-specific.

Discussion

Our study answers one of the oldest questions in chromatin research: what determines the distances of spacing and phasing for nucleosome arrays in absolute terms? Key to the answer are ATP dependent remodelers from the ISWI, CHD and INO80 families with spacing activity. These do not only equalize linker lengths but, as we reveal here, bear rulers for setting distances between nucleosomes and other nucleosomes or other alignment points.

Remodeler rulers explain previous *in vivo* observations. Rulers combined with barriers mechanistically explain *in vivo* observations that involved ISW1a, ISW2, Chd1 and INO80 in +1 nucleosome positioning and/or array regularity and phasing (Gkikopoulos et al., 2011; Hennig et al., 2012; Kubik et al., 2019; Ocampo et al., 2016; Parnell et al., 2015; Pointner et al., 2012; van Bakel et al., 2013; Whitehouse et al., 2007; Yen et al., 2012).

The average yeast linker length of 18 bp (Thomas and Furber, 1976) results from combined contributions of ISW1a and Chd1 (Ocampo et al., 2016). As we show that ISW1a and Chd1 rulers generate linkers of about 20 and 12 bp, respectively, the 18 bp average linker speaks for ISW1a contributing globally more than Chd1. Indeed, lack of Isw1 *in vivo* globally shortened linkers, while lack of Chd1 affected global spacing only mildly (Kubik et al., 2019; Ocampo et al., 2016). Locally, high transcription rate correlates with shorter spacing (Chereji et al., 2018; Ocampo et al., 2016), which points to increased Chd1 contribution, probably due to increased Chd1 recruitment by elongating RNA polymerase (Simic et al., 2003).

Remodeler-specific rulers can explain how ISW1a, ISW2 and INO80 affect +1 nucleosome positioning *in vivo* (Kubik et al., 2019; Parnell et al., 2015; Whitehouse et al., 2007; Yen et al., 2012) and *in vitro* (Krietenstein et al., 2016), especially in combination with RSC. RSC and SWI/SNF are the only yeast remodelers that disassemble nucleosomes (Clapier and Cairns, 2009; Clapier et al., 2017), particularly at promoter NDRs (Badis et al., 2008; Brahma and Henikoff, 2019; Ganguli et al., 2014; Hartley and Madhani, 2009; Kubik et al., 2019; Kubik et al., 2018; Parnell et al., 2008; Rawal et al., 2018; van Bakel et al., 2013; Wippo et al., 2011). By definition, a promoter NDR has low nucleosome density. Therefore, remodeler rulers will set distances to NDR-bound barriers as measured here at low or medium nucleosome density. *In vivo* distances between Reb1 and +1 nucleosomes are 60-80 bp

(Figure S3B, (Rhee and Pugh, 2011)), which are within remodeler-specific distances to Reb1 at medium or low density (81-86 bp for INO80, 70-74 bp for ISW2, 58-60 bp for ISW1a). ISW2 and INO80 contribute more to +1 nucleosome positioning *in vivo* than ISW1a (Kubik et al., 2019) as their long rulers are more suited for setting long distances across NDRs. Conversely, the short Chd1-ruler hardly contributes to +1 positioning *in vivo* (Kubik et al., 2019; Ocampo et al., 2016; van Bakel et al., 2013). These different ruler characteristics explain why ISW1a and Chd1 are mainly involved in spacing nucleosomes into densely packed arrays and why ISW2 and INO80 mainly use their ruler for +1 alignment at NDRs *in vivo*. This resolves the conundrum (Krietenstein et al., 2016) why yeast has two remodelers, INO80 and ISW2, that seemingly generate “too wide” spacing compared to average *in vivo* spacing. We do not preclude that other mechanisms, like recruitment via histone modifications or transcription factors, also affect where each remodeler is active.

Remodeler rulers regulate nucleosome sliding direction bias in response to nucleosome environment. The protein ruler model was first proposed for ISW1a (Yamada et al., 2011) and suggested that ISW1a shortens the linker until its ruler contacts the neighboring nucleosome. It neither considered GRFs or DNA ends nor why nucleosomes stay positioned at the ruler-specified distance. We now extend the model (Figure 7) into a widely applicable remodeler ruler principle.

A remodeler may slide a nucleosome either to the left or to the right from a given position. If there is no bias for sliding in either direction, the nucleosome will experience a random walk along the DNA (regions C in Figure 7A). Net nucleosome movement in one direction (Gangaraju and Bartholomew, 2007; Langst et al., 1999; McKnight et al., 2011; Stockdale et al., 2006; Udugama et al., 2011; Yang et al., 2006; Zhou et al., 2018) requires an overall sliding direction bias in this direction. We define a remodeler ruler as a remodeler-intrinsic feature that generates an overall sliding direction bias in response to the environment of the nucleosome that the remodeler is remodeling (three hypothetical examples in Figure 7A). The bias may originate from differences, e.g., in binding orientation, ATPase activity, sliding rate or processivity. While the microscopic details may differ for different remodelers, the overall regulation of sliding direction bias by the ruler will share three key elements that constitute the ruler mechanism. First, the ruler has a certain reach (region A + B in Figure 7A), within which it interacts with a generalized “barrier”. This may be a GRF, a DSB, a neighboring nucleosome, or

a DNA sequence element recognized by the ruler. Second, if the position, from where the remodeler slides the nucleosome, is within region B, the interaction between ruler and barrier biases overall sliding direction towards the barrier (red curve is above green curve), e.g., due to binding energy gained upon orienting the remodeler towards vs. away from the barrier. Third, if the nucleosome is in region A, the ruler-barrier interaction disfavors sliding towards relative to sliding away from the barrier (green curve is above red curve), e.g., because the ruler gets sterically in the way. Our study determined the length of region A for each remodeler type. Region B and curve shapes will have to be determined for each remodeler, barrier and condition in future studies. If the above three key elements are met, resulting fluxes will lead to steady-state nucleosome placement at a defined position relative to the barrier (stippled vertical arrows throughout Figure 7). This position is a self-stabilizing dynamic equilibrium point (intersection of red and green curves) without sliding direction bias here, but with biases *towards* this point from neighboring positions. This model applies to how a remodeler with ruler stably positions a nucleosome next to a barrier as well as to another nucleosome and therefore explains both spacing and phasing.

It also explains density-independent clamping. As long as a remodeler is processive enough to fortuitously bring nucleosomes into region B of a barrier also at low density, the ruler mechanism will keep the nucleosome at the dynamic equilibrium point. Nonetheless, the model can also accommodate sensing of nucleosome density and barrier type, e.g., if the ruler offers a hierarchy of interaction points that depends on density or barrier type. For example, INO80 may be able to adopt different conformations that may provide different interaction sites and have different footprint sizes, which may explain why INO80 can remodel arrays with just 30 bp linkers despite a measured footprint of >50 bp (Brahma et al., 2018). INO80 mutants showed not concerted but uncoupled effects on distance to Reb1, DNA ends and nucleosomes, even if the same module, like the Nhp10 module, was differentially mutated. Chd1 generated shorter linker lengths (12-16 bp) than distances to DNA ends or Reb1 (35-40 bp). For Chd1, Reb1 may be a “hard” barrier while nucleosomes are “soft” barriers are partially “invaded” by the ruler. Indeed, Chd1 partially unwraps nucleosomal DNA (Farnung et al., 2017). The way how different remodeler rulers interact with different barriers requires clarification, and we outline our model (Figure 7) in terms of extension-less point particles, but actual footprints have to be taken into account.

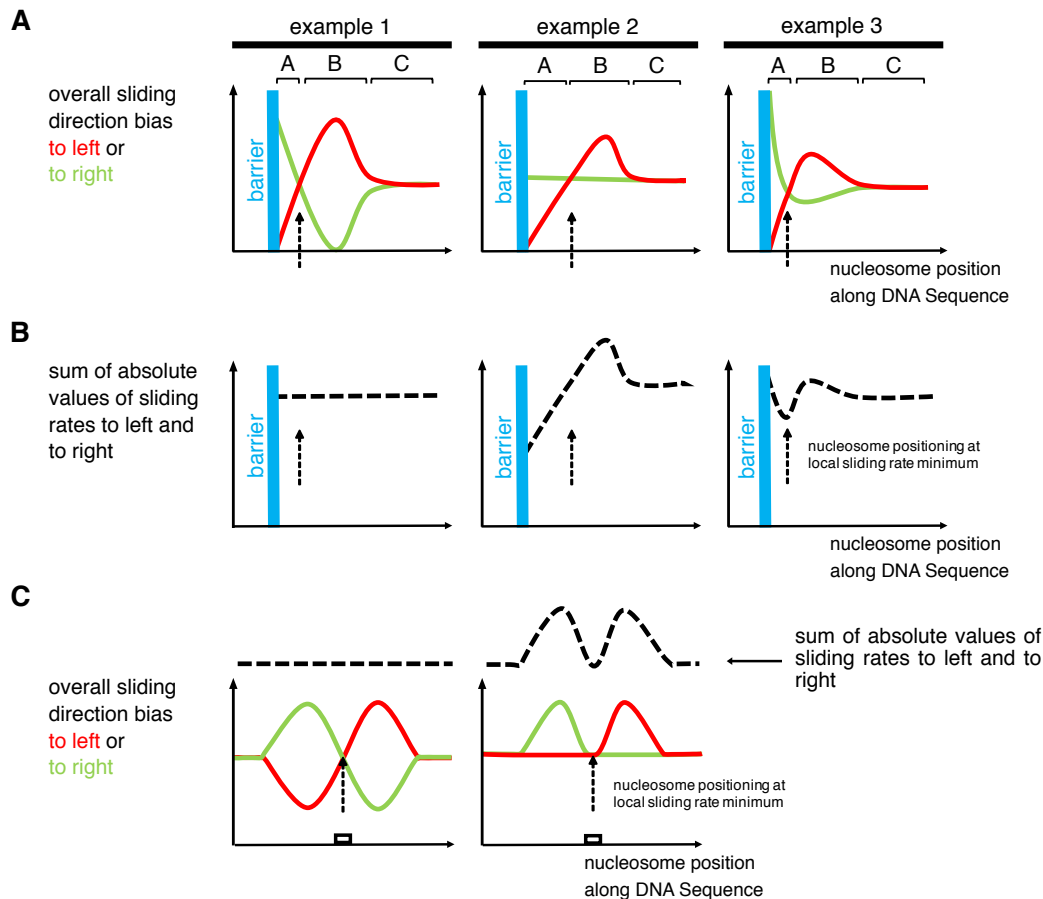


Figure 7. Model for remodeler ruler mechanism. (A) Three hypothetical examples for how a remodeler ruler regulates the overall bias of sliding a nucleosome to left (red curves) or to right (green curves) resulting in nucleosome positioning (stippled vertical arrows) in the vicinity of a barrier. (B) As panel A but plotting sum of absolute values of sliding rates to the left and to the right (stippled black curves). (C) Two hypothetical examples for how a remodeler ruler leads to nucleosome positioning over a DNA site (white box). Symbolics as in panels A and B. For details see text.

The model is fully compatible with the ruler, e.g., the DNA binding domain (DBD) of Chd1 (McKnight et al., 2011) or *Drosophila* ACF (Yang et al., 2006), introducing bias via sensing extranucleosomal DNA length. Indeed, differently long extranucleosomal DNA in mono- or oligonucleosome sliding assays amounts to different distances to barriers like DNA ends or other nucleosomes. Our model is fully consistent with previous data, but offers an alternative interpretation.

We introduced our model in terms of overall sliding direction bias. More specifically, the model may refer to differential regulation of sliding rates, i.e., the y-axis in Figure 7A could correspond to “overall sliding rate to the left or to the right”. If sliding rates are reciprocally regulated (example 1, Figure 7A), the sum of absolute sliding rate values is constant at each position (Figure 7B), but not upon asymmetric regulation of sliding direction (examples 2 and 3, Figure 7A). As special case (example 3, Figure 7A,B), the dynamic equilibrium point may correspond to a minimum

of absolute sliding rate. This case corresponds to the “kinetic release” model (Rippe et al., 2007), which posits that remodelers position nucleosomes at sites where the nucleosome is the (locally) poorest substrate for remodeling.

Ruler-regulated sliding: the unifying principle for nucleosome positioning by remodelers.

As nucleosome positions are defined by the DNA sequence bound by the histone octamer, all mechanisms, that generate distinct nucleosome positions, must select certain DNA sequences in competition with other sequences. As shown here and in the accompanying paper (Krietenstein et al.), remodelers may mediate this selection in two ways. On the one hand, a remodeler may directly choose a sequence, e.g., INO80 turns DNA shape features into +1 nucleosome positions at promoters (accompanying paper Krietenstein et al.) On the other hand, a remodeler ruler may place a nucleosome at a ruler-determined distance to a barrier, e.g., ISW2 aligns nucleosomes to Reb1 and generates a regular array by aligning a second

nucleosome to the first and so on. In the former case, the resulting nucleosomal sequence is selected for its sequence features, while in the latter case, it is selected without regards for its sequence features but merely for its position relative to the barrier, as we show here by using Reb1 sites in *S. pombe* and *E. coli* genomes.

Our ruler model unifies these seemingly opposing positioning mechanisms. The generalized barrier also encompasses DNA sequence elements, with which a remodeler ruler interacts such that sliding direction bias is regulated (Figure 7C). This explains observations for hybrid Chd1 remodelers where the Chd1 DBD was replaced with heterologous sequence-specific DBDs (Donovan et al., 2019; McKnight et al., 2011; McKnight et al., 2016). Such hybrid Chd1 remodelers slide nucleosomes faster towards the cognate site of the heterologous DBD, if it was in reach of this site, until the nucleosome became positioned on the site. In our model, the heterologous DBD is a remodeler ruler. As a DNA sequence element as barrier is no hindrance for nucleosome sliding, the remodeler may slide the nucleosome onto this site. This prevents ruler binding to the site, abolishes the increase in sliding rate linked to ruler binding and makes a nucleosome on the cognate site a poorer nucleosome sliding substrate than at neighboring positions (Figure 7C, right), which corresponds to the kinetic release model as noted (McKnight et al., 2011). Our model now adds that sliding from neighboring positions will always (within ruler reach) convene at the cognate site and stabilize this position, even if there is no local sliding rate minimum, as long as the ruler regulates sliding direction bias according to the three key elements outlined above (Figure 7C, left). As our INO80 mutations differently affected nucleosome positioning via DNA shape (accompanying paper Krietenstein et al.) vs. relative to Reb1 vs. DNA ends vs. nucleosomes, the ruler elements seem to be multilayered and maybe linked to different structural conformations. For example, aligning nucleosomes at high density may not be compatible with positioning +1 nucleosomes via DNA shape.

In vivo there are many ways that may regulate nucleosome positioning by remodelers, e.g., by recruitment, by architectural factors, by nucleosome density fluctuations or by histone variants and modifications, possibly in the context of elongating polymerases. Nonetheless, we expect that the regulation of nucleosome sliding direction

bias via built-in sensing of nucleosome environment, i.e., a remodeler ruler, will be at the heart of each nucleosome positioning mechanism.

References

- Awad, S., Ryan, D., Prochasson, P., Owen-Hughes, T., and Hassan, A.H. (2010). The Snf2 homolog Fun30 acts as a homodimeric ATP-dependent chromatin-remodeling enzyme. *The Journal of biological chemistry* 285, 9477-9484.
- Badis, G., Chan, E.T., van Bakel, H., Pena-Castillo, L., Tillo, D., Tsui, K., Carlson, C.D., Gossett, A.J., Hasinoff, M.J., Warren, C.L., et al. (2008). A library of yeast transcription factor motifs reveals a widespread function for Rsc3 in targeting nucleosome exclusion at promoters. *Molecular cell* 32, 878-887.
- Baldi, S., Jain, D.S., Harpprecht, L., Zabel, A., Scheibe, M., Butter, F., Straub, T., and Becker, P.B. (2018a). Genome-wide Rules of Nucleosome Phasing in *Drosophila*. *Molecular cell* 72, 661-672.e664.
- Baldi, S., Korber, P., and Becker, P.B. (2020). Beads on a string-nucleosome array arrangements and folding of the chromatin fiber. *Nature structural & molecular biology* 27, 109-118.
- Baldi, S., Krebs, S., Blum, H., and Becker, P.B. (2018b). Genome-wide measurement of local nucleosome array regularity and spacing by nanopore sequencing. *Nature structural & molecular biology* 25, 894-901.
- Brahma, S., and Henikoff, S. (2019). RSC-Associated Subnucleosomes Define MNase-Sensitive Promoters in Yeast. *Molecular cell* 73, 238-249.e233.
- Brahma, S., Ngubo, M., Paul, S., Udugama, M., and Bartholomew, B. (2018). The Arp8 and Arp4 module acts as a DNA sensor controlling INO80 chromatin remodeling. *Nature communications* 9, 3309.
- Challal, D., Barucco, M., Kubik, S., Feuerbach, F., Candelli, T., Geoffroy, H., Benaksas, C., Shore, D., and Libri, D. (2018). General Regulatory Factors Control the Fidelity of Transcription by Restricting Non-coding and Ectopic Initiation. *Molecular cell* 72, 955-969.e957.
- Chereji, R.V., Ramachandran, S., Bryson, T.D., and Henikoff, S. (2018). Precise genome-wide mapping of single nucleosomes and linkers in vivo. *Genome biology* 19, 19.
- Clapier, C.R., and Cairns, B.R. (2009). The biology of chromatin remodeling complexes. *Annual review of biochemistry* 78, 273-304.
- Clapier, C.R., Iwasa, J., Cairns, B.R., and Peterson, C.L. (2017). Mechanisms of action and regulation of ATP-dependent chromatin-remodelling complexes. *Nature reviews Molecular cell biology* 18, 407-422.
- Donovan, D.A., Crandall, J.G., Banks, O.G.B., Jensvold, Z.D., Truong, V., Dinwiddie, D., McKnight, L.E., and McKnight, J.N. (2019). Engineered Chromatin Remodeling Proteins for Precise Nucleosome Positioning. *Cell reports* 29, 2520-2535.e2524.
- Eustermann, S., Schall, K., Kostrewa, D., Lakomek, K., Strauss, M., Moldt, M., and Hopfner, K.P. (2018). Structural basis for ATP-dependent chromatin remodelling by the INO80 complex. *Nature* 556, 386-390.
- Farnung, L., Vos, S.M., Wigge, C., and Cramer, P. (2017). Nucleosome-Chd1 structure and implications for chromatin remodelling. *Nature*.
- Flaus, A., Martin, D.M., Barton, G.J., and Owen-Hughes, T. (2006). Identification of multiple distinct Snf2 subfamilies with conserved structural motifs. *Nucleic acids research* 34, 2887-2905.

- Ganapathi, M., Palumbo, M.J., Ansari, S.A., He, Q., Tsui, K., Nislow, C., and Morse, R.H. (2011). Extensive role of the general regulatory factors, Abf1 and Rap1, in determining genome-wide chromatin structure in budding yeast. *Nucleic acids research* 39, 2032-2044.
- Gangaraju, V.K., and Bartholomew, B. (2007). Dependency of ISW1a chromatin remodeling on extranucleosomal DNA. *Molecular and cellular biology* 27, 3217-3225.
- Ganguli, D., Chereji, R.V., Iben, J.R., Cole, H.A., and Clark, D.J. (2014). RSC-dependent constructive and destructive interference between opposing arrays of phased nucleosomes in yeast. *Genome research* 24, 1637-1649.
- Gkikopoulos, T., Schofield, P., Singh, V., Pinskaya, M., Mellor, J., Smolle, M., Workman, J.L., Barton, G.J., and Owen-Hughes, T. (2011). A role for Snf2-related nucleosome-spacing enzymes in genome-wide nucleosome organization. *Science* (New York, NY) 333, 1758-1760.
- Gossett, A.J., and Lieb, J.D. (2012). In vivo effects of histone H3 depletion on nucleosome occupancy and position in *Saccharomyces cerevisiae*. *PLoS genetics* 8, e1002771.
- Gutin, J., Sadeh, R., Bodenheimer, N., Joseph-Strauss, D., Klein-Brill, A., Alajem, A., Ram, O., and Friedman, N. (2018). Fine-Resolution Mapping of TF Binding and Chromatin Interactions. *Cell reports* 22, 2797-2807.
- Hartley, P.D., and Madhani, H.D. (2009). Mechanisms that specify promoter nucleosome location and identity. *Cell* 137, 445-458.
- Hennig, B.P., Bendrin, K., Zhou, Y., and Fischer, T. (2012). Chd1 chromatin remodelers maintain nucleosome organization and repress cryptic transcription. *EMBO reports* 13, 997-1003.
- Ito, T., Bulger, M., Pazin, M.J., Kobayashi, R., and Kadonaga, J.T. (1997). ACF, an ISWI-containing and ATP-utilizing chromatin assembly and remodeling factor. *Cell* 90, 145-155.
- Jaiswal, R., Choudhury, M., Zaman, S., Singh, S., Santosh, V., Bastia, D., and Escalante, C.R. (2016). Functional architecture of the Reb1-Ter complex of *Schizosaccharomyces pombe*. *Proceedings of the National Academy of Sciences of the United States of America* 113, E2267-2276.
- Knoll, K.R., Eustermann, S., Niebauer, V., Oberbeckmann, E., Stoehr, G., Schall, K., Tosi, A., Schwarz, M., Buchfeller, A., Korber, P., *et al.* (2018). The nuclear actin-containing Arp8 module is a linker DNA sensor driving INO80 chromatin remodeling. *Nature structural & molecular biology* 25, 823-832.
- Kornberg, R.D. (1974). Chromatin structure: a repeating unit of histones and DNA. *Science* (New York, NY) 184, 868-871.
- Kornberg, R.D., and Lorch, Y. (1999). Twenty-five years of the nucleosome, fundamental particle of the eukaryote chromosome. *Cell* 98, 285-294.
- Krietenstein, N., Wal, M., Watanabe, S., Park, B., Peterson, C.L., Pugh, B.F., and Korber, P. (2016). Genomic Nucleosome Organization Reconstituted with Pure Proteins. *Cell* 167, 709-721.e712.
- Kubik, S., Bruzzone, M.J., Challal, D., Dreos, R., Mattarocci, S., Bucher, P., Libri, D., and Shore, D. (2019). Opposing chromatin remodelers control transcription initiation frequency and start site selection. *Nature structural & molecular biology* 26, 744-754.
- Kubik, S., O'Duibhir, E., de Jonge, W.J., Mattarocci, S., Albert, B., Falcone, J.L., Bruzzone, M.J., Holstege, F.C.P., and Shore, D. (2018). Sequence-Directed Action of RSC Remodeler and General Regulatory Factors Modulates +1 Nucleosome Position to Facilitate Transcription. *Molecular cell* 71, 89-102.e105.
- Lai, W.K.M., and Pugh, B.F. (2017). Understanding nucleosome dynamics and their links to gene expression and DNA replication. *Nature reviews Molecular cell biology* 18, 548-562.
- Langst, G., Bonte, E.J., Corona, D.F., and Becker, P.B. (1999). Nucleosome movement by CHRAC and ISWI without disruption or trans-displacement of the histone octamer. *Cell* 97, 843-852.
- Lieleg, C., Ketterer, P., Nuebler, J., Ludwigsen, J., Gerland, U., Dietz, H., Mueller-Planitz, F., and Korber, P. (2015). Nucleosome spacing generated by ISWI and CHD1 remodelers is constant regardless of nucleosome density. *Molecular and cellular biology* 35, 1588-1605.
- Luger, K., Mader, A.W., Richmond, R.K., Sargent, D.F., and Richmond, T.J. (1997). Crystal structure of the nucleosome core particle at 2.8 Å resolution. *Nature* 389, 251-260.
- Lusser, A., Urwin, D.L., and Kadonaga, J.T. (2005). Distinct activities of CHD1 and ACF in ATP-dependent chromatin assembly. *Nature structural & molecular biology* 12, 160-166.
- McKnight, J.N., Jenkins, K.R., Nodelman, I.M., Escobar, T., and Bowman, G.D. (2011). Extranucleosomal DNA binding directs nucleosome sliding by Chd1. *Molecular and cellular biology* 31, 4746-4759.
- McKnight, J.N., Tsukiyama, T., and Bowman, G.D. (2016). Sequence-targeted nucleosome sliding in vivo by a hybrid Chd1 chromatin remodeler. *Genome research* 26, 693-704.
- Ngo, H.B., Lovely, G.A., Phillips, R., and Chan, D.C. (2014). Distinct structural features of TFAM drive mitochondrial DNA packaging versus transcriptional activation. *Nature communications* 5, 3077.
- Ocampo, J., Chereji, R.V., Eriksson, P.R., and Clark, D.J. (2016). The ISW1 and CHD1 ATP-dependent chromatin remodelers compete to set nucleosome spacing in vivo. *Nucleic acids research* 44, 4625-4635.
- Olins, A.L., and Olins, D.E. (1974). Spheroid chromatin units (v bodies). *Science* (New York, NY) 183, 330-332.
- Olins, D.E., and Olins, A.L. (2003). Chromatin history: our view from the bridge. *Nature reviews Molecular cell biology* 4, 809-814.
- Parnell, T.J., Huff, J.T., and Cairns, B.R. (2008). RSC regulates nucleosome positioning at Pol II genes and density at Pol III genes. *The EMBO journal* 27, 100-110.
- Parnell, T.J., Schlichter, A., Wilson, B.G., and Cairns, B.R. (2015). The chromatin remodelers RSC and ISW1 display functional and chromatin-based promoter antagonism. *eLife* 4, e06073.
- Patel, A., McKnight, J.N., Genzor, P., and Bowman, G.D. (2011). Identification of residues in chromodomain helicase DNA-binding protein 1 (Chd1) required for coupling ATP hydrolysis to nucleosome sliding. *The Journal of biological chemistry* 286, 43984-43993.
- Pointner, J., Persson, J., Prasad, P., Norman-Axelsson, U., Stralfors, A., Khorosjutina, O., Krietenstein, N., Svensson, J.P., Ekwall, K., and Korber, P. (2012). CHD1 remodelers regulate nucleosome spacing in vitro and align nucleosomal arrays over gene coding regions in *S. pombe*. *The EMBO journal* 31, 4388-4403.
- Rawal, Y., Chereji, R.V., Qiu, H., Ananthkrishnan, S., Govind, C.K., Clark, D.J., and Hinnebusch, A.G. (2018). SWI/SNF and RSC cooperate to reposition and evict promoter nucleosomes at highly expressed genes in yeast. *Genes & development* 32, 695-710.
- Rhee, H.S., and Pugh, B.F. (2011). Comprehensive genome-wide protein-DNA interactions detected at single-nucleotide resolution. *Cell* 147, 1408-1419.

- Rippe, K., Schrader, A., Riede, P., Strohnner, R., Lehmann, E., and Langst, G. (2007). DNA sequence- and conformation-directed positioning of nucleosomes by chromatin-remodeling complexes. *Proceedings of the National Academy of Sciences of the United States of America* *104*, 15635-15640.
- Satchwell, S.C., Drew, H.R., and Travers, A.A. (1986). Sequence periodicities in chicken nucleosome core DNA. *Journal of molecular biology* *191*, 659-675.
- Simic, R., Lindstrom, D.L., Tran, H.G., Roinick, K.L., Costa, P.J., Johnson, A.D., Hartzog, G.A., and Arndt, K.M. (2003). Chromatin remodeling protein Chd1 interacts with transcription elongation factors and localizes to transcribed genes. *The EMBO journal* *22*, 1846-1856.
- Smolle, M., Venkatesh, S., Gogol, M.M., Li, H., Zhang, Y., Florens, L., Washburn, M.P., and Workman, J.L. (2012). Chromatin remodelers Isw1 and Chd1 maintain chromatin structure during transcription by preventing histone exchange. *Nature structural & molecular biology* *19*, 884-892.
- Stockdale, C., Flaus, A., Ferreira, H., and Owen-Hughes, T. (2006). Analysis of nucleosome repositioning by yeast ISWI and Chd1 chromatin remodeling complexes. *The Journal of biological chemistry* *281*, 16279-16288.
- Thomas, J.O., and Furber, V. (1976). Yeast chromatin structure. *FEBS letters* *66*, 274-280.
- Torigoe, S.E., Patel, A., Khuong, M.T., Bowman, G.D., and Kadonaga, J.T. (2013). ATP-dependent chromatin assembly is functionally distinct from chromatin remodeling. *eLife* *2*, e00863.
- Tsankov, A., Yanagisawa, Y., Rhind, N., Regev, A., and Rando, O.J. (2011). Evolutionary divergence of intrinsic and trans-regulated nucleosome positioning sequences reveals plastic rules for chromatin organization. *Genome research* *21*, 1851-1862.
- Tsukiyama, T., Palmer, J., Landel, C.C., Shiloach, J., and Wu, C. (1999). Characterization of the imitation switch subfamily of ATP-dependent chromatin-remodeling factors in *Saccharomyces cerevisiae*. *Genes & development* *13*, 686-697.
- Udugama, M., Sabri, A., and Bartholomew, B. (2011). The INO80 ATP-dependent chromatin remodeling complex is a nucleosome spacing factor. *Molecular and cellular biology* *31*, 662-673.
- Valouev, A., Johnson, S.M., Boyd, S.D., Smith, C.L., Fire, A.Z., and Sidow, A. (2011). Determinants of nucleosome organization in primary human cells. *Nature* *474*, 516-520.
- van Bakel, H., Tsui, K., Gebbia, M., Mnaimneh, S., Hughes, T.R., and Nislow, C. (2013). A compendium of nucleosome and transcript profiles reveals determinants of chromatin architecture and transcription. *PLoS genetics* *9*, e1003479.
- van Holde, K.E. (1989). *Chromatin* (New York: Springer).
- Varga-Weisz, P.D., Wilm, M., Bonte, E., Dumas, K., Mann, M., and Becker, P.B. (1997). Chromatin-remodelling factor CHRAC contains the ATPases ISWI and topoisomerase II. *Nature* *388*, 598-602.
- Whitehouse, I., Rando, O.J., Delrow, J., and Tsukiyama, T. (2007). Chromatin remodelling at promoters suppresses antisense transcription. *Nature* *450*, 1031-1035.
- Wiechens, N., Singh, V., Gkikopoulos, T., Schofield, P., Rocha, S., and Owen-Hughes, T. (2016). The Chromatin Remodelling Enzymes SNF2H and SNF2L Position Nucleosomes adjacent to CTCF and Other Transcription Factors. *PLoS genetics* *12*, e1005940.
- Wippo, C.J., Israel, L., Watanabe, S., Hochheimer, A., Peterson, C.L., and Korber, P. (2011). The RSC chromatin remodelling enzyme has a unique role in directing the accurate positioning of nucleosomes. *The EMBO journal* *30*, 1277-1288.
- Yamada, K., Frouws, T.D., Angst, B., Fitzgerald, D.J., DeLuca, C., Schimmele, K., Sargent, D.F., and Richmond, T.J. (2011). Structure and mechanism of the chromatin remodelling factor ISW1a. *Nature* *472*, 448-453.
- Yan, C., Chen, H., and Bai, L. (2018). Systematic Study of Nucleosome-Displacing Factors in Budding Yeast. *Molecular cell* *71*, 294-305.e294.
- Yang, J.G., Madrid, T.S., Sevastopoulos, E., and Narlikar, G.J. (2006). The chromatin-remodeling enzyme ACF is an ATP-dependent DNA length sensor that regulates nucleosome spacing. *Nature structural & molecular biology* *13*, 1078-1083.
- Yarragudi, A., Miyake, T., Li, R., and Morse, R.H. (2004). Comparison of ABF1 and RAP1 in chromatin opening and transactivator potentiation in the budding yeast *Saccharomyces cerevisiae*. *Molecular and cellular biology* *24*, 9152-9164.
- Yen, K., Vinayachandran, V., Batta, K., Koerber, R.T., and Pugh, B.F. (2012). Genome-wide nucleosome specificity and directionality of chromatin remodelers. *Cell* *149*, 1461-1473.
- Zhang, Y., Moqtaderi, Z., Rattner, B.P., Euskirchen, G., Snyder, M., Kadonaga, J.T., Liu, X.S., and Struhl, K. (2009). Intrinsic histone-DNA interactions are not the major determinant of nucleosome positions in vivo. *Nature structural & molecular biology* *16*, 847-852.
- Zhang, Z., Wippo, C.J., Wal, M., Ward, E., Korber, P., and Pugh, B.F. (2011). A packing mechanism for nucleosome organization reconstituted across a eukaryotic genome. *Science (New York, NY)* *332*, 977-980.
- Zhou, C.Y., Johnson, S.L., Lee, L.J., Longhurst, A.D., Beckwith, S.L., Johnson, M.J., Morrison, A.J., and Narlikar, G.J. (2018). The Yeast INO80 Complex Operates as a Tunable DNA Length-Sensitive Switch to Regulate Nucleosome Sliding. *Molecular cell* *69*, 677-688.e679.

Acknowledgments

We thank Kevin Schall, Nils Krietenstein and Maria Walker for providing purified proteins, Michael Wolff and Ulrich Gerland for helpful discussions of nucleosome positioning mechanisms, Stefan Krebs and Helmut Blum at the Laboratory for Functional Genome Analysis (LAFUGA, Gene Center, LMU München) for high throughput sequencing, and Sigurd Braun for access to and help with the plating robot. This study was funded by the German Research Foundation (SFB1064 to P.K.; SFB860, SPP1935, and EXC 2067/1-390729940 to P.C.), and the European Research Council (grant agreement No 693023 to P.C.).

Author contributions

Conceptualization: PK, SE, EO, KPH; Data curation: EO, VN; Formal analysis: EO, VN; Funding acquisition, Project administration, Supervision: PK, KPH, SE, PC, CLP; Investigation: EO, VN, SW, LF, MM, AS; Methodology: EO, VN, SE, SW, LF, PK; Validation: EO, VN, MM, AS, SW, LF, PK, SE; Visualization: EO, VN, PK, SW, LF; Writing original draft: PK, SE, EO; Writing – review & editing: PK, SE, EO, VN, KPH, LF, SW, CLP, PC.

Competing interests

The authors declare no competing interests.

Methods

Organisms as source for materials used in experiments.

The pGP546 yeast genomic plasmid library was expanded from the clonal plates provided by Open Biosystems. For generation of genomic plasmid libraries, the *S. pombe* strain Hu0303 (Ekwall group) and *E. coli* strain (ATCC 11303 strain, 14380, Affymetrix) were used.

INO80 wild-type and mutant complexes, Chd1 and FACT were expressed in *Trichoplusia insect cells*. *Spodoptera frugiperda sf21* insect cells were used for virus production. The *Saccharomyces cerevisiae* ISW1a and Fun30 remodelers were purified from the correspondingly TAP-tagged yeast strains, Ioc3-TAP, Fun30-Tap, as provided by Open Biosystems. Yeast ISW2 was purified from strain YTT480 (ISW2-2xFLAG, Tsukiyama et al., 1999). Reb1 was purified from *E. coli* BL21 (DE3) cd+ cells. The *Drosophila* embryo histones were prepared from the *Drosophila melanogaster* strain OregonR.

Embryonic *D. melanogaster* histones, whole-genome plasmid libraries and salt gradient dialysis

Embryonic *D. melanogaster* histone purification. The preparation of embryonic *D. melanogaster* histones octamers was carried out as described in Krietenstein et al. 2012 and Simon and Felsenfeld, 1979. Briefly, 50 g of 0-12 hours old *D. melanogaster* embryos were dechorionated in 3 % sodium hypochlorite, washed with dH₂O and resuspended in 40 mL lysis-buffer (15 mM K-HEPES pH 7.5, 10 mM KCl, 5 mM MgCl₂, 0.1 mM EDTA, 0.5 mM EGTA, 1 mM DTT, 0.2 mM PMSF, 10 % glycerol). Embryos were homogenized (Yamamoto homogenizer), filtered through cloth and centrifuged at 6,500 g for 15 min. Nuclei (brownish light pellet) were washed 3 times with 50 mL sucrose-buffer (15 mM K-HEPES pH 7.5, 10 mM KCl, 5 mM MgCl₂, 0.05 mM EDTA, 0.25 mM EGTA, 1 mM DTT, 0.2 mM PMSF, 1.2 % sucrose) and resuspended in 30 mL sucrose-buffer containing 3 mM CaCl₂. To obtain mononucleosomes, nuclei were incubated for 10 min at 26 °C with 6250 Units MNase (Sigma-Aldrich). Reaction was stopped with 10 mM EDTA, nuclei were pelleted and resuspended in 6 mL TE (10 mM Tris-HCl pH 7.6, 1 mM EDTA) containing 1 mM DTT and 0.2 mM PMSF followed by 30 to 45 min of rotation at 4 °C. Nuclei were centrifuged for 30 min at 15,300 g at 4 °C. Solubilized mononucleosomes are found in the supernatant, which was applied to a pre-equilibrated hydroxyapatite column. After washing the hydroxyapatite column with 0.63 M KCl, histone octamers were eluted with 2 M KCl, concentrated and stored in 50 % glycerol and 1x Complete (Roche) protease inhibitors without EDTA at -20 °C.

Whole-genome plasmid library expansion. The *S. cerevisiae* genomic plasmid library (pGP546) was originally described in Jones et al. 2008 and purchased as a clonal glycerol stock collection from Open Biosystems. Library expansion was carried out via a Singer ROTOR plating machine (Singer Instruments) (8-12 rounds, 3 replicas). After 16 hours, colonies were combined into 3x2 L of LB medium containing 50 µg/mL kanamycin and grown for 4 hours. Cells were harvested and subjected to Plasmid Giga Preparation (PC 10 000 Kit, Macherey&Nagel).

For *S. pombe* and *E. coli* plasmid library generation, genomic *S. pombe* (Hu0303) and *E. coli* (type B cells, ATCC 11303 strain, 14380, Affymetrix) DNA was fragmented by a limited SauIIIa or AluI digest. Fragmented DNA was ligated into pJET1.2 vector (ThermoFisher Scientific) and

transformed into electrocompetent DH5α cells. Cells were plated on LB plates containing 100 µg/mL ampicillin, grown for 16 - 20 hours, combined in LB medium containing 100 µg/mL ampicillin and grown for another 4 hours. Plasmids was extracted with Plasmid Mega Preparation Kit (PC 2000 Kit, Macherey&Nagel)

Salt gradient dialysis (SGD). For low, medium and high assembly degrees, 10 µg of plasmid library DNA (*S. cerevisiae*, *S. pombe* or *E. coli*) was mixed with ~2, 4 or 8 µg of *Drosophila* embryo histone octamers, respectively, in 100 µl assembly buffer (10 mM Tris-HCl, pH 7.6, 2 M NaCl, 1 mM EDTA, 0.05 % IGEPAL CA630, 0.2 µg BSA). Samples were transferred to Slide-A-lyzer mini dialysis devices, which were placed in a 3 L beaker containing 300 mL of high salt buffer (10 mM Tris-HCl pH 7.6, 2 M NaCl, 1 mM EDTA, 0.05 % IGEPAL CA630, 14.3 mM β-mercaptoethanol), and dialyzed against a total of 3 L low salt buffer (10 mM Tris-HCl pH 7.6, 50 mM NaCl, 1 mM EDTA, 0.05 % IGEPAL CA630, 1.4 mM β-mercaptoethanol) added continuously via a peristaltic pump over a time course of 16 h while stirring. β-mercaptoethanol was added freshly to all buffers. After complete transfer of low salt buffer, samples were dialyzed against 1 L low salt buffer for 1 h at room temperature. DNA concentration of the SGD chromatin preparations was estimated with a DS-11+ spektrophotometer (Denovix) and could be stored at 4 °C for several weeks. To estimate the extent of the assembly degree, an aliquot of the sample was subjected to MNase digestion (as described below) for MNase-ladder read out.

Purifications of chromatin remodeling enzymes

Expression and purification of INO80 complex and respective mutants. Exact strategy for recombinant expression of *S. cerevisiae* INO80 complex in insect cells and complex purification is described in the accompanying paper Krietenstein et al. Briefly, MultiBac technology (Trowitzsch et al., 2010) was applied to generate two baculoviruses carrying coding sequences for *S. cerevisiae* Ino80 (2xFlag), Rvb1, Rvb2, Arp4, Arp5-His, Arp8, Actin, Taf14, Ies1, Ies2, Ies3, Ies4, Ies5, Ies6 and Nhp10 which were subcloned into pFBDM vectors and sequence verified by Sanger Sequencing (GATC Services at Eurofins Genomics). High Five (Hi5) insect cells (BTI-TN-5B1-4 Invitrogen) were co-infected with two or three baculoviruses 1/100 (v/v) each for expression purposes. The recombinantly expressed INO80 complex and respective INO80 mutant complexes were purified from insect cells according to (Tosi, Haas et al. 2013), which resulted in a pure and monodisperse sample. Shortly, cells were resuspended in lysis buffer (50 mM Tris-HCl pH 7.9, 500 mM NaCl, 10 % glycerol, 1 mM DTT), sonified (Branson Sonifier, 3x 20 s with 40 % duty cycle and output control 3-4) and cleared by centrifugation (Sorvall Evolution RC, SS34 rotor, 15,000 g). The supernatant was incubated with anti-Flag M2 Affinity Gel (Sigma-Aldrich) and centrifuged for 15 min at 1,000 g and 4 °C. The anti-Flag resin was washed with buffer A (25 mM Na-HEPES pH 8.0, 500 mM KCl, 10 % glycerol, 0.025 mM IGEPAL CA630, 4 mM MgCl₂, 1 mM DTT) and buffer B (25 mM Na-HEPES pH 8.0, 200 mM KCl, 10 % glycerol, 0.02 mM IGEPAL CA630, 4 mM MgCl₂, 1 mM DTT). Recombinant INO80 complex was eluted with buffer B containing 1.6 mg Flag Peptide. Anion exchange chromatography (MonoQ 5/50 GL, GE Healthcare) was used for further purification which resulted in a monodisperse and clear INO80 complex. Using standard cloning techniques,

three INO80(2xFlag) HSA domain mutants (HQ1, HQ2, HQ1/2, Figure 4D), one N-terminal deletion mutant (Ino80^{ΔN}, deletion of the first 461 amino acids of the N terminus of Ino80) and two INO80 (2xFlag) Nhp10 module mutants (ΔNhp10 (INO80 complex without Ies1, Ies3, Ies5 and Nhp10 but with Ino80 N-terminus) and HMGII (Figure 4G) were generated and integrated into baculoviruses using MultiBac Technology. Expression and purification of mutant INO80 complexes was carried out as described above. The INO80 core complex from *Chaetomium thermophilum* (equivalent to the *S. cerevisiae* N-terminal deletion mutant) was essentially purified as described in Eustermann et al., 2018.

Expression and purification of full-length Chd1 and FACT. Hi5 cells (600 mL) were grown in ESF-921 media (Expression Systems) and infected with V1 virus for full-length Chd1 (tagged with a N-terminal 6×His tag, followed by a MBP tag, and a tobacco etch virus protease cleavage site) or FACT (Spt16 carries an N-terminal 6×His tag, followed by an MBP tag, and a tobacco etch virus protease cleavage site) for protein expression. Cells were grown for 72 hours at 37 °C and subsequently harvested by centrifugation (238 g, 4 °C, 30 min). Supernatant was discarded and cell pellets resuspended in lysis buffer (300 mM NaCl, 20 mM Na-HEPES pH 7.4, 10 % (v/v) glycerol, 1 mM DTT, 30 mM imidazole pH 8.0, 0.284 μg/mL leupeptin, 1.37 μg/mL pepstatin A, 0.17 mg/mL PMSF, 0.33 mg/mL benzamidine). Resuspended cells were snap frozen and stored at -80 °C.

All protein purifications were performed at 4 °C. Frozen cell pellets were thawed and lysed by sonication. Lysates were cleared using centrifugation (18,000 g, 4 °C, 30 min and 235,000 g, 4 °C, 60 min). The supernatant containing Chd1 was filtered with 0.8-μm syringe filters (Millipore) and applied onto a GE HisTrap HP 5 mL (GE Healthcare). The column was washed with 10 column volumes (CV) lysis buffer, 5 CV high salt buffer (1 M NaCl, 20 mM Na-HEPES pH 7.4, 10 % (v/v) glycerol, 1 mM DTT, 30 mM imidazole pH 8.0, 0.284 μg/mL leupeptin, 1.37 μg/mL pepstatin A, 0.17 mg/mL PMSF, 0.33 mg/mL benzamidine), and 5 CV lysis buffer. Chd1 was eluted using a 40-minute gradient of 0-100 % elution buffer (300 mM NaCl, 20 mM Na-HEPES pH 7.4, 10 % (v/v) glycerol, 1 mM DTT, 500 mM imidazole pH 8.0, 0.284 μg/mL leupeptin, 1.37 μg/mL pepstatin A, 0.17 mg/mL PMSF, 0.33 mg/mL benzamidine). Fractions containing Chd1 were pooled and subjected to dialysis/TEV protease digestion for 16 hours (300 mM NaCl, 20 mM Na-HEPES pH 7.4, 10 % (v/v) glycerol, 1 mM DTT, 30 mM imidazole with 2 mg His6-TEV protease).

The dialyzed sample was again applied to a GE HisTrap HP 5 mL. The flow-through, which contained cleaved tag-less Chd1, was concentrated using an Amicon Millipore 15 mL 50,000 MWCO centrifugal concentrator. The concentrate was applied to a GE S200 16/600 pg size exclusion column in 300 mM NaCl, 20 mM Na-HEPES pH 7.4, 10 % (v/v) glycerol, 1 mM DTT. Fractions containing Chd1 were concentrated to ~100 μM. The sample was aliquoted, snap frozen and stored at -80 °C.

FACT was purified as above with minor modifications. After dialysis, the sample was subjected to a tandem GE HisTrap HP 5 mL and GE HiTrap Q 5 mL columns combination. After sample application, the columns were washed with lysis buffer and the HisTrap removed. FACT was eluted by applying a high salt buffer gradient from 0-100 % high salt buffer (1 M NaCl, 20 mM Na-HEPES pH 7.4, 10 % (v/v) glycerol, 1 mM DTT, 30 mM imidazole pH

8.0). Fractions with FACT were applied to a GE S200 16/600 pg size exclusion column. Peak fractions with FACT were concentrated to a concentration of ~60 μM, aliquoted, snap frozen, and stored at -80 °C.

Expression and purifications of ISW1a, ISW2 and Fun30.

Tandem affinity purification of ISW1a (TAP-Ioc3) and Fun30 (TAP-Fun30) was performed as follows: Cultures were grown in YPD media, harvested cells were washed once with water. The cells were lysed in buffer E (20 mM Na-HEPES pH 7.5, 350 mM NaCl, 10 % glycerol, 0.1 % Tween, and 0.5 mM DTT) and protease inhibitors by grinding in the presence of liquid nitrogen. Lysates were clarified at 40,000 g at 4 °C for 1 h. Cleared lysates were incubated with IgG-Sepharose (GE Healthcare) at 4 °C for 2 h and eluted by TEV protease (Invitrogen) cleavage at 4 °C overnight. The elutions were incubated with calmodulin affinity resin (Agilent Technology) in buffer E plus 2 mM CaCl₂ at 4 °C for 2 h and eluted in buffer E plus 10 mM EGTA.

ISW2 (FLAG-Isw2) was purified as follows: Cleared lysate was incubated with Anti-FLAG M2 affinity gel (Sigma-Aldrich) at 4 °C for 1 h and eluted with 0.1 mg/mL 3X FLAG peptide (Sigma-Aldrich). E-buffer (20 mM Na-HEPES pH 7.5, 350 mM NaCl, 10 % glycerol, 0.1 % Tween, and 0.5 mM DTT) was used during the entire purification.

Purified proteins were concentrated with VIVASPIN concentrators (Sartorius) and dialyzed against E-Buffer with 1 mM DTT. Subunit compositions were confirmed by SDS-PAGE (Figure S1A) and mass spectrometry.

Expression and purification of *S. cerevisiae* Reb1.

Purification of *S. cerevisiae* Reb1 was essentially carried out as described in (Krietenstein et al., 2016). Briefly, using BY4741 genomic *S. cerevisiae* DNA the coding sequence for Reb1 was amplified by PCR and cloned into pET21b (Novagen) via InFusion cloning (Clontech) with a Streptavidin tag at the C terminus. Correct sequences were verified via Sanger sequencing (GATC Services at Eurofins Genomics). Expression plasmids were transformed into BL21 (DE3) cd⁺ cells. Three liters of LB medium supplemented with 600 mg/l ampicillin were inoculated with 200 mL pre-culture. Cells were grown at 37 °C to an OD₆₀₀ of 0.6 (WPA CO8000 cell density meter). Induction was carried out by addition of IPTG to a final concentration of 1 mM. Cells were grown overnight at 18 °C, harvested by centrifugation (3,500 rpm, Sorvall Evolution RC) and stored at -80 °C. Cells were resuspended in lysis buffer (50 mM Tris-HCl pH 7.9, 500 mM NaCl, 7 % glycerol, 1 mM DTT, 7 % sucrose and protease inhibitor 1:100), sonicated (Branson Sonifier 250, 5 min at 40-50 % duty cycle and output control 4) and cleared by centrifugation (Sorvall Evolution RC, SS34 rotor, 15,000 g). The supernatant was dialyzed over night against 2 L low salt buffer (25 mM K-HEPES pH 8.0, 150 mM KCl, 7 % glycerol, 4 mM MgCl₂, 1 mM DTT). Cation ion exchange chromatography (HiTrap SP HP 5 mL, elution buffer: 25 mM K-HEPES pH 8.0, 1 M KCl, 7 % glycerol, 4 mM MgCl₂, 1 mM DTT) followed by size exclusion chromatography (Superdex 200 10/300, buffer: 25 mM K-HEPES pH 8.0, 200 mM KCl, 7 % glycerol, 4 mM MgCl₂, 1 mM DTT) were used for purification. Peak fractions were analyzed by Coomassie SDS-PAGE. Fractions containing Reb1 were pooled, concentrated and stored at -80 °C.

Preparation of mononucleosomes with recombinant human octamers. Canonical human histones were provided by The Histone Source – Protein Expression and Purification

(PEP) Facility at Colorado State University. Lyophilized individual human histones were resuspended in 7 M guanidinium chloride, mixed at a 1.2-fold molar excess of H2A/H2B and dialyzed against 2 M NaCl for 16 h. Histone octamers were purified by size exclusion chromatography (HILoad 16/600 Superdex 200 column, GE Healthcare) and stored at -20 °C in 50 % glycerol.

We used fluorescein-labeled Widom 601 DNA (Lowary and Widom 1998) with 80 bp extranucleosomal DNA (ON80 orientation) harboring an *in vivo* ChIP-Exo verified Reb1 binding site (Rhee and Pugh 2012) of *S. cerevisiae* gene *yGL167c* (Reb1 binding motif: TTACCC) 64 or 84 bp distant to the 601 sequence. The DNA template (*yGL267c_601*) was amplified via PCR, purified by anion exchange chromatography (HiTrap DEAE FF, GE Healthcare) and vacuum concentrated. DNA and assembled histone octamer were mixed in 1.1-fold molar excess of DNA at 2 M NaCl. Over a time-period of 17 h at 4 °C the NaCl concentration was reduced to a final concentration of 50 mM NaCl. Again, anion exchange chromatography was used to purify reconstituted nucleosome core particle (NCP) which were then dialyzed to 50 mM NaCl. NCPs were concentrated to 1 mg/mL and stored at 4 °C.

ATPase Assay. As described previously (Eustermann et al., 2018; Knoll et al., 2018), we applied an NADH-based ATPase assay (Kiianitsa et al., 2003) to determine INO80's ATPase rate. 15 nM INO80 were incubated at 30 °C in a final volume of 50 μ l assay buffer (25 mM K-HEPES pH 8.0, 50 mM KCl, 5 mM MgCl₂, 0.1 mg/mL BSA) with 0.5 mM phosphoenolpyruvate, 2 mM ATP, 0.2 mM NADH and 25 units/mL lactate dehydrogenase/pyruvate kinase (Sigma-Aldrich) to monitor the NADH dependent fluorescence signal in non-binding, black, 384-well plates (Greiner) at an excitation wavelength of 340 nm and an emission wavelength of 460 nm over a 40-min period. We used the Tecan Infinite M1000 (Tecan) plate reader for read out. For all samples, ATPase activity was determined at maximum INO80 WT ATPase activity. ATPase activity was stimulated with 50 nM, 25 nM and 12.5 nM Reb1 site-ON80 mononucleosomes with or without WT Reb1 at indicated concentrations. Using maximal initial linear rates corrected for the buffer blank, we calculated final ATP turnover rates.

Genome-wide remodeling reaction. All remodeling reactions, except Chd1-containing reactions, were performed at 30 °C in 100 μ l with final buffer conditions of 26.6 mM Na-HEPES pH 7.5, 1 mM Tris-HCl pH 7.6, 85.5 mM NaCl, 8 mM KCl, 10 mM ammonium sulfate, 10 mM creatine phosphate (Sigma-Aldrich), 3 mM MgCl₂, 2.5 mM ATP, 0.1 mM EDTA, 0.6 mM EGTA, 1 mM DTT, 14 % glycerol, 20 ng/ μ l creatine kinase (Roche Applied Science).

Chd1-containing reactions were performed in 26.6 mM Na-HEPES pH 7.5, 1 mM Tris-HCl pH 7.6, 50 mM NaCl, 10 mM creatine phosphate (Sigma-Aldrich), 3 mM MgCl₂, 2.5 mM ATP, 0.1 mM EDTA, 0.6 mM EGTA, 1 mM DTT, 14 % glycerol, 20 ng/ μ l creatine kinase. If called for, 10 nM of remodeling enzyme (but 50 nM Chd1/FACT), 40 nM Reb1 and 20 Units of BamHI (NEB) was added. Before full-length Chd1 (in high-salt buffer) was added to the reaction, it was diluted together with FACT into low salt buffer. For that, full-length Chd1 and purified FACT was mixed in a 1.2:1 molar ratio in high salt buffer (300 mM NaCl, 20 mM Na-HEPES pH 7.4, 10 % (v/v) glycerol, 1 mM DTT),

incubated on ice for 5 min and then diluted to 30 mM NaCl final concentration.

Remodeling reactions were started by adding 10 μ l SGD chromatin corresponding to about 1 μ g DNA assembled into nucleosomes and terminated by adding 0.8 Units apyrase (NEB) followed by incubation at 30 °C for 30 min.

MNase-seq. After apyrase addition, remodeling reactions were supplemented with CaCl₂ to a final concentration of 1.5 mM and digested with 100 Units MNase to generate mostly mononucleosomal DNA. Chd1-reaction were incubated with 20 Units MNase to get the same extent of mononucleosomal DNA. 10 mM EDTA and 0.5 % SDS (final concentrations) were added to stop the MNase digest. After proteinase K treatment for 30 min at 37 °C, samples were ethanol precipitated and electrophoresed for 1.5 - 2 h at 100 V using a 1.5 % agarose gel in 1x Tris-acetate-EDTA (TAE) buffer. Mononucleosome bands were excised and purified with PureLink Quick Gel Extraction Kit (ThermoFisher Scientific).

For library preparation, 10-50 ng of mononucleosomal DNA was incubated with 1.25 Units Taq polymerase (NEB), 3.75 Units T4 DNA polymerase (NEB) and 12.5 Units T4-PNK (NEB) in 1x ligation buffer (B0202S, NEB) for 15 min at 12 °C, 15 min at 37 °C and 20 min at 72 °C. To ligate NEBNext Adaptors (0.75 μ M final concentration, NEBNext Multiplex Oligos Kit) to the DNA, samples were incubated with T4 DNA ligase (NEB) at 25 °C for 15 min, followed by incubation with 2 Units USER enzyme (NEB) for 10 min at 37 °C. Fragments were purified using 2 volumes AMPure XP beads (Beckman Coulter) and amplified for 8-10 cycles using NEBNext Multiplex Oligos, Phusion High-Fidelity DNA Polymerase (1 U, NEB), deoxynucleotide solution mix (dNTP, 2.5 mM, NEB) and Phusion HF Buffer (1x, NEB). The following protocol was applied for amplification: 98 °C for 30 s, 98 °C for 10 s, 65 °C for 30 s, 72 °C for 30 s with a final amplification step at 72 °C for 5 min. DNA content was assessed by using Qubit dsDNA HS Assay Kit (Invitrogen). PCR reactions were applied to a 1.5 % agarose gel, needed fragment length (~270 bp) was excised and purified via PureLink Quick Gel Extraction Kit (ThermoFisher Scientific). DNA was measured again with Qubit dsDNA HS Assay Kit and diluted to a final concentration of 10 nM (calculation based on the assumption that the DNA fragment length is 272 bp, i. e., 147 bp nucleosomal DNA and 122 bp sequencing adaptor). Diluted samples were pooled according to sequencing reads (~6 Mio reads/ sample). The final pool was quantified with BioAnalyzer (Agilent) and analyzed on an Illumina HiSeq 1500 in 50 bp single-end mode (Laboratory for Functional Genome Analysis, LAFUGA, LMU Munich).

Data Processing. Sequencing data was mapped to the SacCer3 (R64), EF2 or *E. coli* strain B (REL606) genome using Bowtie (Langmead et al., 2009). Multiple matches were omitted. After mapping, data was imported into R Studio using GenomicAlignments (Lawrence et al., 2013). Every read was shifted by 73 bp to cover the nucleosome dyad and extended to 50 bp. Genome coverage was calculated and either aligned to *in vivo* +1 nucleosome positions (Xu et al., 2009), BamHI cut sites, Reb1 SLIM-ChIP hits (Gutin et al., 2018) or Reb1 PWM hits (Badis et al., 2008). Signal was normalized per gene in a 2001 bp window centered on the alignment point.

Heatmaps were sorted either by NFR length (distance between *in vivo* +1 and -1 nucleosome annotated by calling nucleosomes of *in vivo* MNase-seq by Tirosh) or by Reb1 binding score. For the latter, Reb1 SLIM-ChIP data

(GSM2916407) was aligned to in vivo +1 nucleosome positions and sorted by signal strength in a 120 bp-window 160 bp upstream of every +1 nucleosome.

For promotor grouping according to Reb1 site orientation, Reb1 SLIM-ChIP hits which contain a PWM site (± 50 bp) and which are located within 400 bp upstream of in vivo +1 nucleosomes were used. Cluster 1 contains promoters where the Reb1 PWM motif is located on the sense strand and cluster 2, where the Reb1 PWM motif is located on the antisense strand. Cluster 3 contains Reb1 sites at bidirectional promoters.

Data Resources

All raw and processed sequencing data generated in this study have been submitted to the NCBI Gene Expression Omnibus (GEO; <https://www.ncbi.nlm.nih.gov/geo/>) under accession number GSE140614. Source codes are deposited at <https://github.com/eoberbeckmann/ruler-paper/>.

References

- Badis, G., Chan, E.T., van Bakel, H., Pena-Castillo, L., Tillo, D., Tsui, K., Carlson, C.D., Gossett, A.J., Hasinoff, M.J., Warren, C.L., et al. (2008). A Library of Yeast Transcription Factor Motifs Reveals a Widespread Function for Rsc3 in Targeting Nucleosome Exclusion at Promoters. *Molecular Cell* 32, 878–887.
- Eustermann, S., Schall, K., Kostrewa, D., Lakomek, K., Strauss, M., Moldt, M., and Hopfner, K.-P. (2018). Structural basis for ATP-dependent chromatin remodelling by the INO80 complex. *Nature* 556, 386–390.
- Gutin, J., Sadeh, R., Bodenheimer, N., Joseph-Strauss, D., Klein-Brill, A., Alajem, A., Ram, O., and Friedman, N. (2018). Fine-Resolution Mapping of TF Binding and Chromatin Interactions. *Cell Reports* 22, 2797–2807.
- Jones, G.M., Stalker, J., Humphray, S., West, A., Cox, T., Rogers, J., Dunham, I., and Prelich, G. (2008). A systematic library for comprehensive overexpression screens in *Saccharomyces cerevisiae*. *Nat Meth* 5, 239–241.
- Kiiianitsa, K., Solinger, J.A., and Heyer, W.-D. (2003). NADH-coupled microplate photometric assay for kinetic studies of ATP-hydrolyzing enzymes with low and high specific activities. *Anal. Biochem.* 321, 266–271.
- Knoll, K.R., Eustermann, S., Niebauer, V., Oberbeckmann, E., Stoehr, G., Schall, K., Tosi, A., Schwarz, M., Buchfellner, A., Korber, P., et al. (2018). The nuclear actin-containing Arp8 module is a linker DNA sensor driving INO80 chromatin remodeling. *Nat Struct Mol Biol* 25, 823–832.
- Krietenstein, N., Wippo, C.J., Lileg, C., and Korber, P. (2012). Genome-Wide In Vitro Reconstitution of Yeast Chromatin with In Vivo-Like Nucleosome Positioning. In *Methods in Enzymology*, (Elsevier), pp. 205–232.
- Krietenstein, N., Wal, M., Watanabe, S., Park, B., Peterson, C.L., Pugh, B.F., and Korber, P. (2016). Genomic Nucleosome Organization Reconstituted with Pure Proteins. *Cell* 167, 709–721.e12.
- Langmead, B., Trapnell, C., Pop, M., and Salzberg, S.L. (2009). Ultrafast and memory-efficient alignment of short DNA sequences to the human genome. *Genome Biology* 10, R25.
- Lawrence, M., Huber, W., Pagès, H., Aboyoun, P., Carlson, M., Gentleman, R., Morgan, M.T., and Carey, V.J. (2013). Software for Computing and Annotating Genomic Ranges. *PLOS Computational Biology* 9, e1003118.
- Simon, R.H., and Felsenfeld, G. (1979). A new procedure for purifying histone pairs H2A + H2B and H3 + H4 from chromatin using hydroxylapatite. *Nucleic Acids Res* 6, 689–696.
- Xu, Z., Wei, W., Gagneur, J., Perocchi, F., Clauder-Münster, S., Camblong, J., Guffanti, E., Stutz, F., Huber, W., and Steinmetz, L.M. (2009). Bidirectional promoters generate pervasive transcription in yeast. *Nature* 457, 1033–1037.

3. Discussion

3.1 The sequence-specific general regulatory factor Reb1 as well as double strand DNA ends are potent barriers to set nucleosome phasing distances independent of spacing distances

3.1.1 Density-independent setting of spacing and phasing distances by ISW1a and Chd1

The setting of DNA linker length (spacing) generated by ISW1a as well as Chd1 was constant and independent of nucleosome density. The spacing distance between adjacent nucleosomes was independent of both Reb1 and dsDNA break alignment points. Spacing measured in absolute terms was 12-13bp for Chd1 and 21-26bp for ISW1a. Our findings using a more minimalistic *in vitro* approach are in line with previous *in vivo* linker length assessments for ISW1a (20bp) and Chd1(12bp) (Ocampo *et al.*, 2016). This suggested that both ISWI and CHD chromatin remodelers may have a distinct role in setting the average DNA linker length of 18bp in living yeast cells (Thomas and Furber, 1976) maybe depending on cell cycle state and nucleosome environment including epigenetic mechanisms or DNA binding factor levels. Indeed, actively transcribed genes are characterized by shorter linker lengths, which correlates with the proposed Chd1 recruitment by RNA polymerase II *in vivo* (Simic *et al.*, 2003). Additionally, Chd1 formed a stable complex with the Polymerase II-associated histone chaperone FACT, recently visualized by cryo-EM, suggesting a predominant function of Chd1 at actively transcribed genes (Farnung *et al.*, 2017).

Double strand DNA (dsDNA) breaks with a blunt-end, a 3'- or a 5'-overhang provided sufficient barrier information for ISW1a and Chd1 to align nucleosomes, both generating nucleosomal arrays radiating from the dsDNA break site. The dsDNA break-induced phasing distance measured in this study was density-independent and closely resembled spacing distances for ISW1a but not for Chd1. When determining the phasing distance to the Reb1 barrier, it became apparent that phasing at Reb1 sites is density-independent for both remodelers, but clearly more extended than dsDNA break phasing as well as spacing distances (Chd1: 46bp and ISW1a: 53bp). Based on the (*S.p.*) crystal structure of the Reb1 DNA binding domain, we estimated a Reb1 footprint size of approximately 20bp, which might be sufficient to explain discrepancies between phasing and spacing distances for Chd1 but not for ISW1a. Our study showed that the orientation of the Reb1 binding site does not direct nucleosome array phasing, whereas the respective direction of transcription directs nucleosome array phasing, predominantly for INO80. We concluded that a direct interaction between Reb1 and ISW1a generated a discrete and

Discussion

remodeler-specific phasing distance, which differs from dsDNA break phasing and spacing distances suggesting a separate read-out mechanism. Density-independence of spacing and phasing as well as short spacing by ISW1a and Chd1 might be linked to their functions in generating dense nucleosomal arrays within gene bodies and in the vicinity to the transcription machinery *in vivo*. ISW1a and Chd1 are proposed to be less involved overall in +1 nucleosome positioning *in vivo* as well as *in vitro* (Krietenstein *et al.*, 2016, Challal *et al.*, 2018, Kubik *et al.*, 2019, Kubik *et al.*, 2018). In summary, focusing on dsDNA breaks lacking a promoter context provided sufficient phasing information for ISW1a and Chd1. Phasing at dsDNA breaks is related to spacing distances for ISW1a but not Chd1 and both are nucleosome density-independent. Phasing at Reb1 sites is enlarged and is independent of the density as well as binding site orientation for ISW1a and Chd1. These findings suggest either that spacing and phasing of nucleosomes by chromatin remodelers are likely to be two independent events based on distinct mechanisms or, that spacing and phasing of nucleosomes are directed by a remodeler-intrinsic ruler functionality that processes Reb1 or dsDNA break reference points and adjacent nucleosome information differently. The minimalistic *in vitro* setting provides a launching point for the dissection of the molecular mechanism that function in the background of remodelers attributed *in vivo* functions.

3.1.2 Density-dependent setting of spacing and phasing distances by ISW2 and INO80

The positioning of the +1 nucleosome *in vivo* is the consequence of the combinatorial actions of two antagonistic remodeler families. RSC binds to the majority of gene promoters where it expands the NDR by “pushing out” nucleosomes. This action is antagonized by INO80 as well as partly ISW2 which contract the NDR by “pulling in” the -/+1 nucleosome (Kubik *et al.*, 2019). Based on our findings regarding ISW1a and Chd1, we asked the following questions. Are the pivotal roles of ISW2 and INO80 in shaping the archetypical promoter pattern a direct consequence of density-dependent spacing and phasing? Do absolute spacing and phasing values reflect the remodeler actions at promoter sites? Do both remodelers recognize dsDNA breaks as alignment points for phasing? Indeed, spacing and phasing at Reb1 and dsDNA break sites were partly density-dependent for ISW2. Looking at low and medium densities that might be best suited to resemble *in vivo* promoter densities, absolute linker lengths for ISW2 (54-58bp) clearly extended spacing values measured for ISW1a and Chd1. As suggested previously and measured in this study, ISW2 generated extended spacing that may disfavor acting on densely packed nucleosomal arrays and may favor interaction with the -/+1 nucleosomes flanking the NDR (Kubik

et al., 2019). Earlier studies suggested a critical extranucleosomal DNA length of 26-30 bp for ISW2 remodeling (Zofall *et al.*, 2004) which coincides with values measured for ISW2 spacing at high density in this study.

INO80-driven spacing and phasing at the Reb1 and dsDNA break reference points were highly nucleosome density dependent. Absolute linker length measured in this study for INO80 was 82 bp and could, similar to ISW2, hint towards a preferred action on the +/- 1 nucleosomes flanking NDRs. In parallel, spacing measured for INO80 at high nucleosome density (30bp) is consistent with spacing of tri-nucleosomal arrays *in vitro* (Udugama *et al.*, 2011) as well as ensemble and single molecule enzymology assays that suggest a critical extranucleosomal DNA length of 40 bp for effective INO80 remodeling (Zhou *et al.*, 2018).

The INO80 chromatin remodeler is known to function in DNA repair and checkpoint regulation and is recruited to dsDNA breaks by the Arp4, Ies3 and Nhp10 subunits recognizing γ -H2A.X (Conaway and Conaway, 2009, van Attikum *et al.*, 2004). Both INO80 and ISW2 generated aligned nucleosomal arrays radiating from dsDNA break sites in a density-dependent fashion. Phasing distances at dsDNA breaks were akin to nucleosome spacing distances for both ISW2 and INO80, similar to ISW1a. ChIP-exo *in vivo* mapping measured a distance between the Reb1 binding site located in the NDR of Reb1 bound promoter sites and the +1 nucleosome of 60-80bp (Rhee and Pugh, 2011), which coincided with absolute values for ISW2 (70bp) and INO80 (80-86bp) phasing measured in this study. Orientation of the Reb1 binding site had no effect on array phasing of both ISW2 as well as INO80. Density dependency of spacing and phasing as well as the setting of *in vivo* Reb1 distances implies a causal link between *in vivo* functions of ISW2 and INO80 and their respective mechanistic background dissected *in vitro*.

3.2 Nucleosome positioning driven by ATP-dependent chromatin remodelers is guided by a ruler-like functionality

The question that became clear in this study was what determines spacing and phasing distances of nucleosomal arrays in absolute terms. Spacing and phasing at Reb1 or dsDNA break sites generated by ISW1a, Chd1, ISW2 and INO80 allowed us to derive two main findings. First, remodeler-specific spacing and phasing are independent activities that are driven by distinctive molecular mechanisms, or are directed by a remodeler-intrinsic ruler element generating a reference point or nucleosome-specific response. Second, spacing and phasing can (in case of ISW2 and INO80), but do not need to (in case of ISW1a and Chd1), be nucleosome density-dependent. The “protein ruler” concept was first introduced in a structural and biochemical study

of the *S.c.* chromatin remodeler ISW1a, for which it was proposed that the remodeling reaction on its nucleosomal substrate is influenced by neighboring nucleosomes (Yamada *et al.*, 2011). The term “spacing” as stated in 1.3.2 refers to the equalization of DNA linker length (Ito *et al.*, 1997, Thomas and Furber, 1976). ISW1a was proposed to act as a “protein ruler” setting regular spacing distances between two adjacent nucleosomes directed by a feature intrinsic to remodelers. Earlier studies suggested that chromatin remodelers bear such intrinsic ruler features if the generation of nucleosomal arrays depends on “clamping” activity (Krietenstein *et al.*, 2016, Lieleg *et al.*, 2015a). Our minimalistic genome-wide approach enabled a detailed measurement of the remodeler-intrinsic ruler-mediated linker length and broadens the primary definition of a “protein ruler” by suggesting three pre-requisites: The ruler feature is a remodeler-intrinsic feature that generates the same distance on genomic sequences derived from different organisms. Second, the ruler feature operates independent of nucleosome density and sets constant distances. Third, different remodelers are expected to set specific distances acting on the same chromatin template, due to their intrinsic ruler feature. To answer the question if spacing and phasing is consistent on different chromatin templates we assembled chromatin on genomic sequences of *S.c.*, *S.p.* and *E. coli*. Comparison of spacing and phasing on the aforementioned chromatin templates revealed that spacing and phasing values hardly deviate between *S.c.*, *S.p.* and *E. coli* genomic sequences. Focusing on the aforementioned pre-requisites, ruler functionalities of each remodeler will be discussed in the following. We concluded that ISW1a and Chd1 bear an intrinsic ruler feature that independently reads out spacing as well as phasing parameters. The linker length setting mediated through the ISW1a and Chd1 ruler functionality provides the mechanistic basis for generating dense genic nucleosomal arrays *in vivo* (Ocampo *et al.*, 2016). The linker length setting through the ISW1a ruler feature explains its major contribution to establish compact and regular nucleosome arrays with *in vivo* linker lengths of 18bp on average, and a minor contribution in +1 nucleosome positioning *in vivo* (van Bakel *et al.*, 2013, Ocampo *et al.*, 2016, Kubik *et al.*, 2019). ISWI as well as CHD family remodelers harbor specific auxiliary domains at their N- and C-termini (Figure 5A and B). The proposed mechanism for nucleosome sliding by ISWI remodelers describes a complex cross-communication between the H4 histone tail of the nucleosomal substrate, the conserved AutoN and NegC domains, as well as the extranucleosomal DNA length (Clapier *et al.*, 2001, Clapier and Cairns, 2012, Dang *et al.*, 2006). Recent structural data revealed the molecular interaction of the H4 tail, AutoN, NegC and the ATPase motor domain of ISWI and how this interplay regulates the ATPase activity of ISWI remodelers (Yan *et al.*, 2016). ISWI remodelers persist in an inactive state with the AutoN domain bridging across the N- and C-lobes. Binding of the H4 tail relieves the AutoN inhibition by

competitively binding to the N-lobe of the main ATPase. The NegC domain inhibits by decoupling ATP hydrolysis from DNA translocation and is released by extranucleosomal DNA binding (Clapier *et al.*, 2001, Clapier *et al.*, 2017, Clapier and Cairns, 2012, Sundaramoorthy, 2019). Despite the clear evidence, the exact coordination of all these factors within ISWI remodelers to set absolute spacing and phasing distances is still not entirely clear. CHD remodelers harbor N-terminal chromodomains implicated in binding methylated H3 tails and predominantly involved in regulating the main ATPase lobes of CHD remodelers (Sundaramoorthy, 2019, Hauk *et al.*, 2010). The Chd1 structure showed an important role for the H4 tail interacting with the ATPase N-lobe similar to ISWI, which provides an allosteric regulator of Chd1 action (Hauk *et al.*, 2010, Farnung *et al.*, 2017). Despite only minor sequence conservation of both domains, the structure of the C-terminal CHD DNA binding domain (DBD) revealed high structural conservation with the SANT-SLIDE domain of ISWI remodeler. (Sharma *et al.*, 2011, Ryan *et al.*, 2011, Sundaramoorthy, 2019). Nonetheless, the structural models based on the 3' to 5' directionality of the ATPase motor domain are insufficient to deduce how CHD and ISWI remodelers set spacing and phasing distances in absolute terms. This work adds knowledge to the translocation mechanism of ISWI and CHD remodelers by showing that spacing and phasing information is either independently processed or directed by a remodeler-intrinsic ruler element that individually responds to the type of reference point or adjacent nucleosomes. The role of the ISWI HSS domain and the CHD DBD in building a remodeler ruler element awaits future characterization. Mutational studies within those domains and effects on spacing and phasing will provide evidence if those sub-domains are part of the ruler functionality and if the ruler functionality is tunable similar to the INO80 model system (refer to section 3.3). Replacing the canonical CHD DNA binding domain with sequence-specific engineered domains targeted Chd1 to specific nucleosomes, making the DBD a prime candidate for a ruler feature (McKnight *et al.*, 2011, Nodelman and Bowman, 2013). Our data showed that ISW2 spacing and phasing are density-independent at low and medium densities. Looking at *in vivo* +1 nucleosome positioning, ISW2 predominantly operates at low to medium densities. Its intrinsic ruler probably evolved to set longer spacing and phasing at NDR and flanking +/-1 nucleosomes, consistent with previous *in vivo* data (Kubik *et al.*, 2019).

In theory, a remodeler ruler may function in creating a nucleosome sliding direction bias towards or away from a specific interaction point, by affecting DNA translocation rates in absolute terms or by implementing a preferred binding orientation of the remodeler relative to its nucleosomal substrate. The incorporation of diverse information, such as DNA sequence features or barrier types, into a ruler-directed mechano-chemical reaction that sets spacing and phasing distances in absolute terms will be dissected in future studies.

3.3 The INO80 ruler element is multi-layered and hierarchically organized

Nucleosome density-dependency of spacing and phasing by INO80 raises two possibilities: Either INO80 does not have an intrinsic ruler feature to set spacing and phasing, or the ruler feature of INO80 includes and processes nucleosome density information putatively linked to its integral role in organizing the stereotypical promoter pattern *in vivo* and *in vitro*. The ARP module as well as the NHP10 module binding to linker DNA supposedly provide a sensor that allosterically couples linker DNA length to DNA translocation activity of the Ino80 main ATPase (Knoll *et al.*, 2018, Zhou *et al.*, 2018, Brahma *et al.*, 2018). Mapping the *in vivo* configuration of INO80 at the +1 nucleosome revealed that the ARP and NHP10 modules are located adjacent to each other at promoter regions (Figure 6B) (Yen *et al.*, 2013). Therefore, the ARP as well as the NHP10 modules are prime candidates to dissect mechanistically if INO80 bears an intrinsic ruler feature. Based on high-resolution cryo-EM and crystal structures of the INO80^{core} and ARP module as well as homology modeling of the poorly characterized Nhp10 subunit structure, we aimed for candidate INO80-DNA interactions. Intriguingly, all mutants tested except for Ino80_HSA domain mutants generated regular nucleosomal arrays, but allowed tuning of both INO80 spacing as well as phasing distances. This verifies that INO80 indeed has an intrinsic ruler functionality that is multi-layered with contributions of both the ARP and NHP10 modules. The Ino80_HSA-DNA interaction is a three-way involvement in nucleosome spacing, alignment to barriers, as well as sensing of nucleosome density. Not only Ino80_HSA α 1 but also Ino80_HSA α 2 significantly increased absolute values of spacing and phasing distances to both Reb1 and dsDNA breaks. Strikingly, mutations introduced within the Ino80_HSA α 1 allowed density-independent spacing by INO80, suggesting that the α 1 helix of the Ino80_HSA domain is particularly involved in sensing and processing nucleosome density information. Ino80_HSA α 1 as well as Ino80_HSA α 2 putatively impair ATP-dependent DNA translocation through altered DNA interaction, or by hindering interactions with other subunits required for a conformational rearrangement during remodeling. There is indeed structural evidence for conformational flexibility of the *C.t.* INO80 complex, in which the ARP module rearranges and moves closer the main ATPase (unpublished Data Schall and Kunert *et al.*). Comparing recent cryo-EM structures of ARP module-containing remodelers, such as the yeast RSC, SWI/SNF and human BRG1(BRGM)-associated factors complex (BAF) complexes with INO80 indeed reveals varying arrangements of the respective ARP modules (Knoll *et al.*, 2018, Ayala *et al.*, 2018, Han *et al.*, 2020, He *et al.*, 2020, Wagner *et al.*, 2020).

Deletion of the entire NHP10 module affected spacing as well as phasing akin to point mutations within the HMG-like domain of the Nhp10 subunit. Deletion of either the NHP10 module

Discussion

(INO80_ΔNHP10) or N-terminal residues (Ino80ΔN) mostly affected phasing at dsDNA breaks. The alignment of nucleosomes closer to dsDNA breaks may simply originate from steric reasons, which cannot be ruled out by the experimental setting. Recent smFRET studies showed that deletion of the NHP10 module (with truncated Ino80) as well as deletion of the first 200 residues of Ino80 tremendously changed the extranucleosomal DNA requirements, allowing remodeling of mononucleosomes with only 40bp linker DNA (Zhou *et al.*, 2018) which is consistent with our findings. Earlier studies proposed a direct interaction of the INO80 Nhp10 subunit with γ -H2A.X that specifically localizes to and establishes one of the first hallmarks of dsDNA breaks (Shen *et al.*, 2003a, Morrison *et al.*, 2004). The Nhp10 subunit is integral in targeting INO80 to sites of dsDNA breaks as deletion of Nhp10 led to the loss of Ies3 and significantly reduced INO80 recruitment to γ -H2A.X sites (Morrison *et al.*, 2004). Our findings show that deletion of the NHP10 module akin to point mutations in the HMG-like domain of Nhp10 mainly affects dsDNA break alignment, which might be related to Nhp10-directed recruitment of INO80 to dsDNA break sites *in vivo*. It remains to be elucidated how dsDNA break recognition and processing by the NHP10 module is mechanistically incorporated into the molecular cross-communication of INO80 modules.

3.3.1 Direct interaction between the Ino80 N-terminus and Reb1 governs nucleosome positioning

Biochemical mapping proposed an extended conformation of INO80 bound at the NDR, which is likely to traverse the +1 nucleosome and Reb1 (Yen *et al.*, 2013, Brahma *et al.*, 2017). We applied mononucleosome sliding assays to address the question of whether INO80 is capable of direct transduction of Reb1-provided information into nucleosome positioning through a so far unspecified regulatory mechanism. Based on *in vivo* data we selected the yeast YGL167c promoter sequence due to high INO80 as well as high Reb1 occupancy (Brahma *et al.*, 2017) *in vivo* and according to degree of +1 nucleosome positioning by INO80 on its own *in vitro* (Krietenstein *et al.*, 2016) and replaced the +1 nucleosome sequence with the Widom 601 sequence (Lowary and Widom, 1998). Sliding kinetics for wild type INO80 were drastically reduced in presence of Reb1. To rule out that *in vivo*-like construct design, meaning an *in vivo* distance between the Reb1 binding site and the +1 nucleosome that would mimic a stable steady-state nucleosome position relative to Reb1 mediated by the INO80 ruler functionality, caused this effect, we shifted the Reb1 binding site about 20bp further upstream of the +1 nucleosome. INO80 still showed sliding activity in presence of Reb1 with the shifted Reb1 position, but with slower sliding kinetics. We asked if Reb1 affected the ATPase activity of the wild type INO80 and also

Discussion

mutant constructs. Most mutations tested so far, such as Ino80_HSA (Knoll *et al.*, 2018) and Arp5 (Eustermann *et al.*, 2018) mutations abrogated INO80 sliding activity, but maintained a robust ATPase activity. Surprisingly, INO80 wild type ATPase activity decreased two-fold in presence of Reb1, which also holds true for NHP10 module mutants. In contrast, the Ino80 Δ N mutant showed robust ATPase activity even in the presence of Reb1. We concluded that Reb1 may allosterically regulate INO80 nucleosome positioning via direct interaction with Ino80 N-terminal residues. Further mutational studies on the Reb1 interaction partners are needed to directly show the physical interaction between Reb1 and INO80 and to decipher which residues are interacting with the Ino80 N-terminus. Reb1 harbors sequence peculiarities, such as its predicted unstructured N-terminus or extended poly-alanine stretches that may be main candidates for investigating the interactions between INO80 and Reb1 on a molecular level. If these interactions are conserved among the INO80 remodelers and can be transferred to the *Chaetomium thermophilum* or the human INO80 system remains to be elucidated in future studies.

3.3.2 The INO80 ARP module ruler element evolved to read genomic information

All mutants tested showed minor differences in +1 nucleosome positioning and indicate, in contrast to spacing that was affected in most mutants, that the INO80 driven +1 nucleosome positioning is more robust. The +1 nucleosome positioning of Ino80_HSA α 1 and Ino80 Δ N both deviated, compared with INO80 wild type and NHP10 module mutants, more from the canonical *in vivo* nucleosome position. The Ino80_HSA α 1 mutant generated +1 positions that were on average downstream-shifted by 10 bp with a broader peak, which recapitulated the findings for Ino80 deletion *in vivo* (van Bakel *et al.*, 2013, Kubik *et al.*, 2019, Yen *et al.*, 2013). An earlier study suggested a DNA shape read-out mechanism for INO80 (Krietenstein *et al.*, 2016). To directly test this hypothesis, a question was raised whether mutated INO80-DNA contacts impact the DNA shape read-out by INO80. Composite plots of MNase-sequencing data for SGD chromatin incubated with recombinant remodeler showed striking DNA propeller twist profile differences between the wild type INO80 and chromatin generated by SGD mainly located 100bp and 55bp away from the dyad. This is consistent with the high-resolution structure information and *in vivo* mapping of INO80 that proposed the functional importance for these regions. Contacts made between the Ino80_HSA helix are mapped 100bp away from the nucleosome dyad (Knoll *et al.*, 2018, Brahma *et al.*, 2018) and DNA located between the Ino80 main ATPase and the Arp5/les6 counter grip mapped 55bp away from the dyad. We propose that DNA shape signals in promoter regions exemplify a signal for INO80-mediated +1 nucleosome positioning. Unbiased principal

Discussion

component analysis (PCA) clustering showed that Ino80_HSA mutants generate different clusters of nucleosome positions, whereas NHP10 module mutants and Ino80 Δ N cluster together with the wild type INO80. This rules out a major contribution from the NHP10 module as well as the Ino80 N-terminus in DNA shape read-out, and highlights the impact of the INO80 ARP module. Comparing endogenous *Drosophila melanogaster* histones with recombinant human histones allowed us to rule out shape preferences based on the respective histone sources. DNA propeller twist values 100bp from the dyad where the Ino80_HSA helix contacts DNA shifted, closely associated with a secondary shift 55bp from the dyad. We concluded that the simultaneous shift in propeller twist values hints towards a communication between the ARP module and the main ATPase during ATP-dependent DNA translocation. A crosstalk between the ARP module and the remodeler main ATPase for regulation purpose was recently suggested for the yeast RSC complex (refer to 3.4.1 DNA shape read-out as a common mechanism for genome-wide operating machineries) (Wagner *et al.*, 2020). Mutagenic studies in the *Chaetomium thermophilum* or human INO80 targeting Ino80_HSA domain residues will provide evidence if this is a conserved task for the INO80 ARP module.

3.3.3 The INO80 ruler feature hierarchically processes information

At promoter regions, INO80 is proposed to integrate direct DNA shape information as well as indirect Reb1 phasing information to precisely position the +1 nucleosome. A question was raised whether Reb1 phasing information is processed synergistically, antagonistically, or neutral to DNA shape information read-out by the INO80. With Reb1 binding sites located in NDRs, we focused on low-density measurements, in which +1 nucleosome positions for both DNA shape as well as Reb1 were overlapping. Thus, information processing was proposed to be synergistic. INO80 was still able to position +1 nucleosomes at high densities, but Reb1 phasing distances were shorter. The DNA shape readout was not achievable at high densities. We concluded that Reb1 phasing information read-out is dominant over the DNA shape read-out to position the +1 nucleosomes at higher nucleosome densities, where the latter information input may not be implemented.

Mutations within the Ino80_HSA α 1 led to density-independent spacing, increased phasing distances to both Reb1 and dsDNA breaks and abrogated sliding on ON80 mononucleosomes. Spacing distance in absolute values for Ino80_HSA α 1 was 40bp. Nucleosomes with 80bp of extranucleosomal DNA should provide sufficiently long linker DNA for sliding by the Ino80_HSA α 1 mutant. It was not possible to detect any final sliding event in the nucleosome sliding assays, which raises the possibility that this represents evidence for hierarchical information processing by the INO80 ruler functionality. Phasing at dsDNA breaks in absolute terms for Ino80_HSA α 1

was above 100bp, providing an explanation of no net sliding event in mononucleosome assays if dsDNA break alignment information was processed. Future work will be required to further dissect the hierarchical information processing of the INO80 and the detailed mechanistic background governing this function.

The precise positioning of the +1 nucleosome influences transcription activation as well as repression, and directs transcription initiation by presenting a hallmark for downstream nucleosome array alignment to prevent ectopic transcription initiation (Challal *et al.*, 2018, Kubik *et al.*, 2019, Boeger *et al.*, 2003, Jiang and Pugh, 2009b). A central question to this thesis was to find the mechanisms that determine nucleosome phasing, spacing and positioning by chromatin remodelers. The +1 nucleosome positioning by INO80 involves an integrative, but somehow hierarchical processing of information, combining DNA shape features interpreted mainly by the ARP module and/or phasing at Reb1 sites through direct interaction of Reb1 and Ino80 N-terminal residues. The NHP10 module contributed less to +1 positioning by DNA shape read-out and / or Reb1 phasing, but was significantly involved in dsDNA break alignment. The modular architecture of INO80 is proposed to build a channeling platform to mechanistically and conformationally couple sensing and processing of a myriad of input information by specific sub-modules for precise nucleosome positioning. A division of labor is emerging in a logical way: INO80 harbors a ruler functionality comprised of its NHP10 and ARP modules, as well as the N-terminal Ino80 main ATPase residues for a multi-layered processing of indirect (Reb1 phasing and dsDNA breaks) and direct (DNA shape) information, resulting in ruler-defined spacing and phasing distances. Division of labor and ruler-directed distance setting in spacing and phasing are proposed to be features shared by all chromatin remodelers with spacing activity.

3.4 DNA shape profiles define a new type of positioning sequences

Previous data brought about the concept of ATP-dependent chromatin remodelers as key organizers of chromatin structure with their highly specific function dependent on DNA sequence (Lorch *et al.*, 2014, Krietenstein *et al.*, 2016, Winger and Bowman, 2017). The Widom 601 sequence represents a prime example of an engineered DNA sequence leading to robust nucleosome positioning in salt gradient dialysis (SGD) (Lowary and Widom, 1998). Nucleosome positioning sequences were defined here by their bendability dependent on the DNA sequence and therefore, by the underlying histone-DNA contacts. DNA sequences and their respective conformations direct nucleosome positioning not only during SGD but also by chromatin

remodelers (Rippe *et al.*, 2007). This study expands the definition of nucleosome positioning sequences for chromatin remodelers by incorporating nucleosome positions directed by DNA shape read-out. Tuning the DNA shape read-out by structure-directed mutagenesis provides a causal and mechanistic connection between the DNA shape read-out and the nucleosome positioning by INO80. Mutated DNA binding residues located in the Ino80_HSA helix that contact extranucleosomal DNA 100bp from the dyad changed nucleosome positioning, which is directly linked to altered DNA shape features in the very same region and 55bp from the dyad. A connection between linker DNA sensing by the ARP and the NHP10 module and nucleosome sliding by INO80 was proposed by recent studies (Brahma *et al.*, 2018, Zhou *et al.*, 2018, Knoll *et al.*, 2018). Effects on DNA shape features in both regions, 100 bp and 55bp from the dyad, suggest allosteric coupling of DNA shape-defined under- and overwinding of DNA in front and behind the Ino80 main ATPase to facilitate ATP-dependent DNA translocation. Not only linker DNA sensing, but also DNA shape read-out information is likely transferred to the INO80 main ATPase through the ARP module. Mutagenesis of respective Ino80_HSA domain residues in the *Chaetomium thermophilum* system and subsequent analysis of DNA shape features will elucidate the role of the ARP module in DNA shape read-out in INO80 chromatin remodeler complexes. Our findings provide a starting point for future dissection of the molecular mechanisms guiding DNA shape read-out by the ARP module and its role for other in ARP module-containing chromatin remodelers.

3.4.1 DNA shape read-out as a common mechanism for genome-wide operating machineries

So far, DNA shape has been associated mostly with non-dynamic binding of GRFs or TFs to DNA (Levo *et al.*, 2015, Zentner *et al.*, 2015). Protein-DNA interactions are linked to the recognition of the three-dimensional (3D) arrangement of the DNA structure (Rohs *et al.*, 2009). DNA 3D structure recognition is based on the conformational deviation of short DNA stretches from canonical B-DNA through changes in the minor groove width (MGW), base roll (roll), propeller twist (prT) or helical twist (HeT) (Figure 9C). Consequently, DNA shape is sequence-dependent, but a degenerative sequence-structure relationship allows very similar shapes of dissimilar sequences (Zhou *et al.*, 2013). DNA shape read-out has been proposed so far for TFs (Joshi *et al.*, 2007, Gordan *et al.*, 2013) as well as for other DNA binding proteins (Stella *et al.*, 2010, Chang *et al.*, 2013, Lazarovici *et al.*, 2013). The binding of Hox proteins to cognate DNA sequences established the first direct link between 3D DNA structure read-out and protein binding (Crocker *et al.*, 2015, Zhou *et al.*, 2013).

DNA shape read-out and interpretation by a dynamic DNA tracking machinery, such as the SF2-type Ino80 ATPase has not been reported so far. Chromatin remodelers as well as the transcription and replication machinery are characterized by genome-wide operation where they bind to various sequences *in lieu* of specific sequence motifs as bound by GRFs and TFs. A read-out of mechanical DNA properties, such as DNA shape, for genome-wide operating DNA translocating machineries is more likely than sequence motif-directed binding. Previous studies suggested that the RNA polymerase I promoter specificity is directed by DNA conformation rather than DNA sequence (Kownin *et al.*, 1987). Indeed, recent studies show that RNA polymerase I action at respective promoters is facilitated via DNA bend read-out 12-25bp upstream of the TSS and by sensing the propensity for dsDNA melting around the TSS (Engel *et al.*, 2017). *In vitro* exchange of DNA sequences located 1-30bp upstream of the TSS abolished transcription initiation by the RNA polymerase I. The RNA polymerase II processes a multivalent information input derived from DNA bending 33bp downstream the TATA box, DNA flexibility including helix axis offset and underwinding 20bp downstream of the TATA box and the propensity for dsDNA melting for promoter recognition (Dienemann *et al.*, 2019). For RNA polymerase I DNA shape read-out provided a model for promoter recognition in the absence of a conserved sequence motif, such as the TATA box for RNA polymerase II. If DNA shape read-out by the INO80 and potentially other chromatin remodelers enables genome-wide operation at promoter sites, this may become a key aspect to future studies. Modulation of DNA sequences located 100 bp and 55 bp from the dyad have the potential to dissect DNA shape read-out by the INO80 ARP module and its molecular basis. DNA shape read-out might help to explain the lack of consensus sequences for ATP-dependent chromatin remodelers similar to RNA polymerases.

3.6 Function of the ARP module in genomic information processing

Members of the SWI/SNF as well as the INO80 family of chromatin remodelers are characterized by a highly conserved domain located N-terminal to their respective catalytic ATPase motor called helicase-SANT associated (HSA) domain. The HSA domain of chromatin remodeler including yeast RSC, yeast SWI/SNF, human BAF, yeast SWR1 and INO80 is the primary assembly platform to nucleate N-actin and actin-related proteins (Arps) into respective ARP modules (refer to section 1.5.4 The INO80 ARP module(Clapier *et al.*, 2017, Szerlong *et al.*, 2008, Boyer and Peterson, 2000, Turegun *et al.*, 2018, Brahma *et al.*, 2018, Shen *et al.*, 2003a, Olave *et al.*, 2002, Knoll *et al.*, 2018, Schubert *et al.*, 2013, Peterson *et al.*, 1998)). Both SWI/SNF as well as INO80 remodelers are the essential architects of stereotypical promoter patterns *in vivo* as well as *in vitro*, sharing a preference for widespread operation on strictly nucleosome-depleted regions

Discussion

(Krietenstein *et al.*, 2016, Badis *et al.*, 2008, Yen *et al.*, 2013, Kubik *et al.*, 2019, Kubik *et al.*, 2018).

The INO80 ARP module was proposed to be an extranucleosomal DNA length sensor that directly links extranucleosomal DNA readout to the remodeling activity. This finding was supported by structural as well as biochemical data mapping the INO80 ARP module to extranucleosomal DNA 100bp from the nucleosomal dyad (Knoll *et al.*, 2018, Eustermann *et al.*, 2018, Brahma *et al.*, 2018, Brahma *et al.*, 2017) as well as mutational analysis of the Ino80 HSA domain that demonstrated a causal link between altered Ino80-HSA-DNA contacts and the INO80 ATPase and nucleosome remodeling activity (Knoll *et al.*, 2018). In addition to linker DNA sensing, the ARP module is proposed to be a molecular hub that reads and processes DNA information integrating DNA shape and GRFs as well as dsDNA break barrier recognition to facilitate spacing and phasing (Figure 7A and B).

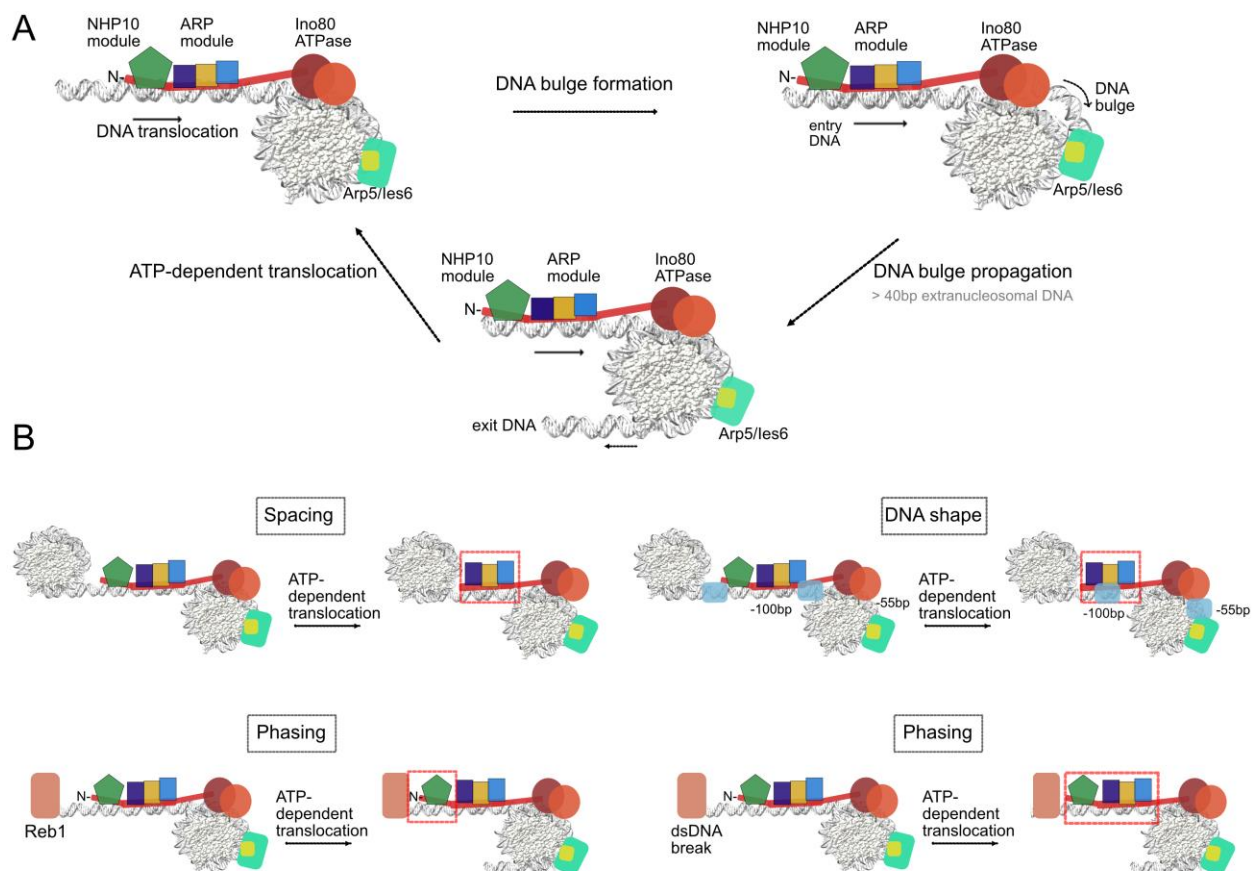


Figure 7: Ratchet-like DNA translocation model implementing spacing, phasing and DNA shape read-out. (A) The model displays the DNA translocation mechanism proposed for INO80, adapted and modified from (Knoll *et al.*, 2018, Eustermann *et al.*, 2018), including the ARP module (light blue Arp8, yellow N-actin and dark blue Arp4) and the NHP10 module bound to the N-terminal Ino80 ATPase residues (entire module depicted in green, comprised of Nhp10, les1, les3 and les5). Ino80 main ATPase lobes are depicted in dark red (N-lobe) and light red (C-lobe) and the Arp5/les6 counter-grip in light yellow and turquoise. The NHP10 and

Discussion

ARP modules bind to the entry side linker DNA adjacent to each other. In the first step, both lobes are conformationally rearranged and DNA is translocated in 1-2bp steps per ATP hydrolysis cycle by pumping in entry side DNA towards the dyad. After 10bp of translocation the resulting DNA bulge slips over the Arp5/les6 counter-grip. Effective DNA translocation requires at least 40bp extranucleosomal DNA. The color coding is the same as in Figure 6. (B) Model for the implementation of INO80 spacing, DNA shape read-out as well as phasing. INO80 sub-modules involved in the respective activity are highlighted. The color coding is the same as in (A).

In the ratchet-like DNA translocation model, the INO80 ARP module binds to linker DNA located at the entry side (Figure 7A). The ARP module is described to prevent DNA back-slippage and to sense linker DNA length at the entry side. The ratchet-like DNA translocation model implementing the NHP10 module on its location based on crosslinking data and low resolution cryoEM density maps is shown in Figure 7A (Knoll *et al.*, 2018, Eustermann *et al.*, 2018, Brahma *et al.*, 2017). Findings of this study broaden the scope of this model implementing spacing between adjacent nucleosomes carried out predominantly by the ARP module, DNA shape feature read-out by the ARP module (Figure 7B, refer to section 3.4) as well as phasing at Reb1 carried out by the Ino80 N-terminus and phasing at dsDNA breaks carried out by the ARP and NHP10 modules (Figure 7B, refer to section 3.3).

3.6.1 A general perspective on the ARP module in chromatin remodeler function based on recent structural data

Based on our findings and recent high-resolution data of ARP module-containing chromatin remodelers, a question was raised whether the decisive role of the ARP module of INO80 in linker DNA length sensing, spacing and phasing, as well as for DNA shape read-out might represent a shared task generally applicable to ARP module-containing chromatin remodelers, such as yeast RSC (HSA^{Sth1}-Arp7-Arp9-Rtt102), human BAF (HSA^{Brg1/Brm}-BAF53A/B-Actin), yeast SWI/SNF (HSA^{Snf2}-Arp7-Arp9-Rtt102) and yeast SWR1 (HSA^{Swr1}-Arp4-Actin). Recent cryo-EM structures of the yeast RSC, the yeast SWI/SNF, the human BAF, as well as the yeast SWR1 complex revealed a modular architecture shared by all remodelers. The ARP module is flexible in all structures and inherits different conformational states resulting in lower-resolution of this particular area than the more rigid core (Eustermann *et al.*, 2018, Willhoft *et al.*, 2018, Wagner *et al.*, 2020, Han *et al.*, 2020, He *et al.*, 2020). In the structure of the SWR1 complex, the ARP module is present, but is highly disordered (Willhoft *et al.*, 2018). Surprisingly, the main ATPase motor domain of RSC, SWI/SNF and BAF engages the nucleosome at SHL+/-2, similar to Chd1, ISWI and SWR1, but in contrast with the INO80 that binds at SHL+/-6 (Willhoft *et al.*, 2018, Ayala *et al.*, 2018, Eustermann *et al.*, 2018, Farnung *et al.*, 2017, Wagner *et al.*, 2020, Han *et al.*, 2020, He *et al.*, 2020, Yan *et al.*, 2016, Yan *et al.*, 2019).

Discussion

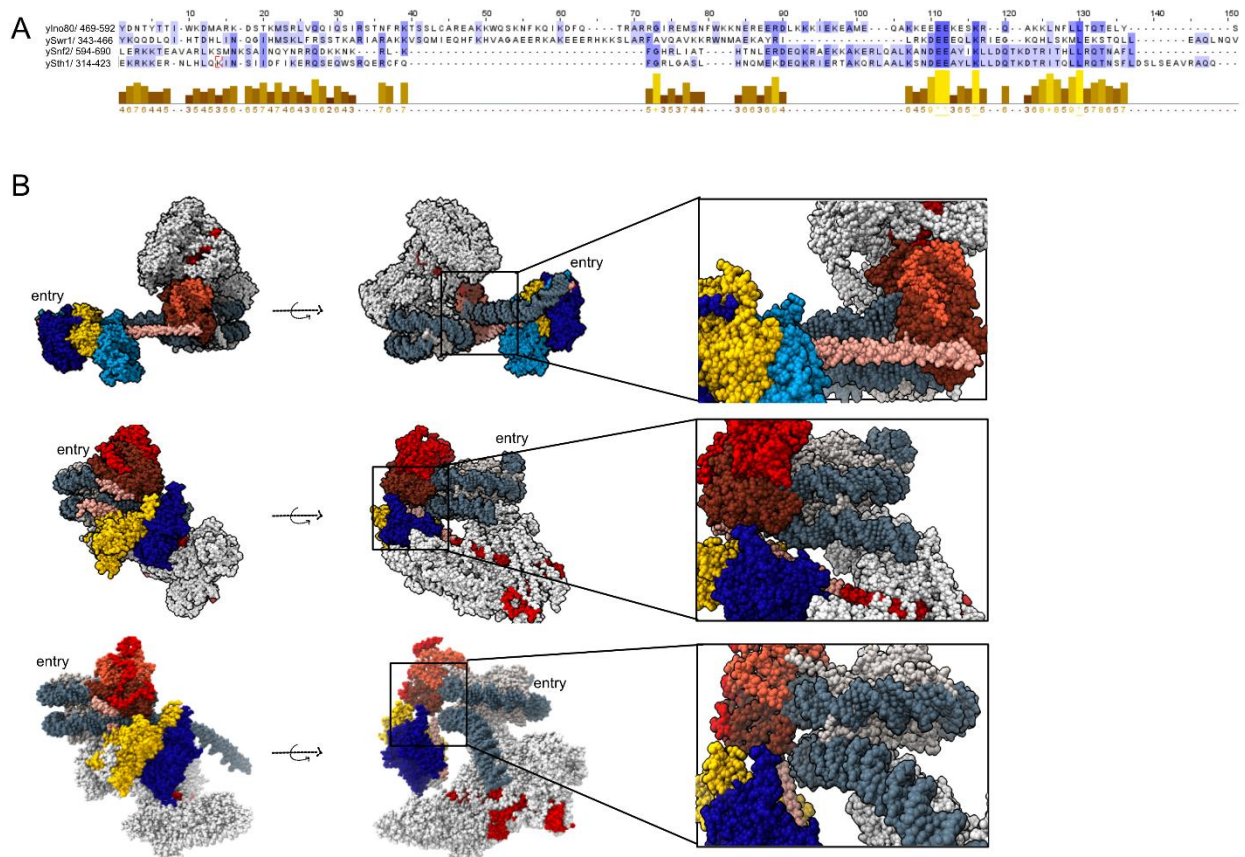


Figure 8: HSA domain organization in Arp module containing remodeler. (A) Sequence alignment of HSA and post-HSA domains of *ylno80*, *ySwr1*, *ySnf2* and *ySth1*. Conservation of residues is indicated in the lower panel with values ranging from 0 (lowest) to 10 (highest conservation) (B) Cryo-EM structures of INO80 (PDB: 6FHS and 5NBN, top), ySWI/SNF (PDB: 6UXW, middle) and yRSC (PDB: 6TDA, bottom). Panel 1 includes the side view on the respective ATPase domains bound at SHL+/-6 or SHL+/-2 with the ARP module in front of ATPase (INO80) bound to entry DNA or behind the ATPase bound to exit DNA (ySWI/SNF and yRSC). A close up into the structural arrangement of post-HSA and HSA domains. HSA and post-HSA domains are colored in light pink. Ino80 HSA and post-HSA domains show an extended helical conformation placing the ARP module distant to the N-lobe of the ATPase. The SWI/SNF and RSC HSA and post-HSA domains are helical but rearranged compared with INO80, placing the ARP modules in close proximity to the N-lobes of the main ATPases. Color code is the same as in figure 5 and the following: The main ATPase is shown in red, with the N-lobe in dark, the C-lobe in light red and the HSA domain in translucent grey. Components of the ARP module are shown in dark blue (Arp4), gold (N-Actin) and light blue (Arp8).

The yeast RSC (HSA^{Sth1}-Arp7-Arp9-Rtt102) and the yeast SWI/SNF (HSA^{Snf2}-Arp7-Arp9-Rtt102) ARP modules are located adjacent to the main ATPase motor domain contacting the nucleosome at SHL+/-6 (Figure 8B) (He *et al.*, 2020, Han *et al.*, 2020, Wagner *et al.*, 2020). The RSC main ATPase motor binds to SHL+2 with the Sth1_HSA domain nucleating Arp7 and Arp9 located adjacent to the main ATPase in close proximity to the exit DNA. The ARP module occupies a defined position in the RSC-nucleosome complex, but is highly mobile in the free RSC structure, suggesting several flexible arrangements of the module within the complex (Wagner *et al.*, 2020). Conformational rearrangements of the ARP module very likely regulate the RSC main ATPase by repositioning the Sth1 ATPase N-lobe via the post-HSA-protrusion-I axis (Wagner *et al.*, 2020).

Interestingly, the DNA interacting module (DIM) of RSC binds extranucleosomal DNA 20-40bp upstream of SHL+/-7, which is the same region that the INO80 ARP module binds to and DNA shape read-out is facilitated (Figure 8B). Binding and recognition of DNA sequences located in promoter regions via the DIM module navigates RSC function (Kubik *et al.*, 2015, Kubik *et al.*, 2018). Binding of the DIM module to DNA and the extended module arrangement suggest a minimum linker length of at least 40-50bp, compared with the average linker length in yeast of 23bp (Brogaard *et al.*, 2012) and may support activity at low density nucleosome areas, such as the NDR and may disfavor activity in densely spaced arrays, explaining impaired binding of RSC to densely packed genic arrays (Dechassa *et al.*, 2010). The DIM module might represent a ruler-related feature as proposed by this study that is guiding RSC action towards specific suited regions and advancing a preferred/certain binding orientation or sliding kinetics of the complex.

The structure of the SWI/SNF complex bound to its nucleosomal substrate displays the Snf2 ATPase bound at SHL+2 similar to SWR1, Chd1 and SNF2h, as well as the SWI/SNF "ATPase only"-nucleosome structure, but quite different to the INO80 (Figure 8B) (Han *et al.*, 2020, Farnung *et al.*, 2017, Eustermann *et al.*, 2018, Willhoft *et al.*, 2018, Armache *et al.*, 2019). The SWI/SNF ARP module is comprised of Arp7, Arp9, Rtt102 and the Snf2-HSA domain. The ARP module in SWI/SNF is sandwiched between the body and the ATPase module, similar to the human BAF complex but quite different to the INO80 (Han *et al.*, 2020, Eustermann *et al.*, 2018, Willhoft *et al.*, 2018). The Snf2_HSA domain is essential for connecting the ARP/ATPase modules to the body module. Interestingly, the arm module of the yeast SWI/SNF complex grips the nucleosome opposite from the main ATPase, such as Arp5/les6 in INO80 or Arp6/Swc6 in SWR1 (Figure 8B) (Willhoft *et al.*, 2018, Eustermann *et al.*, 2018, Han *et al.*, 2020). The SWI/SNF HSA-DNA interface is located at SHL+6 and extranucleosomal exit DNA is contacted by the body module, which contains mainly species-specific subunits (Figure 8B) (Han *et al.*, 2020).

ATP-dependent DNA translocation by INO80 was described in the macromolecular ratchet model (refer to 1.5.1 and 1.4.4) (Eustermann *et al.*, 2018). SWI/SNF and INO80 family remodelers are RecA-like DNA translocases sharing the basic mechanism of ATP-dependent DNA translocation based on C-lobe movement pumping in 1 bp DNA per step while tracking along one strand in 3' to 5' direction (Yan and Chen, 2020, Saha *et al.*, 2005, Harada *et al.*, 2016). Comparing the structural arrangements of yeast RSC, SWI/SNF, and INO80 reveals a significantly different orientation and binding mode of the main ATPase as well as the ARP module (Figure 8B). The INO80 ARP module binds to the entry side DNA possibly to provide stability and prevent back-slippage of translocated entry DNA (Knoll *et al.*, 2018, Eustermann *et al.*, 2018) and to read the

DNA environment on the entry side (Figure 7B, Figure 8B). In contrast, the main ATPase domains of SWI/SNF and RSC reside at SHL \pm 2 with the ARP module located at SHL \pm 6 on the exit side DNA (Figure 8B). As a consequence, the SWI/SNF chromatin remodeler main ATPase is in front of the ARP module, whereas the INO80 ATPase is located behind the ARP module. Sequence conservation of Arps and nuclear Actin, as well as the structural arrangements of the HSA-Arp-N-Actin modules itself suggest evolution from a common ancestor and similar cellular functions (Figure 8A) (Szerlong *et al.*, 2008, Knoll *et al.*, 2018, Schubert *et al.*, 2013, Chen *et al.*, 2011, Turegun *et al.*, 2013)). Indeed, the ARP module is a key regulator of remodeling activity *in vitro* as well as *in vivo* (Szerlong *et al.*, 2008, Szerlong *et al.*, 2003, Kapoor *et al.*, 2013, Knoll *et al.*, 2018, Brahma *et al.*, 2018, Olave *et al.*, 2002, Zhang *et al.*, 2018).

Recent structural data delineate the critical role of interactions between the conserved post-HSA domain and the ATPase N-lobe to regulate the activity of the main ATPase motor domain (Clapier *et al.*, 2016, Wagner *et al.*, 2020, He *et al.*, 2020, Li *et al.*, 2019, Turegun *et al.*, 2018). A direct interaction between the post-HSA domain residues and the protrusion-I helix, which is a conserved structural motif located in the N-lobe of Snf2-type ATPases, was proposed in biochemical and observed in structural studies (Eustermann *et al.*, 2018, Wagner *et al.*, 2020, He *et al.*, 2020, Liu *et al.*, 2017, Clapier *et al.*, 2016). Genetic studies in yeast could establish a direct link between the regulation of the ATPase motor and post-HSA–protrusion-I interaction, as well as a modulation of the post-HSA-protrusion-I interaction by the ARP module (Clapier *et al.*, 2016, Turegun *et al.*, 2018). In summary, interaction between the ARP module and DNA is allosterically linked to the main ATPase activity by the post-HSA–protrusion-I axis in SWI/SNF, and also likely in INO80 family remodelers.

3.6.2 DNA length sensing and DNA shape read-out by the ARP module

3.6.2.1 The ARP module as a linker DNA length sensor and a DNA shape reader

A conserved task for ARP modules in sensing linker DNA length, as seen for the INO80 remodeler, for SWI/SNF chromatin remodelers is due to recent structural data quite unlikely (Figure 8B) (Willhoft *et al.*, 2018, Ayala *et al.*, 2018, Han *et al.*, 2020, He *et al.*, 2020, Wagner *et al.*, 2020). INO80 carries out DNA translocation by pumping entry DNA towards the dyad with the ARP module bound to entry DNA. The conformational arrangement of the ARP module in SWI/SNF remodelers suggests a DNA translocation mechanism different to the INO80, but in line with the conserved basic 1bp DNA translocation steps carried out by the N- and C-lobe of the main

ATPases (Figure 8B). The SWI/SNF remodeler ARP module is located at SHL6/7 on exit site DNA with the main ATPase in front, suggesting a minor role of the ARP module in linker DNA length sensing. Mutagenesis of the Ino80_HSA domain residues within the *Chaetomium thermophilum* or human INO80 complex are potent for deciphering whether DNA linker length sensing is indeed a conserved task of the INO80 ARP module. Future studies based on biochemical as well as structural data are needed to elucidate whether and how the ARP modules of SWI/SNF complexes rearrange for binding of linker and/or nucleosomal DNA, and whether DNA length sensing by the ARP module can be tuned by mutagenesis that may point towards a conserved task for the ARP module in ARP-containing chromatin remodelers. Optimization of remodeler substrates for cryo-EM analysis using di-, tri- or tetra-nucleosomes with certain linker lengths will be a key factor in determining the structural arrangements of remodeler ARP modules as well as auxiliary domains.

Could DNA shape read-out as proposed for the INO80 ARP module putatively be a shared task of ARP modules in ARP-containing chromatin remodeling complexes? As stated above, the overall conformation of the ARP module in INO80 and SWI/SNF remodelers is quite different with respect to the front or back of the main ATPase motor domain arrangement. Direct interaction between the HSA domain of INO80 and entry side DNA and mutagenesis of Ino80-HSA residues established a direct link between the DNA shape read-out and the Ino80-HSA domain residues. Based on this assumption, DNA shape read-out by the SWI/SNF family remodelers through their respective HSA domains seems unlikely, due to missing structural evidence for direct HSA-DNA contact (Wagner *et al.*, 2020, Han *et al.*, 2020, He *et al.*, 2020). However, there is emerging evidence that the ARP module is highly flexible and acts as a conformational switch (Knoll *et al.*, 2018, Clapier *et al.*, 2016, Szerlong *et al.*, 2008, Zhang *et al.*, 2019). The main ATPase of yeast RSC as well as SWI/SNF in the presence of ADP-BeF_x and ATP- γ -S showed the N- and C-lobes residing in the closed conformation (Wagner *et al.*, 2020, Han *et al.*, 2020). The conformation of the ARP module with DNA bound as seen in the INO80 structure or not contacting DNA as seen in SWI/SNF family remodeler structures may be related to the nucleotide state of the main ATPase and/or the arrangement of the N-terminal modules. Conformational flexibility of the ARP module in all structures suggests a transition between the two captured conformational states. The conformational switch of the ARP module in SWI/SNF and INO80 family remodelers may be accommodated via the Ino80 post-HSA–protrusion I helix interaction as suggested for the yeast RSC complex (Wagner *et al.*, 2020). Assuming HSA-DNA contacts, DNA shape read-out would theoretically be possible. In contrast to INO80, DNA shape read-out by SWI/SNF remodeler would happen behind the main ATPase motor at SHL6/7. The conformational architecture of remodeling

complexes and the relative arrangement and conformational transitions of sub-modules within the complexes awaits further structural investigation. It remains to be analyzed whether DNA shape read-out by SWI/SNF family remodelers influences NDR formation and +/-1 nucleosome positioning and whether DNA shape read-out can be directly manipulated through HSA domain mutations similar to those of INO80 or sequence exchange in important regions, such as 100bp and 55bp from the dyad and its consequence on the +1 nucleosome positioning. It will be of great interest to see if and how mutations within the post-HSA and/or protrusion I helix affect the conformational arrangement of the ARP module and how this is cross-communicated to spacing, phasing and DNA shape read-out in these complexes.

3.6.2.2 Comparison of yeast RSC and INO80 ARP modules in a promoter-focused context

RSC as well as INO80 predominantly operate at promoter sites, shaping the stereotypical promoter pattern (Krietenstein *et al.*, 2016, Badis *et al.*, 2008, Lorch *et al.*, 2014, Brahma and Henikoff, 2019, Kubik *et al.*, 2018, Wagner *et al.*, 2020, Brahma *et al.*, 2018, van Bakel *et al.*, 2013, Yen *et al.*, 2012, Brahma *et al.*, 2017, Knoll *et al.*, 2018, Eustermann *et al.*, 2018, Yen *et al.*, 2013, Kubik *et al.*, 2019). RNA polymerases are operating at active promoter sites and there is convincing evidence that these macromolecular machines read DNA structures rather than sequences (refer to section 3.4.1) (Dienemann *et al.*, 2019, Engel *et al.*, 2017). The question arises whether DNA shape reading may be an integral part of INO80 as well as SWI/SNF remodeler-guided NDR establishment and +/-1 nucleosome positioning. Further questions arise on whether the same DNA shape features are read by both complexes or a complex-intrinsic ruler functionality is reading the 3D DNA structures.

Discussion

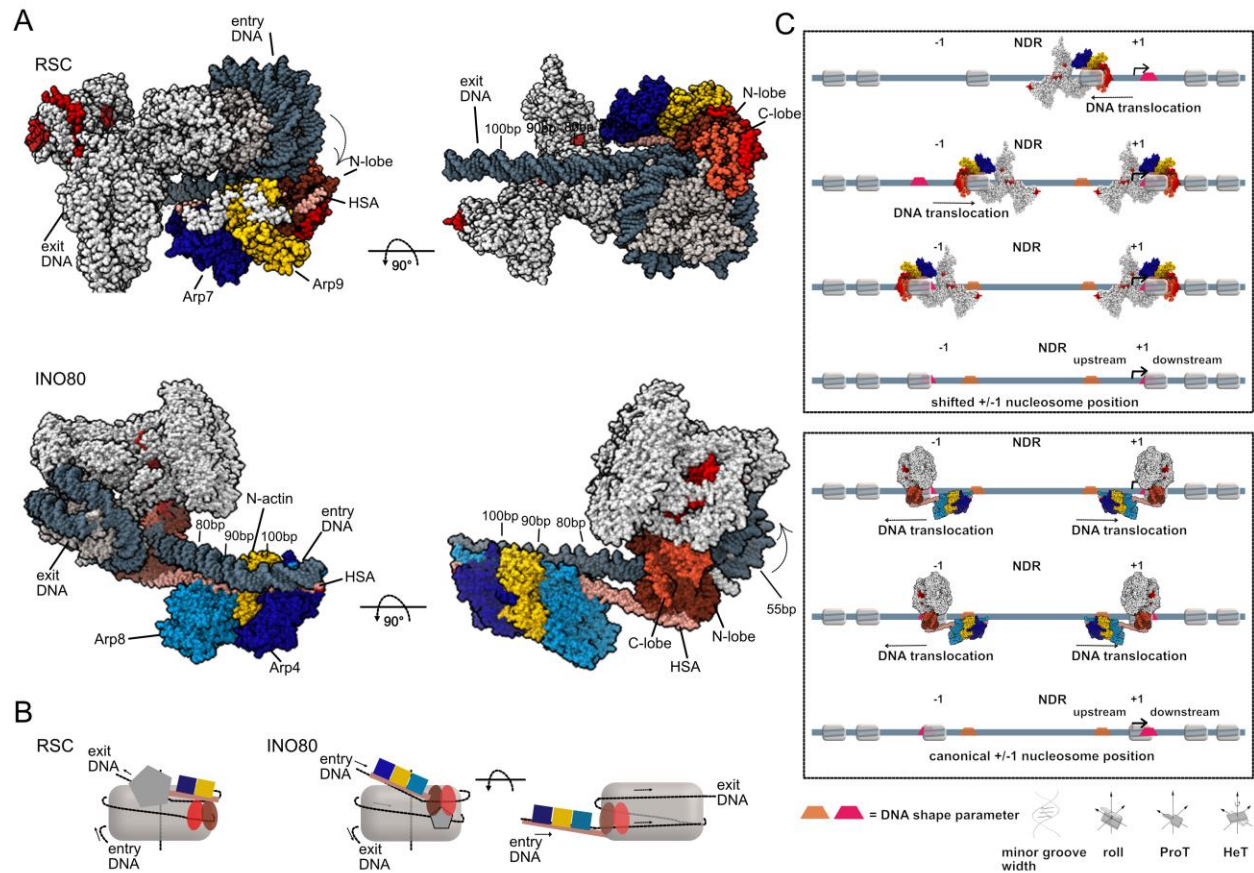


Figure 9: Comparison of RSC and INO80 in a promoter-focused context. (A) High-resolution structures of yRSC (PDB: 6TDA) and ctINO80 (PDB: 6FHS) bound to the nucleosomal substrate. Color coding matches Figure 7: The respective main ATPases are shown in red with the N-lobe in dark and the C-lobe in light red. The ATPase HSA domains are shown in translucent grey. The ARP module is depicted in light blue (Arp8), gold (N-Actin and Arp9) and dark blue (Arp4 and Arp7). Entry as well as exit DNA locations are indicated. Extranucleosomal DNA is highlighted in 10bp steps from the nucleosomal dyad. DNA translocation direction is indicated. (A) Upper panel: RSC bound to the nucleosome focusing on extranucleosomal exit DNA binding by the DIM module as well as the ARP module arrangement in proximity to the ATPase N-lobe. (A) Lower panel: ctINO80 bound to the nucleosome focusing on the ARP module binding to entry DNA 100bp from the dyad. (B) Model for RSC and INO80 nucleosome binding highlighting exit and entry DNA sites, as well as differences in nucleosome engagement. The RSC main ATPase binds at SHL \pm 2 with the ARP module in close proximity interacting with the exit site DNA. Applying the same perspective, the INO80 main ATPase binds at SHL \pm 6 with the ARP module bound to the entry side DNA. (C) Model describing the mechanism for establishing the stereotypical promoter patterns, including binding orientations of RSC and INO80, DNA translocation direction and a hypothetical DNA shape read-out step. RSC establishes NDR regions by clearing them of nucleosomes. The binding orientation of the RSC and the INO80 complexes in this process is indicated. Parameters defining DNA shape features are indicated in orange and pink and described on the bottom.

In vitro studies showed that RSC is sufficient for clearing promoter regions and for establishing the NDR with a relatively imprecise \pm 1 nucleosome positioning, shifted 20bp on average from the canonical *in vivo* positions, creating an NDR with at least physiological width (Krietenstein *et al.*, 2016). Targeting of RSC may be carried out by the Rsc3 and Rsc30 subunits recognizing promoter-specific DNA elements (Badis *et al.*, 2008). The HSA domain of the remodeler main ATPase is highly conserved throughout different remodeler family members, suggesting a model for RSC activity including DNA shape information read-out by the ARP module (Figure 8A, Figure

9). RSC may get oriented and activated upon binding to poly-(dT):(dA) elements translocating DNA by its main ATPase residing at SHL+/-2 (Krietenstein *et al.*, 2016, Wagner *et al.*, 2020). The RSC main ATPase may translocate DNA in an ATP-dependent manner until the ARP module positioned at SHL+/-6 reads out the DNA shape information located adjacent to the +1 nucleosome position (Figure 9C, upper panel). During information processing, the ARP module may rearrange to regulate the main ATPase presumably through the post-HSA–protrusion I helix axis. The DNA shape signal processing stops the DNA translocation by RSC and generates, since the main ATPase is working in front of the ARP module, nucleosome positioning downstream of its *in vivo* position, which would explain previous results (Figure 9C, upper panel) (Krietenstein *et al.*, 2016). Mirroring the binding orientation of RSC would result in nucleosome movement towards the NDR, which has not been described so far and limits the engagement of the nucleosome by RSC as depicted in Figure 9. INO80 may bind at SHL+/-6 on the same nucleosome with its ARP module located at the entry side extranucleosomal DNA (Figure 9C, bottom panel). The INO80 main ATPase may start pumping in entry side DNA until an intrinsic DNA shape pattern is recognized by the INO80 ARP module based on HSA-DNA interactions 100bp and 55bp away from the dyad (Figure 9C). This stop signal is possibly back-communicated through the post-HSA–protrusion I helix axis similar to RSC (Wagner *et al.*, 2020). Considering both possible binding orientations of INO80 on the nucleosomal substrate, the read-out of the same RSC DNA shape feature seems rather unlikely. The RSC-generated nucleosome position would in theory place its DNA shape feature downstream of the canonical +1 nucleosome position (Figure 9C, upper panel, bottom). Binding of the INO80 ARP module to downstream DNA would result in an even more extended NFR, for which there is no evidence *in vivo* nor *in vitro*, without any contact of the INO80 ARP module to the RSC DNA shape feature. Binding of the INO80 ARP module to DNA upstream the +1 nucleosome would pull-in the RSC positioned nucleosome to its canonical position. The ARP module binds to approximately 40bp extranucleosomal DNA that would be in close proximity to, but not in direct contact with, the RSC DNA shape feature. As a consequence, it seems more likely that, if DNA shape read-out by the ARP module is a shared feature of the ARP-containing chromatin remodelers, the type of DNA shape that is read-out is inherent to the remodelers. Since the human BAF complex as well as the yeast SWI/SNF complex lack sequence-specific Rsc3 and Rsc30 homologue subunits guiding the complexes to the NDR regions, the establishment of NDRs by SWI/SNF complexes solely based on DNA sequence seems unlikely. Mutagenesis of the SWI/SNF ARP modules and biochemical assessment of respective changes in the NDR pattern formation will improve the overall understanding of the suggested role of ARP modules in DNA shape read-out and the molecular integration of this information into downstream processes.

Discussion

A central question of future studies may be whether DNA shape features read by RNA polymerases I and II that are located 20-30bp upstream of the TSS overlap with the INO80 DNA shape features located 100bp from the dyad as defined by this study. Since ISWI and Chd1 remodeler ATPases lack HSA domains, and therefore ARP modules, the question arises whether DNA shape can actually be read by these remodelers, and, if so, how the respective auxiliary domains might be involved.

4. References

- ADAM, M., ROBERT, F., LAROCHELLE, M. & GAUDREAU, L. 2001. H2A.Z is required for global chromatin integrity and for recruitment of RNA polymerase II under specific conditions. *Mol Cell Biol*, 21, 6270-9.
- ALATWI, H. E. & DOWNS, J. A. 2015. Removal of H2A.Z by INO80 promotes homologous recombination. *EMBO Rep*, 16, 986-94.
- ALLFREY, V. G., FAULKNER, R. & MIRSKY, A. E. 1964. Acetylation and Methylation of Histones and Their Possible Role in the Regulation of Rna Synthesis. *Proc Natl Acad Sci U S A*, 51, 786-94.
- ALLSHIRE, R. C. & MADHANI, H. D. 2018. Ten principles of heterochromatin formation and function. *Nat Rev Mol Cell Biol*, 19, 229-244.
- ANDREEV, V., HRISTOVA, R., ASPARUHOVA, M., DANOVSKI, G., STOYNOV, S. & GOSPODINOV, A. 2019. Mammalian INO80 chromatin remodeler cooperates with FANCM to mediate DNA interstrand crosslink-induced checkpoint activation and repair. *DNA Repair (Amst)*, 74, 38-50.
- ARAMAYO, R. J., WILLHOFT, O., AYALA, R., BYTHELL-DOUGLAS, R., WIGLEY, D. B. & ZHANG, X. 2018. Cryo-EM structures of the human INO80 chromatin-remodeling complex. *Nat Struct Mol Biol*, 25, 37-44.
- ARENTS, G., BURLINGAME, R. W., WANG, B. C., LOVE, W. E. & MOUDRIANAKIS, E. N. 1991. The nucleosomal core histone octamer at 3.1 Å resolution: a tripartite protein assembly and a left-handed superhelix. *Proc Natl Acad Sci U S A*, 88, 10148-52.
- ARMACHE, J. P., GAMARRA, N., JOHNSON, S. L., LEONARD, J. D., WU, S., NARLIKAR, G. J. & CHENG, Y. 2019. Cryo-EM structures of remodeler-nucleosome intermediates suggest allosteric control through the nucleosome. *Elife*, 8.
- AYALA, R., WILLHOFT, O., ARAMAYO, R. J., WILKINSON, M., MCCORMACK, E. A., OCLOO, L., WIGLEY, D. B. & ZHANG, X. 2018. Structure and regulation of the human INO80-nucleosome complex. *Nature*, 556, 391-395.
- BADIS, G., CHAN, E. T., VAN BAKEL, H., PENA-CASTILLO, L., TILLO, D., TSUI, K., CARLSON, C. D., GOSSETT, A. J., HASINOFF, M. J., WARREN, C. L., GEBBIA, M., TALUKDER, S., YANG, A., MNAIMNEH, S., TERTEROV, D., COBURN, D., LI YEO, A., YEO, Z. X., CLARKE, N. D., LIEB, J. D., ANSARI, A. Z., NISLOW, C. & HUGHES, T. R. 2008. A library of yeast transcription factor motifs reveals a widespread function for Rsc3 in targeting nucleosome exclusion at promoters. *Mol Cell*, 32, 878-87.
- BALDI, S., KORBER, P. & BECKER, P. B. 2020. Beads on a string-nucleosome array arrangements and folding of the chromatin fiber. *Nat Struct Mol Biol*, 27, 109-118.
- BALDI, S., KREBS, S., BLUM, H. & BECKER, P. B. 2018. Genome-wide measurement of local nucleosome array regularity and spacing by nanopore sequencing. *Nat Struct Mol Biol*, 25, 894-901.
- BARNES, C. E., ENGLISH, D. M. & COWLEY, S. M. 2019. Acetylation & Co: an expanding repertoire of histone acylations regulates chromatin and transcription. *Essays Biochem*, 63, 97-107.
- BERGER, F. 2019. Emil Heitz, a true epigenetics pioneer. *Nat Rev Mol Cell Biol*, 20, 572.
- BESHNOVA, D. A., CHERSTVY, A. G., VAINSHTEIN, Y. & TEIF, V. B. 2014. Regulation of the nucleosome repeat length in vivo by the DNA sequence, protein concentrations and long-range interactions. *PLoS Comput Biol*, 10, e1003698.
- BOEGER, H., GRIESENBECK, J., STRATTAN, J. S. & KORNBERG, R. D. 2003. Nucleosomes unfold completely at a transcriptionally active promoter. *Mol Cell*, 11, 1587-98.
- BORNELOV, S., REYNOLDS, N., XENOPHONTOS, M., GHARBI, S., JOHNSTONE, E., FLOYD, R., RALSER, M., SIGNOLET, J., LOOS, R., DIETMANN, S., BERTONE, P. & HENDRICH, B. 2018. The Nucleosome

References

- Remodeling and Deacetylation Complex Modulates Chromatin Structure at Sites of Active Transcription to Fine-Tune Gene Expression. *Mol Cell*, 71, 56-72 e4.
- BOYER, L. A. & PETERSON, C. L. 2000. Actin-related proteins (Arps): conformational switches for chromatin-remodeling machines? *Bioessays*, 22, 666-72.
- BRAHMA, S. & HENIKOFF, S. 2019. RSC-Associated Subnucleosomes Define MNase-Sensitive Promoters in Yeast. *Mol Cell*, 73, 238-249 e3.
- BRAHMA, S., NGUBO, M., PAUL, S., UDUGAMA, M. & BARTHOLOMEW, B. 2018. The Arp8 and Arp4 module acts as a DNA sensor controlling INO80 chromatin remodeling. *Nat Commun*, 9, 3309.
- BRAHMA, S., UDUGAMA, M. I., KIM, J., HADA, A., BHARDWAJ, S. K., HAILU, S. G., LEE, T. H. & BARTHOLOMEW, B. 2017. INO80 exchanges H2A.Z for H2A by translocating on DNA proximal to histone dimers. *Nat Commun*, 8, 15616.
- BRANGWYNNE, C. P., ECKMANN, C. R., COURSON, D. S., RYBARSKA, A., HOEGE, C., GHARAKHANI, J., JULICHER, F. & HYMAN, A. A. 2009. Germline P granules are liquid droplets that localize by controlled dissolution/condensation. *Science*, 324, 1729-32.
- BROGAARD, K., XI, L., WANG, J. P. & WIDOM, J. 2012. A map of nucleosome positions in yeast at base-pair resolution. *Nature*, 486, 496-501.
- BROWNELL, J. E. & ALLIS, C. D. 1996. Special HATs for special occasions: linking histone acetylation to chromatin assembly and gene activation. *Curr Opin Genet Dev*, 6, 176-84.
- BYRD, A. K. & RANEY, K. D. 2012. Superfamily 2 helicases. *Front Biosci (Landmark Ed)*, 17, 2070-88.
- CAI, S., SONG, Y., CHEN, C., SHI, J. & GAN, L. 2018. Natural chromatin is heterogeneous and self-associates in vitro. *Mol Biol Cell*, 29, 1652-1663.
- CAO, T., SUN, L., JIANG, Y., HUANG, S., WANG, J. & CHEN, Z. 2016. Crystal structure of a nuclear actin ternary complex. *Proc Natl Acad Sci U S A*, 113, 8985-90.
- CARROZZA, M. J., UTLEY, R. T., WORKMAN, J. L. & COTE, J. 2003. The diverse functions of histone acetyltransferase complexes. *Trends Genet*, 19, 321-9.
- CHALLAL, D., BARUCCO, M., KUBIK, S., FEUERBACH, F., CANDELLI, T., GEOFFROY, H., BENAKSAS, C., SHORE, D. & LIBRI, D. 2018. General Regulatory Factors Control the Fidelity of Transcription by Restricting Non-coding and Ectopic Initiation. *Mol Cell*, 72, 955-969 e7.
- CHANG, Y. P., XU, M., MACHADO, A. C., YU, X. J., ROHS, R. & CHEN, X. S. 2013. Mechanism of origin DNA recognition and assembly of an initiator-helicase complex by SV40 large tumor antigen. *Cell Rep*, 3, 1117-27.
- CHEN, C., LIM, H. H., SHI, J., TAMURA, S., MAESHIMA, K., SURANA, U. & GAN, L. 2016. Budding yeast chromatin is dispersed in a crowded nucleoplasm in vivo. *Mol Biol Cell*, 27, 3357-3368.
- CHEN, L., CAI, Y., JIN, J., FLORENS, L., SWANSON, S. K., WASHBURN, M. P., CONAWAY, J. W. & CONAWAY, R. C. 2011. Subunit organization of the human INO80 chromatin remodeling complex: an evolutionarily conserved core complex catalyzes ATP-dependent nucleosome remodeling. *J Biol Chem*, 286, 11283-9.
- CHEN, L., CONAWAY, R. C. & CONAWAY, J. W. 2013. Multiple modes of regulation of the human Ino80 SNF2 ATPase by subunits of the INO80 chromatin-remodeling complex. *Proc Natl Acad Sci U S A*, 110, 20497-502.
- CHEREJI, R. V., KAN, T. W., GRUDNIEWSKA, M. K., ROMASHCHENKO, A. V., BEREZIKOV, E., ZHIMULEV, I. F., GURYEV, V., MOROZOV, A. V. & MOSHKIN, Y. M. 2016. Genome-wide profiling of nucleosome sensitivity and chromatin accessibility in *Drosophila melanogaster*. *Nucleic Acids Res*, 44, 1036-51.
- CHEREJI, R. V., RAMACHANDRAN, S., BRYSON, T. D. & HENIKOFF, S. 2018. Precise genome-wide mapping of single nucleosomes and linkers in vivo. *Genome Biol*, 19, 19.
- CIABRELLI, F. & CAVALLI, G. 2015. Chromatin-driven behavior of topologically associating domains. *J Mol Biol*, 427, 608-25.

References

- CLAPIER, C. R. & CAIRNS, B. R. 2009. The biology of chromatin remodeling complexes. *Annu Rev Biochem*, 78, 273-304.
- CLAPIER, C. R. & CAIRNS, B. R. 2012. Regulation of ISWI involves inhibitory modules antagonized by nucleosomal epitopes. *Nature*, 492, 280-4.
- CLAPIER, C. R., IWASA, J., CAIRNS, B. R. & PETERSON, C. L. 2017. Mechanisms of action and regulation of ATP-dependent chromatin-remodelling complexes. *Nat Rev Mol Cell Biol*, 18, 407-422.
- CLAPIER, C. R., KASTEN, M. M., PARNELL, T. J., VISWANATHAN, R., SZERLONG, H., SIRINAKIS, G., ZHANG, Y. & CAIRNS, B. R. 2016. Regulation of DNA Translocation Efficiency within the Chromatin Remodeler RSC/Sth1 Potentiates Nucleosome Sliding and Ejection. *Mol Cell*, 62, 453-461.
- CLAPIER, C. R., LANGST, G., CORONA, D. F., BECKER, P. B. & NIGHTINGALE, K. P. 2001. Critical role for the histone H4 N terminus in nucleosome remodeling by ISWI. *Mol Cell Biol*, 21, 875-83.
- CLAYTON, A. L., HEBBES, T. R., THORNE, A. W. & CRANE-ROBINSON, C. 1993. Histone acetylation and gene induction in human cells. *FEBS Lett*, 336, 23-6.
- CONAWAY, R. C. & CONAWAY, J. W. 2009. The INO80 chromatin remodeling complex in transcription, replication and repair. *Trends Biochem Sci*, 34, 71-7.
- COTE, J., QUINN, J., WORKMAN, J. L. & PETERSON, C. L. 1994. Stimulation of GAL4 derivative binding to nucleosomal DNA by the yeast SWI/SNF complex. *Science*, 265, 53-60.
- CROCKER, J., ABE, N., RINALDI, L., MCGREGOR, A. P., FRANKEL, N., WANG, S., ALSAWADI, A., VALENTI, P., PLAZA, S., PAYRE, F., MANN, R. S. & STERN, D. L. 2015. Low affinity binding site clusters confer hox specificity and regulatory robustness. *Cell*, 160, 191-203.
- CUI, Y. & BUSTAMANTE, C. 2000. Pulling a single chromatin fiber reveals the forces that maintain its higher-order structure. *Proc Natl Acad Sci U S A*, 97, 127-32.
- CUTTER, A. R. & HAYES, J. J. 2015. A brief review of nucleosome structure. *FEBS Lett*, 589, 2914-22.
- DABAN, J. R. & BERMUDEZ, A. 1998. Interdigitated solenoid model for compact chromatin fibers. *Biochemistry*, 37, 4299-304.
- DANG, W., KAGALWALA, M. N. & BARTHOLOMEW, B. 2006. Regulation of ISW2 by concerted action of histone H4 tail and extranucleosomal DNA. *Mol Cell Biol*, 26, 7388-96.
- DAVEY, C. A., SARGENT, D. F., LUGER, K., MAEDER, A. W. & RICHMOND, T. J. 2002. Solvent mediated interactions in the structure of the nucleosome core particle at 1.9 a resolution. *J Mol Biol*, 319, 1097-113.
- DECHASSA, M. L., SABRI, A., PONDUGULA, S., KASSABOV, S. R., CHATTERJEE, N., KLADDE, M. P. & BARTHOLOMEW, B. 2010. SWI/SNF has intrinsic nucleosome disassembly activity that is dependent on adjacent nucleosomes. *Mol Cell*, 38, 590-602.
- DEINDL, S., HWANG, W. L., HOTA, S. K., BLOSSER, T. R., PRASAD, P., BARTHOLOMEW, B. & ZHUANG, X. 2013. ISWI remodelers slide nucleosomes with coordinated multi-base-pair entry steps and single-base-pair exit steps. *Cell*, 152, 442-52.
- DIENEMANN, C., SCHWALB, B., SCHILBACH, S. & CRAMER, P. 2019. Promoter Distortion and Opening in the RNA Polymerase II Cleft. *Mol Cell*, 73, 97-106 e4.
- DIXON, J. R., GORKIN, D. U. & REN, B. 2016. Chromatin Domains: The Unit of Chromosome Organization. *Mol Cell*, 62, 668-80.
- DORIGO, B., SCHALCH, T., KULANGARA, A., DUDA, S., SCHROEDER, R. R. & RICHMOND, T. J. 2004. Nucleosome arrays reveal the two-start organization of the chromatin fiber. *Science*, 306, 1571-3.
- DUBOCHET, J., ADRIAN, M., SCHULTZ, P. & OUDET, P. 1986. Cryo-electron microscopy of vitrified SV40 minichromosomes: the liquid drop model. *EMBO J*, 5, 519-28.
- DURR, H., FLAUS, A., OWEN-HUGHES, T. & HOPFNER, K. P. 2006. Snf2 family ATPases and DExx box helicases: differences and unifying concepts from high-resolution crystal structures. *Nucleic Acids Res*, 34, 4160-7.

References

- DURR, H., KORNER, C., MULLER, M., HICKMANN, V. & HOPFNER, K. P. 2005. X-ray structures of the *Sulfolobus solfataricus* SWI2/SNF2 ATPase core and its complex with DNA. *Cell*, 121, 363-73.
- EBBERT, R., BIRKMANN, A. & SCHULLER, H. J. 1999. The product of the SNF2/SWI2 paralogue INO80 of *Saccharomyces cerevisiae* required for efficient expression of various yeast structural genes is part of a high-molecular-weight protein complex. *Mol Microbiol*, 32, 741-51.
- ELTSOV, M., MACLELLAN, K. M., MAESHIMA, K., FRANGAKIS, A. S. & DUBOCHET, J. 2008. Analysis of cryo-electron microscopy images does not support the existence of 30-nm chromatin fibers in mitotic chromosomes in situ. *Proc Natl Acad Sci U S A*, 105, 19732-7.
- ENGEL, C., GUBBEY, T., NEYER, S., SAINSBURY, S., OBERTHUER, C., BAEJEN, C., BERNECKY, C. & CRAMER, P. 2017. Structural Basis of RNA Polymerase I Transcription Initiation. *Cell*, 169, 120-131 e22.
- EUSTERMANN, S., SCHALL, K., KOSTREWA, D., LAKOMEK, K., STRAUSS, M., MOLDT, M. & HOPFNER, K. P. 2018. Structural basis for ATP-dependent chromatin remodelling by the INO80 complex. *Nature*, 556, 386-390.
- FALCIOLA, L., SPADA, F., CALOGERO, S., LANGST, G., VOIT, R., GRUMMT, I. & BIANCHI, M. E. 1997. High mobility group 1 protein is not stably associated with the chromosomes of somatic cells. *J Cell Biol*, 137, 19-26.
- FAN, J. Y., GORDON, F., LUGER, K., HANSEN, J. C. & TREMETHICK, D. J. 2002. The essential histone variant H2A.Z regulates the equilibrium between different chromatin conformational states. *Nat Struct Biol*, 9, 172-6.
- FARNUNG, L., VOS, S. M., WIGGE, C. & CRAMER, P. 2017. Nucleosome-Chd1 structure and implications for chromatin remodelling. *Nature*, 550, 539-542.
- FEDOR, M. J., LUE, N. F. & KORNBERG, R. D. 1988. Statistical positioning of nucleosomes by specific protein-binding to an upstream activating sequence in yeast. *J Mol Biol*, 204, 109-27.
- FEI, J., TORIGOE, S. E., BROWN, C. R., KHUONG, M. T., KASSAVETIS, G. A., BOEGER, H. & KADONAGA, J. T. 2015. The prenucleosome, a stable conformational isomer of the nucleosome. *Genes Dev*, 29, 2563-75.
- FENG, Q. & ZHANG, Y. 2003. The NuRD complex: linking histone modification to nucleosome remodeling. *Curr Top Microbiol Immunol*, 274, 269-90.
- FENN, S., BREITSPRECHER, D., GERHOLD, C. B., WITTE, G., FAIX, J. & HOPFNER, K. P. 2011. Structural biochemistry of nuclear actin-related proteins 4 and 8 reveals their interaction with actin. *EMBO J*, 30, 2153-66.
- FINCH, J. T. & KLUG, A. 1976. Solenoidal model for superstructure in chromatin. *Proc Natl Acad Sci U S A*, 73, 1897-901.
- FINCH, J. T., LUTTER, L. C., RHODES, D., BROWN, R. S., RUSHTON, B., LEVITT, M. & KLUG, A. 1977. Structure of nucleosome core particles of chromatin. *Nature*, 269, 29-36.
- FLAUS, A., MARTIN, D. M., BARTON, G. J. & OWEN-HUGHES, T. 2006. Identification of multiple distinct Snf2 subfamilies with conserved structural motifs. *Nucleic Acids Res*, 34, 2887-905.
- FLAUS, A. & OWEN-HUGHES, T. 2003. Mechanisms for nucleosome mobilization. *Biopolymers*, 68, 563-78.
- FRANKE, M., IBRAHIM, D. M., ANDREY, G., SCHWARZER, W., HEINRICH, V., SCHOPFLIN, R., KRAFT, K., KEMPFER, R., JERKOVIC, I., CHAN, W. L., SPIELMANN, M., TIMMERMANN, B., WITTLER, L., KURTH, I., CAMBIASO, P., ZUFFARDI, O., HOUGE, G., LAMBIE, L., BRANCATI, F., POMBO, A., VINGRON, M., SPITZ, F. & MUNDLOS, S. 2016. Formation of new chromatin domains determines pathogenicity of genomic duplications. *Nature*, 538, 265-269.
- FUSSNER, E., CHING, R. W. & BAZETT-JONES, D. P. 2011. Living without 30nm chromatin fibers. *Trends Biochem Sci*, 36, 1-6.

References

- GALLINARI, P., DI MARCO, S., JONES, P., PALLAORO, M. & STEINKUHLER, C. 2007. HDACs, histone deacetylation and gene transcription: from molecular biology to cancer therapeutics. *Cell Res*, 17, 195-211.
- GERHOLD, C. B. & GASSER, S. M. 2014. INO80 and SWR complexes: relating structure to function in chromatin remodeling. *Trends Cell Biol*, 24, 619-31.
- GERHOLD, C. B., WINKLER, D. D., LAKOMEK, K., SEIFERT, F. U., FENN, S., KESSLER, B., WITTE, G., LUGER, K. & HOPFNER, K. P. 2012. Structure of Actin-related protein 8 and its contribution to nucleosome binding. *Nucleic Acids Res*, 40, 11036-46.
- GKIKOPOULOS, T., SCHOFIELD, P., SINGH, V., PINSKAYA, M., MELLOR, J., SMOLLE, M., WORKMAN, J. L., BARTON, G. J. & OWEN-HUGHES, T. 2011. A role for Snf2-related nucleosome-spacing enzymes in genome-wide nucleosome organization. *Science*, 333, 1758-60.
- GORDAN, R., SHEN, N., DROR, I., ZHOU, T., HORTON, J., ROHS, R. & BULYK, M. L. 2013. Genomic regions flanking E-box binding sites influence DNA binding specificity of bHLH transcription factors through DNA shape. *Cell Rep*, 3, 1093-104.
- GRIGORYEV, S. A. 2018. Chromatin Higher-Order Folding: A Perspective with Linker DNA Angles. *Biophys J*, 114, 2290-2297.
- GRIGORYEV, S. A. & WOODCOCK, C. L. 2012. Chromatin organization - the 30 nm fiber. *Exp Cell Res*, 318, 1448-55.
- HAN, Y., REYES, A. A., MALIK, S. & HE, Y. 2020. Cryo-EM structure of SWI/SNF complex bound to a nucleosome. *Nature*, 579, 452-455.
- HANSEN, A. S., PUSTOVA, I., CATTOGLIO, C., TJIAN, R. & DARZACQ, X. 2017. CTCF and cohesin regulate chromatin loop stability with distinct dynamics. *Elife*, 6.
- HANSEN, J. C., CONNOLLY, M., MCDONALD, C. J., PAN, A., PRYAMKOVA, A., RAY, K., SEIDEL, E., TAMURA, S., ROGGE, R. & MAESHIMA, K. 2018. The 10-nm chromatin fiber and its relationship to interphase chromosome organization. *Biochem Soc Trans*, 46, 67-76.
- HARADA, B. T., HWANG, W. L., DEINDL, S., CHATTERJEE, N., BARTHOLOMEW, B. & ZHUANG, X. 2016. Stepwise nucleosome translocation by RSC remodeling complexes. *Elife*, 5.
- HAUK, G., MCKNIGHT, J. N., NODELMAN, I. M. & BOWMAN, G. D. 2010. The chromodomains of the Chd1 chromatin remodeler regulate DNA access to the ATPase motor. *Mol Cell*, 39, 711-23.
- HAVAS, K., FLAUS, A., PHELAN, M., KINGSTON, R., WADE, P. A., LILLEY, D. M. & OWEN-HUGHES, T. 2000. Generation of superhelical torsion by ATP-dependent chromatin remodeling activities. *Cell*, 103, 1133-42.
- HE, S., WU, Z., TIAN, Y., YU, Z., YU, J., WANG, X., LI, J., LIU, B. & XU, Y. 2020. Structure of nucleosome-bound human BAF complex. *Science*, 367, 875-881.
- HO, L. & CRABTREE, G. R. 2010. Chromatin remodelling during development. *Nature*, 463, 474-84.
- HOCK, R., WILDE, F., SCHEER, U. & BUSTIN, M. 1998. Dynamic relocation of chromosomal protein HMG-17 in the nucleus is dependent on transcriptional activity. *EMBO J*, 17, 6992-7001.
- HOPFNER, K. P., GERHOLD, C. B., LAKOMEK, K. & WOLLMANN, P. 2012. Swi2/Snf2 remodelers: hybrid views on hybrid molecular machines. *Curr Opin Struct Biol*, 22, 225-33.
- HORN, P. J. & PETERSON, C. L. 2002. Molecular biology. Chromatin higher order folding--wrapping up transcription. *Science*, 297, 1824-7.
- HSIEH, T. H., WEINER, A., LAJOIE, B., DEKKER, J., FRIEDMAN, N. & RANDO, O. J. 2015. Mapping Nucleosome Resolution Chromosome Folding in Yeast by Micro-C. *Cell*, 162, 108-19.
- HYLAND, E. M., COSGROVE, M. S., MOLINA, H., WANG, D., PANDEY, A., COTTEE, R. J. & BOEKE, J. D. 2005. Insights into the role of histone H3 and histone H4 core modifiable residues in *Saccharomyces cerevisiae*. *Mol Cell Biol*, 25, 10060-70.
- IOSHIKHES, I. P., ALBERT, I., ZANTON, S. J. & PUGH, B. F. 2006. Nucleosome positions predicted through comparative genomics. *Nat Genet*, 38, 1210-5.

References

- IRVINE, D., TUERK, C. & GOLD, L. 1991. SELEXION. Systematic evolution of ligands by exponential enrichment with integrated optimization by non-linear analysis. *J Mol Biol*, 222, 739-61.
- ITO, T., BULGER, M., PAZIN, M. J., KOBAYASHI, R. & KADONAGA, J. T. 1997. ACF, an ISWI-containing and ATP-utilizing chromatin assembly and remodeling factor. *Cell*, 90, 145-55.
- IYER, V. & STRUHL, K. 1995. Poly(dA:dT), a ubiquitous promoter element that stimulates transcription via its intrinsic DNA structure. *EMBO J*, 14, 2570-9.
- JANSSEN, A., COLMENARES, S. U. & KARPEN, G. H. 2018. Heterochromatin: Guardian of the Genome. *Annu Rev Cell Dev Biol*, 34, 265-288.
- JIANG, C. & PUGH, B. F. 2009a. A compiled and systematic reference map of nucleosome positions across the *Saccharomyces cerevisiae* genome. *Genome Biol*, 10, R109.
- JIANG, C. & PUGH, B. F. 2009b. Nucleosome positioning and gene regulation: advances through genomics. *Nat Rev Genet*, 10, 161-72.
- JOSHI, R., PASSNER, J. M., ROHS, R., JAIN, R., SOSINSKY, A., CRICKMORE, M. A., JACOB, V., AGGARWAL, A. K., HONIG, B. & MANN, R. S. 2007. Functional specificity of a Hox protein mediated by the recognition of minor groove structure. *Cell*, 131, 530-43.
- KAPLAN, N., MOORE, I. K., FONDUFE-MITTENDORF, Y., GOSSETT, A. J., TILLO, D., FIELD, Y., LEPROUST, E. M., HUGHES, T. R., LIEB, J. D., WIDOM, J. & SEGAL, E. 2009. The DNA-encoded nucleosome organization of a eukaryotic genome. *Nature*, 458, 362-6.
- KAPOOR, P., CHEN, M., WINKLER, D. D., LUGER, K. & SHEN, X. 2013. Evidence for monomeric actin function in INO80 chromatin remodeling. *Nat Struct Mol Biol*, 20, 426-32.
- KINGSTON, R. E. & NARLIKAR, G. J. 1999. ATP-dependent remodeling and acetylation as regulators of chromatin fluidity. *Genes Dev*, 13, 2339-52.
- KLOPF, E., SCHMIDT, H. A., CLAUDER-MUNSTER, S., STEINMETZ, L. M. & SCHULLER, C. 2017. INO80 represses osmotic stress induced gene expression by resetting promoter proximal nucleosomes. *Nucleic Acids Res*, 45, 3752-3766.
- KLUG, A., RHODES, D., SMITH, J., FINCH, J. T. & THOMAS, J. O. 1980. A low resolution structure for the histone core of the nucleosome. *Nature*, 287, 509-16.
- KNOLL, K. R., EUSTERMANN, S., NIEBAUER, V., OBERBECKMANN, E., STOEHR, G., SCHALL, K., TOSI, A., SCHWARZ, M., BUCHFELLNER, A., KORBER, P. & HOPFNER, K. P. 2018. The nuclear actin-containing Arp8 module is a linker DNA sensor driving INO80 chromatin remodeling. *Nat Struct Mol Biol*, 25, 823-832.
- KOBAYASHI, W. & KURUMIZAKA, H. 2019. Structural transition of the nucleosome during chromatin remodeling and transcription. *Curr Opin Struct Biol*, 59, 107-114.
- KOONIN, E. V. 1993. A superfamily of ATPases with diverse functions containing either classical or deviant ATP-binding motif. *J Mol Biol*, 229, 1165-74.
- KORNBERG, R. 1981. The location of nucleosomes in chromatin: specific or statistical. *Nature*, 292, 579-80.
- KORNBERG, R. D. 1974. Chromatin structure: a repeating unit of histones and DNA. *Science*, 184, 868-71.
- KORNBERG, R. D. & STRYER, L. 1988. Statistical distributions of nucleosomes: nonrandom locations by a stochastic mechanism. *Nucleic Acids Res*, 16, 6677-90.
- KORNBERG, R. D. & THOMAS, J. O. 1974. Chromatin structure; oligomers of the histones. *Science*, 184, 865-8.
- KOWNIN, P., BATEMAN, E. & PAULE, M. R. 1987. Eukaryotic RNA polymerase I promoter binding is directed by protein contacts with transcription initiation factor and is DNA sequence-independent. *Cell*, 50, 693-9.
- KRIETENSTEIN, N. & RANDO, O. J. 2020. Mesoscale organization of the chromatin fiber. *Curr Opin Genet Dev*, 61, 32-36.

References

- KRIETENSTEIN, N., WAL, M., WATANABE, S., PARK, B., PETERSON, C. L., PUGH, B. F. & KORBER, P. 2016. Genomic Nucleosome Organization Reconstituted with Pure Proteins. *Cell*, 167, 709-721 e12.
- KUBIK, S., BRUZZONE, M. J., CHALLAL, D., DREOS, R., MATTAROCCHI, S., BUCHER, P., LIBRI, D. & SHORE, D. 2019. Opposing chromatin remodelers control transcription initiation frequency and start site selection. *Nat Struct Mol Biol*, 26, 744-754.
- KUBIK, S., BRUZZONE, M. J., JACQUET, P., FALCONE, J. L., ROUGEMONT, J. & SHORE, D. 2015. Nucleosome Stability Distinguishes Two Different Promoter Types at All Protein-Coding Genes in Yeast. *Mol Cell*, 60, 422-34.
- KUBIK, S., O'DUIBHIR, E., DE JONGE, W. J., MATTAROCCHI, S., ALBERT, B., FALCONE, J. L., BRUZZONE, M. J., HOLSTEGE, F. C. P. & SHORE, D. 2018. Sequence-Directed Action of RSC Remodeler and General Regulatory Factors Modulates +1 Nucleosome Position to Facilitate Transcription. *Mol Cell*, 71, 89-102 e5.
- LADEMANN, C. A., RENKAWITZ, J., PFANDER, B. & JENTSCH, S. 2017. The INO80 Complex Removes H2A.Z to Promote Presynaptic Filament Formation during Homologous Recombination. *Cell Rep*, 19, 1294-1303.
- LAFON, A., TARANUM, S., PIETROCOLA, F., DINGLI, F., LOEW, D., BRAHMA, S., BARTHOLOMEW, B. & PAPAMICHOS-CHRONAKIS, M. 2015. INO80 Chromatin Remodeler Facilitates Release of RNA Polymerase II from Chromatin for Ubiquitin-Mediated Proteasomal Degradation. *Mol Cell*, 60, 784-796.
- LAI, A. Y. & WADE, P. A. 2011. Cancer biology and NuRD: a multifaceted chromatin remodelling complex. *Nat Rev Cancer*, 11, 588-96.
- LAI, B., GAO, W., CUI, K., XIE, W., TANG, Q., JIN, W., HU, G., NI, B. & ZHAO, K. 2018. Publisher Correction: Principles of nucleosome organization revealed by single-cell micrococcal nuclease sequencing. *Nature*, 564, E17.
- LANGST, G. & BECKER, P. B. 2001. Nucleosome mobilization and positioning by ISWI-containing chromatin-remodeling factors. *J Cell Sci*, 114, 2561-8.
- LARSON, A. G., ELNATAN, D., KEENEN, M. M., TRNKA, M. J., JOHNSTON, J. B., BURLINGAME, A. L., AGARD, D. A., REDDING, S. & NARLIKAR, G. J. 2017. Liquid droplet formation by HP1alpha suggests a role for phase separation in heterochromatin. *Nature*, 547, 236-240.
- LATHAM, J. A. & DENT, S. Y. 2007. Cross-regulation of histone modifications. *Nat Struct Mol Biol*, 14, 1017-24.
- LAZAROVICI, A., ZHOU, T., SHAFER, A., DANTAS MACHADO, A. C., RILEY, T. R., SANDSTROM, R., SABO, P. J., LU, Y., ROHS, R., STAMATOYANNOPOULOS, J. A. & BUSSEMAKER, H. J. 2013. Probing DNA shape and methylation state on a genomic scale with DNase I. *Proc Natl Acad Sci U S A*, 110, 6376-81.
- LEVO, M., ZALCKVAR, E., SHARON, E., DANTAS MACHADO, A. C., KALMA, Y., LOTAM-POMPAN, M., WEINBERGER, A., YAKHINI, Z., ROHS, R. & SEGAL, E. 2015. Unraveling determinants of transcription factor binding outside the core binding site. *Genome Res*, 25, 1018-29.
- LI, M., HADA, A., SEN, P., OLUFEMI, L., HALL, M. A., SMITH, B. Y., FORTH, S., MCKNIGHT, J. N., PATEL, A., BOWMAN, G. D., BARTHOLOMEW, B. & WANG, M. D. 2015. Dynamic regulation of transcription factors by nucleosome remodeling. *Elife*, 4.
- LI, M., XIA, X., TIAN, Y., JIA, Q., LIU, X., LU, Y., LI, M., LI, X. & CHEN, Z. 2019. Mechanism of DNA translocation underlying chromatin remodelling by Snf2. *Nature*, 567, 409-413.
- LIELEG, C., KETTERER, P., NUEBLER, J., LUDWIGSEN, J., GERLAND, U., DIETZ, H., MUELLER-PLANITZ, F. & KORBER, P. 2015a. Nucleosome spacing generated by ISWI and CHD1 remodelers is constant regardless of nucleosome density. *Mol Cell Biol*, 35, 1588-605.
- LIELEG, C., KRIETENSTEIN, N., WALKER, M. & KORBER, P. 2015b. Nucleosome positioning in yeasts: methods, maps, and mechanisms. *Chromosoma*, 124, 131-51.

References

- LIU, X., LI, M., XIA, X., LI, X. & CHEN, Z. 2017. Mechanism of chromatin remodelling revealed by the Snf2-nucleosome structure. *Nature*, 544, 440-445.
- LIU, Y., ZHOU, K., ZHANG, N., WEI, H., TAN, Y. Z., ZHANG, Z., CARRAGHER, B., POTTER, C. S., D'ARCY, S. & LUGER, K. 2020. FACT caught in the act of manipulating the nucleosome. *Nature*, 577, 426-431.
- LO, W. S., DUGGAN, L., EMRE, N. C., BELOTSEKOVSKAYA, R., LANE, W. S., SHIEKHATTAR, R. & BERGER, S. L. 2001. Snf1--a histone kinase that works in concert with the histone acetyltransferase Gcn5 to regulate transcription. *Science*, 293, 1142-6.
- LORCH, Y., MAIER-DAVIS, B. & KORNBERG, R. D. 2014. Role of DNA sequence in chromatin remodeling and the formation of nucleosome-free regions. *Genes Dev*, 28, 2492-7.
- LORCH, Y., ZHANG, M. & KORNBERG, R. D. 1999. Histone octamer transfer by a chromatin-remodeling complex. *Cell*, 96, 389-92.
- LORCH, Y., ZHANG, M. & KORNBERG, R. D. 2001. RSC unravels the nucleosome. *Mol Cell*, 7, 89-95.
- LOWARY, P. T. & WIDOM, J. 1998. New DNA sequence rules for high affinity binding to histone octamer and sequence-directed nucleosome positioning. *J Mol Biol*, 276, 19-42.
- LU, Q., WALLRATH, L. L. & ELGIN, S. C. 1994. Nucleosome positioning and gene regulation. *J Cell Biochem*, 55, 83-92.
- LUGER, K., DECHASSA, M. L. & TREMETHICK, D. J. 2012. New insights into nucleosome and chromatin structure: an ordered state or a disordered affair? *Nat Rev Mol Cell Biol*, 13, 436-47.
- LUGER, K., MADER, A. W., RICHMOND, R. K., SARGENT, D. F. & RICHMOND, T. J. 1997. Crystal structure of the nucleosome core particle at 2.8 Å resolution. *Nature*, 389, 251-60.
- LUGER, K. & RICHMOND, T. J. 1998. DNA binding within the nucleosome core. *Curr Opin Struct Biol*, 8, 33-40.
- LUK, E., RANJAN, A., FITZGERALD, P. C., MIZUGUCHI, G., HUANG, Y., WEI, D. & WU, C. 2010. Stepwise histone replacement by SWR1 requires dual activation with histone H2A.Z and canonical nucleosome. *Cell*, 143, 725-36.
- LUSSER, A., URWIN, D. L. & KADONAGA, J. T. 2005. Distinct activities of CHD1 and ACF in ATP-dependent chromatin assembly. *Nat Struct Mol Biol*, 12, 160-6.
- MAESHIMA, K., HIHARA, S. & ELTSOV, M. 2010. Chromatin structure: does the 30-nm fibre exist in vivo? *Curr Opin Cell Biol*, 22, 291-7.
- MAVRICH, T. N., IOSHIKHES, I. P., VENTERS, B. J., JIANG, C., TOMSHO, L. P., QI, J., SCHUSTER, S. C., ALBERT, I. & PUGH, B. F. 2008a. A barrier nucleosome model for statistical positioning of nucleosomes throughout the yeast genome. *Genome Res*, 18, 1073-83.
- MAVRICH, T. N., JIANG, C., IOSHIKHES, I. P., LI, X., VENTERS, B. J., ZANTON, S. J., TOMSHO, L. P., QI, J., GLASER, R. L., SCHUSTER, S. C., GILMOUR, D. S., ALBERT, I. & PUGH, B. F. 2008b. Nucleosome organization in the Drosophila genome. *Nature*, 453, 358-62.
- MCGINTY, R. K. & TAN, S. 2015. Nucleosome structure and function. *Chem Rev*, 115, 2255-73.
- MCKNIGHT, J. N., JENKINS, K. R., NODELMAN, I. M., ESCOBAR, T. & BOWMAN, G. D. 2011. Extranucleosomal DNA binding directs nucleosome sliding by Chd1. *Mol Cell Biol*, 31, 4746-59.
- MIZUGUCHI, G., SHEN, X., LANDRY, J., WU, W. H., SEN, S. & WU, C. 2004. ATP-driven exchange of histone H2AZ variant catalyzed by SWR1 chromatin remodeling complex. *Science*, 303, 343-8.
- MORARU, M. & SCHALCH, T. 2019. Chromatin fiber structural motifs as regulatory hubs of genome function? *Essays Biochem*, 63, 123-132.
- MORRISON, A. J., HIGHLAND, J., KROGAN, N. J., ARBEL-EDEN, A., GREENBLATT, J. F., HABER, J. E. & SHEN, X. 2004. INO80 and gamma-H2AX interaction links ATP-dependent chromatin remodeling to DNA damage repair. *Cell*, 119, 767-75.
- MUELLER-PLANITZ, F., KLINKER, H. & BECKER, P. B. 2013. Nucleosome sliding mechanisms: new twists in a looped history. *Nat Struct Mol Biol*, 20, 1026-32.

References

- NARLIKAR, G. J., FAN, H. Y. & KINGSTON, R. E. 2002. Cooperation between complexes that regulate chromatin structure and transcription. *Cell*, 108, 475-87.
- NARLIKAR, G. J., PHELAN, M. L. & KINGSTON, R. E. 2001. Generation and interconversion of multiple distinct nucleosomal states as a mechanism for catalyzing chromatin fluidity. *Mol Cell*, 8, 1219-30.
- NELSON, H. C., FINCH, J. T., LUISI, B. F. & KLUG, A. 1987. The structure of an oligo(dA).oligo(dT) tract and its biological implications. *Nature*, 330, 221-6.
- NGO, T. T., ZHANG, Q., ZHOU, R., YODH, J. G. & HA, T. 2015. Asymmetric unwrapping of nucleosomes under tension directed by DNA local flexibility. *Cell*, 160, 1135-44.
- NISHINO, Y., ELTSOV, M., JOTI, Y., ITO, K., TAKATA, H., TAKAHASHI, Y., HIHARA, S., FRANGAKIS, A. S., IMAMOTO, N., ISHIKAWA, T. & MAESHIMA, K. 2012. Human mitotic chromosomes consist predominantly of irregularly folded nucleosome fibres without a 30-nm chromatin structure. *EMBO J*, 31, 1644-53.
- NODELMAN, I. M., BLEICHERT, F., PATEL, A., REN, R., HORVATH, K. C., BERGER, J. M. & BOWMAN, G. D. 2017. Interdomain Communication of the Chd1 Chromatin Remodeler across the DNA Gyres of the Nucleosome. *Mol Cell*, 65, 447-459 e6.
- NODELMAN, I. M. & BOWMAN, G. D. 2013. Nucleosome sliding by Chd1 does not require rigid coupling between DNA-binding and ATPase domains. *EMBO Rep*, 14, 1098-103.
- NORTH, J. A., JAVAID, S., FERDINAND, M. B., CHATTERJEE, N., PICKING, J. W., SHOFFNER, M., NAKKULA, R. J., BARTHOLOMEW, B., OTTESEN, J. J., FISHEL, R. & POIRIER, M. G. 2011. Phosphorylation of histone H3(T118) alters nucleosome dynamics and remodeling. *Nucleic Acids Res*, 39, 6465-74.
- OCAMPO, J., CHEREJI, R. V., ERIKSSON, P. R. & CLARK, D. J. 2016. The ISW1 and CHD1 ATP-dependent chromatin remodelers compete to set nucleosome spacing in vivo. *Nucleic Acids Res*, 44, 4625-35.
- OHNO, M., ANDO, T., PRIEST, D. G., KUMAR, V., YOSHIDA, Y. & TANIGUCHI, Y. 2019. Sub-nucleosomal Genome Structure Reveals Distinct Nucleosome Folding Motifs. *Cell*, 176, 520-534 e25.
- OLAVE, I. A., RECK-PETERSON, S. L. & CRABTREE, G. R. 2002. Nuclear actin and actin-related proteins in chromatin remodeling. *Annu Rev Biochem*, 71, 755-81.
- OLINS, A. L. & OLINS, D. E. 1974. Spheroid chromatin units (v bodies). *Science*, 183, 330-2.
- OLINS, D. E. & OLINS, A. L. 2003. Chromatin history: our view from the bridge. *Nat Rev Mol Cell Biol*, 4, 809-14.
- OU, H. D., PHAN, S., DEERINCK, T. J., THOR, A., ELLISMAN, M. H. & O'SHEA, C. C. 2017. ChromEMT: Visualizing 3D chromatin structure and compaction in interphase and mitotic cells. *Science*, 357.
- PAPAMICHOS-CHRONAKIS, M. & PETERSON, C. L. 2008. The Ino80 chromatin-remodeling enzyme regulates replisome function and stability. *Nat Struct Mol Biol*, 15, 338-45.
- PAZIN, M. J. & KADONAGA, J. T. 1997. SWI2/SNF2 and related proteins: ATP-driven motors that disrupt protein-DNA interactions? *Cell*, 88, 737-40.
- PETERSON, C. L., ZHAO, Y. & CHAIT, B. T. 1998. Subunits of the yeast SWI/SNF complex are members of the actin-related protein (ARP) family. *J Biol Chem*, 273, 23641-4.
- POLI, J., GASSER, S. M. & PAPAMICHOS-CHRONAKIS, M. 2017. The INO80 remodeler in transcription, replication and repair. *Philos Trans R Soc Lond B Biol Sci*, 372.
- POLI, J., GERHOLD, C. B., TOSI, A., HUSTEDT, N., SEEBER, A., SACK, R., HERZOG, F., PASERO, P., SHIMADA, K., HOPFNER, K. P. & GASSER, S. M. 2016. Mec1, INO80, and the PAF1 complex cooperate to limit transcription replication conflicts through RNAPII removal during replication stress. *Genes Dev*, 30, 337-54.
- QIU, Y., LEVENDOSKY, R. F., CHAKRAVARTHY, S., PATEL, A., BOWMAN, G. D. & MYONG, S. 2017. The Chd1 Chromatin Remodeler Shifts Nucleosomal DNA Bidirectionally as a Monomer. *Mol Cell*, 68, 76-88 e6.

References

- RAISNER, R. M., HARTLEY, P. D., MENEGHINI, M. D., BAO, M. Z., LIU, C. L., SCHREIBER, S. L., RANDO, O. J. & MADHANI, H. D. 2005. Histone variant H2A.Z marks the 5' ends of both active and inactive genes in euchromatin. *Cell*, 123, 233-48.
- RANJAN, A., WANG, F., MIZUGUCHI, G., WEI, D., HUANG, Y. & WU, C. 2015. H2A histone-fold and DNA elements in nucleosome activate SWR1-mediated H2A.Z replacement in budding yeast. *Elife*, 4, e06845.
- RHEE, H. S. & PUGH, B. F. 2011. Comprehensive genome-wide protein-DNA interactions detected at single-nucleotide resolution. *Cell*, 147, 1408-19.
- RICCI, M. A., MANZO, C., GARCIA-PARAJO, M. F., LAKADAMYALI, M. & COSMA, M. P. 2015. Chromatin fibers are formed by heterogeneous groups of nucleosomes in vivo. *Cell*, 160, 1145-58.
- RICHMOND, T. J. & DAVEY, C. A. 2003. The structure of DNA in the nucleosome core. *Nature*, 423, 145-50.
- RIPPE, K., SCHRADER, A., RIEDE, P., STROHNER, R., LEHMANN, E. & LANGST, G. 2007. DNA sequence- and conformation-directed positioning of nucleosomes by chromatin-remodeling complexes. *Proc Natl Acad Sci U S A*, 104, 15635-40.
- ROBINSON, P. J. & RHODES, D. 2006. Structure of the '30 nm' chromatin fibre: a key role for the linker histone. *Curr Opin Struct Biol*, 16, 336-43.
- ROHS, R., WEST, S. M., SOSINSKY, A., LIU, P., MANN, R. S. & HONIG, B. 2009. The role of DNA shape in protein-DNA recognition. *Nature*, 461, 1248-53.
- ROSSI, M. J., LAI, W. K. M. & PUGH, B. F. 2018. Genome-wide determinants of sequence-specific DNA binding of general regulatory factors. *Genome Res*, 28, 497-508.
- ROUTH, A., SANDIN, S. & RHODES, D. 2008. Nucleosome repeat length and linker histone stoichiometry determine chromatin fiber structure. *Proc Natl Acad Sci U S A*, 105, 8872-7.
- RYAN, D. P., SUNDARAMOORTHY, R., MARTIN, D., SINGH, V. & OWEN-HUGHES, T. 2011. The DNA-binding domain of the Chd1 chromatin-remodelling enzyme contains SANT and SLIDE domains. *EMBO J*, 30, 2596-609.
- SABANTSEV, A., LEVENDOSKY, R. F., ZHUANG, X., BOWMAN, G. D. & DEINDL, S. 2019. Direct observation of coordinated DNA movements on the nucleosome during chromatin remodelling. *Nat Commun*, 10, 1720.
- SAHA, A., WITTMAYER, J. & CAIRNS, B. R. 2002. Chromatin remodeling by RSC involves ATP-dependent DNA translocation. *Genes Dev*, 16, 2120-34.
- SAHA, A., WITTMAYER, J. & CAIRNS, B. R. 2005. Chromatin remodeling through directional DNA translocation from an internal nucleosomal site. *Nat Struct Mol Biol*, 12, 747-55.
- SCHAFER, D. A. & SCHROER, T. A. 1999. Actin-related proteins. *Annu Rev Cell Dev Biol*, 15, 341-63.
- SCHALCH, T., DUDA, S., SARGENT, D. F. & RICHMOND, T. J. 2005. X-ray structure of a tetranucleosome and its implications for the chromatin fibre. *Nature*, 436, 138-41.
- SCHNITZLER, G. R., CHEUNG, C. L., HAFNER, J. H., SAURIN, A. J., KINGSTON, R. E. & LIEBER, C. M. 2001. Direct imaging of human SWI/SNF-remodeled mono- and polynucleosomes by atomic force microscopy employing carbon nanotube tips. *Mol Cell Biol*, 21, 8504-11.
- SCHROTER, H. & BODE, J. 1982. The binding sites for large and small high-mobility-group (HMG) proteins. Studies on HMG-nucleosome interactions in vitro. *Eur J Biochem*, 127, 429-36.
- SCHUBERT, H. L., WITTMAYER, J., KASTEN, M. M., HINATA, K., RAWLING, D. C., HEROUX, A., CAIRNS, B. R. & HILL, C. P. 2013. Structure of an actin-related subcomplex of the SWI/SNF chromatin remodeler. *Proc Natl Acad Sci U S A*, 110, 3345-50.
- SCHWANBECK, R., XIAO, H. & WU, C. 2004. Spatial contacts and nucleosome step movements induced by the NURF chromatin remodeling complex. *J Biol Chem*, 279, 39933-41.

References

- SCHWARZ, M., SCHALL, K., KALLIS, E., EUSTERMANN, S., GUARIENTO, M., MOLDT, M., HOPFNER, K. P. & MICHAELIS, J. 2018. Single-molecule nucleosome remodeling by INO80 and effects of histone tails. *FEBS Lett*, 592, 318-331.
- SCULLY, R. & XIE, A. 2013. Double strand break repair functions of histone H2AX. *Mutat Res*, 750, 5-14.
- SHARMA, A., JENKINS, K. R., HEROUX, A. & BOWMAN, G. D. 2011. Crystal structure of the chromodomain helicase DNA-binding protein 1 (Chd1) DNA-binding domain in complex with DNA. *J Biol Chem*, 286, 42099-104.
- SHEN, X., MIZUGUCHI, G., HAMICHE, A. & WU, C. 2000. A chromatin remodelling complex involved in transcription and DNA processing. *Nature*, 406, 541-4.
- SHEN, X., RANALLO, R., CHOI, E. & WU, C. 2003a. Involvement of actin-related proteins in ATP-dependent chromatin remodeling. *Mol Cell*, 12, 147-55.
- SHEN, X., XIAO, H., RANALLO, R., WU, W. H. & WU, C. 2003b. Modulation of ATP-dependent chromatin-remodeling complexes by inositol polyphosphates. *Science*, 299, 112-4.
- SIMIC, R., LINDSTROM, D. L., TRAN, H. G., ROINICK, K. L., COSTA, P. J., JOHNSON, A. D., HARTZOG, G. A. & ARNDT, K. M. 2003. Chromatin remodeling protein Chd1 interacts with transcription elongation factors and localizes to transcribed genes. *EMBO J*, 22, 1846-56.
- SIMPSON, R. T. 1978. Structure of the chromatosome, a chromatin particle containing 160 base pairs of DNA and all the histones. *Biochemistry*, 17, 5524-31.
- SIMPSON, R. T. & STAFFORD, D. W. 1983. Structural features of a phased nucleosome core particle. *Proc Natl Acad Sci U S A*, 80, 51-5.
- SINGLETON, M. R., DILLINGHAM, M. S. & WIGLEY, D. B. 2007. Structure and mechanism of helicases and nucleic acid translocases. *Annu Rev Biochem*, 76, 23-50.
- SIRINAKIS, G., CLAPIER, C. R., GAO, Y., VISWANATHAN, R., CAIRNS, B. R. & ZHANG, Y. 2011. The RSC chromatin remodelling ATPase translocates DNA with high force and small step size. *EMBO J*, 30, 2364-72.
- SIVOLOB, A. & PRUNELL, A. 2003. Linker histone-dependent organization and dynamics of nucleosome entry/exit DNAs. *J Mol Biol*, 331, 1025-40.
- SMITH, R. M. & RILL, R. L. 1989. Mobile histone tails in nucleosomes. Assignments of mobile segments and investigations of their role in chromatin folding. *J Biol Chem*, 264, 10574-81.
- STELLA, S., CASCIO, D. & JOHNSON, R. C. 2010. The shape of the DNA minor groove directs binding by the DNA-bending protein Fis. *Genes Dev*, 24, 814-26.
- STRAHL, B. D. & ALLIS, C. D. 2000. The language of covalent histone modifications. *Nature*, 403, 41-5.
- STROM, A. R., EMELYANOV, A. V., MIR, M., FYODOROV, D. V., DARZACQ, X. & KARPEN, G. H. 2017. Phase separation drives heterochromatin domain formation. *Nature*, 547, 241-245.
- STRUHL, K. & SEGAL, E. 2013. Determinants of nucleosome positioning. *Nat Struct Mol Biol*, 20, 267-73.
- SUNDARAMOORTHY, R. 2019. Nucleosome remodelling: structural insights into ATP-dependent remodelling enzymes. *Essays Biochem*, 63, 45-58.
- SUNDARAMOORTHY, R., HUGHES, A. L., EL-MKAMI, H., NORMAN, D. G., FERREIRA, H. & OWEN-HUGHES, T. 2018. Structure of the chromatin remodelling enzyme Chd1 bound to a ubiquitinated nucleosome. *Elife*, 7.
- SZERLONG, H., HINATA, K., VISWANATHAN, R., ERDJUMENT-BROMAGE, H., TEMPST, P. & CAIRNS, B. R. 2008. The HSA domain binds nuclear actin-related proteins to regulate chromatin-remodeling ATPases. *Nat Struct Mol Biol*, 15, 469-76.
- SZERLONG, H., SAHA, A. & CAIRNS, B. R. 2003. The nuclear actin-related proteins Arp7 and Arp9: a dimeric module that cooperates with architectural proteins for chromatin remodeling. *EMBO J*, 22, 3175-87.
- TALBERT, P. B. & HENIKOFF, S. 2010. Histone variants--ancient wrap artists of the epigenome. *Nat Rev Mol Cell Biol*, 11, 264-75.

References

- TAN, S. & DAVEY, C. A. 2011. Nucleosome structural studies. *Curr Opin Struct Biol*, 21, 128-36.
- THOMAS, J. O. & FURBER, V. 1976. Yeast chromatin structure. *FEBS Lett*, 66, 274-80.
- TONG, J. K., HASSIG, C. A., SCHNITZLER, G. R., KINGSTON, R. E. & SCHREIBER, S. L. 1998. Chromatin deacetylation by an ATP-dependent nucleosome remodelling complex. *Nature*, 395, 917-21.
- TOSI, A., HAAS, C., HERZOG, F., GILMOZZI, A., BERNINGHAUSEN, O., UNGEWICKELL, C., GERHOLD, C. B., LAKOMEK, K., AEBERSOLD, R., BECKMANN, R. & HOPFNER, K. P. 2013. Structure and subunit topology of the INO80 chromatin remodeler and its nucleosome complex. *Cell*, 154, 1207-19.
- TUREGUN, B., BAKER, R. W., LESCHZINER, A. E. & DOMINGUEZ, R. 2018. Actin-related proteins regulate the RSC chromatin remodeler by weakening intramolecular interactions of the Sth1 ATPase. *Commun Biol*, 1, 1.
- TUREGUN, B., KAST, D. J. & DOMINGUEZ, R. 2013. Subunit Rtt102 controls the conformation of the Arp7/9 heterodimer and its interactions with nucleotide and the catalytic subunit of SWI/SNF remodelers. *J Biol Chem*, 288, 35758-68.
- TURNER, B. M. 2000. Histone acetylation and an epigenetic code. *Bioessays*, 22, 836-45.
- UBERBACHER, E. C. & BUNICK, G. J. 1985. X-ray structure of the nucleosome core particle. *J Biomol Struct Dyn*, 2, 1033-55.
- UDUGAMA, M., SABRI, A. & BARTHOLOMEW, B. 2011. The INO80 ATP-dependent chromatin remodeling complex is a nucleosome spacing factor. *Mol Cell Biol*, 31, 662-73.
- VALOUEV, A., JOHNSON, S. M., BOYD, S. D., SMITH, C. L., FIRE, A. Z. & SIDOW, A. 2011. Determinants of nucleosome organization in primary human cells. *Nature*, 474, 516-20.
- VAN ATTIKUM, H., FRITSCH, O., HOHN, B. & GASSER, S. M. 2004. Recruitment of the INO80 complex by H2A phosphorylation links ATP-dependent chromatin remodeling with DNA double-strand break repair. *Cell*, 119, 777-88.
- VAN ATTIKUM, H. & GASSER, S. M. 2009. Crosstalk between histone modifications during the DNA damage response. *Trends Cell Biol*, 19, 207-17.
- VAN BAKEL, H., TSUI, K., GEBBIA, M., MNAIMNEH, S., HUGHES, T. R. & NISLOW, C. 2013. A compendium of nucleosome and transcript profiles reveals determinants of chromatin architecture and transcription. *PLoS Genet*, 9, e1003479.
- VANDEMARK, A. P., KASTEN, M. M., FERRIS, E., HEROUX, A., HILL, C. P. & CAIRNS, B. R. 2007. Autoregulation of the rsc4 tandem bromodomain by gcn5 acetylation. *Mol Cell*, 27, 817-28.
- VARGA-WEISZ, P., VAN HOLDE, K. & ZLATANOVA, J. 1993. Preferential binding of histone H1 to four-way helical junction DNA. *J Biol Chem*, 268, 20699-700.
- VASSILEVA, I., YANAKIEVA, I., PEYCHEVA, M., GOSPODINOV, A. & ANACHKOVA, B. 2014. The mammalian INO80 chromatin remodeling complex is required for replication stress recovery. *Nucleic Acids Res*, 42, 9074-86.
- VELANKAR, S. S., SOULTANAS, P., DILLINGHAM, M. S., SUBRAMANYA, H. S. & WIGLEY, D. B. 1999. Crystal structures of complexes of PcrA DNA helicase with a DNA substrate indicate an inchworm mechanism. *Cell*, 97, 75-84.
- VENNE, A. S., KOLLIPARA, L. & ZAHEDI, R. P. 2014. The next level of complexity: crosstalk of posttranslational modifications. *Proteomics*, 14, 513-24.
- VIGNALI, M., HASSAN, A. H., NEELY, K. E. & WORKMAN, J. L. 2000. ATP-dependent chromatin-remodeling complexes. *Mol Cell Biol*, 20, 1899-910.
- WAGNER, F. R., DIENEMANN, C., WANG, H., STUTZER, A., TEGUNOV, D., URLAUB, H. & CRAMER, P. 2020. Structure of SWI/SNF chromatin remodeler RSC bound to a nucleosome. *Nature*, 579, 448-451.
- WATANABE, S., TAN, D., LAKSHMINARASIMHAN, M., WASHBURN, M. P., HONG, E. J., WALZ, T. & PETERSON, C. L. 2015. Structural analyses of the chromatin remodelling enzymes INO80-C and SWR-C. *Nat Commun*, 6, 7108.
- WATSON, J. D. & CRICK, F. H. 1953. The structure of DNA. *Cold Spring Harb Symp Quant Biol*, 18, 123-31.

References

- WHITEHOUSE, I., FLAUS, A., CAIRNS, B. R., WHITE, M. F., WORKMAN, J. L. & OWEN-HUGHES, T. 1999. Nucleosome mobilization catalysed by the yeast SWI/SNF complex. *Nature*, 400, 784-7.
- WIDOM, J. 1998. Chromatin structure: linking structure to function with histone H1. *Curr Biol*, 8, R788-91.
- WILLHOFT, O., BYTHELL-DOUGLAS, R., MCCORMACK, E. A. & WIGLEY, D. B. 2016. Synergy and antagonism in regulation of recombinant human INO80 chromatin remodeling complex. *Nucleic Acids Res*, 44, 8179-88.
- WILLHOFT, O., GHONEIM, M., LIN, C. L., CHUA, E. Y. D., WILKINSON, M., CHABAN, Y., AYALA, R., MCCORMACK, E. A., OCLOO, L., RUEDA, D. S. & WIGLEY, D. B. 2018. Structure and dynamics of the yeast SWR1-nucleosome complex. *Science*, 362.
- WILSON, B. G. & ROBERTS, C. W. 2011. SWI/SNF nucleosome remodellers and cancer. *Nat Rev Cancer*, 11, 481-92.
- WINGER, J. & BOWMAN, G. D. 2017. The Sequence of Nucleosomal DNA Modulates Sliding by the Chd1 Chromatin Remodeler. *J Mol Biol*, 429, 808-822.
- WINGER, J., NODELMAN, I. M., LEVENDOSKY, R. F. & BOWMAN, G. D. 2018. A twist defect mechanism for ATP-dependent translocation of nucleosomal DNA. *Elife*, 7.
- WOODCOCK, C. L., SAFER, J. P. & STANCHFIELD, J. E. 1976. Structural repeating units in chromatin. I. Evidence for their general occurrence. *Exp Cell Res*, 97, 101-10.
- WORCEL, A., STROGATZ, S. & RILEY, D. 1981. Structure of chromatin and the linking number of DNA. *Proc Natl Acad Sci U S A*, 78, 1461-5.
- WU, J. & GRUNSTEIN, M. 2000. 25 years after the nucleosome model: chromatin modifications. *Trends Biochem Sci*, 25, 619-23.
- YAMADA, K., FROUWS, T. D., ANGST, B., FITZGERALD, D. J., DELUCA, C., SCHIMMELE, K., SARGENT, D. F. & RICHMOND, T. J. 2011. Structure and mechanism of the chromatin remodelling factor ISW1a. *Nature*, 472, 448-53.
- YAN, L. & CHEN, Z. 2020. A Unifying Mechanism of DNA Translocation Underlying Chromatin Remodeling. *Trends Biochem Sci*, 45, 217-227.
- YAN, L., WANG, L., TIAN, Y., XIA, X. & CHEN, Z. 2016. Structure and regulation of the chromatin remodeler ISWI. *Nature*, 540, 466-469.
- YAN, L., WU, H., LI, X., GAO, N. & CHEN, Z. 2019. Structures of the ISWI-nucleosome complex reveal a conserved mechanism of chromatin remodeling. *Nat Struct Mol Biol*, 26, 258-266.
- YANG, J. G., MADRID, T. S., SEVASTOPOULOS, E. & NARLIKAR, G. J. 2006. The chromatin-remodeling enzyme ACF is an ATP-dependent DNA length sensor that regulates nucleosome spacing. *Nat Struct Mol Biol*, 13, 1078-83.
- YEN, K., VINAYACHANDRAN, V., BATTI, K., KOERBER, R. T. & PUGH, B. F. 2012. Genome-wide nucleosome specificity and directionality of chromatin remodelers. *Cell*, 149, 1461-73.
- YEN, K., VINAYACHANDRAN, V. & PUGH, B. F. 2013. SWR-C and INO80 chromatin remodelers recognize nucleosome-free regions near +1 nucleosomes. *Cell*, 154, 1246-56.
- YUAN, G. C., LIU, Y. J., DION, M. F., SLACK, M. D., WU, L. F., ALTSCHULER, S. J. & RANDO, O. J. 2005. Genome-scale identification of nucleosome positions in *S. cerevisiae*. *Science*, 309, 626-30.
- ZANTON, S. J. & PUGH, B. F. 2006. Full and partial genome-wide assembly and disassembly of the yeast transcription machinery in response to heat shock. *Genes Dev*, 20, 2250-65.
- ZENTNER, G. E. & HENIKOFF, S. 2013. Regulation of nucleosome dynamics by histone modifications. *Nat Struct Mol Biol*, 20, 259-66.
- ZENTNER, G. E., KASINATHAN, S., XIN, B., ROHS, R. & HENIKOFF, S. 2015. ChEC-seq kinetics discriminates transcription factor binding sites by DNA sequence and shape in vivo. *Nat Commun*, 6, 8733.
- ZHANG, X., WANG, X., ZHANG, Z. & CAI, G. 2019. Structure and functional interactions of INO80 actin/Arp module. *J Mol Cell Biol*, 11, 345-355.

References

- ZHANG, Y., MOQTADERI, Z., RATTNER, B. P., EUSKIRCHEN, G., SNYDER, M., KADONAGA, J. T., LIU, X. S. & STRUHL, K. 2009. Intrinsic histone-DNA interactions are not the major determinant of nucleosome positions in vivo. *Nat Struct Mol Biol*, 16, 847-52.
- ZHANG, Z., WANG, X., XIN, J., DING, Z., LIU, S., FANG, Q., YANG, N., XU, R. M. & CAI, G. 2018. Architecture of SWI/SNF chromatin remodeling complex. *Protein Cell*, 9, 1045-1049.
- ZHANG, Z., WIPPO, C. J., WAL, M., WARD, E., KORBER, P. & PUGH, B. F. 2011. A packing mechanism for nucleosome organization reconstituted across a eukaryotic genome. *Science*, 332, 977-80.
- ZHENG, C. & HAYES, J. J. 2003. Structures and interactions of the core histone tail domains. *Biopolymers*, 68, 539-46.
- ZHOU, C. Y., JOHNSON, S. L., LEE, L. J., LONGHURST, A. D., BECKWITH, S. L., JOHNSON, M. J., MORRISON, A. J. & NARLIKAR, G. J. 2018. The Yeast INO80 Complex Operates as a Tunable DNA Length-Sensitive Switch to Regulate Nucleosome Sliding. *Mol Cell*, 69, 677-688 e9.
- ZHOU, K., GAULLIER, G. & LUGER, K. 2019. Nucleosome structure and dynamics are coming of age. *Nat Struct Mol Biol*, 26, 3-13.
- ZHOU, T., YANG, L., LU, Y., DROR, I., DANTAS MACHADO, A. C., GHANE, T., DI FELICE, R. & ROHS, R. 2013. DNASHape: a method for the high-throughput prediction of DNA structural features on a genomic scale. *Nucleic Acids Res*, 41, W56-62.
- ZLATANOVA, J. & THAKAR, A. 2008. H2A.Z: view from the top. *Structure*, 16, 166-79.
- ZLATANOVA, J. & VAN HOLDE, K. 1996. The linker histones and chromatin structure: new twists. *Prog Nucleic Acid Res Mol Biol*, 52, 217-59.
- ZOFALL, M., PERSINGER, J. & BARTHOLOMEW, B. 2004. Functional role of extranucleosomal DNA and the entry site of the nucleosome in chromatin remodeling by ISW2. *Mol Cell Biol*, 24, 10047-57.
- ZOFALL, M., PERSINGER, J., KASSABOV, S. R. & BARTHOLOMEW, B. 2006. Chromatin remodeling by ISW2 and SWI/SNF requires DNA translocation inside the nucleosome. *Nat Struct Mol Biol*, 13, 339-46.

5. Acknowledgements

This work would not have been possible without the support from various persons:

First and foremost, I would like to express my deep and sincere gratitude to my research supervisor, Prof. Dr. Karl-Peter Hopfner, for giving me the opportunity to work on the challenging INO80 project, for giving me the freedom to develop and follow my own ideas as well as for providing invaluable guidance whenever I asked for it. I would also like to thank him for his empathy and patience.

I would like to extend my heartfelt thanks to PD. Dr. Philipp Korber who gave me the opportunity to broaden my knowledge of genome-wide in vitro reconstitution systems, who welcomed me to his lab, who gave me advice whenever I needed it and who showed unlimited patience during paper preparation and proof reading of this thesis.

I want to express my profound gratitude to the revisors of the manuscript: PD Dr. Gregor Witte, Elisa Oberbeckmann, Stephan Woike, and especially PD Dr. Philipp Korber and Dr. James Jung.

I would like to express my gratitude to the entire INO80 subgroup (Manu, Stephan, Franzi, Felix and James) as well as to former members for the great working atmosphere and fruitful scientific discussions. I want to thank you, Manu, for introducing me into the lab, for providing practical advice whenever I asked and for continuing the project during maternity protection. I extend my gratitude to the entire Hopfner lab for the great and supportive working atmosphere. Heartfelt thanks to the group of "ANPs" and Sebastian Michalski!

I am extremely grateful to Elisa Oberbeckmann, Franziska Kunert as well as Kilian Knoll for scientific discussions and support, for unlimited patience predominantly during bioinformatic problem solving, but mainly for your great sense of humor, support, sympathy and friendship.

I am extremely grateful to my parents and my brother for their love, sympathy, guidance, unlimited support and their sacrifices to give me the opportunity to complete this thesis successfully.

I sincerely owe my deepest gratitude to you Max.